

ABSTRACT

PATANKAR, NEHA SATISH. Addressing Uncertainty in Energy System Optimization Models Over a Long Planning Horizon. (Under the direction of Dr. Joseph F. DeCarolis).

Rapid technological changes and anthropogenic climate change are motivating a fundamental transformation of the global energy system. That transformation comes with significant uncertainties. Dealing with the effects of future uncertainties in energy systems is a major challenge, particularly over long time horizons. This thesis utilizes Tools for Energy Model Optimization and Analysis (Temoa), an open source energy system optimization model to conduct the analysis. Temoa is used to examine a wide range of future uncertainties across three different applications of the model. The first application uses stochastic programming to address how conflict uncertainty in South Sudan can affect the country's electricity planning. The second application utilizes robust optimization to address parametric uncertainty and explore deep decarbonization pathways in the United States. The third application focuses on modeling consumer behavior regarding the choice between electricity consumption and the adoption of energy efficiency measures.

Chapter 2 describes the ongoing armed conflict uncertainty in South Sudan, the newest country in the world. Assuming that armed conflict might lead to damage to power system infrastructure with a finite probability, we evaluate the importance of uncertainty analysis for power system capacity expansion planning. The model solution obtained with stochastic programming is evaluated by estimating the expected value of perfect information (EVPI), the value of the stochastic solution (VSS), and the expected cost of ignoring conflict (ECIC). The study finds that utilizing distributed solar generation hedges against the risk of conflict. The investment in centralized hydro generation, on the other hand, will lead to higher financial risks despite the lower cost of electricity generation when conflict uncertainty is ignored.

Chapter 3 sheds light on the limitations of using stochastic programming for energy system capacity expansion problems, which leads to the formulation of a robust optimization problem. The objective is to better characterize robust pathways for US deep decarbonization while considering future uncertainty in future fuel prices and technology capital costs. The variations in fuel price projections affect the penetration of renewables and the deployment of more efficient technologies. Moreover, the fuel prices and investment cost of the technologies are autocorrelated. The correlated robust optimization formulation is proposed based on the nature of data uncertainty.

Another key challenge in energy system models is modeling the response of consumers to prices as well as the option to invest in energy efficiency in order to reduce electricity costs. Chapter 4 revises the Temoa formulation to describe the substitution effect between electricity and energy efficiency. The revised model formulated in chapter 4, referred to as the “energy efficiency model,” uses the production function defined in microeconomics theory to consider the substitution effect between electricity supply and the adoption of energy efficiency measures. The model is tested on a hypothetical test case, and sensitivity analysis is performed to quantify the effects of uncertain parameters on total (consumer plus producer) welfare. The sensitivity analysis suggests that lower energy efficiency costs lead to higher welfare recovered for a given efficiency subsidy. Similarly, lower own price elasticity of end-use energy service demand increases the welfare recovered at a given efficiency level. Lastly, the energy efficiency subsidy needs to increase as the carbon tax increases in order to recover the maximum amount of welfare.

© Copyright 2019 by Neha Patankar
All Rights Reserved

Addressing Uncertainty in Energy System Optimization Models Over a Long Planning Horizon

by
Neha Satish Patankar

A dissertation submitted to the Graduate Faculty of
North Carolina State University
in partial fulfillment of the
requirements for the degree of
Doctor of Philosophy

Operations Research

Raleigh, North Carolina
2019

APPROVED BY:

Dr. Joseph F. DeCarolis
Committee Chair

Dr. Anderson de Queiroz

Dr. Harrison Fell

Dr. Reha Uzsoy

DEDICATION

This thesis is dedicated to my wonderful parents who have always been a source of inspiration, encouragement, and resilience to undertake my higher studies and to face the eventualities of life with zeal and enthusiasm.

BIOGRAPHY

Neha Patankar moved from India to the USA to explore her passion for the field of Operations Research and its applications. She started pursuing a Ph.D. in Operations Research at North Carolina State University in 2015. During her Ph.D., she has become immensely interested in the applications of Operations Research in the field of energy system modeling. She has closely worked on the open source energy modelling framework known as Tools for Energy Model Optimization and Assessment (Temoa) to implement techniques from Operations Research in energy system models. Addressing parametric and structural uncertainties in the energy system models has been her prime interest during this period. Apart from her research interests, she is also an avid chess player and has represented her home state on a national level.

TABLE OF CONTENTS

LIST OF TABLES	viii
LIST OF FIGURES	x
Chapter 1 Introduction	1
1 The Utility of Energy System Optimization Models (ESOMs).....	1
2 Motivation	1
3 Objective	2
Chapter 2 Building Conflict Uncertainty into Electricity Planning: A South Sudan Case Study	5
1 Introduction	5
2 Methods.....	6
2.1 Tools for Energy Model Optimization and Analysis (Temoa).....	7
2.2 Input Data.....	7
2.3 Method of Morris.....	10
2.4 Stochastic Problem Formulation.....	11
2.4.1 Scenario Tree Structure.....	12
2.4.2 Damage Estimation.....	13
2.5 Metrics to assess value: EVPI, VSS and ECIC	16
2.5.1 Expected Value of Perfect Information (EVPI).....	16
2.5.2 Value of Stochastic Solution (VSS).....	16
2.5.3 Expected Cost of Ignoring Conflict (ECIC).....	17
3 Results and Discussion.....	18
3.1 Identifying key input sensitivities.....	18
3.2 Capacity expansion under conflict uncertainty.....	19
3.3 The value of hedging.....	23
4 Conclusion and policy implications.....	27
5 Caveats and Future Work.....	27
Chapter 3 A Novel Approach to Consider Parametric Uncertainty in Bottom-Up Energy System Models: US Case Study	30
1 Introduction	32
2 Robust optimization	34
2.1 Robust optimization in power system modeling.....	35
2.2 Robust optimization in energy system modeling.....	36
3 Robust optimization formulation.....	38
3.1 A simplified ESOM formulation	39

3.2 Robust optimization formulation.....	41
3.2.1 RO formulation for uncorrelated variables - R-ESOM.....	41
3.3.2 RO formulation for correlated variables (CR-ESOM).....	45
3.3 Evaluating quality of the RO solution.....	48
4 US case study	49
5 Building the uncertainty set.....	50
5.1 Grouping of the parameters.....	51
5.2 Uncertainty characterization.....	51
5.2.1 Criteria for investigating uncertainty	51
5.2.2 Correlation coefficient	54
5.2.3 Determining the effects of correlation on the uncertain parameters	56
5.3 The uncertainty set.....	58
6 Robust optimization results	59
6.1 Value of the robust optimization	60
6.2 Solution quality of robust vs. naïve solution.....	61
6.3 Robust emission mitigation pathways considering future uncertainty.....	62
6.4 Importance of a parameter in achieving a robust solution.....	65
7 Conclusions	67
Chapter 4 Substitution between Energy Efficiency and Electricity in an Energy System Optimization Model.....	69
1 Introduction	70
2 Energy System Optimization Models	73
2.1 Framework of ESOMs	73
2.2 Economic interpretation of bottom up ESOMs	74
2.3 Elasticity.....	75
2.3.1 Demand elasticity	75
2.3.2 Elasticity of substitution.....	76
3 ESOM Representation with Energy Efficiency Model	77
3.1 Conceptual Framework	77
3.2 Mathematical Formulation	80
3.3 Solution methodology	81
4 Experimental datasets	82
5 Policy Scenario	84
5.1 Results and Discussion.....	87
5.2 Sensitivity Analysis	90

6 Conclusion and Future work.....	93
Chapter 5 Conclusion and Future Work.....	95
1 Research contribution	95
2 Final remarks and future research goals.....	97
REFERENCES	100
Chapter 1	100
Chapter 2	102
Chapter 3	107
Chapter 4.....	113
Chapter 5	116
APPENDICES.....	118
Chapter 2	119
1 Technology representation	119
2 Electricity demand.....	121
3 Damage Value Estimation.....	122
3.1 Regional Conflict Rate.....	122
3.2 Damage Rate	122
Chapter 3	125
1 An overview of the database	125
1.1 Electric sector.....	126
1.1.1 Investment costs of electric sector technologies.....	126
1.1.2 Renewable energies representation.....	126
1.1.2.1 Solar.....	126
1.1.2.2 Wind	129
1.1.4 Capacity reserve margin.....	131
1.1.5 Renewable portfolio standards	132
1.1.6 Cross-State Air Pollution Rule.....	132
1.1.7 Hydrogen combustion.....	133
1.2 Transportation sector	133
1.2.1 Modeling of ethanol E10 and E85	133
1.2.2 Modeling of jet fuel and biodiesel.....	135
1.2.2.1 Description:.....	136
1.2.2.2 Calculations.....	139
1.3 Residential and commercial sectors.....	143
1.4 Industrial sector	143

1.4.1 Background	143
1.4.2 Structure.....	143
1.4.3 Key Assumptions about manufacturing sector.....	146
1.4.4 Key assumptions about non-manufacturing sector.....	149
1.4.5 Fuel Cost.....	150
1.4.6 Hydrogen in industrial sector	150
1.5 Cross-sectoral issues.....	150
1.5.1 Hurdle rate.....	151
1.6 Power to X.....	151
1.6.1 Introduction.....	151
1.6.1.1 Scope of this report.....	152
1.6.2 The Power-to-X technology.....	153
1.6.3 Implementing Power-to-X into Temoa.....	156
1.6.3.1 Transformation of electricity from AC to DC (E_TRS_DC).....	156
1.6.3.2 Technologies for electrolysis (E_ELECAL and E_ELECPEM).....	157
1.6.3.3 Technology for import of Hydrogen (IMPTRNH2).....	159
1.6.3.4 Technology for compression of Hydrogen to 100 bar (H2_COMP10100).....	160
1.6.3.5 Technology for Hydrogen storage at 150 bar (H2_STO150).....	162
1.6.3.6 Technology for compression of Hydrogen to 100 bar (H2_COMP100700).....	163
1.6.3.7 Technologies for blending Hydrogen into natural gas (..._H2BL).....	165
1.6.3.8 Technology for generating SNG from Hydrogen and CO2 (SNGSYN)	167
1.3.6.8 Technology for compression of SNG from 20 to 100 bar (SNG_COMP20100) ...	169
1.3.6.12 Technology for storing Methanol (MEOH_STO)	174
1.3.6.13 Technologies for blending Methanol into gasoline for utilization in the transport sector (..._MEOHBL).....	174
1.7 Biomass.....	175
Chapter 4.....	178
1 Proving global optimality of the IPOPT solution:.....	178
2 Data.....	182
3 Policy Analysis.....	184
Appendix of Chapter 2.....	187
Appendix of Chapter 3.....	188
Appendix of Chapter 4.....	195

LIST OF TABLES

Table 2.1: Node probabilities of a scenario tree	13
Table 3.1: Sectoral-level detail in the Temoa input database	50
Table 3.2: Application of uncertainty characterization method to the US energy system model. We divide 2224 parameters in 22 categories.	54
Table 3.3: Correlation between uncertain parameters used for formulation in 3.2.....	55
Table 3.4: Correlation coefficient for the 22 groups of technologies. For technologies consuming coal, natural gas and solar, we have access to data by technology type.....	56
Table 3.5: Uncertainty set for the US energy system. Abbreviations: Natural Gas (NG), Integrated Gasification Combined Cycle (IGCC), Advanced Combined Cycle (ACC), Carbon Capture and Sequestration (CCS), Photovoltaic (PV), Thermal (TH).....	58
Table 3.6: Uncertainty set for fuel prices. Abbreviations: Commercial (Com), Residential (Res), Industrial (Ind.), Electric (Elc.), Transportation (Trn.), Distillate Fuel Oil (DFO), Residual Fuel Oil (RFO), Gasoline (GSL), Propane (LPG), Diesel (DSL), Jet fuel (JTF), Sub (S)	59
Table 4.1: Test model parameter values.....	84
Appendix Table 2.1: Technology cost and performance assumptions	119
Appendix Table 2.2: Location of all the generators by region.....	121
Appendix Table 2.3: Regional conflict rate (RCR) calculated from frequency of conflict incidences in 2016 for 10 states in South Sudan (Raleigh et al., 2010).	122
Appendix Table 2.4: EFOM represents percent equivalent increase in investment cost while <i>ECF</i> represents equivalent percent of capacity factor remaining for each power plant after damage. EFOM and ECF for Regional damage \leq Intensified regional damage \leq Maximum damage. ‘SO’ indicates solar PV, ‘TH’ indicates thermal plants running on diesel, ‘HY’ indicates hydro power plant.....	124
Appendix Table 3.1: UPV capacity factors	127
Appendix Table 3.2: DPV capacity factors	128
Appendix Table 3.3: STH capacity factors.....	128
Appendix Table 3.4: Solar outputs of the DPV deployments across the regions (GW).....	128
Appendix Table 3.5: Maximum wind capacities (GW).....	129
Appendix Table 3.6: capacity credit values from Figure 3 (Voorspools and D'haeseleer, 2006).	131
Appendix Table 3.7: capacity credit for wind resources in the US database.....	131

Appendix Table 3.8: Minimum generation from renewable energies (RPS).....	132
Appendix Table 3.9: Techno economic parameters for hydrogen combustion to produce electricity	133
Appendix Table 3.10: Description of notations used in Figure 6.....	134
Appendix Table 3.11: Constraints imposed on ethanol use. Numbers are in PJ.....	135
Appendix Table 3.12: Biomass related commodities.....	136
Appendix Table 3.13: Techno-economic data for FISCH_TROP AND HEFA	138
Appendix Table 3.14: Techno-economic data for TRANSEST.....	138
Appendix Table 3.15: Techno-economic data for ethanol.....	139
Appendix Table 3.16: Techno-economic parameters for the technologies (EIA, 2010).....	149
Appendix Table 3.17: Fuel cost projections from AEO (\$Million/PJ).....	150
Appendix Table 3.18: Data for electrolysis technologies E_ELECAL and E_ELECPDM entered to Temoa.....	159
Appendix Table 3.19: Data for Compressor technology H2_COMP10100 entered to Temoa.....	161
Appendix Table 3.20: Data for Hydrogen storage technology H2_STO150 entered to Temoa	163
Appendix Table 3.21: Data for Compressor technology H2_COMP100700 entered to Temoa.....	164
Appendix Table 3.22: Data for SNG generation technology SNGSYN entered to Temoa.....	169
Appendix Table 3.23: Data for Compressor technology SNG_COMP20100 entered to Temoa.....	170
Appendix Table 3.24: Data for Methanol generation technology MEOHSYN entered to Temoa	173
Appendix Table 3.25: sample calculation for IMPSTV	176
Appendix Table 3.26: Energy content of the biomass.....	176
Appendix Table 4.1: Valid range of the model parameters	179
Appendix Table 4.2: Technology specifications for utopia database.....	184

LIST OF FIGURES

Figure 2.1: Layout of the modeled South Sudan system. Proposed locations (see Appendix Table 2.2) for new hydro and thermal capacity are based on Hatch (2014). Solar PV can be constructed within each of the 13 demand centers. Existing and proposed capacities are denoted in GW..... 8

Figure 2.2: (a) Scenario tree representation with three uncertain stages, where each region of South Sudan has its own damage intensity and each demand center within a given region experiences the same damage intensity. (b) Given this tree structure, there are 8 potentially different pathways through the scenario tree representing different combinations of damage versus no damage to generators at each of the three uncertain time stages. Two of the 8 pathways are shown. 12

Figure 2.3: Single forward path in a three-stage problem used to solve $ZDM(\xi)$ 17

Figure 2.4: Change in the total cost of energy supply given a $\pm 20\%$ change in the value of five different input parameters using the Method of Morris. The length of the bars indicates the average effect of each parameter on total system-wide cost, and the error bars indicate the standard deviation across an ensemble of runs. 19

Figure 2.5: Installed capacity in the first model time period (2017) assuming (a) high probability of power plant damage, and (b) medium probability of power plant damage. The stochastic optimization is repeated for different curtailment costs and damage estimation methods: base (no damage), regional, intensified, and max damage. Differences in the total amount of installed capacity stem from differential use of demand curtailment and differences in technology-specific capacity factors. Given a 5-year delay in hydro availability, hydro constructed in 2017 is not available for generation until 2022. 20

Figure 2.6: Difference in installed capacity between the two most extreme forward paths through the scenario tree: no generator damage and damage in every time period. Positive differences indicate higher installed capacity in the all-damage scenario. Differences are shown with (a) high damage probability and (b) medium damage probability, and in both cases, three different damage estimation methods. Differences are also shown at three different curtailment costs given in parentheses: 0.15, 0.25, and 0.8 \$/kWh. 22

Figure 2.7: Cumulative installed capacity of hydro (top two rows) and solar (bottom two rows) as a function of the damage estimation method, damage probabilities (high or medium), and the number of time periods within the model time horizon that include conflict-related damage. Solar and hydro deployment are represented at different curtailment values, given in parentheses within the legend..... 23

Figure 2.8: Measures of economic cost associated with future conflict uncertainty, including (a) the expected value of perfect information (EVPI), (b) value of the stochastic solution (VSS), and (c) the expected cost of ignoring conflict (ECIC). Methods producing higher damage estimates produce higher values for these metrics. 26

Figure 3.1: Methodology for obtaining robust alternate policies for GHG emission mitigation in the absence of federal climate policy..... 39

Figure 3.2: Probability that number of uncertain variables assuming worst case value exceeds Γ . N represents total number of uncertain parameters in a constraint. For example, for an optimization problem with 10 uncertain parameters in a constraint, if we set budget of uncertainty (Γ) = 4, then the probability that more than 4 uncertain variables assume their worst-case value is 17.13%. 45

Figure 3.3: Uncertainty characterization: six criteria are used to select uncertain parameter values in the model. Each criterion corresponds to a different method for investigating the uncertainty of the parameter and the correlation coefficient.	53
Figure 3.4: Effect of the correlation in coal prices. The red line shows the worst case values from the AEO 2019 while the green line shows the reference case values.	57
Figure 3.5: Percent change in objective function as a function of budget of uncertainty. Abbreviations: Worst Case (WC), Nominal (NM). ‘Naïve WC cost’ represents the cost of the naïve solution as the budget of uncertainty increases; ‘Robust WC cost’ represents the same for the robust solution; ‘Robust NM cost’ represents cost of robust solution if all uncertain parameters assume their nominal value.	61
Figure 3.6: Distribution of system cost for naïve and robust solution under uncertain parameter realizations.	62
Figure 3.7: Activity of technologies in different sectors as a function of the budget of uncertainty and time period: (a) electricity generation, (b) commercial space cooling and heating, (c) residential space cooling and space heating, and (d) transportation. The ‘WC’ stacked bars represent the technology activity in a given sector and time period under the worst-case outcome, and ‘naïve’ represents the reference scenario where uncertainty is ignored.	63
Figure 3.8: Sensitivity of the sectors as a function of budget of uncertainty. The importance of a category increases as we move from bottom to top and robustness of a solution increases as we move from left to right. Abbreviations: Synthetic (Syn.); Photovoltaic (PV); Thermal (TH).....	66
Figure 4.1: Economic flow and process flow for energy efficiency model.....	77
Figure 4.2: Supply-demand equilibrium. Note that the supply curve of energy services is a function of supply curve for electricity and energy efficiency. Similarly, the demand curve of energy services is a function of demand curve for electricity and energy efficiency. The dashed line show price P_t and quantity ES_t at equilibrium for a given time period.	78
Figure 4.3: Visualization of policy scenarios along with economic and process flow in energy efficiency model.	86
Figure 4.4: (a) For a given price of electricity, quantity demanded of electricity decreases with increasing efficiency crediting (b) Quantity demanded for energy efficiency increases with increasing efficiency crediting and (c) Quantity demanded for energy service increases with increasing efficiency crediting (d) Price of energy services decreases with increasing efficiency crediting.....	88
Figure 4.5: Welfare gain as a function of the efficiency credit. The gain is expressed as the fraction of welfare recovered through the energy efficiency policy compared with respect to welfare gain with a Pigouvian carbon tax set at 40 \$/ton of CO ₂	89
Figure 4.6: For a given efficiency credit a point of a variable represents the percentage quantity of a variable as compared to the quantity of a variable under carbon tax policy	90
Figure 4.8: Effect of uncertain model parameters on the welfare recovered through energy efficiency credit policy as compared with the Pigouvian tax policy. Uncertain parameters are (a) Energy efficiency cost (b) Substitutability between electricity and energy efficiency (c) Own price elasticity of energy service demand (d) Carbon tax	91

Appendix Figure 2.1: Electricity demand forecast for South Sudan, drawn from AfDB (2013).	122
Appendix Figure 3.1: reference for capacity credit for solar PV as a function of renewable share.....	129
Appendix Figure 3.2: reference for capacity credit of wind as a function of wind share and capacity factor	130
Appendix Figure 3.3: Processes and commodities defined for E10 production. E85 has a similar chain, except T_BLND_ETHGAS_E10 is replaced by T_BLND_ETHGAS_E85.....	134
Appendix Figure 3.4: Structure of bio jet fuel and biodiesel production in Temoa.....	136
Appendix Figure 3.5: Structure of ethanol production in Temoa	139
Appendix Figure 3.6: Conceptual framework of industrial sector.....	144
Appendix Figure 3.7: Energy use in U.S. manufacturing (MECS, 2014).....	145
Appendix Figure 3.8: Industrial subsector and End Uses relevant to electrification scenarios. (Jadun et al., 2017).....	146
Appendix Figure 3.9: Share of energy consumption by end-uses which are included in 'other' end uses	147
Appendix Figure 3.10: Historical renewable energy consumption for industrial sector.....	148
Appendix Figure 3.11: Basic pathways for conversion of renewable electricity to gaseous and liquid fuels by Power-to-X pursued in this report	153
Appendix Figure 3.12: Power to Gas representation in US database.....	154
Appendix Figure 3.13: Implementation of the processes for Hydrogen generation in Temoa (textured commodities/ technologies already existing in Temoa, fully colored commodities/technologies new to Temoa)	157
Appendix Figure 3.14: Implementation of the processes for blending Hydrogen in natural gas in Temoa (textured commodities/ technologies already existing in Temoa, fully colored commodities/technologies new to Temoa).....	166
Appendix Figure 3.15: Implementation of the processes for generating SNG and methanol in Temoa (textured commodities/ technologies already existing in Temoa, fully colored commodities/technologies new to Temoa).....	167
Appendix Figure 3.16: CO ₂ input for SNG production.....	171
Appendix Figure 4.1: Graphical representation of a modified version of a test case called 'utopia' (developed for MARKAL). Energy technology is represented by green arrows, flow out by red arrows. Energy sources are shown on the left edge of the diagram (i.e., the import technologies), and on the right edge are the end-use electricity demand. This image was dynamically generated with an open source graphing utility called Graphviz	183
Appendix Figure 4.2: Welfare gain with respect to welfare gain with carbon tax = 40 \$/tonCO ₂	185

Appendix Figure 4.3: Capacity expansion in GW for 40 \$/ton Carbon tax (CT), no efficiency credit (EC0), 10% efficiency credit (EC10) and 20% efficiency credit (EC20)186

Appendix Figure 4.4: For a given efficiency credit a point of a variable represents the percentage quantity of a variable as compared to the quantity of a variable under emission tax policy186

Chapter 1 Introduction

“In the real world applications of linear programming one cannot ignore the possibility that a small uncertainty in the data can make the usual optimal solution completely meaningless from a practical viewpoint.” — Ben-Tal and Nemirovski (2000)

1 The Utility of Energy System Optimization Models (ESOMs)

The global community faces a daunting transition to a clean, affordable, and reliable energy system. The threat of climate change and the rapid pace of technological change are transforming the global energy system. Because energy technologies – ranging from resource extraction technologies to power plants to heating and cooling systems – are long-lived and capital intensive, it is critical to plan those investments while considering uncertainty that could affect future system performance.

Energy system optimization models (ESOMs) are developed and utilized to explore the future decision landscape and deliver insights that can inform policy (DeCarolis et al., 2017). ESOMs are described algebraically as a network of linked processes that convert raw energy commodities such as coal, oil, and biomass into end-use demands such as lighting, transport, water heating. Each process is defined by a set of engineering, economic, and environmental characteristics associated with converting an energy commodity from one form to another. The engineering-economic input parameters that characterize each technology include capital cost, fixed and variable operations and maintenance cost, conversion efficiency, and capacity factor. Processes are linked together in a network via model constraints representing the allowable flow of energy commodities. ESOMs are typically formulated as linear programming models that perform capacity expansion in which technology capacity is installed and utilized to meet end-use demands. The objective of ESOMs is to meet a set of exogenously specified end-use demands at the minimum net present cost of energy supply by utilizing energy processes and commodities over a set time horizon. ESOMs simultaneously make technology investment decisions and operating decisions while maintaining energy balance between primary energy resources, secondary fuels, final energy consumption and end-use energy services.

2 Motivation

ESOM-based analysis often includes conventional scenario analysis to investigate different technical, economic, and policy assumptions in energy system capacity expansion plans. Given the complexity of real-world energy systems and long time horizons for planning, it is critical to apply ESOMs using

techniques that address future uncertainty. However, inherent structural and parametric uncertainties in energy systems are often underemphasized or overlooked in these models. Structural uncertainty arises from the difficulty in precisely modeling real world dynamics with a limited set of mathematical equations. Parametric uncertainty arises from the imprecise specification of input parameter values. Model-based analysis that ignores future uncertainty has a strong potential to mislead decision makers and planners, who deal with critical issues such as Green House Gas (GHG) emission mitigation and maintaining a reliable energy supply. ESOMs such as MARKAL, MESSAGE and TIMES have been used to address some of the uncertainty in planning of energy systems (Kanudia, 1998; Messner, 1996; Loulou, 2012). Yue et al. (2018) and DeCarolis (2016) both note that even though uncertainty in energy models is a widely accepted issue, the number of studies that formally apply uncertainty analysis techniques is still limited. Moreover, they emphasize the need to explore new techniques that consider broader range of parametric, political and policy uncertainty in ESOMs.

3 Objective

The goal of this thesis is to address two key challenges in energy system modeling. First, decision makers must act before uncertainty is resolved, and thus need planning strategies that explicitly consider future uncertainty. This thesis demonstrates how planning strategies can be produced with both stochastic linear programming (SLP) and robust optimization (RO). Second, ESOMs do a poor job capturing the uptake of energy technologies on the consumer side, often assuming that consumers simply select the most energy efficient technologies. This thesis presents a new way to model the uptake of energy efficiency, which is more consistent with microeconomic theory. All the model-based analysis presented here utilizes Tools for Energy Optimization and Analysis (Temoa), an open source energy system model developed at NC State (Hunter et al., 2013). The model code and data developed under this thesis is archived on GitHub (TemoaProject, 2019), allowing third parties to replicate the analysis presented in this thesis.

The first model application explicitly considers the effects of conflict on electrification strategies in South Sudan. Such an approach is rare; for example, EAPP (2011) examined future electricity development in South Sudan by employing a least-cost capacity planning model. They concluded that South Sudan should focus on developing a series of large-scale hydroelectric projects. However, the least-cost capacity planning model applied in this study did not consider the role of conflict. Ignoring such risk can lead to inefficient outcomes in capacity expansion planning. To address this planning challenge, we build an SLP model that explicitly considers the possibility of damage to electricity infrastructure as a result of ongoing conflict. SLP works well in the South Sudan context where the scope is limited to the electric sector and only one uncertain parameter is considered. The resultant hedging strategy suggested by the SLP can inform future

electricity system planning efforts. We employ a stochastic energy system optimization model that explicitly considers the possibility of armed conflict leading to electric power generator damage. Given the deep uncertainty surrounding conflict and its effect on power system planning, planning strategies are generated under varying input assumptions. While this analysis focuses on South Sudan, the analytical framework can be applied to other conflict-prone countries.

The second application examines the future development of the US energy system under a deep decarbonization scenario. The objective is to develop a planning strategy for technology deployment that considers uncertainty in future fuel prices and technology investment costs. In this case, the full energy system is considered with potentially thousands of uncertain input parameters. Under these circumstances, SLP is an inappropriate method because it suffers from the curse of dimensionality (Shapiro et al., 2009). Instead, RO is applied. RO generates series of solutions that are progressively less sensitive to the realization of input parameter uncertainty, thus yielding energy development pathways that are robust to future cost uncertainty. Previous literature has demonstrated the usefulness of robust optimization (RO) for analyzing energy systems (Babonneau, F. et al., 2009; Babonneau et al., 2012, Lorne and Tchong-Ming, 2012, Labriet et al., 2015, Morel et al., 2019). This chapter extends the application of RO in ESOMs by considering correlation between uncertain parameters. A detailed methodology is provided to characterize the uncertainty in the energy system. We consider the uncertainty in fuel prices and technology investment costs by assessing the impact of uncertainty on energy planning decisions for the United States.

The third application explores the combination of structural and parametric uncertainty in ESOMs. While common practice in ESOMs, the specification of exogenously specified end-use demands restrict the feedback from consumers side, leading to a structural uncertainty. We address this structural uncertainty by revising the model to represent the consumer's choice between electricity and energy efficiency in a manner that is consistent with microeconomic theory. Advocates of ambitious climate policies often support simultaneously imposing a price on carbon and alternative policies, such as crediting energy efficiency (Baranzini, et al. 2015). Efficiency crediting policy provides an incentive to utilize energy-efficient technologies. The parametric uncertainties in the revised model arise from the cost and productivity of energy efficiency, elasticity of energy services, and the marginal external damage cost. Being able to more accurately model policy interactions can yield valuable insights that inform the development of efficient policy mechanisms to reduce emissions. In traditional least-cost, bottom-up ESOMs, exogeneous end-use energy service demand (e.g., cooking and lighting) are satisfied by a range of technologies with varying costs and efficiencies at minimum cost. However, such a simplistic approach ignores the role of consumers, and their willingness to tradeoff energy efficiency and electricity supply in order to meet end-use energy

service demands. In the fourth chapter, a revised model is constructed where, on the production side, electric utilities have an option of investing in electricity generation and investing in energy efficiency as a way to satisfy future demands. While on the demand side, consumers meet their demand for energy services by purchasing electricity and energy efficiency from a supplier. A wide range of consumer behavior including substitutability between electricity and energy efficiency and productivity of energy efficiency can be analyzed with this model. Moreover, we develop a hypothetical test case to analyze welfare gain from efficiency crediting policy as compared to welfare gain from carbon tax policy.

The thesis is organized as follows. Chapters 2 and 3 quantify parametric uncertainty and incorporate the uncertainty into the model formulation using stochastic optimization and robust optimization, respectively. Chapters 4 present a new model formulation that incorporates energy efficiency into the satisfaction of end-use demand in a way that is consistent with microeconomic theory. Chapter 5 provides a synthesis of insights and draws high-level conclusions across the various chapters.

Chapter 2 Building Conflict Uncertainty into Electricity Planning: A South Sudan Case Study

1 Introduction

Electricity supply security is critically important, especially in fragile and conflict-affected states where resumption of electricity services can restore confidence in the government and society, strengthen security, and revive the economy (World Bank, 2013). Addressing fragility, conflict, and violence (FCV) is required to end poverty and promote shared prosperity (World Bank, 2015). While the provision of affordable and reliable electricity supply can promote economic development and help countries exit the conflict trap (Collier, 2003), electric power systems are also vulnerable to conflict conditions. Attackers in many conflict environments have targeted electricity transmission lines and power generation plants, which can lead to long outages and the need for system restoration (Zerriffi, H. et. al., 2002).

Acknowledging that each conflict has its own unique dynamics (Goldstone, 2008), recommendations should be based on a thorough examination of specific conflict situations. In this chapter, we explore potential electricity development pathways in South Sudan. South Sudan has been ranked as the most fragile country in the world for the last several years (Fund for Peace, 2017), and it is also one of the least developed countries in the world. There are approximately 250 km of paved roads and less than 30 MW of installed electric generating capacity serving 13 million people in a landlocked area slightly smaller than the US state of Texas (CIA, 2018). Soon after South Sudan gained its independence in 2011, the government started to attract investment funding for hydropower installations (IEA, 2014). Two years later, in 2013, a civil war erupted, and it is still ongoing despite a peace agreement signed in 2015 (The Guardian, 2016). To the best of our understanding, most of the investments in the electricity infrastructure expansion have been suspended. Despite having an abundance of natural resources, conflict in South Sudan makes the country prone to economic collapse (World Bank, 2016).

Electrification strategies under FCV conditions should explicitly consider the risk of conflict in the decision-making process. However, this is often not the case. For example, EAPP (2011) examined future electricity development by employing a conventional least-cost capacity planning model and concluded that South Sudan should focus on developing a series of large-scale hydroelectric dams along the White Nile. Political issues were considered, but only exogenously to the optimization model. Such a focus on large scale infrastructure projects with long construction times produces inefficient outcomes. These

hydroelectric projects never broke ground, and instead hundreds of millions of dollars have been spent on generators and diesel fuel (Mozersky and Kammen, 2018). While incorporating conflict risk in energy system planning is challenging and subject to considerable uncertainty, it should not be ignored (Bazilian and Chattopadhyay, 2016).

This chapter focuses on developing planning strategies for the South Sudan electric power system that explicitly consider conflict uncertainty. We model the South Sudan system using an open source energy system optimization model and incorporate conflict by performing multi-stage stochastic optimization (Birge and Louveaux, 2011; Pereira and Pinto, 1991; de Queiroz, 2016). Optimization is performed over a scenario tree that represents different conflict-related outcomes in the future, and the resultant stochastic solution suggests a near-term planning strategy. Given the paucity of data and large future uncertainties, we perform sensitivity analysis to identify critical assumptions and develop insights that explicitly consider conflict-related uncertainty.

While the application of stochastic optimization yields a planning strategy, this analysis should nonetheless be viewed as an exercise to explore the decision space when conflict is explicitly considered. We are not able to capture all of the real-world conflict dynamics and potential power system failure modes. In addition, we emphasize that models alone cannot provide a solution in such complex decision landscapes but can yield insight that informs decision making. This chapter is intended to further the discussion between modelers and the decision makers, planners, and consultants who develop electrification strategies in FCV countries.

The results presented here suggest promise for further application. Much of the analysis focused on energy development in Africa has been focused on universal access and climate change mitigation through renewables deployment (Lucas et. al., 2017; Africa Progress Report, 2015; AREI, 2017; Wu et. al., 2017; Deichmann et. al., 2011). Considering conflict-related uncertainty can add another dimension to future analysis, ensuring that energy supply is also resilient in the face of conflict, fragility, and violence.

2 Methods

Key aspects of the modeling effort are described in this section. We begin by describing Tools for Energy Model Optimization and Analysis (Temoa), the open source energy system optimization model and the South Sudan input dataset used to conduct this work. Next, we describe Method of Morris, a sensitivity analysis technique that allows us to identify the input parameters with the largest effect on total system cost. Then we describe the stochastic model formulation, the method by which generator damage is estimated,

and the metrics used to assess the cost of conflict uncertainty. The appendix provides additional detail on technology specifications, demand projection, and the estimation of damages.

2.1 Tools for Energy Model Optimization and Analysis (Temoa)

Tools for Energy Model Optimization and Analysis (Temoa) is an open source, Python-based framework to conduct energy systems analysis. The core component of Temoa is a bottom-up, technology rich energy system optimization model (ESOM). The Temoa model formulation is similar to the MARKAL/TIMES model generators (Fishbone and Abilock, 1981), MESSAGE (Messner and Strubegger, 1995), and OSeMOSYS (Howells et al., 2011). Technologies are represented by a set of engineering-economic parameters and linked together in an energy system network through a user-specified series of commodity flows. The model employs linear optimization to minimize the system-wide cost of energy supply over the user-defined time horizon by optimizing the installed capacity and utilization of energy technologies. Several constraints ensure appropriate system performance, including energy supply sufficient to meet demand, energy balance at both the process and system-wide levels, and operating limits on baseload plants. The complete algebraic formulation of Temoa is published (Hunter et. al., 2013), and the model source code is publicly available through a GitHub repository (TemoaProject, 2018).

2.2 Input Data

A Temoa-compatible dataset to represent South Sudan was created for this analysis. The model time horizon extends from 2017 to 2037, with five-year time periods defined at 2017, 2022, 2027, and 2032. When performing stochastic optimization, conflict uncertainty is resolved in the latter three time stages. The climate of South Sudan is tropical and has a wet and dry season. Most rainfall occurs from May to October while December, January, and February are the driest months. To capture diurnal variation in electricity production from solar Photovoltaic (PV), each day is split into day and night, and to represent the tropical climate of South Sudan, each year is split in two seasons: wet (May to October) and dry (November to April). For simplicity, we assume that demand is equally divided across all the time slices: wet-day, wet-night, dry-day, and dry-night.

South Sudan has very little existing infrastructure, including 30 MW of electricity generation capacity mainly from portable diesel generators (World Bank, 2013). Based on a planning report by Hatch (2014), we model a largely hypothetical electricity grid connecting 5 hydro power plants and 11 thermal power plants to meet electricity demand at 13 different demand centers located across 10 constitutionally established states. Electricity transmission links between demand centers and between demand centers and the proposed hydro and thermal plants are modeled explicitly, as shown in Figure 2.1.

As an alternative to the proposed hydro and thermal plants, we also include distributed solar photovoltaics (PV), which can be built at each demand point as an alternative source of electricity generation (Figure 2.1) but produce no electricity at night. An advantage of distributed solar PV is its modularity; it can be deployed on a small scale at critical locations and built up over time. For example, Mozersky and Kammen (2018) suggest that solar PV could initially be funded by international donor governments and used to generate electricity on protected compounds associated with non-governmental organizations, UN agencies and peacekeeping bases, and protection of civilians (POC) camps. We omit consideration of centralized solar PV facilities, as they suffer from the same vulnerabilities as the centralized hydro and thermal plants. In this analysis, we also omit consideration of storage coupled to the solar PV systems. While storage is a feasible option that could allow solar generated electricity to meet demand at night, modeling it properly requires a higher temporal resolution of electricity supply and demand, ideally hourly, in order to capture the individual store and dispatch decisions. Such a representation is beyond the scope of this study.

Generator locations are based on Hatch (2014), and Appendix Table 2.1 maps each existing and proposed generator to South Sudan’s ten states.

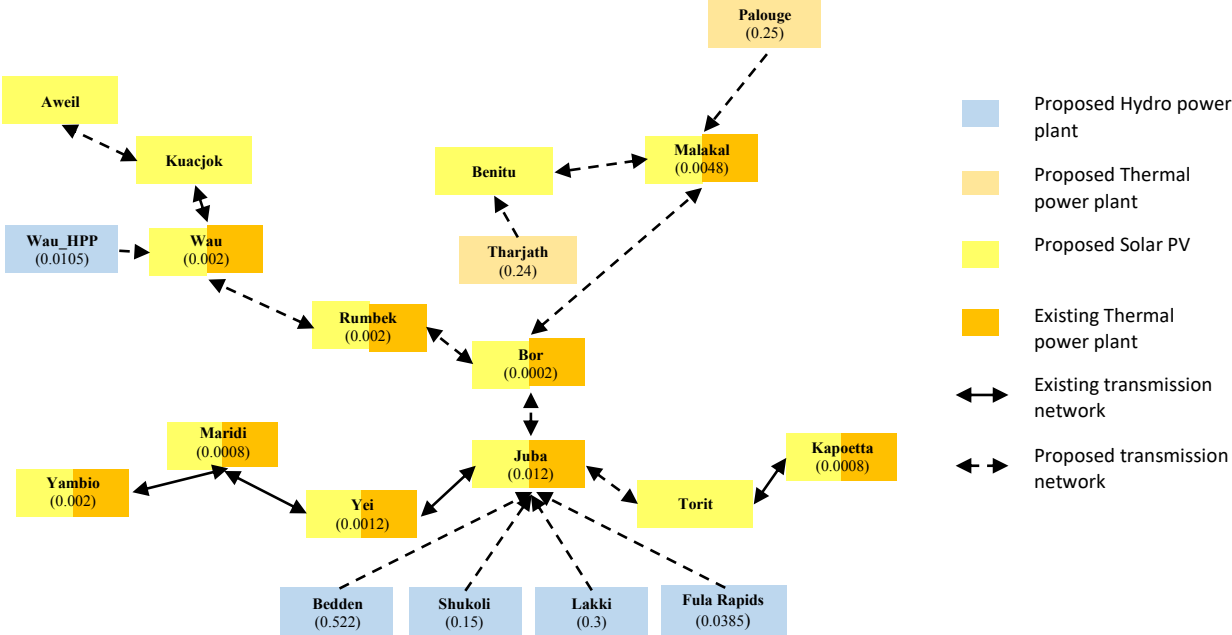


Figure 2.1: Layout of the modeled South Sudan system. Proposed locations (see Appendix Table 2.2) for new hydro and thermal capacity are based on Hatch (2014). Solar PV can be constructed within each of the 13 demand centers. Existing and proposed capacities are denoted in GW.

For simplicity, we assume that the investment cost, fixed cost, variable cost, capacity factor and efficiency of a technology remain unchanged over the model time horizon. Cost and performance associated with hydro power plants are taken from Hatch (2014). EIA (2013) is used to estimate solar PV cost, and the location-specific solar PV capacity factors are taken from IRENA (2018). Both the investment costs associated with proposed thermal power plants and the efficiency of existing thermal power plants are taken from Hatch (2014). The rest of the cost and performance coefficients are taken from Trüby, J. (2014) due to the unavailability of region-specific data. All of the thermal power plants are assumed to run on diesel. The most recent available estimate on the diesel price is \$1.98/liter (World Bank, 2017). Operations and maintenance costs for the transmission lines are omitted, as we assume they are small relative to their investment cost. Investments in new hydro and thermal capacity (Figure 2.1) also require dedicated transmission lines. The model ensures that the transmission lines are built along with the power plants. No new investment in thermal or hydro capacity other than the proposed capacity denoted in Figure 2.1 is permitted. Because hydro capacity requires a significant lead time, we model a 5-year, 1-period delay between hydro capacity construction and when it can generate electricity. All future costs associated with technology deployment, operations, and incurred damage are discounted to the base year (2017) using a 3% global discount rate. For simplicity, all generating technologies are assumed to have a 30-year technical lifetime.

Electricity demand is an exogenous input taken from a comprehensive infrastructure action plan produced by the African Development Bank Group in 2013 (AfDB, 2013). The report includes a load forecast for the ten former South Sudan state capitals as well as for three additional important population centers. The demand growth in the short-term is estimated based on the historical demand growth trends of the South Sudan Electricity Corporation (SSEC). The demand forecast for the medium- to long-term is estimated based on projected consumption by customer and tariff categories, including domestic/household, commercial, and government. The potential demand in Juba and Malakal is based on field surveys undertaken by the SSEC. Commercial demand is assumed to grow at 10% per year while the government demand is projected to grow at 6% per year. Estimated demand by region as given in Hatch (2014) is provided in the Appendix.

Conflict will likely raise the electricity price, which in turn will suppress projected demand growth. Estimating demand elasticity in a country such as South Sudan is extremely difficult given the paucity of data, but we can assume that most of the population will be unwilling to tolerate high electricity prices. For simplicity, we assume that when electricity prices exceed a threshold value, consumers will choose to curtail their demand. We refer to this threshold as the curtailment cost. We assume that curtailment cost varies

from 0.1 to 0.8 \$/kWh, which encapsulates the range estimated by Oseni and Pollitt (2013). In addition, Steinbuks and Foster (2010) use the marginal cost method of revealed preference approach and estimate the outage cost in sub-Saharan Africa between 0.13 – 0.76 \$/kWh (2007 prices). Throughout our analysis, we vary the curtailment cost, which serves as a sensitivity on the level of consumer demand met by electricity supply. The required amount of electricity supply decreases as the prescribed curtailment cost decreases.

2.3 Method of Morris

Before conducting the stochastic optimization, we apply the Method of Morris (Morris, 1991) in order to identify the input parameters that produce the largest change on total system cost. The results are used to prioritize data collection needs and inform the stochastic program model formulation (Francesca, 2007). Unlike other sensitivity methods (Saltelli et al., 2004, 2005; Cacuci and Ionesco-Bujor, 2004, Pappenberger et al., 2006), the Method of Morris falls under the simplest class of one-factor-at-a-time (OAT) screening techniques. It assumes l levels per input factor and generates a set of trajectories through the input space. As such, the Method of Morris generates a grid of uncertain model input parameters, $x_i, i = 1, \dots, k$, where the range $[x_i^-, x_i^+]$ of each uncertain input parameter i is split into l intervals of equal length. Each trajectory starts at different realizations of input parameters chosen at random and are built by successively selecting one of the inputs randomly and moving it to an adjacent level. These trajectories are used to estimate the mean and the standard deviation of each input parameter on total system cost. A high estimated mean indicates that the input parameter is important; a high estimated standard deviation indicates important interactions between that input parameter and other inputs.

In this analysis, we consider curtailment cost, electricity demand as well as generator capacity factor, fixed operations and maintenance costs, and investment costs as uncertain parameters. While the latter three parameters vary by generator type, they were grouped together in Method of Morris such that the same proportional perturbation to each parameter is made across each of the three generator technologies. For example, in a given Method of Morris iteration, a 3% perturbation to capacity factor is applied to solar PV, thermal, and hydro plants uniformly. This approach reduces the number of required trajectories and therefore the computational burden associated with the Method of Morris. Given five model inputs, we have l^5 points in the grid, which we call the ‘experimental space’ \mathcal{F} . From \mathcal{F} , r points are drawn at random, and the model is evaluated to obtain its objective function value at each of the r points. For each model input value defined as $x_i, i = 1, \dots, k$, the elementary effect of i^{th} input factor on the objective function $F(x)$ is defined as

$$d_i(x) = \left(\frac{F(x_1, \dots, x_{i-1}, x_i + \Delta, \dots, x) - F(x)}{\Delta} \right) \quad (1)$$

where, Δ is a value such that the point $(x_1, \dots, x_{i-1}, x_i + \Delta, \dots, x_k)$ remains in the experimental space \mathcal{F} for all $i, i = 1, \dots, k$. Further, μ_i^* is the estimated mean of the distribution of elementary effects, $G_i: \mu_i^* = |d_i(x)| \sim G_i$ (Campolongo et al., 2007). It addresses the screening problem by identifying the subset of the model parameters that are not influential and hence can be fixed to any value within their ranges of uncertainty without significantly affecting the model outcome of interest. To conduct this part of the analysis, we utilized SALib (Herman and Usher, 2017), an open source Python library, which includes a complete implementation of the Method of Morris.

2.4 Stochastic Problem Formulation

Planners in countries such as South Sudan must make decisions in the face of deep uncertainty regarding future conflict. Energy system models often ignore future uncertainty by assuming perfect foresight across the entire model time horizon. In this case, individual model scenarios assume the future is known with certainty prior to the model run. In the case of conflict modeling, conventional scenario analysis would mean assuming a specific conflict scenario for a given model run. While such an approach using conventional scenario analysis can yield insight, it does not lead to a single unified strategy in the face of future uncertainty (Kann and Weyant, 2000). A key challenge for planners in FCV countries is to develop a near-term investment strategy that accounts for future conflict uncertainty.

To address this challenge, we frame the problem as a multi-stage stochastic optimization, which allows us to directly account for conflict uncertainty by incorporating it within the model formulation. Performing stochastic optimization requires us to consider future outcomes, assign probabilities to those outcomes, and quantify the effects of those outcomes. This information is organized in a scenario tree (Figure 2.2), which describes the set of possible outcomes that may unfold over time¹. Optimization is performed simultaneously over the entire scenario tree. Because the scenario tree accounts for different probability-weighted outcomes, the resultant model solution provides a near-term planning strategy that account for future conflict-related uncertainty.

Conflict can result in many forms of damage within the power system, including damage to generators, transmission and distribution lines, fuel supply infrastructure and logistics, and maintenance. For simplicity,

¹ For a formal mathematical treatment of stochastic optimization, see [Dantzig, \(2010\)](#), [Shapiro et al. \(2009\)](#), and [Birge and Louveaux \(2011\)](#).

we focus on potential damage to the generators themselves. Thus, we design a scenario tree that considers a binary outcome at each time stage: either generator damage occurs, or it does not. Subjective probabilities denoting the probability of damage to generators during conflict are assigned to each branch in the scenario tree. Whether armed conflict leads to generator damage is deeply uncertain; and thus, we create the scenario tree around this factor in order to explicitly test the effect of different damage probabilities on the deployment of new capacity. We assume that damage to generators results in increased fixed operations and maintenance (O&M) cost and a decrease in capacity factor for 5 years following the time of damage. We begin by describing the scenario tree structure, followed by the damage estimation method.

2.4.1 Scenario Tree Structure

The stochastic programming model includes three uncertain time stages and two branches (realizations) per node within the event tree. The two branches emanating from each node represent the possibility that generator damage either occurs with probability $Pr(D)$ or does not occur with probability $(1 - Pr(D))$ in the next time stage. To test the system response to uncertain damage probabilities, we assume two sets of nodal probabilities: high ($Pr(D) = 0.9$) and medium ($Pr(D) = 0.5$), as shown in Table 2.1. We also tested a low nodal ($Pr(D) = 0.1$) probability of damage but found results similar to the base case, and therefore omitted them in the results section. Considering conflict-related damage with a binary outcome over three uncertain time stages leads the scenario tree shown in Figure 2.2.

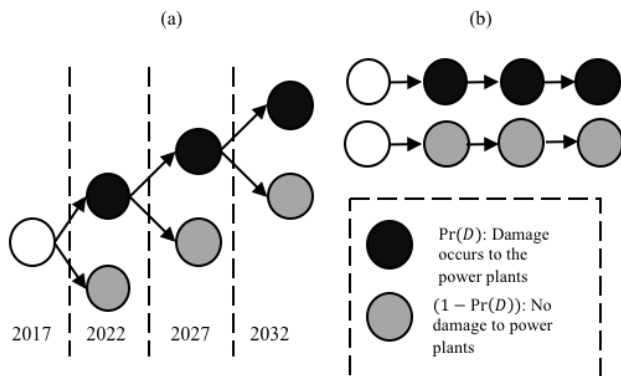


Figure 2.2: (a) Scenario tree representation with three uncertain stages, where each region of South Sudan has its own damage intensity and each demand center within a given region experiences the same damage intensity. (b) Given this tree structure, there are 8 potentially different pathways through the scenario tree representing different combinations of damage versus no damage to generators at each of the three uncertain time stages. Two of the 8 pathways are shown.

Table 0.1: Node probabilities of a scenario tree.

Damage probability	High	Medium
Probability of generator damage: $Pr(D)$	0.90	0.50
Probability of no generator damage: $1 - Pr(D)$	0.10	0.50

2.4.2 Damage Estimation

With the scenario tree shown in Figure 2.2, we must quantify the damage on the branches where conflict-related damage occurs. The resultant damage quantification is embedded within the scenario tree used to perform the stochastic optimization and affects the investment decisions in different capacity types. In this analysis, we assume that conflict-related damage takes two forms: an increase in fixed operations and maintenance (O&M) cost, and a decrease in capacity factor. The increased cost and degraded capacity factor are both incurred for one model time period following the occurrence of damage. This section focuses on the damage estimation method; the numerical values are provided in the appendix. Notation used to estimate damage includes the following:

$Pr(C)$	Probability of conflict in South Sudan
RCR	Regional conflict rate, which represents the percentage of conflict occurring in a specific region given that conflict occurs in South Sudan
FOM	Fixed operations and maintenance cost (\$/kW-yr)
EFOM	Estimated increase in FOM based on the investment cost, RCR , $Pr(C)$, and DR
DR	Damage rate representing the rate of FOM increase
CF	Capacity factor
ECF	Estimated capacity factor following damage; based on CF, RCR , $Pr(C)$, and DCF
DCF	Percent reduction in CF following damage

Because conflict is likely to persist in South Sudan over the next two decades, we set the conflict probability, $Pr(C)$, at 0.9 in all scenarios. The regional conflict rate (RCR) is estimated from Raleigh et al. (2010), which has monitored the conflicts occurring in South Sudan since its independence in 2011. South Sudan is constitutionally divided into 10 regions. We assume that conflict occurs in each of these regions with frequency values based on conflicts in 2016 (see Appendix Table 2.3 for RCR values). Generator damage, represented by an increase in FOM (denoted EFOM) and decrease in CF (denoted ECF), varies by generator type and the location of the generator.

Following Mozersky and Kammen (2018), we make the critical assumption that solar photovoltaics (PV) will be more resilient to conflict-related damage, and thus the changes to solar-related fixed O&M and capacity factor are less severe compared to hydro and thermal plants. In this analysis, the damage rate (DR) represents the increase in the fixed operations and maintenance cost (FOM) equivalent to the annual payment on investment cost. For thermal and hydro power plants, the DR is calculated using 100% of the annual payment on capital, while for solar PV, the DR is calculated using 10% of the annual payment on capital. For example, we assume an investment cost of 3350 \$/kW for solar photovoltaics. Over a 30-year lifetime, the annual payment on capital is 171 \$/kW-yr using a 3% discount rate. The damage is assumed to be 10% of this cost, or 17.1 \$/kW-yr. Since the solar fixed O&M is 25 \$/kW-yr (see Appendix Table 2.3), the damage rate is calculated as $(17.1 + 25) / 25$ \$/kW-yr, which equals 1.68. Thus damage to solar increases its fixed O&M by 68%. (See Appendix for detailed calculations of DR.)

We do not have data to derive an empirical value for the DR, and thus the assumed values here represent an informed judgment on our part. The difference in DR between solar versus hydro and thermal plants is intended to reflect the modularity and smaller scale of the solar installations. For example, 100 installations of 10 kW solar are likely to incur less damage than a single 1000 kW installation of thermal capacity.

While stochastic optimization explicitly addresses conflict uncertainty and how it could shape power system development, additional exogenous uncertainties are considered. First, as mentioned above, the subjective probability of conflict-related damage within a given model time period was tested at high (90%) and medium (50%) levels (Table 2.1). Second, given the high sensitivity to curtailment cost as illustrated in Figure 2.1, the stochastic optimization is repeated at different curtailment cost values. Third, we test three different methods that translate the presence of conflict into power plant damage. The first damage estimation method calculates damage based on historical tallies of armed conflict by region within South Sudan (Raleigh et al., 2010). The second method is similar to the first, but the damage estimates are scaled up such that maximum damage is incurred by at least one generator of each type. The third method ignores differences in regional conflict frequencies and maximizes damage estimates assigned to each individual generator. The three different damage estimation methods are described below.

Regional Damage

In this method, generator damage is proportional to past conflict frequency by region, such that power plants in more conflict-prone regions will have higher damage costs. In this case, we increase the base FOM by the product of FOM, the maximum damage rate, DR, the regional conflict rate, RCR, and the probability of conflict, $Pr(C)$. We use a similar formula to evaluate the reduced capacity factor, ECF. Most of the

proposed hydro capacity is in Eastern and Central Equatoria, where a higher rate of conflict was observed in 2016. As a result, the model prefers to build relatively expensive distributed solar PV over the cheap hydro power to avoid the damage cost.

$$EFOM = FOM \times (1 + DR \times RCR \times Pr(C)) \quad (2)$$

$$ECF = CF \times (1 - (1 - DCF) \times RCR \times Pr(C)) \quad (3)$$

Intensified Regional Damage

In this method, a scaling factor α is added to Equation (2) and a scaling factor β is added to Equation (3). The value of α is calibrated such that the annual damage cost incurred by at least one hydro and one thermal unit over a single model time period is equivalent to the annual payment on its capital cost. Likewise, the α value for solar is calibrated such that the annual damage cost associated with at least one solar installation is equivalent to 10% of the annual payment on its capital cost over one model time period. Similarly, the value of β is calculated so that capacity factor of the same thermal and hydro power plants is decreased by 90% while the capacity factor of the same solar PV units is decreased by 10%. We note that the damage cost varies across individual generators because the RCR varies by region and the DR varies by plant type. This method leads to higher damage costs compared to the “regional damage method” above.

$$EFOM = FOM \times (1 + \alpha \times DR \times RCR \times Pr(C)) \quad (4)$$

$$ECF = CF \times (1 - \beta \times (1 - DCF) \times RCR \times Pr(C)) \quad (5)$$

Max Damage

This method produces the highest damage estimates. In this case, the RCR and $Pr(C)$ terms are removed. For all hydro and thermal plants, the annual increase in FOM for each year in one time period is equal to the annual payment on its capital, and for all solar units, the annual increase in FOM is equal to 10% of the annual payment on its capital. Similarly, for all years in a single model time period, the capacity factor of all the thermal and hydro power plants is decreased by 90%, and all solar PV capacity factors are decreased by 10%.

$$EFOM = FOM \times DR \quad (6)$$

$$ECF = CF \times (1 - DCF) \quad (7)$$

2.5 Metrics to assess value: EVPI, VSS and ECIC

Decision makers should be able to assess the economic value of plans made using stochastic programs. In this chapter, we use the expected value of perfect information (EVPI) (Birge and Louveaux, 2011) and the value of the stochastic solution (VSS) (Birge, 1982) to characterize the economic impact of conflict damage on power systems and the economic value of the hedging strategy, respectively. In addition, we introduce a third metric called the ‘expected cost of ignoring conflict’ (ECIC) that estimates the savings associated with pursuing the stochastic programming solution rather than a least cost (naive) solution that ignores conflict completely. The resultant values associated with all three metrics vary depending on the ESOM parameterization and the scenario tree representation used in the stochastic optimization.

2.5.1 Expected Value of Perfect Information (EVPI)

The EVPI represents the amount of money that decision makers should be willing to pay in order to eliminate future uncertainty. Even when the EVPI is low, naïve decisions that ignore future uncertainty can perform poorly (Mercier and Van Hentenryck, 2007). Each forward path in the scenario tree is first solved deterministically and then the expected cost over those scenarios is calculated. This is known as the expected value of the wait-and-see solution (Madansky, 1960):

$$\mathbb{E}_\omega[Z_{DM}^\omega] = \sum_{\omega \in \Omega} p_\omega(Z_{DM}^\omega) \quad (1)$$

where Z_{DM}^ω is a deterministic model specified according to the set of forward paths Ω , and ω represents a single scenario realization. The EVPI, which represents the difference between the wait-and-see and stochastic solutions, is then computed for multi-stage stochastic programs:

$$EVPI = Z_{RP} - \mathbb{E}_\omega[Z_{DM}^\omega] \quad (2)$$

where Z_{RP} represents the multi-stage, stochastic program solved using the entire scenario tree instead of optimizing a single forward path.

2.5.2 Value of Stochastic Solution (VSS)

The VSS assesses the incremental value of the stochastic solution compared to a deterministic solve that considers the uncertain parameters represented at their expected values. The expected value of the uncertain parameters in the scenario tree is given as:

$$\bar{\xi}_t = \sum_{\omega \in \Omega} p_\omega(\xi_t^\omega) \quad (3)$$

where ξ_t^ω is the realization of the uncertain parameters in scenario ω at time stage t which has a probability p_ω of occurrence. The deterministic model is specified for this purpose by considering the future realization of the uncertain parameter, ξ_t , for time period, $t = 2, \dots, T$, at the expected value $\bar{\xi}_t$. We define $\bar{\xi} = [\bar{\xi}_2 \ \bar{\xi}_3 \ \dots \ \bar{\xi}_t \ \dots \ \bar{\xi}_T]$ and we represent this problem by $Z_{DM}(\bar{\xi})$. Figure 2.3 depicts a deterministic three-stage problem where the uncertain parameters are defined to be at their expected values for Stages 2 and 3 respectively.

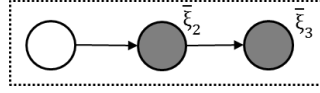


Figure 2.3: Single forward path in a three-stage problem used to solve $Z_{DM}(\bar{\xi})$.

Results obtained in the first time stage of the deterministic model $Z_{DM}(\bar{\xi})$ are fixed as the first stage decisions for the stochastic program, and the optimization over the scenario tree is performed. Following Escudero et. al. (2007), we let $\bar{x}_t, \forall t \in T$, be the optimal solution at a given time stage obtained by solving the deterministic problem, $Z_{DM}(\bar{\xi})$. For calculating VSS, the decision vector of a recourse problem at Stage 1, x_1 , is fixed as the optimal decision vector at Stage 1, \bar{x}_1 , obtained by solving $Z_{DM}(\bar{\xi})$. If we let the solution to the recourse problem be denoted by $Z_{RP}(x_1 = \bar{x}_1)$, then the value of the stochastic solution can be defined as:

$$VSS = Z_{RP}(x_1 = \bar{x}_1) - Z_{RP} \quad (3)$$

If the VSS is small, it implies that the stochastic optimization conveys little value, since the future uncertainty can be well-represented by a deterministic formulation.

2.5.3 Expected Cost of Ignoring Conflict (ECIC)

The expected cost of ignoring conflict (ECIC) represents the savings associated with following the hedging strategy produced by the stochastic optimization instead of naively following a forward path that does not consider conflict and then having to take recourse action. ECIC is conceptually similar to a well-known metric, the expected cost of ignoring uncertainty (ECIU) (Birge and Louveaux, 2011), however, here we focus on only one particular naïve scenario in which conflict is ignored entirely. ECIC is also similar to the

VSS, except the first stage decisions reflect the solution to the naïve scenario rather than the solution to deterministic scenario based on expected values for uncertain parameters.

We have two scenarios emanating from each node in the scenario tree: generator damage occurs (ω_1) and no generator damage occurs (ω_2). Hence, the deterministic model is represented as $Z_{DM}(\xi^{\omega_2})$, where ξ^{ω_2} represents the realization of uncertain parameters when no damage occurs across the planning horizon. Once the decision is made at Stage 1 using the naïve solution, we consider its cost in all the forward paths represented in the scenario tree. ECIC assesses the incremental value of a decision plan obtained using the recourse problem (Z_{RP}), where future uncertainty is explicitly considered instead of the naïve solution that ignores it and requires significant recourse action in future periods.

We let $\tilde{x}_t, \forall t \in T$, be the optimal solution at a given time stage obtained by solving the deterministic problem, $Z_{DM}(\xi^{\omega_2})$. To calculate ECIC, the decision vector of a recourse problem at Stage 1, x_1 , is fixed at the optimal decision vector at Stage 1, \tilde{x}_1 , obtained by solving the naïve scenario $Z_{DM}(\xi^{\omega_2})$. If we let the solution to this recourse problem be denoted by $Z_{RP}(x_1 = \tilde{x}_1)$, then the expected cost of ignoring conflict can be defined as:

$$ECIC = Z_{RP}(x_1 = \tilde{x}_1) - Z_{RP} \quad (12)$$

A small ECIC suggests that ignoring generator damage is inexpensive, and hence the stochastic solution does not yield much value

3 Results and Discussion

We begin by describing the Method of Morris results, which inform the analysis performed with the stochastic version of the model. Next, results from the stochastic optimization are presented under different assumed conflict scenarios. We conclude by discussing the stochastic output metrics – EVPI, VSS and ECIC – and use them to draw insights about future electric power development in South Sudan.

3.1 Identifying key input sensitivities

Before conducting the stochastic optimization, we run a base case that serves as a benchmark and assumes no conflict in South Sudan. We apply Method of Morris to the base case in order to identify the input parameters that produce the largest effect on total electricity supply cost over the time horizon. This initial sensitivity analysis ignores conflict risk, which is addressed explicitly in the stochastic programming model. Key parameters tested include the electricity curtailment cost and end-use electricity demand as well as the

capacity factors, investment costs, and fixed operations and maintenance costs associated with new electric generating units. Figure 2.4 indicates that the cost of electricity supply is most sensitive to electricity curtailment costs.

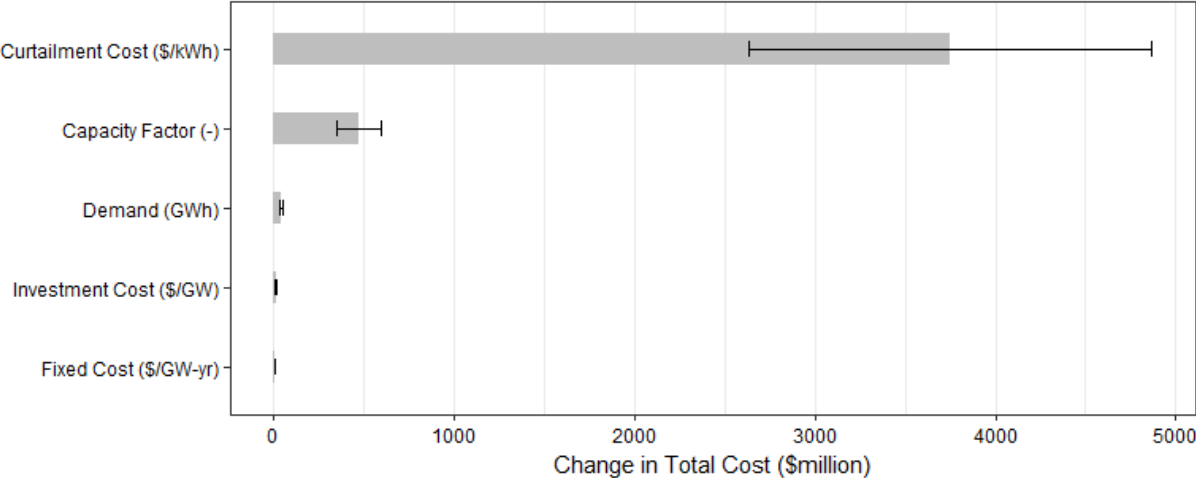


Figure 2.4: Change is the total cost of energy supply given a $\pm 20\%$ change in the value of five different input parameters using the Method of Morris. The length of the bars indicates the average effect of each parameter on total system-wide cost, and the error bars indicate the standard deviation across an ensemble of runs.

3.2 Capacity expansion under conflict uncertainty

Results from the first model time period (2017) reveal how the near-term hedging strategy produced by the stochastic optimization accounts for conflict uncertainty (Figure 2.5). The amount of installed capacity varies by the damage probability, curtailment cost, and damage estimation method. However, some patterns are evident. At all but the lowest curtailment value of 0.10 \$/kWh, solar PV is a cost-effective option to meet demand given its greater resilience in the face of conflict. The combination of high damage probability and high damage values decreases the deployment of large hydro plants. In the case with high damage probability and maximum damage (Figure 2.5a), it is most-effective to utilize solar PV and simply curtail demand at night when the curtailment cost is less than 0.6 \$/kWh. Thermal capacity is only deployed when the curtailment cost is 0.6 \$/kWh or above. Figure 2.5 suggests that an explicit consideration of conflict can have a large effect on near-term electric sector planning.

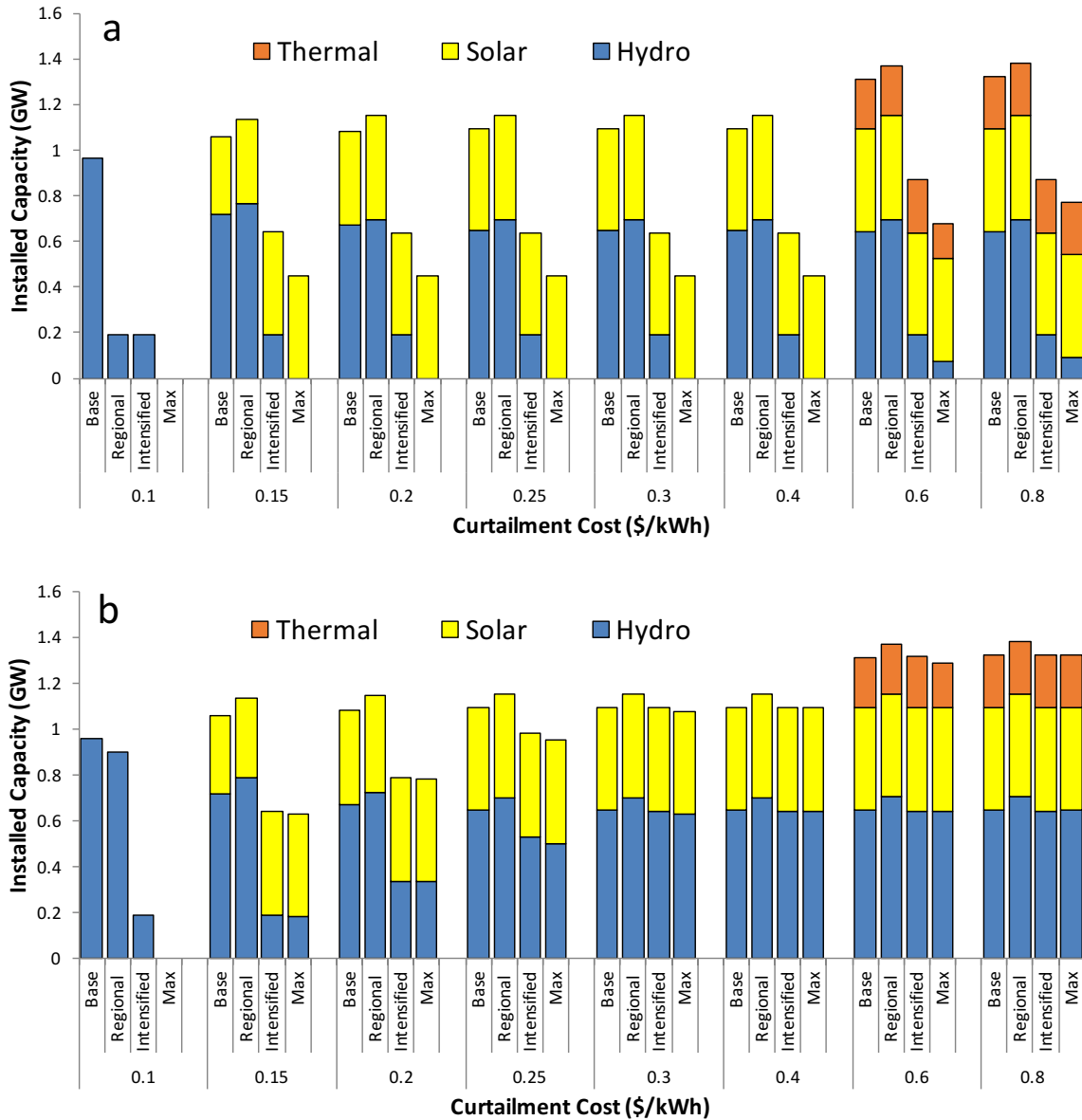


Figure 2.5: Installed capacity in the first model time period (2017) assuming (a) high probability of power plant damage, and (b) medium probability of power plant damage. The stochastic optimization is repeated for different curtailment costs and damage estimation methods: base (no damage), regional, intensified, and max damage. Differences in the total amount of installed capacity stem from differential use of demand curtailment and differences in technology-specific capacity factors. Given a 5-year delay in hydro availability, hydro constructed in 2017 is not available for generation until 2022.

The different conflict pathways represented in the scenario tree can lead to diverging deployment pathways over time. Figure 2.6 illustrates how the deployment pathways of solar, hydro, and thermal differ under extreme scenarios; the vertical axis represents the difference in installed capacity between the scenario

where generator damage occurs in each of the three future time periods, and the scenario where no generator damage occurs throughout the planning horizon. Under high damage probability (Figure 2.6a), the expansion of hydro capacity is limited and there is little divergence between the no damage and all damage scenarios. As the expected damage increases (moving left-to-right in Figure 2.6), there is greater divergence in the installed capacity by technology. Persistent conflict-related damage across the time horizon suggests the use of more solar PV and less hydro and thermal capacity. Differences in installed capacity between these extreme scenarios are larger under moderate damage probabilities because the expected damage costs are lower, allowing for greater variations in installed capacity as uncertainty about generator damage is revealed. This effect is amplified at higher curtailment costs because it is more cost-effective to build additional capacity than curtail demand. For example, under moderate damage probability and maximum damage, differences in 2032 installed capacity between different scenarios range up to 1 GW out of a total of 2.4 - 3.0 GW installed.

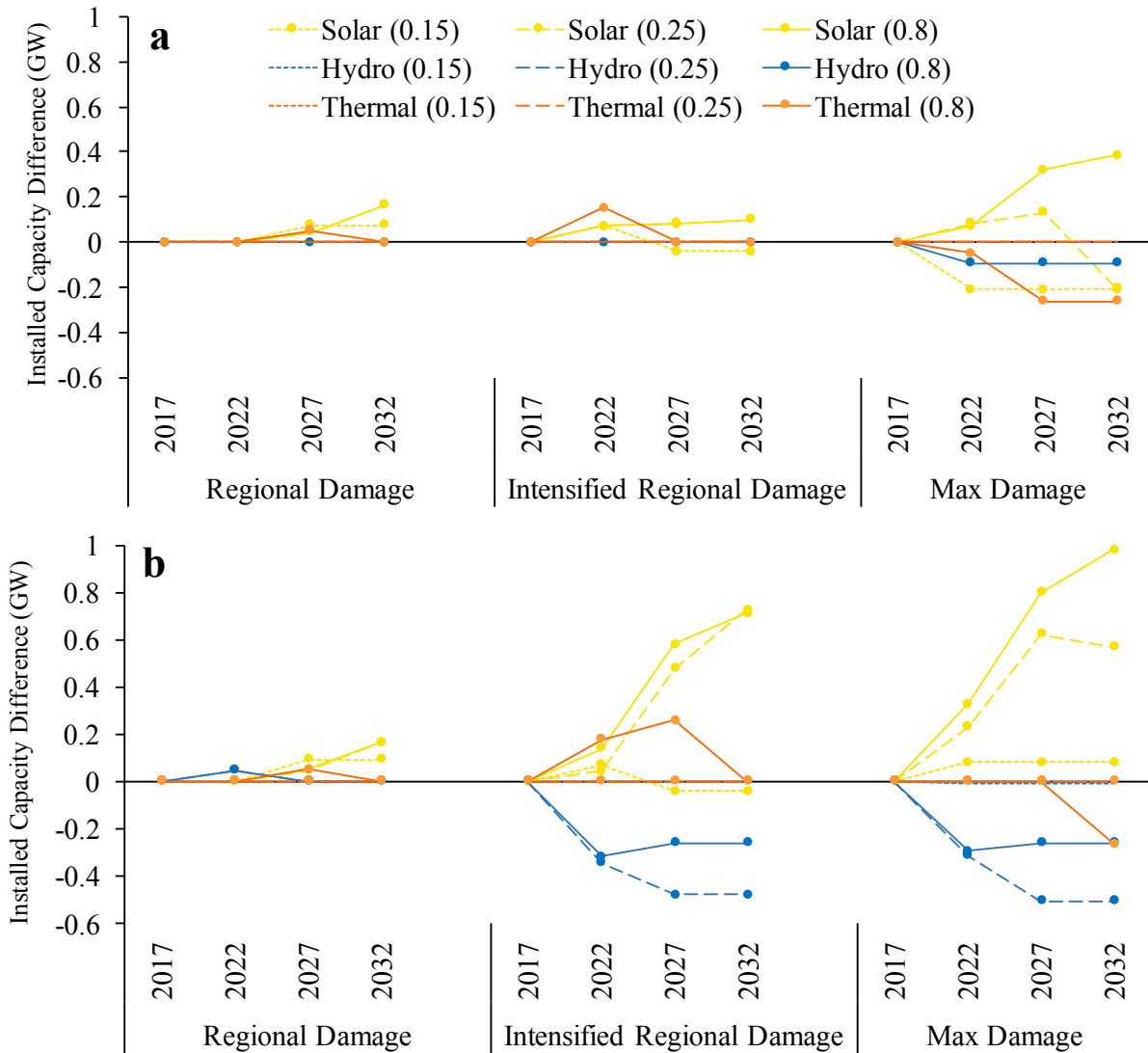


Figure 2.6: Difference in installed capacity between the two most extreme forward paths through the scenario tree: no generator damage and damage in every time period. Positive differences indicate higher installed capacity in the all-damage scenario. Differences are shown with (a) high damage probability and (b) medium damage probability, and in both cases, three different damage estimation methods. Differences are also shown at three different curtailment costs given in parentheses: 0.15, 0.25, and 0.8 \$/kWh.

Figure 2.7 presents the total cumulative installed capacity of hydro and solar by 2032 across all scenarios. Under low curtailment values of 0.15 \$/kWh, only modest amounts of hydro and solar are deployed; it is more cost-effective to simply curtail demand. Under high damage probability (first and third rows of Figure 2.7), only the scenario with regionalized damage costs and moderate to high curtailment costs allow for appreciable amounts of hydro capacity. In general, the high expected damages associated with high damage probabilities suppress the construction of hydro and increase the deployment of solar PV. By contrast,

cumulative hydro capacity increases under medium damage probabilities (second row of Figure 2.7). In this case, hydro remains cost-effective despite the anticipated damage costs.

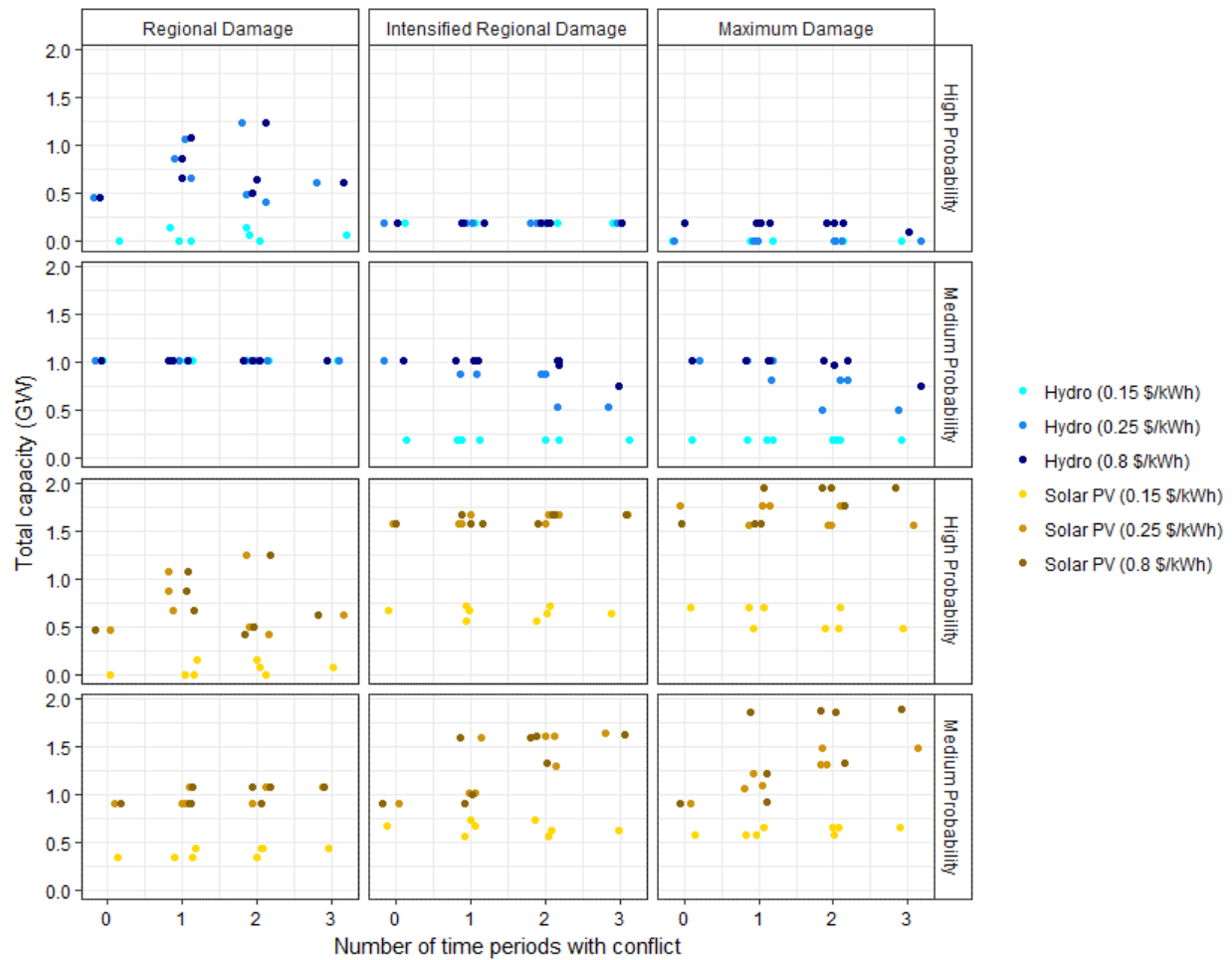


Figure 2.7: Cumulative installed capacity of hydro (top two rows) and solar (bottom two rows) as a function of the damage estimation method, damage probabilities (high or medium), and the number of time periods within the model time horizon that include conflict-related damage. Solar and hydro deployment are represented at different curtailment values, given in parentheses within the legend.

3.3 The value of hedging

Figs. 5-7 illustrate how assumptions about the probability of generator damage, method to estimate damages, curtailment cost, and number of time periods with conflict affect the installed capacity over time. It is also critical to assess how these factors affect the economics of electricity supply in South Sudan, and whether hedging strategies produced by the stochastic optimization provide economic value beyond a simpler deterministic model.

Figure 2.8a presents the expected value of perfect information (EVPI), which can be interpreted in this context as the amount that South Sudan electricity planners should be willing to pay in order to eliminate uncertainty over future conflict. Figure 2.8 plots the EVPI as a function of the exogenously prescribed curtailment cost, ranging from 0.1 to 0.8 \$/kWh. The results indicate that the EVPI increases as the damage costs increase from the “regional damage” to “maximum damage” scenarios. In other words, as the economic impacts of conflict-related damage increase, the EVPI increases. Under high probability of damage, the EVPI increases with curtailment cost. Higher curtailment costs imply that electricity is more highly valued, which means the model must rely more on electricity supply to meet demand at high curtailment costs. As a result, the value of information increases with curtailment cost under the high damage scenario, because the cost of damage can have a large effect on the total system cost. By contrast, under medium damage probability, the EVPI peaks at around 8% of the total baseline cost under the “intensified regional damage” and “maximum damage” scenarios at a curtailment cost value of 0.20 \$/kWh. At higher curtailment values, the EVPI decreases because curtailment is effectively too expensive, and the strategy relies on building generating capacity, thus reducing the value of information. We also tested curtailment values exceeding 1 \$/kWh in the high probability of damage case, and see the same decline in EVPI as shown in the medium probability case. The difference between the two scenarios is that the high damage probability makes the expected damage more costly, and thus the peak in EVPI occurs at a higher curtailment cost. Overall, the EVPI results indicate that when key input parameters take on intermediate values, the results are sensitive to how the uncertainty is resolved and therefore the value of information is comparatively high.

The value of the stochastic solution (VSS) in Figure 2.8b follows a similar pattern to EVPI. The VSS indicates the relative value of the stochastic solution compared with a deterministic formulation that uses expected values for the uncertain damages. In the high damage probability case, the damages are high enough that the planning strategy is more straightforward and relies more on curtailment, which can be well-represented by a deterministic version. By contrast, the VSS results indicate that a medium damage probability and moderate curtailment values produce the largest VSS, reaching a peak of approximately 4% of the baseline cost. Thus, stochastic optimization has the greatest value in scenarios with intermediate values for damage probability and curtailment cost, where future uncertainty is highest.

The ECIC shown in Figure 2.8c represents the difference between the hedging strategy and the naive solution that ignores conflict-related damage and requires recourse. Similar to the VSS, a small ECIC value implies that the hedging strategy produced by stochastic optimization, which accounts for future uncertainty in generator damage, conveys little economic advantage over a naïve least-cost pathway. The results

indicate that the ECIC is at a maximum when the curtailment value is lowest (0.10 \$/kWh), and decreases as the curtailment cost increases. Because the naïve solution does not consider conflict at all, a large amount of hydro capacity is built in 2017. However, conflict-related damage in later periods leads to expensive recourse that requires a shift toward solar. Recourse is more expensive under the high probability of damage case because the anticipated damages are higher. Because hydro includes a one-period delay in construction, more solar and thermal capacity is deployed in 2017 as the curtailment costs increase. Thus, higher curtailment costs force more solar deployment in the naïve scenario, which leads to less expensive recourse action in future periods when conflict occurs. Hence the decline in ECIC as a function of curtailment cost.

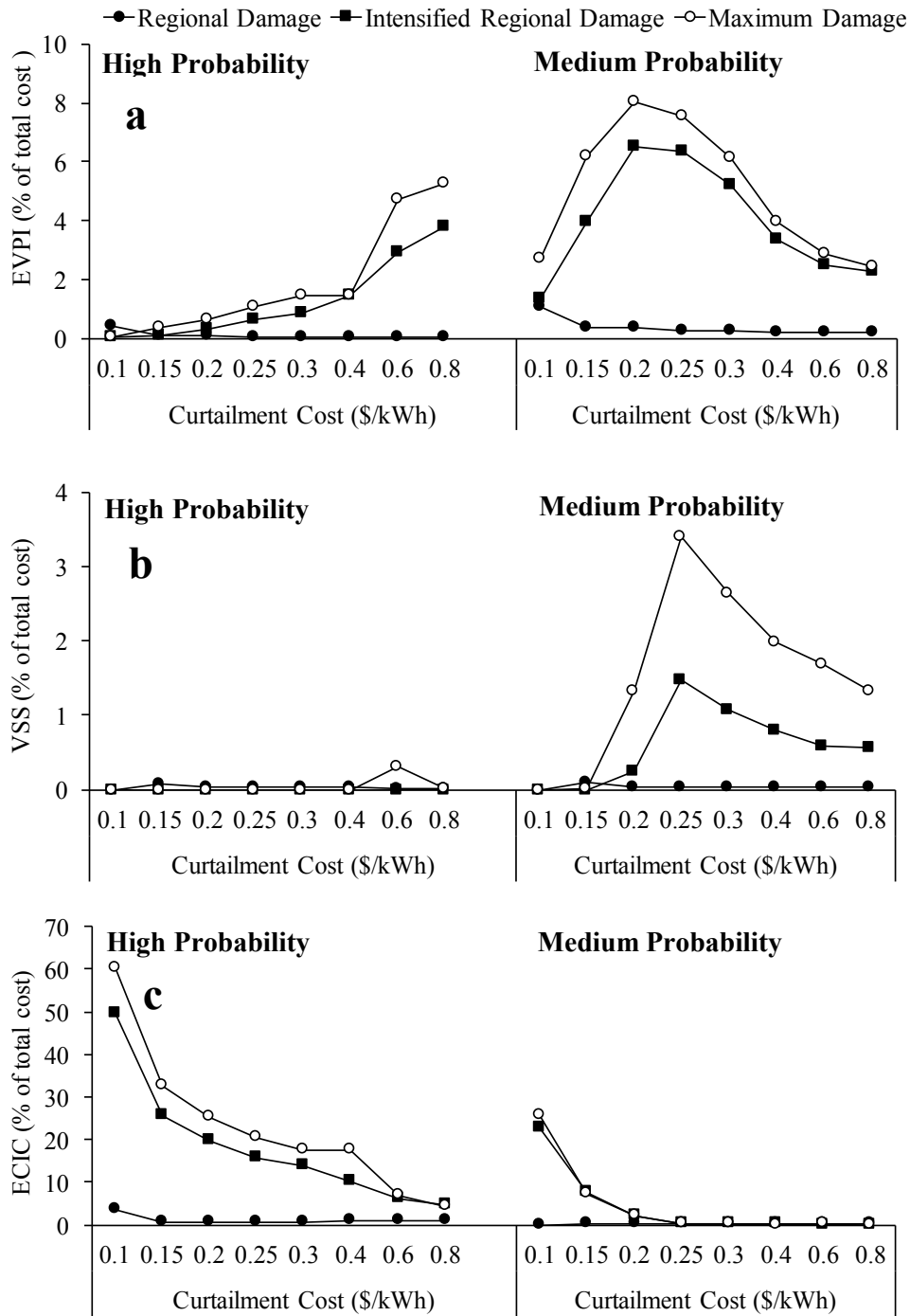


Figure 2.8: Measures of economic cost associated with future conflict uncertainty, including (a) the expected value of perfect information (EVPI), (b) value of the stochastic solution (VSS), and (c) the expected cost of ignoring conflict (ECIC). Methods producing higher damage estimates produce higher values for these metrics.

4 Conclusion and policy implications

Fourteen of the top 20 most fragile countries are in sub-Saharan Africa (Fund for Peace, 2017). This modeling exercise demonstrates the need for such countries to explicitly consider the risk of conflict as they build out their electric power systems. We construct an analytical framework that employs an energy system optimization model along with sensitivity analysis and stochastic optimization to examine how potential future conflict can affect near-term electricity planning. We apply this framework to examine planning alternatives for South Sudan. We emphasize that the results presented here are meant to demonstrate how consideration of conflict in model-based analysis can inform planning, but additional refinement is required before it is used to inform decision making.

Even with the use of stochastic optimization, near-term deployment strategies still depend on exogenous assumptions; in this case, curtailment cost, damage probabilities, and the estimation method by which the presence of conflict can result in damage to electric generators. The ECIC results indicate that naively following a least cost planning strategy results in expensive recourse actions, particularly when the naïve scenario relies heavily on hydro. The ECIC peaks at approximately 60% of the baseline cost, which is extremely high because conflict-related damage converts much of the installed hydro capacity into a stranded asset. By comparison, van der Weijde and Hobbs (2012) examine transmission planning in Great Britain and estimate an overall ECIU value of 0.08% of the stochastic solution cost. Such high ECIC values in the South Sudan case suggest the potential for large economic losses in a country that can ill afford them.

Both the EVPI and VSS reach peak values under moderate damage probability and curtailment cost. In this intermediate range of input values, hedging based on consideration of future outcomes provides the most economic benefit. By contrast, more extreme scenario assumptions that make conflict-related generator damage either a near certainty or a remote possibility result in relatively straightforward decision strategies that do not require much hedging. Therefore, future work aimed at refining the range of input assumptions can help determine the utility of applying stochastic optimization to develop electric sector planning strategies under conflict.

5 Caveats and Future Work

As mentioned in the introduction, this analysis explores a simplified decision landscape that includes the explicit consideration of conflict in an electricity expansion planning exercise. Given the complexity of real-world conflict dynamics, we made a number of simplifying assumptions.

First, we assume an exogenously specified demand increase over time, with demand curtailment occurring at a prescribed cost. The use of a curtailment cost – above which electricity is no longer demanded – is a simplifying assumption employed to make the model computationally tractable. Repeating the stochastic optimization at different curtailment cost values is functionally equivalent to adjusting the level of electricity demand that must be met. As the curtailment cost is lowered, less electricity demand will be met with supply. In reality, there would be a continuous response to prices: as prices increase, demand decreases, and vice versa. Future effort should focus on estimating the demand elasticity for electricity, which would allow the demand to adjust endogenously to realized electricity prices. Because South Sudan has never had significant electricity infrastructure, such elasticities would be highly uncertain, and could be incorporated as an uncertain parameter into the stochastic optimization.

Second, while we characterized three different methods to calculate damage to generators, more empirical data that quantifies how conflict affects electricity infrastructure would improve our analysis. We assume, for example, that the probability of conflict, $Pr(C)$, and regional conflict rate, RCR , do not vary with time. In addition, we assume independence among key damage-related parameters, including the probability of damage, $Pr(D)$, regional conflict rate, RCR , probability of conflict, $Pr(C)$, and the damage rate, DR . In reality, we would expect, for example, that the regional conflict would affect the damage rate, which would in turn affect the probability of damage. We are not aware of an existing dataset that would allow us to derive the correlation between these parameters. Future work could include additional sensitivity analysis to quantify how parameter correlation affects the damage estimates. The importance of time dependence and correlation among parameters also depends on the timeframe for analysis and the characteristics of the conflict. For example, given the persistence of the South Sudan conflict, assuming the conflict dynamics remain largely the same over the next 15 years may result in a plausible capacity expansion plan under conflict.

Also, in addition to considering damage to generators, future analysis should also consider damage to transmission and distribution lines, fuel supply infrastructure, and the resultant effect on cost and delay associated with maintenance. Damage to transmission and distribution infrastructure would disproportionately affect the centralized hydro and thermal plants, which typically rely on long distance, high voltage transmission lines to deliver electricity. By contrast, the modularity of solar allows for separate installations or microgrids with a limited amount of distribution infrastructure. While this vulnerability is partially captured by the higher damage rate for hydro and thermal facilities compared to solar, the effect on transmission and distribution lines could be modeled explicitly. The vulnerability of fuel supply infrastructure would only affect the thermal plants, which only see limited deployment in the current

analysis. Consideration of maintenance and repair should also be considered in future work. The effect on maintenance should consider plant locations, the ability to move through the terrain and source parts, and human capital required to repair and maintain the facilities. Given the modularity of solar and the ability to place it strategically within currently protected locations, we speculate that maintenance would incur larger costs and delays on the centralized plants.

Chapter 3 A Novel Approach to Consider Parametric Uncertainty in Bottom-Up Energy System Models: US Case Study

A. Abbreviations

<i>ESOM</i>	<i>Energy system optimization model</i>
<i>SLP</i>	<i>Stochastic Linear Program</i>
<i>SA</i>	<i>Sensitivity Analysis</i>
<i>RO</i>	<i>Robust Optimization</i>
<i>ESPP</i>	<i>Energy system planning problem</i>
<i>PDF</i>	<i>Probability density function</i>
<i>RPS</i>	<i>Renewable Portfolio Standard</i>
<i>Temoa</i>	<i>Tools for Energy Model Optimization and Analysis</i>
<i>MCS</i>	<i>Mid Century strategy</i>
<i>MCA</i>	<i>Monte Carlo Analysis</i>
<i>GHG</i>	<i>Green House Gas</i>

B. Sets

$i \in I$	<i>Technologies</i>
$v, \tilde{v} \in V_i$	<i>Vintages associated with technology i</i>
$t, \tilde{t} \in T_i$	<i>Time period associated with technology i</i>
T	<i>All model time periods</i>
\hat{I}_1	<i>Technologies with uncertain investment cost</i>
\hat{I}_2	<i>Technologies representing fuels</i>
S	<i>Feasible domain for the maximization problem given in (6a)</i>
η	<i>Feasible domain for the maximization problem given in (11a)</i>

C. Parameters

$IC_{i,v}$	<i>Nominal investment cost of technology i and vintage v [\$ Million/GW]</i>
$IC_{i,v}^*$	<i>Realization of investment cost of technology i and vintage v [\$ Million/GW]</i>
$\Delta IC_{i,v}$	<i>Investment costs deviation of technology i and vintage v [\$ Million/GW]</i>

$FC_{i,v,t}$	<i>Fixed costs of technology i, vintage v at time period t [\$ Million/GWh]</i>
$VC_{i,v,t}$	<i>Nominal variable cost of technology i, vintage v at time period t [\$ Million/GWh]</i>
$VC_{i,v,t}^*$	<i>Realization of variable cost of technology i, vintage v at time period t [\$ Million/GWh]</i>
$\Delta VC_{i,v,t}$	<i>Maximum deviation in variable cost of technology i, vintage v at time period t [\$ Million/GWh]</i>
$\gamma_{i,v,t}$	<i>Conversion from capacity to activity [h]</i>
$Demand_t$	<i>Demand at time period t [GWh]</i>
B	<i>Matrix of coefficients for constraint (1c)</i>
b	<i>Right-hand-side of constraint (1c)</i>
Γ	<i>Budget of uncertainty</i>
ε	<i>Probability that more than n uncertain parameters assume their worst case value</i>
$g_{\tilde{v},i,v}$	<i>Correlation between $IC_{i,v}$ and $IC_{i,\tilde{v}}$, $v, \tilde{v} \in V_i$</i>
$g_{\tilde{t},\tilde{v},i,v,t}$	<i>Correlation between $VC_{i,v,t}$ and $IC_{i,\tilde{v}}$, $v, \tilde{v} \in V_i, \tilde{t} \in T_i$</i>
$\mathbf{X}_{i,t}$	<i>Random variable used to represent the uncertain parameters</i>
$X_{i,t}^{max}$	<i>Worst case value of the random variable $\mathbf{X}_{i,t}$</i>
$\sigma_{i,t}$	<i>Standard deviation of the random variable $\mathbf{X}_{i,t}$</i>
ρ_i	<i>Temporal correlation coefficient of technology i</i>
$\mu_{i,t}$	<i>Mean of a random variable $\mathbf{X}_{i,t}$</i>
$\mathbf{Z}_{t+1} = \mathbf{X}_{i,t+1} \mathbf{X}_{i,t}$	<i>A random variable denoting a value of $\mathbf{X}_{i,t+1}$ given the value of $\mathbf{X}_{i,t}$</i>
$\mu_{\mathbf{Z}_{t+1}}$	<i>Mean of a random variable \mathbf{Z}_{t+1}</i>

D. Decision Variables

$CAP_{i,v}$	<i>Capacity of technology i with vintage v in [GW]</i>
$ACT_{i,v,t}$	<i>Activity associated with technology i, vintage v at time period t [GWh]</i>
\mathbf{X}	<i>Vector of decision variables in constraint (1c)</i>
$\mathbf{s}_{i,v}$	<i>Scaled deviation of investment cost associated with technology i, vintage v. Varies within $[-1,1]$ (7)</i>
$\mathbf{s}_{i,v,t}$	<i>Scaled deviation of variable cost associated with technology i, vintage v. Varies within $[-1,1]$ (7)</i>
\mathbf{p}	<i>Dual variable associated with constraint (5)</i>

$q_{i,v}^1$	<i>Dual variables associated with constraint $s_{i,v}^{IC} \leq 1$</i>
$q_{i,v,t}^2$	<i>Dual variables associated with constraint $s_{i,v,t}^{VC} \leq 1$</i>
$r_{i,v}^1$	<i>Dual variables for the maximization problem in (6a)</i>
$r_{i,v,t}^2$	<i>Dual variables for the maximization problem in (6a)</i>
W	<i>Continuous variable used to convert objective function into a constraint</i>
$\eta_{\bar{v},i,v}$	<i>Independent symmetrically distributed random variable</i>
$\eta_{\bar{t},\bar{v},i,v,t}$	<i>Independent symmetrically distributed random variable</i>
$q_{\bar{v},i}^1$	<i>Dual variables associated with constraint $\eta_{\bar{v},i,v}^{IC} \leq 1$</i>
$q_{\bar{t},\bar{v},i}^2$	<i>Dual variables associated with constraint $\eta_{\bar{t},\bar{v},i,v,t}^{VC} \leq 1$</i>
$y_{\bar{v},i}^1$	<i>Dual variables for the maximization problem in (11a)</i>
$y_{\bar{t},\bar{v},i}^2$	<i>Dual variables for the maximization problem in (11a)</i>

1 Introduction

Energy system optimization models (ESOMs) provide a way to explore the future decision space by providing a self-consistent framework for evaluation. As a result, ESOMs are widely used to analyze energy system capacity expansion plans to investigate different technical, economic, and policy assumptions. The insights obtained from ESOMs can be used to inform policy decisions, and thus energy models should account for uncertainty that can affect policy outcomes (Turton and Barreto, 2006; Kannan, and Strachan, 2009; Li et al., 2011). However, inherent uncertainties are often underemphasized or ignored altogether in ESOMs. Uncertainties in ESOMs can be categorized as parametric and structural. Structural uncertainty arises from the inability of the mathematical equations embedded in the model to fully represent real systems. By contrast, parametric uncertainty arises from imperfect knowledge of the parameter values used in the model. Policy makers are confronted with decisions that must be taken before future uncertainty is resolved, and models should reflect that reality by embedding the uncertainty into the model formulation, thereby yielding a strategy that accounts for future uncertainty.

Developing a hedging strategy that provides one single best course of action while accounting for future uncertainty can generally be accomplished by two different methods: stochastic linear programming (SLP) and robust optimization (RO) (Yue et al., 2018; Hu and Hobbs, 2010). Stochastic linear programming requires the modeler to develop a scenario tree, assign subjective probabilities and outcomes to each branch in the tree, and then optimize the model over the whole tree. A key limitation of SLP is the curse of dimensionality (Shapiro et al., 2009), whereby the number of decision variables are an exponential function of the number of uncertain parameters and time periods. A second approach, which does not suffer from

the curse of dimensionality, is RO. Robust Optimization combines features of sensitivity analysis (SA), multi-objective optimization, and stochastic linear programming (SLP) to generate a series of solutions that are progressively less sensitive to the realization of uncertainty associated with the inputs, thereby providing robust solutions to decision makers (Mulvey et al., 1995). This method requires the modeler to choose a set of uncertain parameters, assign a range of potential values to those parameters, and then iteratively perform optimization runs, where each run includes a given number of parameters assuming their worst-case value. Given that ESOMs have to work with uncertain technology cost and performance data, the number of uncertain parameters is often more than what SLP can consider. RO on the other hand, is a more suitable approach for finding a hedging strategy when considering a large number of uncertain parameters.

The purpose of this chapter is to apply RO to develop a strategy for deep decarbonization in the United States. The United States currently has no federal greenhouse gas (GHG) emission mitigation policy, has withdrawn from the Paris Climate Accord, and repealed the EPA's Clean Power Plan. Given the lack of near-term federal action to address climate change, it is critical to evaluate other potential policies for emission reduction. In this work, we perform RO to develop insights about robust future technology pathways that achieve the targets set forth in the Obama's Mid-Century Strategy (MCS). While the MCS may not be a feasible option from a political perspective, results from the RO can be used to inform alternative policy options that can achieve deep emissions reductions with a similar portfolio of technologies. The RO formulation is implemented in an open source ESOM called Tools for Energy Model Optimization and Analysis (Temoa), in conjunction with a US input dataset to explore robust technology development pathways that result in deep decarbonization. To perform this analysis, we develop an emissions constraint to represent the MCS developed under the Obama Administration. The MCS is designed to meet the US nationally determined contribution under the Paris Agreement. While RO has been used for several decades, its application to energy system optimization models has been very limited. The RO formulation presented here is generalized, and can be applied to other ESOMs and datasets.

The RO approach was first developed by Soyster (1973) and was first applied to environmental model by Babonneau et al. (2009). It was later developed by Babonneau et al. (2012), Lorne and Tchong-Ming (2012), Labriet et al. (2015), Morel et al. (2019) for the energy system models. However, there are several limitations in this previous work: they do not provide a methodology for assigning ranges to uncertain input parameters, do not consider correlation between the uncertain parameters, and do not provide a general RO formulation for bottom up ESOMs.

Building on the existing literature related to RO in energy system capacity expansion planning, this chapter makes three key contributions. First, preliminary screening techniques are used to select the most sensitive cost parameters. The ranges of uncertain parameters have been arbitrarily assigned in the literature. We introduce a systematic methodology to form the uncertainty set. Second, the cost parameters in the ESOM are temporally correlated. The correlated RO methodology (CR-ESOM) is applied to ESOMs for the first time. Third, this chapter is the first application of the RO methodology to a large scale representation of US energy system.

The remainder of the chapter is organized as follows. Section 2 provides a detailed literature review of RO development and application, and also highlights the advantages and disadvantages of RO compared to SA and SLP. Section 3 describes the specific RO methodology used in this chapter, including the formulation of the RO counterpart for ESOMs with and without temporal correlation between uncertain data. A description of the US energy system database is given in Section 4. Section 5 presents the methodology to build the uncertainty set while Section 6 presents the results and provides discussion. Section 7 presents conclusions from the analysis.

2 Robust optimization

In energy systems, it is critical to develop plans that account for this future uncertainty. Soyster (1973) proposed a first step towards finding a feasible solution by constructing a model that provides a feasible solution under any realization of uncertain parameters. His approach has two drawbacks. First, his model is nonlinear, which resulted in a high computational burden. Second, the resulting solution is highly conservative since the model remains feasible for even the worst-case value of all uncertain parameters. To improve his approach, subsequent developments were made to explore the tradeoff between the conservativeness of the solution and optimality (Ghaoui et al., 1998; Ben-Tal et al., 2002; Bertsimas and Sim, 2004; Bertsimas et al., 2008). In particular, the approach proposed by Bertsimas and Sim (2004) stands out as it lets the decision maker choose the tolerance towards risk by specifying budget of uncertainty. For the highest budget of uncertainty, the formulation proposed by Soyster (1973) becomes a special case of the formulation proposed by Bertsimas and Sim (2004).

SLP has been used in the ESOM community for addressing uncertainty (Kanudia, 1998; Messner, 1996; Loulou, 2012). However, the RO approach provided by Bertsimas and Sim (2004) provides distinct advantages for real world application of ESOMs: it is not necessary to specify the probability distribution of uncertain parameters or choose a particular realization (scenario) of an uncertain parameter. As mentioned above, RO lets the modeler specify the range of an uncertain parameter, whereas SLP quickly

becomes computationally intensive when considering a large number of possible realizations for an uncertain parameter. Moreover, RO enables the modeler to find a solution to a problem with the least amount of infeasibility, whereas SLP may become infeasible under the realization of an uncertain parameter not included in the scenario tree.

Along with some distinct advantages of RO over SA and SLP, it also has some limitations. Rather than a more fine-grained probability distribution, RO only considers the worst case value for each parameter, which may skew the model results. However, parametric uncertainty in ESOMs is high, and the data required to construct a probability distribution often does not exist.

2.1 Robust optimization in power system modeling

While the focus of this paper is on energy system models, RO has been more widely applied to power system models (i.e., models that focus exclusively on electricity), and thus a summary is presented here. Power and energy system models rely input parameters whose values must be estimated. The estimated parameter values, however, may be different from the actual values because of data limitations, biased data, unrealistic assumptions, numerical errors in the estimation process, or the nonstationary nature of the data. An RO formulation for a power system capacity expansion problem was first developed by Malcol and Zenios (1994) for uncertain power demand. They analyze the tradeoff between the inability to recover the cost of excess capacity and a need to curtail electricity demand. They introduce a variance and penalty term in the objective function of a cost-minimizing problem to reduce the volatility of the total system cost and discourage the curtailment of electricity demand. Since the electric utilities are often penalized for excess capacity as well as for curtailing demand, considering the parameter uncertainties leads to a more robust planning strategy. Several papers have also explored the application of RO in generation expansion planning using different variations of the methodology to answer generation expansion planning related questions (Chen, C. et al., 2012; Hajimiragha, H. et al., 2011; Dehghan, S. et al., 2014; Baringo, L., and Baringo, A., 2018). Chen et al. (2012) developed a robust interval stochastic optimization (RISO) considering uncertain pollutant transfer within the region, uncertain electricity demand, and uncertain cost. Hajimiragha et al. (2011) and Dehghan et al. (2014) present noteworthy applications of RO on a real-world power system. Hajimiragha et al. (2011) uses the methodology proposed by Bertsimas and Sim (2004) for analyzing the potential for Ontario's grid to handle a transition to plug-in-hybrid vehicles considering uncertainty in electricity price, while Dehghan et al. (2014) develops single- and two-stage RO formulation to demonstrate the effect of uncertain demand, operation cost and investment cost on Iran's power system planning.

Uncertainties present in the power system also affect transmission capacity expansion planning. Since electricity transmission infrastructure is usually built to withstand severe conditions, the RO approach becomes an apt choice for decision-making under uncertainty (Ruiz and Conejo, 2015). Alizadeh et al. (2013) first formulated the transmission expansion planning problem based on the RO formulation proposed by Bertsimas and Sim (2004). They tested the formulation on three different IEEE test cases to find the optimal transmission capacity expansion plan under various uncertainties. Several papers have then used various RO formulations to analyze the impact of unforeseen equipment failure, adverse weather, and other uncertain techno-economic parameters with IEEE test cases (Chen et al., 2014; Ruiz and Conejo, 2015; Yuan et al., 2016; Baringo and Baringo, 2018). Chen et al. (2014) compares the min-max cost RO model with the min-max regret RO model while Baringo and Baringo (2018) as well as Ruiz and Conejo (2015) use a variation of the well-known adaptive RO methodology proposed by Bertsimas et al. (2011). The MILP formulation in these papers, where the transmission line is represented as a binary variable, provides a robust transmission expansion plan under various types of uncertainties.

Another growing source of uncertainty in power system operations and planning is associated with supply uncertainty associated with an increasing share of renewable sources in electricity generation. Real-world case studies of Belgium and China have been analyzed under variable renewable generation for dispatch planning (Martinez-Mares and Fuerte-Esquivel, 2013; Wei et al., 2015). Zhang et al. (2018) and Zhao et al. (2013) formulate multi-stage RO problems to analyze the effect of uncertain renewable generation with demand response and test the model on IEEE test cases.

An additional focus of RO applied to renewable energy generation pertains to microgrid planning problems (Yu et al., 2016; Hussain et al., 2016; Zhang et al., 2018; Hosseinzadeh and Salmasi, 2015). Accurately scheduling dispatchable power is essential for the reliability of microgrids. However, the uncertainty with demand response and renewable generation represents a scheduling challenge. Hussain et al. (2016) formulates a min-max cost RO model that considers renewable generation and demand forecast uncertainties for scheduling multiple microgrids. Yu et al. (2016) develops a multi-objective RO model as an MILP that minimizes the expected cost as well as the worst-case cost considering operational uncertainties (load variations, weather fluctuations, fuel price fluctuations) and conflicting interests (minimizing expected cost and worst-case scenario cost) among the microgrid stakeholders.

2.2 Robust optimization in energy system modeling

Since this work is focused on energy system optimization models (ESOMs), we provide a brief description of these models before reviewing previous applications. ESOMs can be described algebraically as a network

of linked processes that convert raw energy commodities (e.g., coal, oil, biomass) into end-use demands (e.g., lighting, transport, water heating) through a series of one or more intermediate energy forms (e.g., electricity, gasoline, ethanol). Each process is defined by a set of engineering, economic, and environmental characteristics (e.g., capital, fixed and/or variable cost, efficiency, capacity factor) associated with converting an energy commodity from one form to another. Processes are linked together in a network via model constraints representing the allowable flow of energy commodities. The objective of ESOMs is to minimize the net present cost of energy supply (composed of capital costs, operation & maintenance costs, and fuel costs) by utilizing energy processes and commodities over a under-specified time horizon to meet a set of exogenously specified end-use demands. ESOM simultaneously make technology investment and operating decisions while enforcing an energy balance between primary energy resources, secondary fuels, final energy consumption, and end-use energy services. ESOMs are typically formulated as linear programming models, where installed technology capacity is treated as a continuous variable. In the analysis described below, we utilize an open source ESOM called ‘Temoa.’

Uncertainties in peak electricity demand, renewable generation, future fuel prices and technology investment costs are also a part of ESOMs, which unlike power system models, cover the entire energy system, ranging from fuel resource extraction to the satisfaction of end-use demands across the commercial, residential, industrial, and transportation sectors. Since ESOMs usually deal with planning strategies over decades, addressing the uncertainty in fuel prices and technologies investment costs under different future scenarios is critical to developing robust planning and investment strategies.

In a methodology-oriented paper, Babonneau et al. (2009) first proposed the use of RO in environment and energy optimization models. The authors apply RO to a simple test case under an emission target policy where pollutant transfer within regions as well as end use demand is uncertain. Such an application can assist in forming regional emission reduction policies. Babonneau et al. (2012) further applied RO to examine energy security issues in Europe with the TIAM-world model. The authors find that nearly 100% reliability of the European Union (EU) energy supply could be guaranteed with an extra 0.7% of total energy cost. The reliability improvement is achieved mainly through shifts from imports to domestic resources. The work of Lorne and Tchong-Ming (2012) applied the RO methodology proposed by Bertsimas and Sim (2004) to analyze the impact of energy technology cost and CO₂ price uncertainties in the achievement of biofuels policies in France with the MIRET model. The paper concludes that given fuel cost uncertainty, biofuels are an excellent way to overcome fossil fuel dependency. However, Babonneau et al. (2012) considers uncertainty only in the availability of the resources. Moreover, both Babonneau et

al. (2012) and Lorne and Tchung-Ming (2012) assign a range based on expert's judgement, $\pm M\%$, that remains constant over all the uncertain parameters.

In addition to policy insights, RO can point out critical sources of uncertainty in the energy system. Labriet et al. (2015) analyzed the impacts of uncertainties in investment costs and primary energy costs in France on carbon mitigation using the TIAM-WORLD and the MIRET models. The analysis concludes that scenarios with higher uncertainty budgets have more diversified fuel usage, which demonstrates that diversification is a good hedging strategy. Technologies that use biofuels have a higher penetration in scenarios with higher uncertainty budgets. As a result, biofuels can be considered as a robust hedging strategy against cost uncertainties.

3 Robust optimization formulation

The purpose of this chapter is to build parametric uncertainty related to future fuel prices and capital costs into an RO formulation in order to develop a strategy for deep decarbonization in the United States. The approach is divided into four parts: gathering the data for the US energy system, designing an optimization problem to consider parametric uncertainty, characterizing the uncertainty, and providing robust strategies for GHG emission mitigation. Figure 3.1 outlines the flow of information through analysis. First, beginning in the upper left hand corner, we compile data from public sources into a Temoa-compatible, relational database representing the US energy system as a single region (Section 4). Second, we feed the data to Temoa under a constraint on CO₂ emissions that follows the Mid-Century Strategy (MCS) developed by the Obama Administration (House, 2016). The US nationally determined contribution (NDC) was 26-28% below 2005 levels by 2025 under the Paris Accord (Climate Action Tracker), and the MCS released under the Obama Administration suggests an 80% reduction below 2005 levels by 2050. The solution obtained from this step provides the optimal capacity expansion plan that does not consider any future parametric uncertainty. Henceforth, this solution is called the '*naïve*' solution.

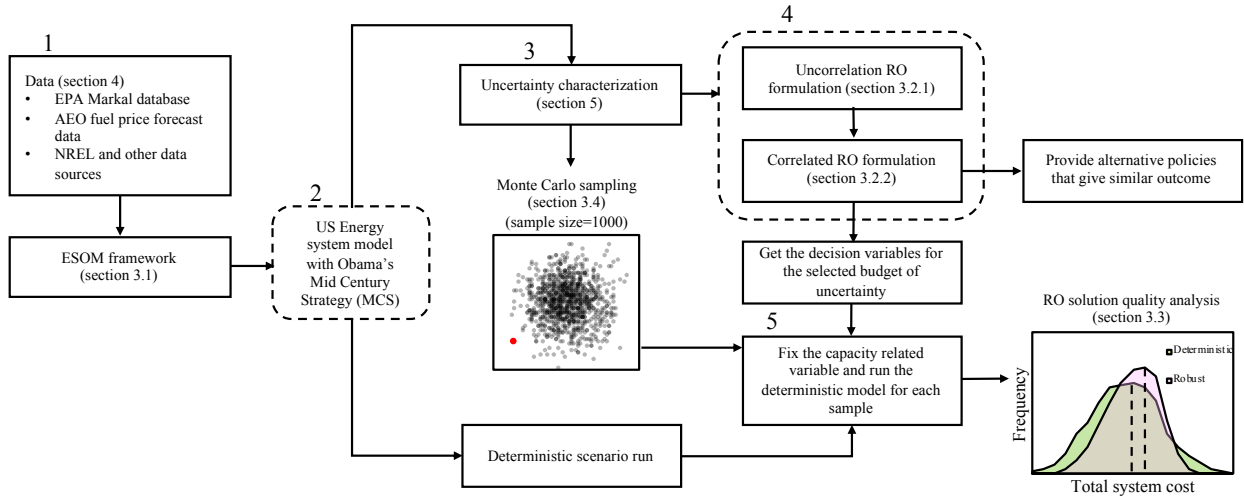


Figure 3.1: Methodology for obtaining robust alternate policies for GHG emission mitigation in the absence of federal climate policy.

Third, the worst case values and autocorrelation are estimated for the input fuel prices and capital costs (Section 5). Fourth, we formulate the RO model in two steps. The first RO (R-ESOM) formulation does not consider temporal autocorrelation in uncertain parameters (Section 3.2.1). Such autocorrelation is important in capacity expansion models because most input parameters are indexed by model time period, but the RO procedure assumes that each parameter value in each time period can be treated independently. As an example, in this basic R-ESOM formulation natural gas prices can take on their worst-case value in 2030, but the prices in other time periods remain at their baseline values. Building on this formulation, we construct a correlated RO (CR-ESOM) formulation (section 3.2.2). In this version, a parameter taking on its worst-case value in a given time period will in turn affect the parameter value in the other time periods through a correlation parameter. We do not present the results for R-ESOM; however, we provide the description of the model as CR-ESOM is an extension of the R-ESOM.

The solution obtained by solving CR-ESOM represents the ‘robust’ solution. Fifth, to compare the effectiveness of the robust solution over the naïve solution, we perform a solution quality evaluation using Monte Carlo Analysis (MCA) (Section 3.3). Results from the RO analysis are used to draw insight about robust pathways for deep decarbonization.

3.1 A simplified ESOM formulation

For the exogenously specified end-use demand, a simplified form of a general ESOM formulation with the objective to minimize total system costs can be written as the following linear program.

$$\begin{aligned}
\min \quad & \sum_{v \in V_i} \sum_{i \in I} IC_{i,v} \cdot \mathbf{CAP}_{i,v} + \sum_{t \in T_i} \sum_{v \in V_i} \sum_{i \in I} FC_{i,v,t} \cdot \mathbf{CAP}_{i,v} + \sum_{t \in T_i} \sum_{v \in V_i} \sum_{i \in I} VC_{i,v,t} \cdot \mathbf{ACT}_{i,v,t} \quad (1) \\
\text{s. t.} \quad & \sum_{v \in V_i} \sum_{i \in I} \mathbf{ACT}_{i,v,t} \geq \text{Demand}_t \quad \forall t \in T \quad (1a) \\
& \sum_{v_i \leq T_i} \gamma_{i,v,t} \cdot \mathbf{CAP}_{i,v} \geq \mathbf{ACT}_{i,v,t} \quad \forall t \in T_i, v \in V_i, i \in I \quad (1b) \\
& \mathbf{BX} \geq b \quad \in I \quad (1c)
\end{aligned}$$

In the above model (1)-(1c), V, I and T are the set of all vintages, technologies and model time periods, respectively where, v is the vintage of the capacity of technology i in time period t . $IC_{i,v}, FC_{i,v,t}$ and $VC_{i,v,t}$ are the investment cost, fixed and variable operations and maintenance costs of technology i , respectively. $\mathbf{CAP}_{i,v}$ is the decision variable representing available capacity of technology i of vintage v . In the above model formulation, the total commodity production from a process is referred to as ‘‘activity’’. $\mathbf{ACT}_{i,v,t}$ is the decision variable representing activity of technology i of vintage v in time period t . Moreover, $\gamma_{i,v,t}$ is the factor that converts available capacity to available activity. Demand_t is the demand in time period t . Furthermore, B represents the coefficients of all the other constraints, and b represents the right-hand side of such constraints. Equation (1) expresses the total discounted cost to be minimized, (1a) is the set of demand satisfaction constraints, where the right-hand-side Demand_t are the exogenous demands that needs to be satisfied, (1b) represents the relationship between available capacity and activity and (1c) is the set of all other constraints such as flow balance, resource availability, technology share, process balance, lower and upper bounds on decision variables, limit on technology lifetime, reserve margin and storage constraints. Hunter et al. (2013) provides a detailed formulation for the constraints included in (1c). The model (1)-(1c) can also be written as (2)-(2d) stated next.

$$\begin{aligned}
\min \quad & W \quad (2) \\
\text{s. t.} \quad & W - \left(\sum_{v \in V_i} \sum_{i \in I} IC_{i,v} \cdot \mathbf{CAP}_{i,v} + \sum_{t \in T_i} \sum_{v \in V_i} \sum_{i \in I} FC_{i,v,t} \cdot \mathbf{CAP}_{i,v} \right. \\
& \quad \left. + \sum_{t \in T_i} \sum_{v \in V_i} \sum_{i \in I} VC_{i,v,t} \cdot \mathbf{ACT}_{i,v,t} \right) \geq 0 \quad (2a) \\
& \sum_{v \in V_i} \sum_{i \in I} \mathbf{ACT}_{i,v,t} \geq \text{Demand}_t \quad \forall t \in T \quad (2b)
\end{aligned}$$

$$\sum_{v_i \leq T_i} \gamma_{i,v,t} \cdot \mathbf{CAP}_{i,v} \geq \mathbf{ACT}_{i,v,t} \quad \forall t \in T_i, i \in I \quad (2c)$$

$$\mathbf{BX} \geq b \quad (2d)$$

Where, W is a dummy variable introduced to write the model's objective function in the form of a constraint. Since we assume uncertainty in variable cost and technologies investment cost as well as fuel costs, only constraint (2a) will contain uncertain parameters when attempting to solve an extension of model (2) under uncertainty.

3.2 Robust optimization formulation

The first RO formulation proposed by Soyster (1973) constructs a solution that is feasible for any realization of uncertain data. As a result, the solution is too conservative in the sense that we give up too much of the optimality of the 'naive' solution in order to guarantee robustness. Bertsimas and Sim (2004), on the contrary, formulates the RO model based on the stipulation that nature will be restricted in its behavior. In other words, only a subset of the uncertain parameters will change in order to affect the system cost adversely. This approach has the property that if nature behaves like this, then the robust solution will be feasible deterministically. The literature for the application of RO in ESOM has adopted the Bertsimas and Sim (2004) formulation for uncorrelated uncertain parameters. Even though for the results presented in this chapter we use correlated version of the RO formulation, we provide the uncorrelated RO formulation for maintaining the consistency.

3.2.1 RO formulation for uncorrelated variables - R-ESOM

In this section we assume that the uncertain ESOM parameters are independently random. We provide a formulation for the uncertain investment cost and fuel prices; however, the formulation can be extended to consider the uncertainty in fixed operations and maintenance cost. Let \widehat{I}_1 be the set of technologies with uncertain investment cost and \widehat{I}_2 be the set of technologies with uncertain variable cost. The elements of the vector, $IC_{i,v}$ i.e., investment cost of a technology i with vintage v , for $i \in \widehat{I}_1$ and $VC_{i,v,t}$ i.e., variable cost of a technology i with vintage v in time period t for $i \in \widehat{I}_2$, are assumed to be subjected to uncertainty. Let the uncertain realization associated with investment cost and variable cost be denoted as $IC_{i,v}^*$ and $VC_{i,v,t}^*$, respectively. $IC_{i,v}^*$ belongs to a symmetrical interval $[IC_{i,v} - \Delta IC_{i,v}, IC_{i,v} + \Delta IC_{i,v}]$ defined by the decision maker, where $IC_{i,v}$ and $\Delta IC_{i,v}$ are used to represent nominal values and deviation magnitudes, respectively. This interval is centered at the point forecast $IC_{i,v}$, while $\Delta IC_{i,v}$ measures the precision of the estimate. Similarly, $VC_{i,v,t}^*$ belongs to a symmetrical interval $[VC_{i,v,t} - \Delta VC_{i,v,t}, VC_{i,v,t} +$

$\Delta VC_{i,v,t}$] defined by the decision maker. The scaled deviation $s_{i,v}^{IC}$ of uncertain investment cost $IC_{i,v}^*$ and $s_{i,v,t}^{VC}$ of uncertain variable cost $VC_{i,v,t}^*$ from its nominal value can then be defined as (3) and (4), respectively.

$$\mathbf{s}_{i,v}^{IC} = \frac{IC_{i,v}^* - IC_{i,v}}{\Delta IC_{i,v}} \quad \forall i \in \widehat{I}_1, v \in V_i \quad (3)$$

$$\mathbf{s}_{i,v,t}^{VC} = \frac{VC_{i,v,t}^* - VC_{i,v,t}}{\Delta VC_{i,v,t}} \quad \forall i \in \widehat{I}_2, v \in V_i, t \in T_i \quad (4)$$

The scaled deviation $s_{i,v}^{IC}$ belongs to $[-1,1]$ as $(IC_{i,v}^* - IC_{i,v})$ varies within $[-\Delta IC_{i,v}, \Delta IC_{i,v}]$. Similarly, $\mathbf{s}_{i,v,t}^{VC}$ belongs to $[-1,1]$. The aggregate scaled deviation for the constraint with uncertain parameters, $\sum_{v \in V_i} \sum_{i \in \widehat{I}_1} |\mathbf{s}_{i,v}^{IC}| + \sum_{t \in T_i} \sum_{v \in V_i} \sum_{i \in \widehat{I}_2} |\mathbf{s}_{i,v,t}^{VC}|$, which is more accurate than individual ones, can take any value between 0 and n , where n is the total number of uncertain parameters. However, it is unlikely that all of the coefficients take their worst cases simultaneously. Consequently, the true value of $\sum_{v \in V_i} \sum_{i \in \widehat{I}_1} |\mathbf{s}_{i,v}^{IC}| + \sum_{t \in T_i} \sum_{v \in V_i} \sum_{i \in \widehat{I}_2} |\mathbf{s}_{i,v,t}^{VC}|$ can be assumed to be in a narrower range as given in (5), i.e.,

$$\sum_{v \in V_i} \sum_{i \in \widehat{I}_1} |\mathbf{s}_{i,v}^{IC}| + \sum_{t \in T_i} \sum_{v \in V_i} \sum_{i \in \widehat{I}_2} |\mathbf{s}_{i,v,t}^{VC}| \leq \Gamma \quad (5)$$

where $\Gamma \in [0, N]$, referred to as the budget of uncertainty of the constraint containing uncertain parameters, is used to adjust the robustness against the level of conservatism of the solution. Its value reflects the decision maker's tolerance for risk. Thus, $\Gamma = 0$ indicates no "protection" against uncertainty and $\Gamma = N$ yields a very conservative solution since it can be interpreted as all the uncertain parameters' taking their worst-case values at the same time. For any values between 0 and N , the decision maker makes a trade-off between the protection level of the constraint and the degree of conservatism of the solution. Based on (Bertsimas and Sim, 2004), on the general ESOM model (2)-(2d) and on Equations (3)-(5) the R-ESOM formulation can be written as (6)-(6d).

$$\min W \quad (6)$$

$$\text{s. t. } W - \left(\sum_{v \in V_i} \sum_{i \in I} IC_{i,v} \cdot CAP_{i,v} + \sum_{t \in T_i} \sum_{v \in V_i} \sum_{i \in I} FC_{i,v,t} \cdot CAP_{i,v} + \sum_{t \in T_i} \sum_{v \in V_i} \sum_{i \in I} VC_{i,v,t} \cdot ACT_{i,v,t} \right) \quad (6a)$$

$$- \max_{\substack{s_{i,v}^{IC} \\ s_{i,v,t}^{VC} \in S}} \left(\sum_{v \in V_i} \sum_{i \in \hat{I}_1} \Delta IC_{i,v} \cdot CAP_{i,v} \cdot s_{i,v}^{IC} + \sum_{t \in T_i} \sum_{v \in V_i} \sum_{i \in \hat{I}_2} \Delta VC_{i,v,t} \cdot ACT_{i,v,t} \cdot s_{i,v,t}^{VC} \right) \geq 0$$

$$\sum_{v \in V} \sum_{i \in I} ACT_{i,v,t} \geq Demand_t \quad \forall t \in T \quad (6b)$$

$$\sum_{V_i \leq T_i} \gamma_{i,v,t} \cdot CAP_{i,v} \geq ACT_{i,v,t} \quad \forall t \in T, v \in V_i, i \in I \quad (6c)$$

$$BX \geq b \quad (6d)$$

$$S = \left\{ |s_{i,v}^{IC}| \leq 1 \forall i \in \hat{I}_1, v \in V_i; |s_{i,v,t}^{VC}| \leq 1 \forall i \in \hat{I}_2, v \in V_i, t \in T_i; \sum_{v \in V_i} \sum_{i \in \hat{I}_1} |s_{i,v}^{IC}| + \sum_{t \in T_i} \sum_{v \in V_i} \sum_{i \in \hat{I}_2} |s_{i,v,t}^{VC}| \leq \Gamma \right\} \quad (6e)$$

In the above model, (6e) is a feasible domain for the maximization problem given in (6a). For a user selected Γ , maximization problem in constraint (6a) provides a protection against infeasibility by assuming that total system cost includes the worst case cost of Γ uncertain parameters. It maximizes the protection for a given $CAP_{i,v}$ and $ACT_{i,v,t}$ by varying $s_{i,v}^{IC}$ and $s_{i,v,t}^{VC}$ over S . Note that maximization model is a linear programming problem as we keep the $CAP_{i,v}$ and $ACT_{i,v,t}$ constant as defined by the minimization model. Problem (6) can be solved by iteratively solving minimization and maximization models to minimize W . To avoid the iterative method, we can simplify model (6)-(6d) through the application of strong duality, which says that at the optimum, objective function value of the dual problem is same as primal problem (Bertsimas and Tsitsiklis, 1997). The dual of the maximization problem is given below in (7)-(7e)

$$\min \sum_{v \in V_i} \sum_{i \in \hat{I}_1} q_{i,v}^{IC} + \sum_{t \in T_i} \sum_{v \in V_i} \sum_{i \in \hat{I}_2} q_{i,v,t}^{VC} + \Gamma \cdot p \quad (7)$$

$$p + q_{i,v}^{IC} \geq \Delta IC_{i,v} \cdot r_{i,v}^{IC} \quad \forall v \in V_i, i \in \hat{I}_1 \quad (7a)$$

$$p + q_{i,v,t}^{VC} \geq \Delta VC_{i,v,t} \cdot r_{i,v,t}^{VC} \quad \forall v \in V_i, i \in \hat{I}_2, t \in T_i \quad (7b)$$

$$-r_{i,v}^{IC} \leq CAP_{i,v} \leq r_{i,v}^{IC} \quad \forall v \in V_i, i \in \widehat{I}_1 \quad (7c)$$

$$-r_{i,v,t}^{VC} \leq ACT_{i,v,t} \leq r_{i,v,t}^{VC} \quad \forall v \in V_i, i \in \widehat{I}_2, t \in T_i \quad (7d)$$

$$\mathbf{p}, \mathbf{q}_{i,v}^{IC}, \mathbf{q}_{i,v,t}^{VC}, r_{i,v}^{IC}, r_{i,v,t}^{VC} \geq 0 \quad \forall i \in I, v \in V_i, t \in T_i \quad (7e)$$

Where, $\mathbf{p}, \mathbf{q}_{i,v}^{IC}, \mathbf{q}_{i,v,t}^{VC}, r_{i,v}^{IC}, r_{i,v,t}^{VC}$ are the dual variables associated with the constraints (6e). The simplified version of (6)-(6d) is given in (8)-(8i) where we replace the maximization problem with the objective function of the dual problem. Constraints of (7)-(7e) can be added as they are without changing the solution to the problem (6)-(6d).

$$\min W \quad (8)$$

$$\text{s. t. } W - \left(\sum_{v \in V_i} \sum_{i \in I} IC_{i,v} \cdot CAP_{i,v} + \sum_{t \in T_i} \sum_{v \in V_i} \sum_{i \in I} FC_{i,v,t} \cdot CAP_{i,v} + \sum_{t \in T_i} \sum_{v \in V_i} \sum_{i \in I} VC_{i,v,t} \cdot ACT_{i,v,t} \right) \quad (8a)$$

$$- \left(\sum_{v \in V_i} \sum_{i \in \widehat{I}_1} \mathbf{q}_{i,v}^{IC} + \sum_{t \in T_i} \sum_{v \in V_i} \sum_{i \in \widehat{I}_2} \mathbf{q}_{i,v,t}^{VC} + \Gamma \cdot \mathbf{p} \right) \geq 0$$

$$\sum_{v \in V_i} \sum_{i \in I} ACT_{i,v,t} \geq Demand_t \quad \forall t \in T \quad (8b)$$

$$\sum_{V_i \leq T_i} \gamma_{i,v,t} \cdot CAP_{i,v} \geq ACT_{i,v,t} \quad \forall t \in T_i, v \in V_i, i \in I \quad (8c)$$

$$BX \geq b \quad (8d)$$

$$\mathbf{p} + \mathbf{q}_{i,v}^{IC} \geq \Delta IC_{i,v} \cdot r_{i,v}^{IC} \quad \forall v \in V_i, i \in \widehat{I}_1 \quad (8e)$$

$$\mathbf{p} + \mathbf{q}_{i,v,t}^{VC} \geq \Delta VC_{i,v,t} \cdot r_{i,v,t}^{VC} \quad \forall v \in V_i, i \in \widehat{I}_2, t \in T_i \quad (8f)$$

$$-r_{i,v}^{IC} \leq CAP_{i,v} \leq r_{i,v}^{IC} \quad \forall v \in V_i, i \in \widehat{I}_1 \quad (8g)$$

$$-r_{i,v,t}^{VC} \leq ACT_{i,v,t} \leq r_{i,v,t}^{VC} \quad \forall v \in V_i, i \in \widehat{I}_2, t \in T_i \quad (8h)$$

$$\mathbf{p}, \mathbf{q}_{i,v}^{IC}, \mathbf{q}_{i,v,t}^{VC}, r_{i,v}^{IC}, r_{i,v,t}^{VC} \geq 0 \quad \forall i \in I, v \in V_i, t \in T_i \quad (8i)$$

Observe that this robust formulation requires the determination of a budget of uncertainty for each constraint subject to uncertainty, as well as the definition of new decision variables $\mathbf{p}, \mathbf{q}_{i,v}^{IC}, \mathbf{q}_{i,v,t}^{VC}, r_{i,v}^{IC}$, and $r_{i,v,t}^{VC}$. In (Bertsimas, 2004), it is shown that irrespective of the distribution of uncertain parameters, the probability, ε , can be calculated as $1 - \phi\left(\frac{\Gamma-1}{\sqrt{N}}\right)$, where $\phi(\cdot)$ represents the cumulative density function (CDF) of a normal distribution and N is the total number of uncertain parameters. It is the probability that the number of uncertain parameters assuming worst case value exceeds the specified budget of uncertainty

$\Gamma \in [0, N]$, In other words, if the decision maker chooses the budget of uncertainty Γ , then the probability of total system cost going beyond the optimal objective function value of R-ESOM is less than ε . Figure 3.2 plots ε for example values of N .

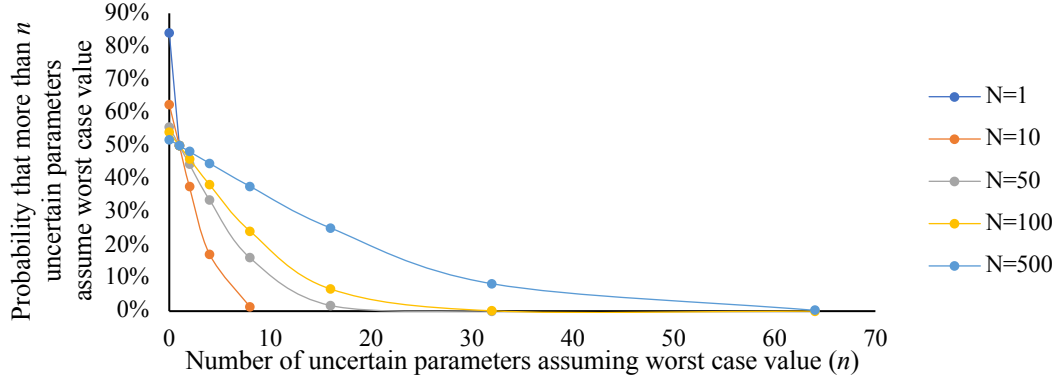


Figure 3.2: Probability that number of uncertain variables assuming worst case value exceeds Γ . N represents total number of uncertain parameters in a constraint. For example, for an optimization problem with 10 uncertain parameters in a constraint, if we set budget of uncertainty (Γ) = 4, then the probability that more than 4 uncertain variables assume their worst-case value is 17.13%.

3.3.2 RO formulation for correlated variables (CR-ESOM)

In reality, the ESOM parameters are not independently random. For example, investment cost of technology i with vintage v_1 , IC_{i,v_1} , might depend on IC_{i,v_n} and vice versa, where $v_1, \dots, v_n, \dots, v_{|V_i|} \in V_i$ and V_i is the set of vintages of technology i . Now, to model temporal correlation for uncertain parameters, we assume that investment cost of a technology has a positive correlation with the investment cost of the same technology of all available vintages. In other words, an increase in IC_{i,v_1} leads to an increase in $IC_{i,v_n}, \forall v_n \in V_i$ and a decrease in IC_{i,v_1} leads to a decrease in IC_{i,v_n} . Each entry $IC_{i,v}, i \in \hat{I}_1$ and $VC_{i,v,t}, i \in \hat{I}_2$ is modeled as:

$$IC_{i,v}^* = IC_{i,v} + \sum_{\tilde{v} \in V_i} \eta_{\tilde{v},i,v}^{IC} \cdot g_{\tilde{v},i,v}^{IC} \cdot IC_{i,v} \quad (9)$$

$$VC_{i,v,t}^* = VC_{i,v,t} + \sum_{\tilde{t} \in T_i} \sum_{\tilde{v} \in V_i} \eta_{\tilde{t},\tilde{v},i,v,t}^{VC} \cdot g_{\tilde{t},\tilde{v},i,v,t}^{VC} \cdot VC_{i,v,t} \quad (10)$$

Where, $\eta_{\tilde{v},i,v}^{IC}$ and $\eta_{\tilde{t},\tilde{v},i,v,t}^{VC}$ are independent and symmetrically distributed random variables in $[-1,1]$, $g_{\tilde{v},i,v}^{IC}$ is the effect of $IC_{i,\tilde{v}}$ on $IC_{i,v}$ for $\tilde{v} \in V_i$ and $g_{\tilde{t},\tilde{v},i,v,t}^{VC}$ is the effect of $VC_{i,\tilde{v},\tilde{t}}$ on $VC_{i,v,t}$ for $\tilde{v} \in V_i, \tilde{t} \in T_i$. For

example, from the methodology in section 5 if we determine that $IC_{i,v}$ may increase by 20% then $g_{\tilde{v},i,v}^{IC} = 0.2$. Note that under this model there are $|\hat{I}_1| \cdot |V_i| + |\hat{I}_2| \cdot |V_i| \cdot |T_i|$ potential sources of uncertainty.

Analogously to (8), the CR-ESOM formulation can be given as (11)-(11d).

$$\min W \quad (11)$$

$$\text{s. t. } W - \left(\sum_{v \in V_i} \sum_{i \in I} IC_{i,v} \cdot \mathbf{CAP}_{i,v} + \sum_{t \in T_i} \sum_{v \in V_i} \sum_{i \in I} FC_{i,v,t} \cdot \mathbf{CAP}_{i,v} + \sum_{t \in T_i} \sum_{v \in V_i} \sum_{i \in I} VC_{i,v,t} \cdot \mathbf{ACT}_{i,v,t} \right) \quad (11a)$$

$$- \max_{\eta_{\tilde{v},i,v}^{IC}, \eta_{\tilde{t},\tilde{v},i,v,t}^{VC} \in \eta} \left(\sum_{\tilde{v} \in V_i} \sum_{v \in V_i} \sum_{i \in \hat{I}_1} \eta_{\tilde{v},i,v}^{IC} \cdot g_{\tilde{v},i,v}^{IC} \cdot IC_{i,v} \cdot \mathbf{CAP}_{i,v} + \sum_{\tilde{t} \in T_i} \sum_{\tilde{v} \in V_i} \sum_{t \in T_i} \sum_{v \in V_i} \sum_{i \in \hat{I}_2} \eta_{\tilde{t},\tilde{v},i,v,t}^{VC} \cdot g_{\tilde{t},\tilde{v},i,v,t}^{VC} \cdot VC_{i,v,t} \cdot \mathbf{ACT}_{i,v,t} \right) \geq 0$$

$$\sum_{v \in V} \sum_{i \in I} \mathbf{ACT}_{i,v,t} \geq \text{Demand}_t \quad \forall t \in T \quad (11b)$$

$$\sum_{v \leq t} \gamma_{i,v,t} \cdot \mathbf{CAP}_{i,v} \geq \mathbf{ACT}_{i,v,t} \quad \forall t \in T, i \in I \quad (11c)$$

$$\mathbf{BX} \geq b \quad (11d)$$

$$\eta = \left\{ \begin{array}{l} |\eta_{\tilde{v},i,v}^{IC}| \leq 1 \forall i \in \hat{I}_1, v \in V_i, \tilde{v} \in V_i; |\eta_{\tilde{t},\tilde{v},i,v,t}^{VC}| \leq 1, \forall i \in \hat{I}_2, v \in V, t \in T, \tilde{v} \in V_i, \tilde{t} \end{array} \right. \quad (11e)$$

$$\in T_i; \left. \sum_{\tilde{v} \in V_i} \sum_{v \in V} \sum_{i \in \hat{I}_1} |\eta_{\tilde{v},i,v}^{IC}| + \sum_{\tilde{t} \in T_i} \sum_{\tilde{v} \in V_i} \sum_{t \in T} \sum_{v \in V} \sum_{i \in \hat{I}_2} |\eta_{\tilde{t},\tilde{v},i,v,t}^{VC}| \leq \Gamma \right\}$$

Where, (11e) is the feasible domain of the maximization problem given in (11a). Similar to the methodology presented in R-ESOM, through the application of strong duality (11) can be written as the linear program represented by (13)-(13i).

$$\min W \quad (13)$$

$$\text{s. t. } W - \left(\sum_{v \in V_i} \sum_{i \in I} IC_{i,v} \cdot \mathbf{CAP}_{i,v} + \sum_{t \in T_i} \sum_{v \in V_i} \sum_{i \in I} FC_{i,v,t} \cdot \mathbf{CAP}_{i,v} \right. \quad (13a)$$

$$\left. + \sum_{t \in T_i} \sum_{v \in V_i} \sum_{i \in I} VC_{i,v,t} \cdot \mathbf{ACT}_{i,v,t} \right) - \left(\Gamma \cdot \mathbf{p} + \sum_{\tilde{v} \in V_i} \sum_{i \in \hat{I}_1} \mathbf{q}_{\tilde{v},i}^{IC} + \sum_{\tilde{t} \in T_i} \sum_{\tilde{v} \in V_i} \sum_{i \in \hat{I}_2} \mathbf{q}_{\tilde{t},\tilde{v},i}^{VC} \right) \geq 0$$

$$\sum_{v \in V} \sum_{i \in I} \mathbf{ACT}_{i,v,t} \geq \text{Demand}_t \quad \forall t \in T \quad (13b)$$

$$\sum_{v \leq t} \gamma_{i,v,t} \cdot \mathbf{CAP}_{i,v} \geq \mathbf{ACT}_{i,v,t} \quad \forall t \in T_i, i \in I \quad (13c)$$

$$\mathbf{BX} \geq b \quad (13d)$$

$$\mathbf{p} + \mathbf{q}_{\tilde{v},i}^{IC} \geq \mathbf{y}_{\tilde{v},i}^{IC} \quad \tilde{v} \in V_i, i \in \hat{I}_1 \quad (13e)$$

$$\mathbf{p} + \mathbf{q}_{\tilde{t},\tilde{v},i}^{VC} \geq \mathbf{y}_{\tilde{t},\tilde{v},i}^{VC} \quad \tilde{v} \in V_i, i \in \hat{I}_2, \tilde{t} \in T_i \quad (13f)$$

$$-\mathbf{y}_{\tilde{v},i}^{IC} \leq \sum_{v \in V_i} g_{\tilde{v},i,v}^{IC} \cdot IC_{i,v} \cdot \mathbf{CAP}_{i,v} \leq \mathbf{y}_{\tilde{v},i}^{IC} \quad \tilde{v} \in V_i, i \in \hat{I}_1 \quad (13g)$$

$$-\mathbf{y}_{\tilde{t},\tilde{v},i}^{VC} \leq \sum_{t \in T_i} \sum_{v \in V_i} g_{\tilde{t},\tilde{v},i,v,t}^{VC} \cdot VC_{i,v,t} \cdot \mathbf{ACT}_{i,v,t} \leq \mathbf{y}_{\tilde{t},\tilde{v},i}^{VC} \quad \tilde{v} \in V_i, i \in \hat{I}_2, \tilde{t} \in T_i \quad (13h)$$

$$\mathbf{p}, \mathbf{q}_{\tilde{v},i}^{IC}, \mathbf{q}_{\tilde{t},\tilde{v},i}^{VC}, \mathbf{y}_{\tilde{v},i}^{IC}, \mathbf{y}_{\tilde{t},\tilde{v},i}^{VC} \geq 0 \quad (13i)$$

Similar to (8), in the constraint (13a), $(\Gamma \cdot \mathbf{p} + \sum_{\tilde{v} \in V_i} \sum_{i \in \hat{I}_1} \mathbf{q}_{\tilde{v},i}^{IC} + \sum_{\tilde{t} \in T_i} \sum_{\tilde{v} \in V_i} \sum_{i \in \hat{I}_2} \mathbf{q}_{\tilde{t},\tilde{v},i}^{VC})$ represents the objective function of the dual problem of $\max_{\eta_{\tilde{v},i,v}^{IC}, \eta_{\tilde{t},\tilde{v},i,v,t}^{VC} \in \eta} (\sum_{\tilde{v} \in V_i} \sum_{v \in V_i} \sum_{i \in \hat{I}_1} \eta_{\tilde{v},i,v}^{IC} \cdot g_{\tilde{v},i,v}^{IC} \cdot IC_{i,v} \cdot \mathbf{CAP}_{i,v} + \sum_{\tilde{t} \in T_i} \sum_{\tilde{v} \in V_i} \sum_{t \in T_i} \sum_{v \in V_i} \sum_{i \in \hat{I}_2} \eta_{\tilde{t},\tilde{v},i,v,t}^{VC} \cdot g_{\tilde{t},\tilde{v},i,v,t}^{VC} \cdot VC_{i,v,t} \cdot \mathbf{ACT}_{i,v,t})$ while constraints (13e), (13f), (13g), (13h) and (13i) are the corresponding constraints of the dual problem.

We created an embarrassingly parallel implementation of the CR-ESOM framework to minimize the computational time (Allen and Wilkinson, 1999). We use the ‘‘joblib’’ library in python to parallelize all the iterative runs of the model (Joblib, 2019). We run the model using a workstation containing two Multi-Core Intel Xeon E5-2600 series processors, representing a total of 24 compute cores. The resulting linear model is solved using CPLEX. The computational time to solve the deterministic model is 8-9 minutes while solving the CR-ESOM formulation takes 20-22 minutes.

3.3 Evaluating quality of the RO solution

Solution quality analysis in the context of SLPs is generally concerned with evaluating solutions or policies obtained by an optimization algorithm in out-of-sample cases. Previous work has evaluated solution quality for SLPs (Bayraksan and Morton, 2006; Bayraksan and Morton, 2009; Mak et al., 1999; de Queiroz, 2011). The goal is to verify how good the solution or policy would be compared to other potential solutions. This approach is based on Monte Carlo Sampling and the fact that in reality, parameters rarely assume their worst possible values. Rather, the realization of uncertain parameters is between the nominal and worst case value. Generally, decisions associated to the first stage problem are fixed and recourse actions are made in Stages 2 up to Stage T following the defined optimization policy and the realization of the uncertainty in each of the stages according to the sampled scenarios.

For the purpose of evaluating solution quality of the CR-ESOM, we let the model make capacity investment decisions based on the worst-case scenario for the uncertain parameters, but the model bases operational decisions on the realization of uncertain parameters simulated using Monte Carlo Sampling.

We use Monte Carlo Analysis (MCA) to address parametric uncertainties and analyze the problem in a systematic manner. The principle of MCA is to propagate uncertainties by simultaneously sampling multiple uncertain input parameters represented by probability distributions. From this analysis, we can compare the quality of the robust solution with the naïve solution under potential future realization of uncertain parameters. The MCA is carried out in the following steps.

1. Define the upper and lower bound for uncertain parameters. Nominal values are considered as the lower bound while the methodology to determine the upper bound is given in Section 5.
2. Given the high uncertainty associated with these future parameter values, we do not attempt to quantify different probability distributions for each parameter. Instead, a uniform distribution is assumed for each parameter over the uncertain range.
3. Sample size is set equal to 1000 and a sample of random values is generated based on the uniform probability distributions.
4. The budget of uncertainty is selected based on modeler's judgement.
5. Optimal decision variables for technology capacity is obtained by solving the CR-ESOM for a given budget of uncertainty.
6. In a naïve, least-cost version of ESOM, decision variables for technology capacity are set equal to the decision variables obtained from the robust solution.

7. Realization of uncertain parameters from the first randomly generated sample is fed into the least-cost version of the ESOM.
8. The total system cost of the naïve run is stored.
9. The procedure is repeated 1000 times.
10. For the same set of randomly generated samples, the same procedure is applied where optimal decision variables for technology capacity are obtained by solving by naïve version without RO.
11. The expected cost and standard deviation of the naïve solution is compared with the robust solution

4 US case study

The Temoa-compatible input database is drawn from the US EPA MARKAL database (Lenox, et al., 2013), NREL (NREL, 2019), and the EIA Annual Energy Outlook (AEO, 2018) and includes residential, commercial, transportation, industrial and electric sectors. The model time horizon spans from 2017 to 2050, with 5-year time periods. To represent seasonal and diurnal variations in energy supply and demand, the model must perform energy commodity balances across a set of time slices that represent different combinations of seasons and times of day. In the input database used in this analysis, we represent three seasons (summer, winter, intermediate) and four times of times of day: AM (6AM - 12PM), peak (12PM - 3PM), PM (3PM - 9PM), and night (9PM - 6AM).

The end-use sectors (residential, commercial, transportation and industrial sectors) include demand technologies that convert secondary energy carriers (e.g., electricity, natural gas, liquid fuels) into useful energy services (e.g., space heating, space cooling, vehicle miles traveled). These energy service demands are specified exogenously and are drawn from the USEPA9r database. For example, the residential sector includes demands for space heating, space cooling, water heating, freezing, refrigeration, lighting, and miscellaneous electricity for appliances.

Data on existing capacities of technologies in the residential, commercial and transportation sectors as well as their techno-economic parameters are drawn from the USEPA9r (Lenox, et al., 2013). These parameters include overnight investment costs, conversion efficiencies and technology lifetime. Existing capacities data on electric sector technologies are drawn from 2018 EIA data. We develop our own simplified representation of the industrial sector, which includes options for deep decarbonization via power-to-gas technologies. Finally, instead of modeling extraction and transport of fossil fuels such as natural gas, coal and liquid fuels, we simply define import technologies for these fuels into each of the nine regions. Fuel prices are exogenous to the model and are taken from the AEO 2018 Outlook (AEO, 2018). While we make the simplifying assumption that fuel prices are not responsive to endogenous changes within the model,

retrospective analysis indicates that there is considerable uncertainty associated with the projection of future fuel prices (AEO, 2018). A brief sectoral description of the input dataset is provided in Table 3.1. The database itself is publicly available for testing and verification through Github (Github, 2019).

Table 0.1: Sectoral-level detail in the Temoa input database.

Sector	Description
Fuel Supply	Fuel prices are specified exogenously. Baseline projections are drawn from the 2018 Annual Energy Outlook (EIA, 2017). There is no limit on fuel availability except for biofuel use in the transportation sector (Babae et al., 2014).
Electric	The electric sector includes 34 generating technologies. Air pollution control retrofits for coal include low NOx burners, selective catalytic reduction, selective non-catalytic reduction, and flue gas desulfurization. Costs and performance characteristics are largely drawn from the EPA US MARKAL database (Lenox et al., 2013), and existing capacity estimates are drawn from the US EIA (EIA, 2017).
Transportation	The transportation sector is divided into four modes: road, rail, air, and water. Road transport is modeled with greater detail by dividing it into three subsectors: light duty transportation, heavy duty transportation, and off-highway transportation. The light duty sector includes 6 size classes and 9 different vehicle technologies. Data is largely drawn from EPA US MARKAL database (Lenox et al., 2013).
Industrial	Given the high degree of heterogeneity in the industrial sector, it is modeled simplistically. The process heat and CHP are modeled in detail while the other industrial end uses are modeled as a set of fuel share constraints that are calibrated to the 2017 Annual Energy Outlook (EIA, 2017).
Commercial	The commercial sector includes the following end-use demands: space heating, space cooling, water heating, refrigeration, lighting, cooking, and ventilation. A total of 83 demand technologies are included to meet these end-use demands. Data is largely drawn from EPA US MARKAL database (Lenox et al., 2013).
Residential	The residential sector includes the following end-use demands: space heating, space cooling, water heating, freezing, refrigeration, lighting, cooking, and appliances. A total of 69 demand technologies are included to meet these end-use demands. Data is largely drawn from EPA US MARKAL database (Lenox et al., 2013).
Power to Gas	The power to gas sector in Temoa uses electricity to produce hydrogen, which is then converted to methanol and synthetic natural gas. Cost and performance characteristics are drawn from various sources which are listed in the Appendix.

To orient our baseline to a familiar projection, our baseline assumptions draw heavily on the AEO (2018) and Assumptions to the AEO (2018b). The detailed description of the database is given in the Appendix.

5 Building the uncertainty set

To solve the CR-ESOM, bounds on the uncertain input parameter and the parameter autocorrelation are required. Though beyond the scope of this analysis, the same approach can be extended to include the correlation between two different parameters; for example, between natural gas and coal prices. Using

historical fuel price data, we observe that fuel prices are temporally correlated. For example, after the 1979 oil embargo, natural gas prices remained higher than usual for the next few years. The existing literature applying RO to ESOMs ignores this temporal autocorrelation, which diminishes the effect of fuel price uncertainty.

For simplicity, uncertain parameters are first categorized into groups: fuel price and investment cost. We then determine the uncertainty bounds and the autocorrelation coefficients for each group based on various sources of data.

5.1 Grouping of the parameters

In total, the model has 6415 uncertain cost parameters, which includes investment costs, fixed operations and maintenance (O&M), variable O&M, and fuel prices. Eshraghi et al. (2018) conducts a Monte Carlo analysis for the US ESOM and shows that among the cost parameters, investment cost and fuel price have the highest impact on the objective function. As a result, uncertainty in the O&M costs are not considered in this analysis. After excluding the fixed and variable O&M cost parameters, the remaining 2224 uncertain parameters are divided into 22 groups of investment cost and fuel price parameters. As a trade-off between time and accuracy, the parameters are divided into groups based on the similarities in the base technology. For example, rooftop solar PV and centralized solar PV represent different implementations of the same underlying technology. Similarly, the uncertainty in electric vehicle cost is tied to the cost of Lithium-ion batteries, which are also used in stationary storage applications. As a result, different types of electric vehicles are grouped together to form one category called ‘electric vehicles’.

5.2 Uncertainty characterization

Figure 3.3 provides a general flowchart to characterize the range and autocorrelation for the uncertain input parameters. The method consists of six criteria applied to the uncertain parameter. Each criteria corresponds to a different data source for determining the uncertainty of the parameter. If the uncertain parameter satisfies the given criteria, then the corresponding data is collected for the computation of correlation coefficient and uncertainty range. Then, we calculate the standard deviation and the correlation coefficient considering a five-year time lag. The highest cost associated with each fuel price and capital cost is considered to be its worst-case value.

5.2.1 Criteria for investigating uncertainty

The six criteria shown in Figure 3.3 are applied to each selected uncertain parameter in the US energy system. We use an ‘if-else’ strategy to choose the data for each parameter. For example, if the criteria P1

is not satisfied then we move to criteria P2. For characterizing the uncertainty in the investment cost of relatively new technologies, we use criteria P1-P4. Criteria P2, P5 and P6 are used for the uncertainty characterization of fuel cost as follows.

P1: Can we obtain a range from the Open EI data? Open Energy Information (EI) is a platform created and managed by NREL (NREL, 2019) that collects energy-related data from various national labs, agencies, journal chapters and experts. They act as a reliable platform for gathering power plant and transportation sector investment cost data from various sources. We use the data published after 2010 since Open EI has very few studies that provide data prior to 2010. Not all the studies provide data for all our model time periods, which extend from 2017 to 2050. Hence, we collect the worst case values, i.e., the highest value of the parameter projection given in the literature for 2020 and 2050. We assume that 2017 investment cost and fuel cost is certain since it is a historical year. For the remaining time periods, we linearly interpolate the upper bound for the uncertain investment cost parameter from 2020 and 2050 values.

P2: Is the range proposed in the literature? In some cases, uncertainty ranges for key parameters are provided. For example, open EI does not report biomass feedstock costs. However, Moret et al. (2019) reports the uncertainty bound for the feedstock. If the case study is not for the United States, then we look at case studies for other countries.

P3: Can we obtain the range from NREL? If the data for the group of the technologies cannot be obtained by P1 or P2, then we check the ATB report provided by NREL. The ATB report gives the investment cost values for electric generating technologies for 3 scenarios – low, medium and constant. We treat the ‘constant’ scenario as the upper bound for the uncertain investment cost parameter that falls in this category.

P4: What if the data for the parameter is not readily available? Data for some of the groups of the parameters is not readily available. As a result, we divide these parameters in two groups: relatively new technologies and mature technologies. We then characterize the uncertainty for these parameters based on the other technologies that are in a similar research phase. The majority of the residential, commercial and industrial sector technologies have been well developed over several decades. Moreover, LPG vehicles and aviation technologies are also well developed. As a result, we assume that all the technologies in these sectors fall under the ‘mature technology’ category. Technologies related to power-to-X and biofuels are still in the research phase. Therefore, they are categorized as ‘relatively new’. This technology categorization involves judgment and should be iteratively refined over time. We follow the methodology proposed in Moret et al. (2019) to determine the worst-case investment cost for both new and mature technologies. We choose a representative technology based on data availability. The uncertainty bounds for all the mature technologies is then set as per the uncertainty bound of the representative technology. For the US database, natural gas boiler technology is chosen as a representative technology. From the available

data for natural gas boilers, we find that the worst case value is 21.6% higher than its nominal value. Hence, the upper bound for all mature technologies is set at 21.6% above their nominal values. We apply a similar methodology for the relatively new technology category with solar PV as a representative technology.

P5: *Is the range available in AEO forecast?* We use this category for determining the fuel price uncertainty. AEO provides the fuel prices for 8 different scenarios. The scenario that gives the highest price for a given fuel is used as the worst case value. This scenario provides the upper bound for the uncertain parameter.

P6: *Can we determine the range from the historical data?* If the AEO does not provide the upper bound for the fuel, then the historical upper bound is set as the worst case value of the fuel. For the US database, only uranium falls in this category. The upper bound for this fuel remains the same through the time horizon.

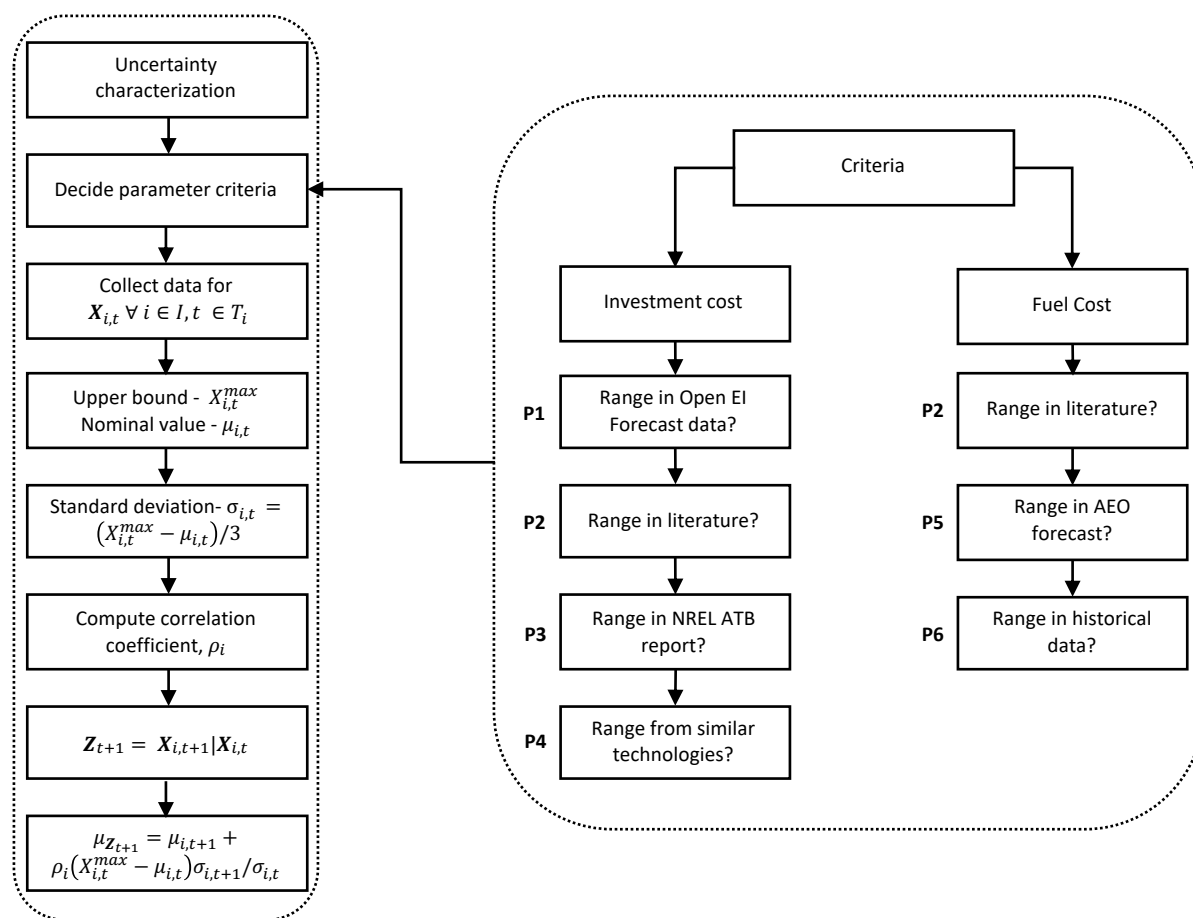


Figure 3.3: Uncertainty characterization: six criteria are used to select uncertain parameter values in the model. Each criterion corresponds to a different method for investigating the uncertainty of the parameter and the correlation coefficient.

The results obtained from the above analysis are summarized in the following Table 3.2.

Table 0.1: Application of uncertainty characterization method to the US energy system model. We divide 2224 parameters in 22 categories.

Category	Criteria (section 5.2.1)						Correlation (section 5.2.2)		By type
	P1	P2	P3	P4	P5	P6	Forecast	Hist. data	
Investment cost									
New coal		✓					✓	✓	✓
Natural gas		✓					✓	✓	✓
Nuclear		✓					✓	✓	
Solar		✓					✓	✓	✓
Wind		✓					✓	✓	
Storage			✓				✓		
Biopower		✓					✓	✓	
Electric vehicles		✓					✓	✓	
Diesel		✓					✓	✓	
Diesel hybrid		✓					✓	✓	
Gasoline		✓					✓	✓	
Gasoline hybrid		✓					✓	✓	
PHEV		✓					✓	✓	
Relatively new				✓			-	-	
Mature technologies				✓			-	-	
Fuel price									
Natural gas					✓			✓	
Coal					✓			✓	✓
Oil					✓			✓	✓
Biomass	✓							✓	
Nuclear						✓		✓	

5.2.2 Correlation coefficient

We assume that the unit price of fuel and investment cost of technology are subject to uncertainty. We follow different methodologies to obtain data for computing correlation for fuel prices and investment costs. First, we model the temporal correlation ρ_i for fuel price i using the correlated RO (CR-ESOM) formulation. To represent the real-world correlation, we use historical fuel price data from AEO (2018). The time horizon for the US database extends to 2050 with 5 year time periods. Hence, we consider the data for the last 50 years, i.e., since 1970 and compute the autocorrelation with a 5-year lag to match the length of future model time periods. Data for the sub-bituminous coal is available from 1979. No historical

data for industrial coal was obtained, therefore, the weighted average of bituminous, sub-bituminous and lignite coal was used to determine the correlation coefficient for the industrial coal price. The share of bituminous, sub-bituminous, and lignite coal in 2017 was 46.6%, 46.4% and 8.1% respectively. Auto-correlation between the uncertain fuel price parameters is given in Table 3.3.

Table 0.1: Correlation between uncertain parameters used for formulation in 3.2.

Fuel	Correlation	Data	Reference
Natural Gas	0.5798	1970 -	http://www.eia.gov/dnav/ng/ng_pri_sum_dcu_nus_a.htm
Bituminous coal	0.3857	1970 -	https://www.eia.gov/totalenergy/data/annual/showtext.php?t=ptb0709
Lignite coal	0.3492	1970 -	https://www.eia.gov/totalenergy/data/annual/showtext.php?t=ptb0709
Sub bituminous coal	0.871	1979 -	https://www.eia.gov/totalenergy/data/annual/showtext.php?t=ptb0709
oil	0.3015	1970 -	https://www.eia.gov/totalenergy/data/annual/showtext.php?t=ptb0523
Industrial coal	0.6017	-	Weighted average of the other types of coal (2017 share – Bituminous coal - 46.6%; Sub Bituminous coal – 46.4%; Lignite coal – 8.1%)
Biomass	0.5868	1970 -	https://www.macrotrends.net/2531/soybean-prices-historical-chart-data
Nuclear	0.6701	1981 -	https://www.eia.gov/totalenergy/data/browser/index.php?tbl=T08.02#/?f=Aandstart=1949andend=2018andcharted=10-11

Next, we consider the uncertainty in investment cost. Similar to the correlation in fuel prices, the investment cost of technology i also experiences temporal correlation. For example, the investment cost of solar PV has been decreasing for the last few years. As a result, it will likely decrease for the next several years. To find the correlation for technology investment costs, we use historical data collected by Open EI (NREL, 2019). However, for some technologies, the historical data collected by Open EI is not sufficient to compute correlation. Consequently, we also include future projection data through 2050 for computing the correlation of all technologies with investment cost uncertainty. The resultant correlation coefficients for the 22 groups of technologies is given in Table 3.4. For simplicity, we assume that the temporal correlation for mature technologies is 100%, such that when a mature technology takes on its worst-case value in a particular time period, it retains that worst-case value for all preceding and subsequent time periods.

Table 0.2: Correlation coefficient for the 22 groups of technologies. For technologies consuming coal, natural gas and solar, we have access to data by technology type.

Category	Type	Correlation coefficient
New coal	Coal IGCC	0.334
	Coal IGCC CCS	0.547
Natural gas	NG ACC	0.135
	NG ACC CCS	0.644
	NG ACT	0.527
Nuclear	-	0.597
Solar	Solar PV	0.534
	Solar TH	0.809
Wind	-	0.309
Storage	-	0.996
Biopower	-	0.752
Electric vehicles	-	0.691
Diesel	-	0.174
Diesel hybrid	-	0.606
Gasoline	-	0.597
Gasoline hybrid	-	0.108
PHEV	-	0.233
Relatively new	-	0.534
Mature technologies	-	1

5.2.3 Determining the effects of correlation on the uncertain parameters

If the fuel price in time period t assumes the worst case value, it affects the fuel price for the entire time horizon. For the CR-ESOM formulation we assume that the fuel price in time period t is a normally distributed random variable, $\mathbf{X}_{i,t}$ with mean, $\mu_{i,t}$, given by the AEO 2019 reference case values. AEO 2019 provides fuel prices for 8 scenarios. The scenario with the highest fuel price is considered as a worst case scenario for each of the fuel price parameter, $X_{i,t}^{max}$.

$\mathbf{X}_{i,t}$ is correlated with $\mathbf{X}_{i,t+1}$, with a correlation coefficient given in Table 3.3. Assuming that both $\mathbf{X}_{i,t}$ and $\mathbf{X}_{i,t+1}$ are normally distributed random variables, $\mathbf{Z}_{t+1} = \mathbf{X}_{i,t+1} | \mathbf{X}_{i,t}$ is also a normally distributed random variable with $\mu_{\mathbf{Z}_{t+1}} = \mu_{i,t+1} + \rho_i (X_{i,t}^{max} - \mu_{i,t}) \sigma_{i,t+1} / \sigma_{i,t}$. The mean of \mathbf{Z} , $\mu_{\mathbf{Z}_{t+1}}$, provides the value of $\mathbf{X}_{i,t+1}$ given that $\mathbf{X}_{i,t}$ assumes the worst-case value, $X_{i,t}^{max}$. Similarly, the value of $\mathbf{X}_{i,t+2}$ given the value of $\mathbf{X}_{i,t}$ is given by $\mu_{\mathbf{Z}_{t+2}} = \mu_{i,t+2} + \rho_i (\mu_{\mathbf{Z}_{t+1}} - \mu_{i,t+1}) \sigma_{i,t+2} / \sigma_{i,t+1}$. Note that $t + 1$ corresponds to the next time period and $t + 2$ to the time period after that. The same procedure can be applied for previous time

periods. The computation of $\mu_{Z_{t+1}}$ requires the data for the standard deviation, $\sigma_{i,t}$, of the random variable. Since we are assuming that $X_{i,t}$ is normally distributed, the standard deviation can be given as $\sigma_{i,t} = (X_{i,t}^{max} - \mu_{i,t})/n$ where, n depends on $X_{i,t}^{max}$. If the worst case fuel price, $X_{i,t}^{max}$, provided by AEO 2019 is beyond 99.7 percentile of the normal distribution, i.e. 3 standard deviations away from the mean, the standard deviation $\sigma_{i,t}$ of a fuel i in time period t is given by $(X_{i,t}^{max} - \mu_{i,t})/3$. However, since we need the ratio of standard deviation, $\sigma_{i,t+1}/\sigma_{i,t}$, we do not need to know the exact value of n . The mean of the random variable Z can be given as (14).

$$\mu_{Z_{t+1}} = \mu_{i,t+1} + \rho_i (X_{i,t}^{max} - \mu_{i,t}) (X_{i,t+1}^{max} - \mu_{i,t+1}) / (X_{i,t}^{max} - \mu_{i,t}) = \mu_{i,t+1} + \rho_i (X_{i,t+1}^{max} - \mu_{i,t+1}) \quad (14)$$

The CR-ESOM formulation given in (13)-(13e) requires the computation of $g_{\tilde{t},\tilde{v},i,v,t}^{VC}$ as an input parameter. As per the above computations $g_{t+1,t,i,t,t}^{VC}$ can be computed using (15), where, $\tilde{v} == v == t$.

$$g_{t+1,t,i,t,t}^{VC} = \mu_{Z_{t+1}} / \mu_{i,t+1} \quad (15)$$

Figure 3.4 shows an example of the coal prices over the time horizon given that the worst case occurs in every time period.

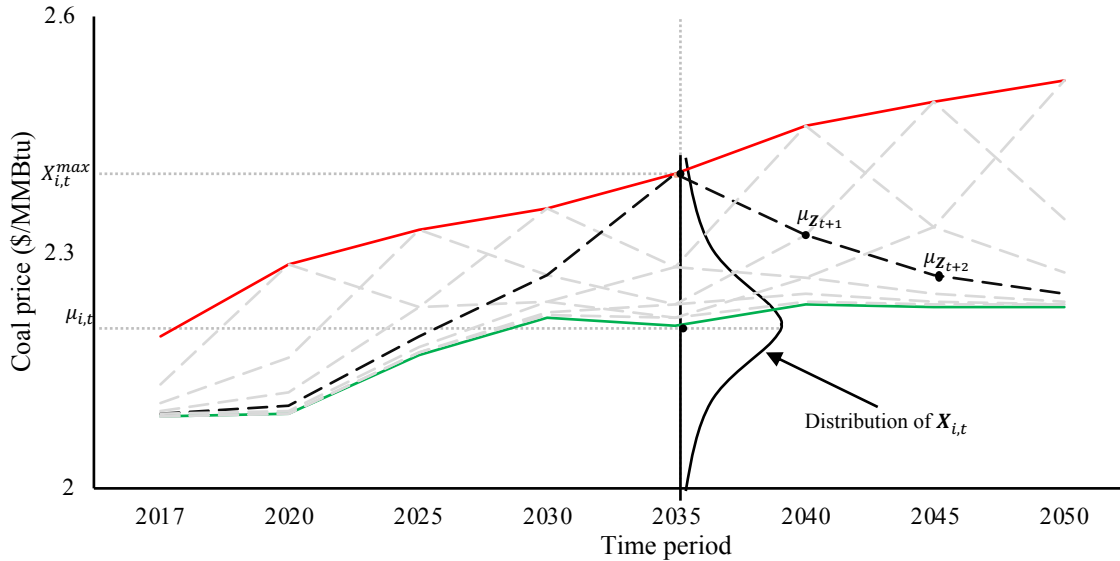


Figure 3.4: Effect of the correlation in coal prices. The red line shows the worst case values from the AEO 2019 while the green line shows the reference case values.

5.3 The uncertainty set

Table 3.5 below provides the percent increase in the nominal value of the uncertain investment cost parameter in the worst case scenario. We vary the upper bound of an uncertain parameter by time period since the uncertainty bounds for the parameter, as obtained from the historical data or open EI or literature, varies over time.

Table 0.1: Uncertainty set for the US energy system. Abbreviations: Natural Gas (NG), Integrated Gasification Combined Cycle (IGCC), Advanced Combined Cycle (ACC), Carbon Capture and Sequestration (CCS), Photovoltaic (PV), Thermal (TH).

Category	Type	Correlation coefficient	Increase in nominal value (%)	
			2020	2050
New coal	Coal IGCC	0.334	103.6	103.6
	Coal IGCC CCS	0.547	99.0	84.9
Natural gas	NG ACC	0.135	46.6	47.1
	NG ACC CCS	0.644	164.9	203.9
Nuclear	NG ACT	0.527	70.3	38.9
	-	0.597	61.3	89.4
Solar	Solar PV	0.534	99.0	131.3
	Solar TH	0.809	85.4	75.1
Wind	-	0.309	56.6	76.2
Storage	-	0.996	44.4	53.1
Biopower	-	0.752	175.1	202.0
Electric vehicles	-	0.691	67.0	68.3
Diesel	-	0.174	51.8	69.0
Diesel hybrid	-	0.606	41.3	21.7
Gasoline	-	0.597	58.2	63.6
Gasoline hybrid	-	0.108	56.4	61.7
PHEV	-	0.233	61.6	75.1
Relatively new	-	0.534	99.0	131.3
Mature technologies	-	1	21.6	21.6

Table 3.6 provides the same information for the fuel cost uncertainty. The AEO provides future projection of natural gas and oil by type, however, sector and type wise historical data for computing correlation coefficient is not readily available. As a result, correlation coefficient remains the same over all types of natural gas and oil.

Table 0.2: Uncertainty set for fuel prices. Abbreviations: Commercial (Com), Residential (Res), Industrial (Ind.), Electric (Elc.), Transportation (Trn.), Distillate Fuel Oil (DFO), Residual Fuel Oil (RFO), Gasoline (GSL), Propane (LPG), Diesel (DSL), Jet fuel (JTF), Sub (S).

Category	Type	Increase in nominal value (%)							
		2017	2020	2025	2030	2035	2040	2045	2050
Natural gas	Com.	0.0	5.5	9.4	15.7	18.0	20.6	21.9	26.1
	Elc.	0.0	15.7	26.3	41.4	44.8	49.6	50.4	60.8
	Ind.	0.0	14.9	25.0	39.7	44.3	49.5	51.3	59.3
	Res.	0.0	4.5	7.5	12.4	14.2	16.2	17.3	20.7
	Trn.	0.0	4.2	4.2	14.2	16.7	19.6	21.5	26.2
Coal	Bituminous	4.8	9.1	7.3	6.3	8.8	10.2	11.7	12.8
	Lignite	4.8	9.1	7.3	6.3	8.8	10.2	11.7	12.8
	S. Bituminous	4.8	9.1	7.3	6.3	8.8	10.2	11.7	12.8
Oil	Industrial	0.0	2.4	4.5	3.9	4.0	3.5	4.0	4.6
	Com. DFO	0.0	0.0	39.2	72.4	64.8	65.7	65.7	75.5
	Com. LPG	0.0	38.9	71.0	73.9	63.5	59.7	59.1	60.3
	Com. RFO	0.0	72.9	112.3	103.1	101.3	97.8	99.1	109.8
	Ind. DFO	0.0	39.4	72.1	65.0	65.8	65.9	69.8	76.1
	Ind. GSL	0.0	36.8	56.2	52.7	51.6	51.1	53.4	53.2
	Ind. LPG	0.0	57.2	100.1	104.0	88.2	83.1	82.1	84.2
	Ind. RFO	0.0	79.9	89.0	83.3	83.0	81.0	82.7	88.1
	Res. DFO	0.0	37.7	58.9	54.3	55.5	55.6	58.8	63.9
	Res. LPG	0.0	28.4	78.9	90.9	80.9	74.2	72.8	73.7
	Trn. DSL	0.0	36.1	59.2	53.8	54.6	55.1	59.0	64.8
	Trn. GAS	0.0	36.1	56.1	52.2	51.1	50.7	53.0	52.7
	Trn. JTF	0.0	48.8	84.3	75.7	77.0	76.9	79.3	83.8
	Trn. LPG	0.0	36.0	62.6	63.4	54.5	51.7	51.2	52.4
	Trn. RFO	0.0	64.6	120.9	106.3	96.4	91.7	96.3	92.8
Biomass	-	3.0	3.0	3.0	3.0	3.0	3.0	3.0	3.0
Nuclear	-	1.7	1.7	1.7	1.7	1.7	1.7	1.7	1.7

6 Robust optimization results

We begin by solving the CR-ESOM formulation for the budget of uncertainty varying from 0 to 100%. The total number of uncertain parameters considered for the analysis is $N = 2224$. We then calculate the probability of constraint violation as given in section 3.2.1 (see Figure 3.2 for reference). In this section, we provide insights specifically for the US energy system under emission mitigation target. However, the

same methodology can be applied for obtaining robust strategies under various different objectives for energy systems on any scale.

6.1 Value of the robust optimization

Figure 3.5 presents the total system cost under three different scenarios versus the budget of uncertainty (Γ), which represents the percentage of uncertain parameters that assume their worst-case (WC) value. In both the worst-case (WC) and nominal (NM) scenarios, the RO formulation is solved, and the optimized capacity and activity values are fixed. In the WC scenario, the total system cost is calculated assuming that a progressively larger number of uncertain parameters take on their worst case values, as indicated by the budget of uncertainty. In the NM scenario, the total system cost reflects the case where the worst case values actually correspond to the nominal values. Thus, the NM case represents a situation where we optimize assuming worst-case, but the realized values correspond with the nominal values. In the naïve scenario, the model optimizes assuming no future uncertainty, and the optimized capacity and activity values are fixed under these naïve assumptions. Then, as in the WC case, the total system cost is calculated assuming that a progressively larger number of uncertain parameters take on their worst case values.

For any robust solution exceeding a 7% budget of uncertainty, the probability (ϵ) that the total system cost of the robust solution exceeds the worst-case value of the robust solution (Robust WC cost) is practically zero. Hence, there is little economic incentive to choose a solution with higher robustness. Now, a naïve solution is the one which does not consider any uncertainty. As shown in Figure 3.5, the naïve solution is clearly more expensive than the robust solution regardless of the budget of uncertainty. In addition, the robust solution is more expensive than the naïve solution if no parameters assume their worst case value. However, the downside risk is lower than the upside risk: at a 7% budget of uncertainty, the robust solution will only cost 6% more than the naïve solution if no parameters assume their worst case value, but the naïve solution may be 91% higher than the robust solution if 7% of the uncertain parameters assume their worst case value.

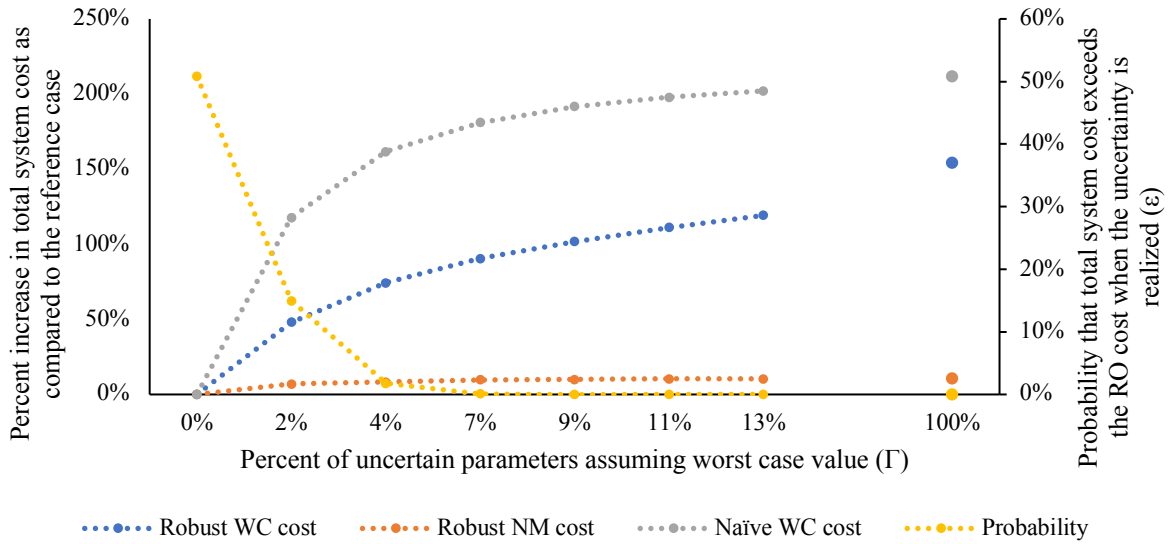


Figure 3.5: Percent change in objective function as a function of budget of uncertainty. Abbreviations: Worst Case (WC), Nominal (NM). ‘Naïve WC cost’ represents the cost of the naïve solution as the budget of uncertainty increases; ‘Robust WC cost’ represents the same for the robust solution; ‘Robust NM cost’ represents cost of robust solution if all uncertain parameters assume their nominal value.

6.2 Solution quality of robust vs. naïve solution

For this analysis, we investigate the investment cost decisions when the budget of uncertainty is set equal to 7%, since Figure 3.5 indicates that there is a nearly zero probability of exceeding the RO cost in this case. We plot the Monte Carlo simulation results, which are based on 1000 runs. All uncertain parameters are selected for inclusion in a suite of Monte Carlo simulations that indicate how the total system cost may change under different realizations of the uncertain parameters. From this analysis, we compare the quality of the robust solution to the naïve solution under potential future realization of uncertain parameters. This approach allows us to estimate the economic savings associated with following a robust versus naïve strategy. The expected cost is approximately equal to the area under the curve given in Figure 3.6. The expected cost of the RO solution, μ_{rob} , is 5.5% lower than the expected cost of the naïve solution, μ_{det} . The standard deviation for the total system cost obtained by solving CR-ESOM is 7% of the mean, μ_{rob} , while for the naïve ESOM it is 7.5% of the mean, μ_{det} . Thus, making the investment decision considering the future uncertainties yields significant economic benefits.

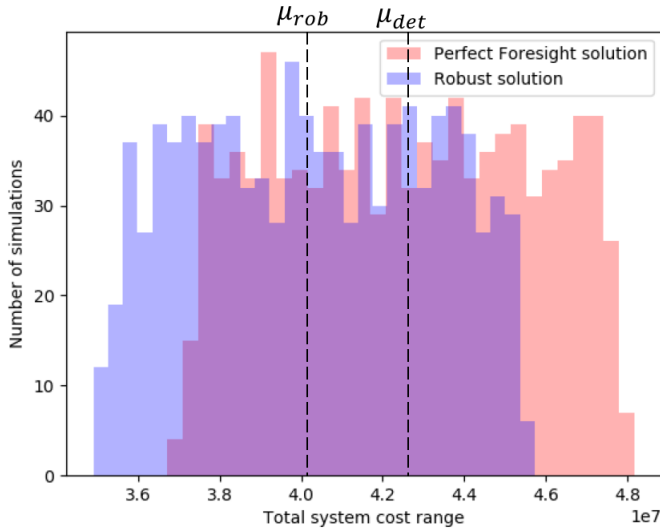


Figure 3.6: Distribution of system cost for naïve and robust solution under uncertain parameter realizations.

6.3 Robust emission mitigation pathways considering future uncertainty

Figure 3.7 shows the change in the energy system activity in three representative time periods spanning the modeled time horizon under different robustness assumptions. The 0% budget of uncertainty represents the naïve solution under Obama’s Mid Century Strategy (MCS), while 100% represents the most robust solution, which hedges against the scenario where all uncertain parameters assume their worst-case (WC) value. The first RO formulation proposed by Soyster (1973) only provides the WC RO solution. However, the revised methodology by Bertsimas and Sim (2004) allows us to identify the solutions obtained for a medium budget of uncertainty. For T varying between 0 to 24% with 2% steps, the RO approach encourages the diversification of resources to hedge against uncertainty. These solutions do not emerge in the more traditional Soyster (1973) approach. For a budget of uncertainty greater than 24%, the RO solution remains relatively constant. A similar result is observed for the numerical simulations presented by Bertsimas and Sim (2004). In Figure 3.7, we vary the budget of uncertainty from 0 to 24% to observe the robust technology deployment options available to decision makers based on their risk tolerance.

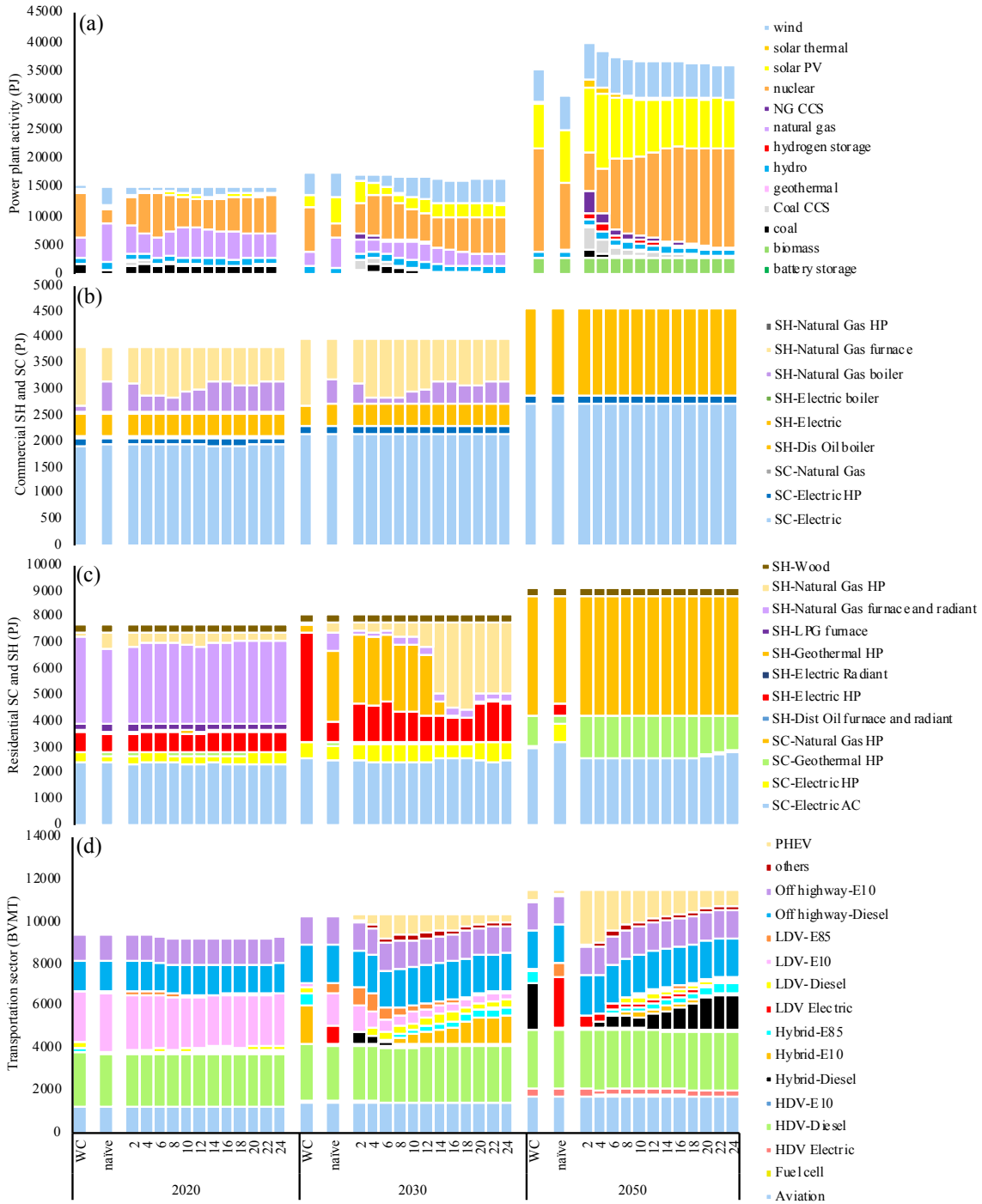


Figure 3.7: Activity of technologies in different sectors as a function of the budget of uncertainty and time period: (a) electricity generation, (b) commercial space cooling and heating, (c) residential space cooling and space heating, and (d) transportation. The ‘WC’ stacked bars represent the technology activity in a given sector and time period under the worst-case outcome, and ‘naive’ represents the reference scenario where uncertainty is ignored.

The composition of the energy system changes dramatically when we account for uncertainty. In Figure (3.7a), the naïve solution with an emission target set forth by Obama’s MCS achieves 40% electricity generation by nuclear power plants. However, the robust solution suggests diversifying the sources of electricity generation. Carbon Capture and Sequestration (CCS), underground hydrogen storage, and solar thermal play a more significant role to achieve a robust technology mix even though these technologies are not cost optimal in the naïve case. In other words, if we assume a rational, cost-minimizing decision maker, that ignores future uncertainty, then the optimal technology mix would not include these technologies. The relative capacity of the technologies, however, depends on the decision maker’s tolerance towards risk. For example, with increased budget of uncertainty, the investment in new CCS decreases while investment in new nuclear increases. Bertsimas and Sim (2004) observe similar results whereby the diversity of the solution decreases with higher budgets of uncertainty. The rationale behind this observation is that $\Gamma = 100\%$, solving the RO model is equivalent to solving a deterministic model where all cost parameters are at a worst case value. As a result, the model chooses the least-cost option instead of diversifying the resources. Overall electricity generation in 2050 increases by approximately 20% in the robust solution as compared to the naïve solution. However, the focus of electrification is shifted from the transportation to the industrial sector. The RO solution also suggests delaying some investments in wind and solar generation until 2030, due to high investment cost uncertainty. Instead, the required emission reduction is achieved using nuclear power plants and CCS. Note that this insight is driven by our selection of worst-case values. With the increase observed in CCS, the robust solution suggests delaying the retirement of coal power plants even though natural gas combined cycle power plants are cheaper to operate. The main reason behind this shift is the multiple types of coal that can be fed into the coal power plant, and the relative variation in coal prices is lower than the variation in natural gas prices. Since the robust solution tends to diversify the resource base, the retirement of coal is delayed until 2030. After 2030, with the reduced uncertainty in the cost of renewable generation, coal is replaced by solar PV and wind.

Figure 3.7(b) and 3.7(c) plot the changes in space heating and space cooling for commercial and residential sectors, respectively. The technology mix for both the sectors in 2050 is robust, however, in earlier time periods, increasing electrification and heat pumps leads to a more robust solution. De Villiers et al. (2000) show a similar solution suggesting mitigating emissions from the residential sector by increasing electrification. Moreover, the electrification in the residential sector is partially shifted from water heating to electric heat pumps due to high variability in natural gas prices. Water heating via electric heat pumps is replaced by solar water heating after 2025.

The transportation sector, plotted in Figure 3.7(d), experiences more drastic changes under uncertainty compared to the residential and commercial sectors. The first significant shift from the naïve solution is reducing the dependency on electric cars alone and replacing it with PHEVs and hybrid vehicles. The robust strategy shifts the required emissions reductions from the transportation sector to other sectors. The model results indicate that the desired share of PHEVs and hybrid vehicles depends on the decision maker's tolerance towards risk. As mentioned above, the diversity of the resources in the robust solution tends to decrease for higher budget of uncertainty. Consequently, the share of emissions reduction achieved by each sector depends on the decision maker. The naïve solution suggests focusing on the transportation sector for emissions reductions; however, the robust strategy, prioritizes the electrification of process heating in the industrial sector over investment in electric vehicles. Since the process heating technologies in the industrial sector have conservative worst-case values, the model tends to choose them over electric cars, which have a wider potential cost range. This observation illustrates a broader point: the results are contingent on how the worst-case values are calibrated. Many technologies lack a detailed cost range, and under a conservative assumption about their worst-case value, can be over emphasized by the model. A critical focus of this work needs to be an extended effort to develop an improved representation of uncertain input parameters. Section 6.4 outlines a method to target the most sensitive input parameters in the model.

6.4 Importance of a parameter in achieving a robust solution

For a given budget of uncertainty, Γ , CR-ESOM determines the uncertain parameters, among all 2224 uncertain parameters considered for this analysis, that produce the highest impact on the total system cost. Obtaining the most impactful parameters helps to identify the parts of the energy system that are most sensitive. Improved characterization of these most sensitive parameters by gathering better data could help achieve a robust strategy. To do so, we sort the shadow prices of the constraints, corresponding to the uncertain variables, in decreasing order in the robust formulation. Specifically, we combine the $\mathbf{y}_{\bar{v},i}^{IC}$ and $\mathbf{y}_{\bar{t},\bar{v},i}^{VC}$ vectors and put them in decreasing order, since higher values of y lead to a higher impact of the uncertain parameter in the cost function. The higher the shadow price, the higher the impact of the uncertain parameter on the objective function. We plot the parameters corresponding to the highest $\mathbf{y}_{\bar{v},i}^{IC}$ and $\mathbf{y}_{\bar{t},\bar{v},i}^{VC}$ in Figure 3.8. From bottom to top, the importance of the parameter increases. From left to right, the robustness of the solution increases. For example, for the budget of uncertainty = 1, a parameter in the transportation sector influences the objective function the most (top-left corner). For a budget of uncertainty = 50, i.e., for $\Gamma = 2.2\%$, solar PV investment cost becomes the most influential parameter (top-right). As we move down a column in the triangle, corresponding to a given budget of uncertainty, the importance of the parameter in determining the robust solution decreases. For example, at $\Gamma = 2.2\%$, the investment cost uncertainty

related to solar water heating in the commercial sector (far right-bottom) is less influential in determining the robust solution than the investment cost of solar PV (top-far right). This result also suggests that resolving the uncertainty in solar PV investment cost would assist more in achieving a robust strategy. Furthermore, if the uncertainty is irreducible through improved data analysis, then at least the parameter range and autocorrelation should be well-calibrated. Other critical costs are the investment cost of some light duty vehicle technologies, particularly PHEV, coal with CCS, biomass IGCC with CCS, nuclear, hydrogen electrolysis, and synthetic natural gas production. The low carbon technologies in the electric sector tend to have a higher impact on the objective function than the high carbon emission technologies.

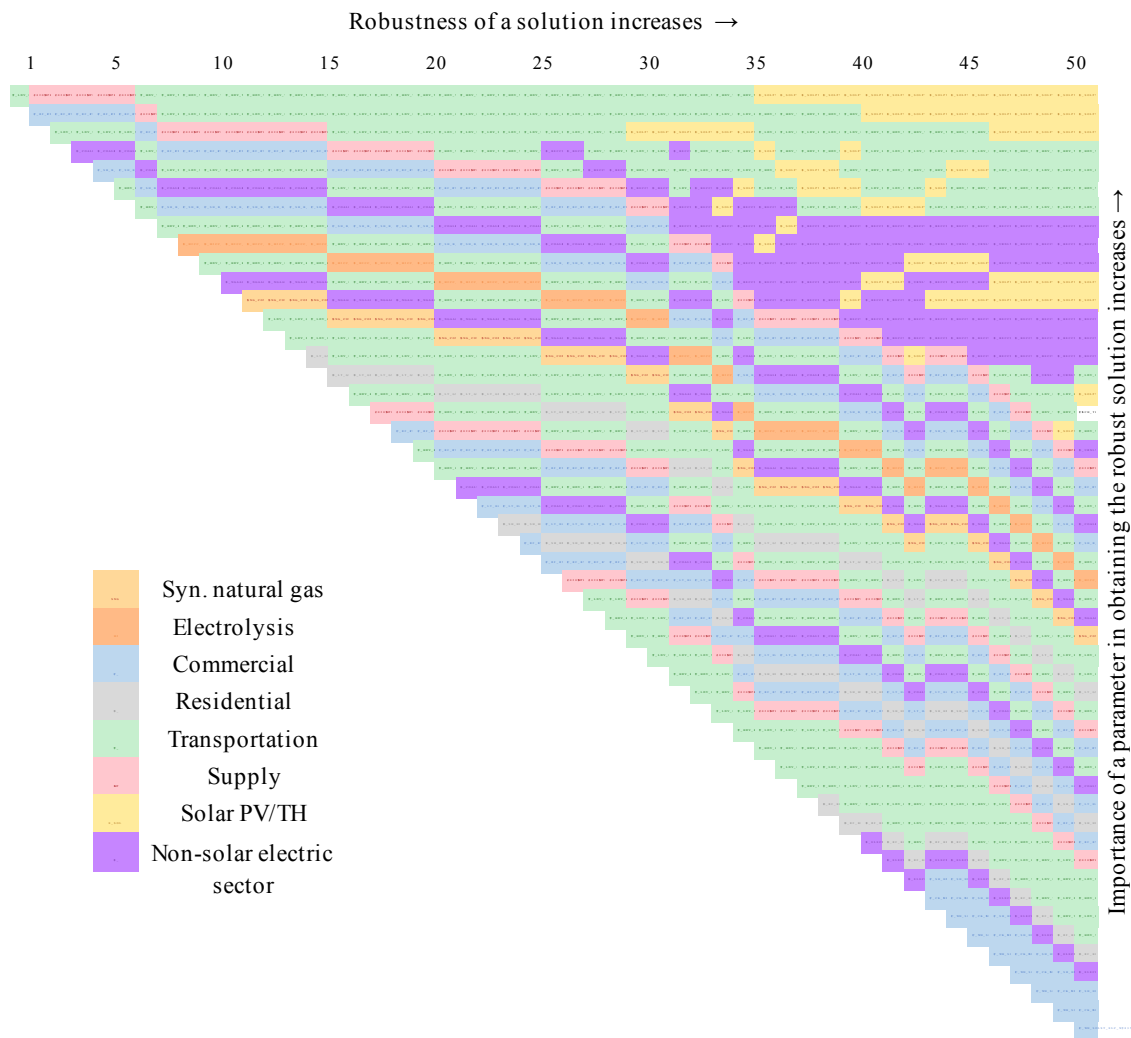


Figure 3.8: Sensitivity of the sectors as a function of budget of uncertainty. The importance of a category increases as we move from bottom to top and robustness of a solution increases as we move from left to right. Abbreviations: Synthetic (Syn.); Photovoltaic (PV); Thermal (TH).

7 Conclusions

Highly uncertain input data is a reality of using ESOMs. Since the insights obtained from such models are often used to inform policy, the uncertainties should be considered to build robust strategies. The main goal of this chapter is to find GHG emission mitigation pathways that are robust to uncertainties related to future fuel prices and investment costs. The second goal of this chapter is to provide a methodology to obtain a robust solution that considers temporal autocorrelation in parameter values.

Building on previous ESOM-related work, we introduce a robust optimization framework that is the first to consider the temporal autocorrelation (CR-ESOM) in uncertain parameters. Because most input parameters are indexed by time period, it is important to consider how the assumption of a worst-case value achieved in a particular time period affects the value of that parameter in other time periods. Ignoring autocorrelation can diminish the effect of any single worst-case value realized in a single time period. The robust solution suggests diversifying the resource for satisfying energy demand and encouraging investment in wide range more expensive technologies with low carbon emissions.

Several open issues deserve further investigation. First, the process of estimating autocorrelation associated with uncertain parameters needs improvement. For some parameters, data for computing autocorrelation is limited. For example, to compute the correlation coefficient for industrial coal, we use the weighted average of the other types of coal. For future work, sensitivity analysis for the correlation coefficients is needed to ensure the robustness of the strategy. Second, the formulation in this chapter only considers autocorrelation for uncertain parameters but does not consider the correlation between different uncertain parameters, which might exist in the real world. Though such a formulation can be written as a natural extension of model (13)-(13i), it is not given in this chapter. Third, we assume the uncertain parameters are a normally distributed random variable for constructing the uncertainty set. However, the CR-ESOM formulation itself ignores information about the distribution of the parameter and merely works with the nominal value and parameter deviation. Fourth, the data and methodology used to determine the ranges for uncertain parameters needs to be refined. Figure 3.8 can serve as a guide to prioritize future data collection efforts. Given the data intensive nature of ESOMs generally and this RO method specifically, it would be beneficial to make this data gathering a community effort, with contributions and critical reviews provided by a broad array of modelers and analysts.

Despite the daunting task of quantifying the uncertainty for solving the robust optimization model, it can provide valuable insights to policymakers who must act before uncertainty is resolved. While further research is needed to improve the construction of uncertainty set and the underlying data, the simplicity and

computational tractability of RO can be an essential tool for uncertainty analysis in ESOMs. While the application of robust optimization yields a hedging strategy, this analysis should nonetheless be viewed as an exercise to explore the decision space when the parametric uncertainty is explicitly considered. In addition, we emphasize that models alone cannot provide a solution in such complex decision landscapes but can yield insight that informs decision making. Moreover, changed in the uncertainty set, emissions mitigation target ,or policy objectives can significantly change the insights obtained from the above analysis.

Chapter 4 Substitution between Energy Efficiency and Electricity in an Energy System Optimization Model

A. Abbreviations

<i>ESOMs</i>	<i>Energy System Optimization Models</i>
<i>CPP</i>	<i>Clean Power Plan</i>
<i>EPA</i>	<i>Environmental Protection Agency</i>
<i>Temoa</i>	<i>Tools for Energy Model Optimization and Analysis</i>
<i>CES</i>	<i>Constant Elasticity of Substitution</i>

B. Indices

t	<i>Index of model time period</i>
i	<i>Index for technology type</i>
v	<i>Index of technology vintages</i>

C. Sets

I	<i>Technologies</i>
V_i	<i>Vintages of technology i</i>
T_i	<i>Time periods in which technology i is active</i>
T	<i>All time periods</i>

D. Parameters

α	<i>Energy efficiency productivity in the production of energy services</i>
σ	<i>Elasticity of substitution between electricity and energy efficiency</i>
ϵ	<i>Price elasticity of energy service demand</i>
$\gamma_{i,t,v}$	<i>Emission activity in time period t</i>
$P\theta_t$	<i>Energy efficiency marginal cost in time period t</i>
PE_t^0	<i>Electricity reference price in time period t corresponding to E_t^0</i>
E_t^0	<i>Electricity demand reference in time period t</i>
φ_t	<i>Constant derived from E_t^0 and PE_t^0</i>
ES_t^{\min}	<i>Lower bound of energy service demand</i>

B	<i>Coefficients of all the other ESOM' constraints</i>
b	<i>Right hand side of all the other ESOM' constraints</i>
$IC_{i,v}$	<i>Nominal investment cost</i>
$FC_{i,v,t}$	<i>Nominal fixed cost</i>
$VC_{i,v,t}$	<i>Nominal variable cost</i>
$\delta_{i,v,t}$	<i>Conversion from capacity to activity</i>
$Demand_t$	<i>Demand in time period t</i>
β	<i>Efficiency credit (ranges from 0.0 - 1.0)</i>
$\zeta_{i,v,t}$	<i>Factor converting $CAP_{i,v}$ to $ACT_{i,v,t}$</i>

E. Variables

$CAP_{i,v}$	<i>Capacity</i>
$ACT_{i,v,t}$	<i>Activity</i>
X	<i>All other variables</i>
E_t	<i>Quantity demanded of electricity in time period t</i>
θ_t	<i>Energy efficiency amount required in time period t</i>
PE_t	<i>Electricity price in time period t</i>
P_t	<i>Marginal price of energy service demand in time period t</i>
ES_t	<i>Energy service demand in time period t</i>

F. Functions

$Q(Y)$	<i>Quantity demanded of Y</i>
$P(Y)$	<i>Price of Y</i>
$f(E, \theta)$	<i>Dummy function used for explaining elasticity of substitution</i>
U	<i>Utility function</i>
e	<i>Expenditure function</i>
$g(ES)$	<i>Dummy function used for explaining utility of energy services</i>

1 Introduction

During the last few decades, energy efficiency started to play a central role in the design of policy goals related to energy security, economic growth, and environmental sustainability. Strong efficiency gains have shown a significant impact on global energy demand, reducing consumers' energy bills, holding back emissions growth (IEA, 2017), and making energy systems more secure by reducing the dependency on

energy imports (Gillingham et al., 2009). In the current environment, advocates of ambitious climate policies often support simultaneously imposing a price on carbon and alternative policies, such as the renewable portfolio standards, which also credit energy efficiency (Baranzini, et al. 2015). Crediting of energy efficiency was identified as one of the means to comply with the intensity standards under the US Environmental Protection Agency's (EPA) Clean Power Plan (CPP). Efficiency crediting policy provides an incentive for deployment of energy-efficient technologies in energy systems' expansion plans. One key effect of this policy is a reduction in electricity generation as well as a reduction in investment in electricity generation capacity expansion. Depending on various factors in the system such as efficiency cost, cost saving from emission reduction and expenditure in energy efficiency dominate each other. Reduction in electricity generation and incentive for deployment of energy efficient technologies affect the price of electricity as well as the price of energy efficiency since the quantity demanded of the good is intrinsically dependent on its price. Variation in the price of energy efficiency affects the unit price of energy services (e.g. lighting, heating, cooling). It leads to a substitution effect, which influences consumers' consumption of energy services and ultimately, energy demand.

To model these system-wide effects, historically, top-down and bottom-up approaches have been used (Van Beeck et al., 2000), and their contrasting styles have led to divergent predictions of technological change and the cost of that change (Horne, et al., 2005). Top-down approaches typically take an aggregate view of the economy and consider market distortions, income effects, and the relations between various economic agents such as households and government. By contrast, bottom-up approaches represent individual technologies so that changes in the technology mix can be modeled explicitly. Energy system optimization models (ESOMs) have typically minimized the present cost of energy supply by deploying and utilizing energy technologies over time to meet a set of exogenously specified end-use demands. Although rich in technology representation, exogenously specified end-use demands restrict the feedback effect from the consumer side. Exposing electricity end-users to varying prices inevitably results in behaviors that maximize the welfare of the consumers (Nardelli et al., 2017). In order to represent feedback effect from the consumer side, many ESOMs have replaced exogenously specified end-use demand by a demand curve which maps the quantity demanded of energy services to their market price. However, representation of consumer behavior in ESOMs is still in the early stages of development. Recent developments in the literature (DeCarolis et al., 2017; Herbst et al., 2012) have addressed fundamental limitations of energy systems models, which are the modest representation of the economy and limited treatment of human behavior.

The conventional way to handle energy efficiency policy analysis and related consumer behavior in an ESOM is to model a suite of different technologies with varying degrees of energy efficiency, market availability and technology penetration or hurdle rates. The ESOM then selects efficient technologies and the level of demand response based on price elasticities of end-use demand (Kadian et al., 2007; Božić, H., 2007). Another common tool to model higher penetration of efficient technologies is to assume efficiency ratios higher than the baseline (Yanbing, K. and Qingpeng, W., 2005). In some cases, the modeling approach simply uses technology adoption targets driven by the energy efficiency policy based on expert knowledge, (e.g., McNeil, M., 2008). While this can provide a useful prescription, it can often lead to unrealistic results. Modelers often then add hurdle rates to control the rate of efficient technology adoption, but, in general, there is a little empirical basis for the choice of the hurdle rates (DeCarolis et al., 2017). Despite these common modeling approaches, there are some recent efforts to model market heterogeneity, consumer behavior and intangible cost (Frederiks, E. et al., 2015; García, Ó. Et al., 2017). The review of modeling efforts for energy efficiency policy analysis, Mundaca, L. et al., 2010, thus concludes that the modeling and evaluation of policy instruments addressing consumer behavior through informative policy instruments remains a challenge for the modelling community.

Many complex factors that affect end-use demand, and price response is only one of them (Jones et al., 2015). In this chapter, we represent other factors that affect end-use demand such as the willingness of a consumer to reduce electricity usage by investing in energy efficient technologies and consumer's perception about how good/bad the energy service is after investing in energy efficient technology. To do so, we build on the model proposed by (Fell et al., 2017) to represent substitution effect between electricity supply and energy efficiency along with the price response for energy service demand for a capacity expansion problem. Therefore, the goal of this research is to propose a novel approach to model energy efficiency policy in a way that is theoretically consistent with the microeconomic theory in the context of ESOMs. We assume that electricity and energy efficiency are two separate means of meeting the end-use energy service demand. To do so, a partial equilibrium modeling framework is implemented with a hypothetical test case database as input. We further consider imposing a carbon tax as the first-best policy while efficiency crediting, in the form of subsidy for energy efficiency, as an alternative policy for reducing emissions. Computational experiments then determine the welfare gain from efficiency credit policy with the welfare gain from carbon tax policy. Furthermore, we perform a sensitivity analysis on selected parameters in order to analyze the effect of uncertain consumer behavior and cost of energy efficiency on the overall welfare gain. The purpose of this approach is not to perfectly forecast electricity prices but to quantify the impact of emission reduction policies on the system in a theoretically consistent manner (Fell et al., 2017). The resulting model is termed as the “energy efficiency model” throughout the chapter.

The rest of the chapter is organized as follows. Section 2 describes the ESOMs and their economic interpretation. In Section 3, we provide a mathematical formulation describing the substitution between electricity and energy efficiency. Section 4 describes a hypothetical test case used to illustrate the effects of substitution on the energy system. The first part of Section 5 analyzes the efficiency crediting policy compared to carbon tax while the second part includes sensitivity analysis for uncertain parameters. Section 6 concludes the chapter by outlining the policy implications associated with the substitution effect. Our chapter documents the algebraic model formulation and data inputs used for the simulation. We implemented this model in an open source ESOM, and the full model implementation along with the data set used for the analysis can be found in the associated Github repository (Temoa GitHub).

2 Energy System Optimization Models

For conducting analysis in this chapter, we utilize Tools for Energy Model Optimization and Assessment (Temoa) which is an open source, energy system optimization model (ESOM), similar to MARKAL/TIMES (Loulou et al., 2004), OSeMOSYS (Howells et al., 2011) and MESSAGE (IIASA, 2011). The model formulation is detailed in Hunter et al. (2013) and the Temoa source code is publicly available on Github (Github/TemoaProject) (Temoa Project, 2018).

2.1 Framework of ESOMs

ESOMs are widely used to analyze energy system capacity expansion plans and employ scenario analysis to investigate different technical, economic, and policy assumptions. The energy system is described algebraically as a network of linked processes that convert raw energy commodities (e.g., coal, oil, biomass) into end-use demands (e.g., lighting, transport, water heating) through a series of one or more intermediate energy forms (e.g., electricity, gasoline, ethanol). Each process is defined by a set of engineering, economic, and environmental characteristics (e.g., capital cost, fixed and variable operations and maintenance cost, efficiency, capacity factor, emission factor) associated with converting an energy commodity from one form to another. Processes are linked together in a network via model constraints representing the allowable flow of energy commodities. The objective of ESOMs is to minimize the net present cost of energy supply (composed by investment, operation & maintenance, fixed and fuel costs) by utilizing energy processes and commodities over a user-specified time horizon to meet a set of exogenously specified end-use demands. ESOM simultaneously make technology investment decisions and operating decisions while maintaining energy balance between primary energy resources, secondary fuels, final energy consumption and end-use energy services. ESOMs are typically formulated as linear programming models in which technology capacity are utilized to meet end-use demands.

For the exogenously specified end-use demand, a simplified form of ESOMs with the objective to minimize total system cost can be written as the following linear program.

$$\begin{aligned}
& \text{minimize } \sum_{v \in V_i} \sum_{i \in I} IC_{i,v} CAP_{i,v} + \sum_{t \in T_i} \sum_{v \in V_i} \sum_{i \in I} FC_{i,v,t} CAP_{i,v} + \sum_{t \in T_i} \sum_{v \in V_i} \sum_{i \in I} VC_{i,v,t} ACT_{i,v,t} & (1) \\
& \text{s. t. } \sum_{v \in V_i} \sum_{i \in I} ACT_{i,v,t} \geq Demand_t & \forall t \in T & (1a) \\
& \zeta_{i,v,t} CAP_{i,v} \geq ACT_{i,v,t} & \forall t \in T_i, v \in V_i, i \in I & (1b) \\
& BX \geq b & & (1c)
\end{aligned}$$

In the above formulation, V, I and T are the set of all vintages, technologies and model time periods, respectively, where, v, i and t are the indices of these sets. $IC_{i,v}, FC_{i,v,t}$ and $VC_{i,v,t}$ are the discounted investment cost, fixed operations and maintenance cost and variable operations and maintenance cost of technology i , respectively. $CAP_{i,v}$ is the decision variable representing available capacity of technology i of vintage v . In the above model formulation, the total commodity production, e.g. electricity, from a process is referred to as “activity”, ACT . $ACT_{i,v,t}$ is the decision variable representing output of technology i of vintage v in time period t . $CAP_{i,v}$ and $ACT_{i,v,t}$ are two inherently different units of measure. $CAP_{i,v}$ is a unit of energy per time, while $ACT_{i,v,t}$ is a unit of total energy actually emitted. Moreover, $\zeta_{i,v,t}$ is the factor that converts available capacity to maximum available activity, $\zeta_{i,v,t} CAP_{i,v}$. Temoa constraints the capacity variable to at least be able to meet the activity of that process, $ACT_{i,v,t}$. $Demand_t$ is the demand in time period t . Furthermore, B represents the coefficients of all the other constraints, such as commodity and process balance constraints, and b represents the right-hand side of such constraints. In words, (1) expresses the total discounted system cost to be minimized, (1a) is the set of demand satisfaction constraints, where the right-hand-side represent the exogenous demands to satisfy, (1b) denotes the relation between available capacity and activity and (1c) is the set of all other constraints, which includes process balance, resource availability, fuel share, lower bound constraints on the variables and other environmental or policy related constraints.

2.2 Economic interpretation of bottom up ESOMs

In bottom up ESOMs, each technology is identified by a detailed description of its inputs, outputs, unit costs, and several other technical and economic characteristics. In these so-called “Bottom-Up” models, a sector is constituted by a number of logically arranged technologies, linked together by their inputs and outputs (which may be energy forms or carriers, materials, emissions and/or demand services). Some

bottom-up models compute a partial equilibrium via maximization of the total net (consumer and producer) surplus; while others meet exogenously specified end-use demand at the least total system cost. In partial equilibrium models, prices and quantities in each time period are such that at those prices the suppliers produce exactly the quantities demanded by the consumers. Further, this equilibrium has the property that the total surplus is maximized over the whole horizon. Investments made at any given period are optimal over the horizon as a whole. The concept of total surplus maximization extends the cost minimization approach upon which earlier bottom-up energy system models were based. These simpler models have fixed energy service demands, and thus are content to minimize the cost of supplying these demands. In bottom-up models, one unit of sectoral output (e.g., a billion vehicle kilometers of heavy truck service or a Peta Joule of residential cooling service) is produced using a mix of individual technologies' outputs. Thus, the production function that defines the physical relation between end-use services and fuel inputs of a sector is implicitly constructed, rather than explicitly specified as in more aggregated models. Such implicit production functions may be quite complex, depending on the complexity of the energy system.

2.3 Elasticity

The above-mentioned welfare maximization models introduce an end use demand that is responsive to prices. It provides a useful first step in capturing both human behavior and economic feedback to changes in energy system. These model use demand elasticity to replace exogeneous demand with inverse demand function (Loulou, R., & Lavigne, D.,1996).

2.3.1 Demand elasticity

The demand elasticity ϵ of a good, Y , is defined as

$$\epsilon(Y) = \frac{\frac{dQ(Y)}{dP(Y)}}{\frac{Y}{P(Y)}} \quad (2)$$

where, $Q(Y)$ is a quantity demanded and $P(Y)$ is the price. From Equation 2, we see that the demand elasticity of Y is the ratio of the percent change in $Q(Y)$ to the corresponding percent change in $P(Y)$. Measuring the responsiveness of a dependent variable to an independent variable in percentage terms rather than simply as the derivative of the function has the attractive feature that this measure is invariant to the units in which the independent and the dependent variable are measured. In this chapter, we use an own price elasticity to specify the responsiveness of demand of energy service to its price.

2.3.2 Elasticity of substitution

Now we introduce elasticity of substitution for a function of two variables. The elasticity of substitution is most often discussed in the context of production functions. While the elasticity of a single variable function measures the percentage response of a dependent variable to a percentage change in the independent variable, the elasticity of substitution between two-factor inputs measures the percentage response of the relative marginal products of the two factors to a percentage change in the ratio of their quantities. We can represent the utility function, U , as a function of quantity demanded of energy services:

$$U = g(ES) \quad (3)$$

Since, quantity demanded of energy services is a function of quantity demanded of electricity, E_t and energy efficiency, θ_t , utility, U , can be given as $g(f(E, \theta))$. Then the elasticity of substitution between electricity and energy efficiency is given by:

$$\sigma_{\theta E} = - \frac{d(\theta/E)}{\theta/E} \bigg/ \frac{d \left(\frac{dg/d\theta}{dg/dE} \right)}{\frac{dg/d\theta}{d\theta} / \frac{dg}{dE}} \quad (4)$$

A special class of production functions include a constant elasticity of substitution (CES), σ . CES functions were first explored by Arrow et al. (1961), who proved that a production function with two inputs has a constant elasticity of substitution σ between inputs if and only if the production function is either of the functional form:

$$f(E, \theta) = (\alpha\theta^\rho + (1 - \alpha)E^\rho)^{1/\rho} \quad (5)$$

or else of the Cobb-Douglas form when elasticity of substitution is 1:

$$f(E, \theta) = (\theta^\alpha E^{1-\alpha}) \quad (6)$$

Where, α is a parameter representing share of an input, $0 \leq \alpha \leq 1$ and ρ is a constant equal to $(\sigma - 1)/\sigma$. Now, electricity and energy efficiency are substitute goods, i.e., one good can be used in place of other. The substitutability leads the elasticity of substitution between electricity and energy efficiency to be greater than one, hence, we use the production function given by Equation (5) for the formulation in Section 3.

3 ESOM Representation with Energy Efficiency Model

3.1 Conceptual Framework

The conceptual starting point for the energy efficiency model is the flow of processes and money in an economy as shown in Figure 4.1. The first actor in the diagram is the group of consumers, who pay for energy efficient technologies as well as electricity in order to receive the energy services. The second is the group of electric utilities, who invest in the electricity generators and energy efficient technologies required for the generation of energy services demanded by consumers. In tracing the circular flow, one can start with the supply of fuel (e.g. coal, natural gas, wind) to the electricity generators and continue to the supply of electricity from the electric utilities to the consumers (e.g. households), who in turn pay for electricity.

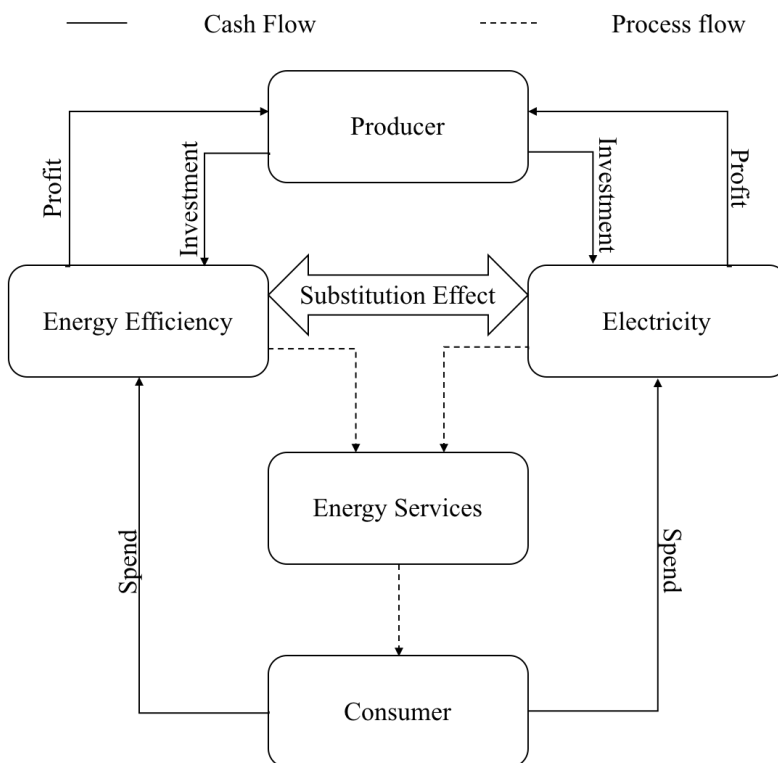


Figure 4.1: Economic flow and process flow for energy efficiency model.

Equilibrium in the economic flows represented in Figure 4.1 results in the partial conservation of both product and value since we are not considering other factors in the economy such as labor, wages and the circulation of earnings. The difference between payment from consumers and cost of production for utilities is the producer surplus (profit). Whereas difference between consumer's willingness to pay for the energy services and what the consumer actually pays is the consumer surplus. The energy efficiency model

maximizes the producer and consumer surplus. We assume that customers choose a combination of electricity consumption and energy efficiency consumption to maximize their utility which results in maximization of consumer surplus. Similarly, the producer maximizes profits or equivalently, producer surplus, by choosing the investment in electricity generation and/or energy efficiency. In general, the model maximizes the total welfare, which is the sum of producer surplus and consumer surplus as shown in Figure 4.2.

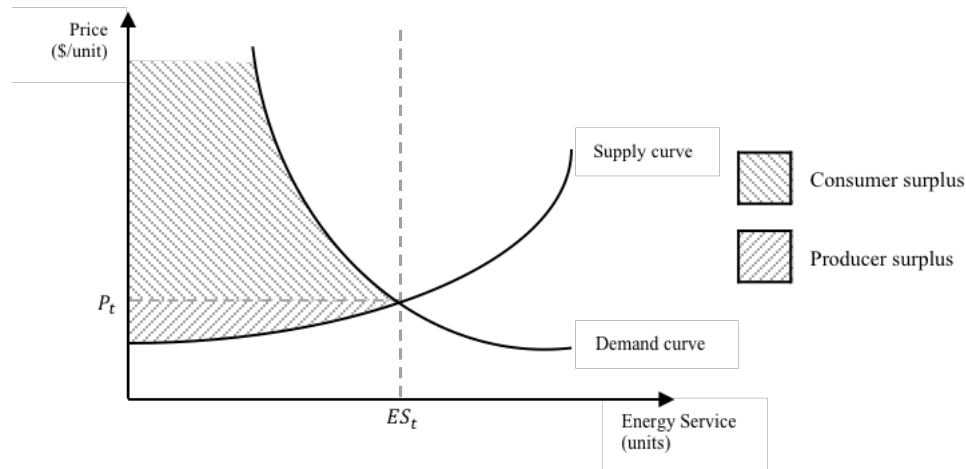


Figure 4.2: Supply-demand equilibrium. Note that the supply curve of energy services is a function of supply curve for electricity and energy efficiency. Similarly, the demand curve of energy services is a function of demand curve for electricity and energy efficiency. The dashed line show price P_t and quantity ES_t at equilibrium for a given time period.

In the model, consumer’s demand of energy services is dependent on price and quantity demanded of energy efficiency and electricity, where price and quantity demanded of electricity and energy efficiency affect each other. This effect is captured by assuming a constant elasticity of substitution production function for the production of energy services.

We implement the formulation of energy efficiency model within the ESOM, Temoa. In this analysis, we develop a hypothetical test case that represents the electric sector on an island where, the investors have an option of having a lump sum investment in energy efficiency. One could assume a supply curve for an investment in energy efficiency that considers technological details; however, such a representation is not required in the analysis provided in Section 5. Details about the characteristics and main assumptions of the case study are provided in Section 4.

The energy efficiency model has two inputs for the consumption of energy services, ES_t , which are electricity, E_t , and energy efficiency, θ_t . We start with the energy service demand as a function of price of energy services and we perform a series of calculations to get a constraint set consisting of Equations (7), (8), (11), and (12) that will be directly implemented in the model. Now, we know that the quantity demanded of most of the energy services is inversely proportional to its price, i.e., the quantity demanded decreases with increase in unit price of energy service, we assume that demand of energy services ES_t have a constant own-price elasticity form:

$$ES_t = \varphi_t P_t^\epsilon \quad (7)$$

The unit cost corresponding to the energy service demand is given as a function of the electricity price and price of energy efficiency. It is a tedious but straightforward application of calculus to demonstrate that in the CES form (Rutherford, T., 2002), the unit cost function is given by:

$$P_t = (\alpha^\sigma P \theta_t^{1-\sigma} + (1 - \alpha)^\sigma P E_t^{1-\sigma})^{1/(1-\sigma)} \quad (8)$$

As a result, ES_t , is given by a convex, differentiable function of the electricity price, $P E_t$, and the energy efficiency price, $P \theta_t$. Shephard's lemma states that demand for a particular good, for a give price, equals the derivative of the expenditure function with respect to the price of the good. The expenditure function, which is given as the minimum amount spent by consumers on energy services, is hence given as a product of the unit cost of energy services, given in Equation (8), and the quantity of energy services, given by Equation (7):

$$e = ES_t P_t \quad (9)$$

After substituting Equations (7) and (8) in (9), the simplified form of Equation (9) can be written as:

$$e = \varphi_t (\alpha^\sigma P \theta_t^{1-\sigma} + (1 - \alpha)^\sigma P E_t^{1-\sigma})^{1+\epsilon/(1-\sigma)} \quad (10)$$

Applying Shephard's lemma, we differentiate the expenditure function with respect to $P E_t$ to obtain the electricity demand and with respect to $P \theta_t$ to obtain the energy efficiency demand as a function of the electricity price and the energy efficiency price:

$$\frac{\partial e}{\partial PE_t} = E_t = \varphi_t (1 - \alpha)^\sigma PE_t^{-\sigma} (\alpha^\sigma P\theta_t^{1-\sigma} + (1 - \alpha)^\sigma PE_t^{1-\sigma})^{(\epsilon+\sigma)/(1-\sigma)} \quad (11)$$

$$\frac{\partial e}{\partial P\theta_t} = \theta_t = \varphi_t \alpha^\sigma P\theta_t^{-\sigma} (\alpha^\sigma P\theta_t^{1-\sigma} + (1 - \alpha)^\sigma PE_t^{1-\sigma})^{(\epsilon+\sigma)/(1-\sigma)} \quad (12)$$

To derive the constant, φ_t , we substitute the historical data for quantity demanded of electricity, E_t^0 , and the corresponding price, PE_t^0 , in Equation (11). As a result, φ_t can be given by

$$\varphi_t = \frac{E_t^0}{((1 - \alpha)^\sigma (PE_t^0)^{-\sigma} (\alpha^\sigma P\theta_t^{1-\sigma} + (1 - \alpha)^\sigma (PE_t^0)^{1-\sigma})^{(\epsilon+\sigma)/(1-\sigma)}} \quad \forall t \in T \quad (13)$$

3.2 Mathematical Formulation

We assume that the market is competitive, and the optimization problem is set up as follows.

$$\max \sum_{t \in T} \int_{ES_t^{min}}^{ES_t} P_t(q) dq - \beta \sum_{t \in T} P\theta_t \theta_t - \sum_{v \in V_i} \sum_{i \in I} IC_{i,v} CAP_{i,v} - \sum_{t \in T_i} \sum_{v \in V_i} \sum_{i \in I} FC_{i,v,t} CAP_{i,v} \quad (14)$$

$$- \sum_{t \in T_i} \sum_{v \in V_i} \sum_{i \in I} VC_{i,v,t} ACT_{i,v,t}$$

$$\text{s. t. } \sum_{v \in V_i} \sum_{i \in I} ACT_{i,v,t} \geq E_t \quad \forall t \in T \quad (14a)$$

$$\zeta_{i,v,t} CAP_{i,v} \geq ACT_{i,v,t} \quad \forall t \in T_i, v \in V_i, i \in I \quad (14b)$$

$$ES_t = \varphi_t P_t^\epsilon \quad \forall t \in T \quad (14c)$$

$$P_t = (\alpha^\sigma (\beta P\theta)_t^{1-\sigma} + (1 - \alpha)^\sigma PE_t^{1-\sigma})^{1/(1-\sigma)} \quad \forall t \in T \quad (14d)$$

$$E_t = \varphi_t (1 - \alpha)^\sigma PE_t^{-\sigma} (\alpha^\sigma (\beta P\theta)_t^{1-\sigma} + (1 - \alpha)^\sigma PE_t^{1-\sigma})^{(\epsilon+\sigma)/(1-\sigma)} \quad \forall t \in T \quad (14e)$$

$$\theta_t = \varphi_t \alpha^\sigma (\beta P\theta)_t^{-\sigma} (\alpha^\sigma (\beta P\theta)_t^{1-\sigma} + (1 - \alpha)^\sigma PE_t^{1-\sigma})^{(\epsilon+\sigma)/(1-\sigma)} \quad \forall t \in T \quad (14f)$$

$$BX \geq b \quad (14g)$$

The objective function given in (14) can be divided into three parts: the area under the energy service demand curve represented by $\sum_{t \in T} \int_{ES_t^{min}}^{ES_t} P_t(q) dq$, the area under energy efficiency supply curve represented by $\sum_{t \in T} P\theta_t \theta_t$, and the area under the electricity supply curve represented as $\sum_{v \in V_i} \sum_{i \in I} IC_{i,v} CAP_{i,v} + \sum_{t \in T_i} \sum_{v \in V_i} \sum_{i \in I} FC_{i,v,t} CAP_{i,v} + \sum_{t \in T_i} \sum_{v \in V_i} \sum_{i \in I} VC_{i,v,t} ACT_{i,v,t}$. We choose an arbitrary lower bound on the integral, ES_t^{min} such that $ES_t^{min} < ES_t$, in the first part of the objective

function to prevent consumer surplus from being unbounded as $ES_t \rightarrow 0$. The pictorial representation of the demand curve for energy services can be seen in Figure 4.2. Note that we do not have a direct representation of a supply curve of energy services in the above model. Since the producer invests in electricity and energy efficiency, the supply curve for energy services is indirectly a function of supply curve of electricity and energy efficiency.

For the optimal value of independent decision variables PE_t , $CAP_{i,v}$ and $ACT_{i,v,t}$, and derived decision variables ES_t , E_t , P_t and θ_t , the nonlinear objective function represented in (14) maximizes the total welfare of the system. Constraint (14a) represents a set of linear constraints that represent supply-demand equilibrium, where demand is a dependent variable. Constraint (14b) is same as constraint (1b) which represents the relation between available capacity and available activity. Constraint (14c to 14f) are a set of nonlinear constraints that evaluate the quantity demanded of energy service, marginal price of energy service demand, the quantity of electricity produced, and the quantity of energy efficiency required, respectively, for a given price of electricity, PE_t and a given price of energy efficiency, $P\theta_t$. Constraint (14g), which is same as constraint (1c), is a set of all other linear constraints in the ESOM. The above optimization problem finds the optimal market clearing conditions, i.e., the optimal value of variables that maximizes the consumer and producer surplus.

3.3 Solution methodology

Given the assumptions for the underlying demand function, the resulting model (14) is a large-scale, welfare maximization problem with a nonlinear objective function, non-linear and linear equality constraints, and linear inequality constraints. Since the resulting ESOM with energy efficiency representation has non-linear terms in the objective function as well as in the constraints, it is necessary to use non-linear optimization methods and solvers to attempt to solve it. To solve this model implemented in Python-Pyomo (Hart, W. E. et al., 2012), we use Interior Point Optimizer (Ipopt) (Biegler, L. T., and Zavala, V. M., 2009) which is a software package for large-scale nonlinear optimization. Ipopt is written in C++ and is released as open source code under the Eclipse Public License and it is designed to find solutions of mathematical optimization problems of the form

$$\begin{aligned} & \min f(X) \\ & \text{s. t. } g_L \leq g(X) \leq g_U \\ & X_L \leq X \leq X_U \end{aligned}$$

Where, $f(X): R^n \rightarrow R$ is an objective function, and $g(X): R^n \rightarrow R^m$ is a constraint functions. The vectors g_L and g_U denote the lower and upper bounds on the constraints, and the vectors X_L and X_U are the bounds on the decision variables X . The functions $f(X)$ and $g(X)$ can be nonlinear and nonconvex but should be twice continuously differentiable.

Due to the nonlinear nature of the model, Ipopt only guarantees local optimality of the solution. However, to generate insights for policy analysis, finding the global optimal solution is necessary. In order to prove the global optimality of the solution, we modify the model give in (14) by introducing the production function for ES_t according to Equation (5). Hence, ES_t can be written as

$$ES_t = \left(\alpha \theta_t^{(\sigma-1)/\sigma} + (1-\alpha) E_t^{(\sigma-1)/\sigma} \right)^{\sigma/(\sigma-1)}$$

We replace the price of energy services denoted by $P_t(q)$ in the objective function (14) by $(q/\varphi)^{1/\epsilon}$ since P_t can be written as $(ES_t/\varphi_t)^{1/\epsilon}$ from equation (14c). The resulting mathematical model is given in (15).

$$\begin{aligned} \max \sum_{t \in T} \int_{ES_t^{min}}^{\left(\alpha \theta_t^{(\sigma-1)/\sigma} + (1-\alpha) E_t^{(\sigma-1)/\sigma} \right)^{\sigma/(\sigma-1)}} (q/\varphi)^{1/\epsilon} dq - \beta \sum_{t \in T} P \theta_t \theta_t - \sum_{v \in V} \sum_{i \in I} IC_{i,v} CAP_{i,v} \\ - \sum_{t \in T} \sum_{v \in V} \sum_{i \in I} FC_{i,v,t} CAP_{i,v} - \sum_{t \in T} \sum_{v \in V} \sum_{i \in I} VC_{i,v,t} ACT_{i,v,t} \end{aligned} \quad (15)$$

$$\text{s. t. } \sum_{v \in V} \sum_{i \in I} ACT_{i,v,t} \geq E_t \quad \forall t \in T \quad (15a)$$

$$\zeta_{i,v,t} CAP_{i,v} \geq ACT_{i,v,t} \quad \forall t \in T, v \in V, i \in I \quad (15b)$$

$$BX \geq b \quad (15c)$$

We then prove that the objective function of (15) is concave and the feasible domain is closed and convex. Since, local minima is a global minimum for a concave function on a closed, convex feasible domain, we conclude that the solution obtained by Ipopt is in fact a global maximum. The proof of global optimality of a solution obtained for the nonlinear energy efficiency model is given in Appendix A.

4 Experimental datasets

To clearly demonstrate the energy efficiency model (within the mathematical formulation of an ESOM) and the effects of uncertain parameters, imagine an island, which has one diesel generator to satisfy all its

electricity demand. For the sake of simplicity, we assume that the island has only one season and that the electricity consumption is equally distributed over the entire day. Suppose that electricity consumption of the island was 66 GWh in 2017, which was satisfied by a diesel generator with 10 MW of existing capacity. The electricity price in 2017 was 0.12 \$Million/GWh or equivalently 12 cents/kWh. Due to the sudden rise in popularity, the projected electricity demand of the island in 2018 is 450 GWh. Now, the central authority for the island has a choice to invest in energy efficient technologies or in diesel power plants to expand the power generation capacity of the existing system. Historical demand-price data of electricity is commonly available. For the purpose of this test system, the electricity demand in 2017 (66 GWh) is considered to be the reference electricity demand, E_t^0 , while the electricity price, considered as reference electricity price, PE_t^0 , is 12 cents/kWh.

We use energy efficiency as the energy consumption avoided, hence referred to as “negawatt” (Palmer and Paul 2015). There is a fairly extensive literature examining the cost-effectiveness of energy efficiency or demand-side management programs. Common values in the literature of the “negawatt cost” (i.e., the total expense of running the program and installing equipment) per megawatt-hour saved as a result of a program range from below \$10/MWh to above \$200/MWh saved (in real 2002 dollars) (Gillingham et al., 2009). Hence, we assume an arbitrary marginal cost of energy efficiency which is within the observed range, 50 \$/MWh, which is equivalent to 0.05 \$Million/GWh. (Ricke, K. et al., 2018) calculated social cost of carbon for US to be between 10 to 50 \$/tCO₂. Hence, for the test case we choose an arbitrary carbon tax equal to 40 \$/tCO₂ on carbon within this range. All the parameters that are required to represent the hypothetical test case are given in Table 4.1. Note that the fuel cost is included in the variable cost of the power plant.

Table 0.1: Test model parameter values.

Model parameter	Value
Existing time period	2017
Future time period	2018
Input commodity	Diesel
Output commodity	Electricity
Existing capacity (GW)	0.01
Investment cost (\$Million/GW)	1500
Fixed cost (\$Million/GW-year)	20
Variable cost (\$Million/GWh)	0.25
Marginal cost of meeting demand in 2017 (\$Million/GWh)	0.12
Energy efficiency productivity in the production of energy services, α	0.4
Elasticity of substitution between electricity and energy efficiency, σ	2.0
Own price demand elasticity of energy service, ϵ	-0.4
Marginal cost of energy efficiency in time period t , $P\theta_t$ (\$Million/GWh)	0.05
Marginal damage of CO ₂ emissions, τ (\$/tCO ₂)	40

This simplistic, hypothetical test case demonstrates the functionalities of the energy efficiency model. Moreover, the effects of uncertain input parameters can be observed much more clearly for two reasons. First, the size of the test case lowers the computational power required for uncertainty analysis. Second, the techno-economic details in the more realistic representation of energy system might overshadow some of the effects of uncertain parameters. The simple test case avoids this complication in building insights. This test case does not, however, represent the full energy system. We utilize a well-known test case called ‘utopia’ which is introduced in MARKAL (Hewells et al., 2011) to further this analysis. We discuss the policy scenario in the Appendix B. The results show similar behavior as can be observed in the test case.

5 Policy Scenario

Economists refer to the first-best policy as the option that gives the welfare maximizing outcome, which is equivalent to the optimal strategy while the second-best policy is a suboptimal strategy that is closest to the optimal strategy. We consider a Pigouvian tax (Pigou, A., 2017), where the tax value is set equal to the marginal external damage τ since the Pigouvian tax achieves the first-best policy outcome in the case of a single pollutant. Electricity producers must account for the additional cost associated with the emissions tax, such that the marginal cost of energy services from each generation technology, inclusive of emissions damages, is equated across sources and with energy efficiency. To compute the welfare considering a Pigouvian tax, the objective function represented by (14) is modified to include an emissions tax as follows

$$\begin{aligned}
\max \sum_{t \in T} \int_{ES_t^{min}}^{ES_t} P_t(q) dq - \beta \sum_{t \in T} P\theta_t \theta_t - \sum_{v \in V_i} \sum_{i \in I} IC_{i,v} CAP_{i,v} - \sum_{t \in T_i} \sum_{v \in V_i} \sum_{i \in I} FC_{i,v,t} CAP_{i,v} \\
- \sum_{t \in T_i} \sum_{v \in V_i} \sum_{i \in I} VC_{i,v,t} ACT_{i,v,t} - \sum_{t \in T_i} \sum_{v \in V_i} \sum_{i \in I} \tau \gamma_{i,v,t} ACT_{i,v,t}
\end{aligned} \tag{16}$$

Where, $\gamma_{i,v,t}$ is the emission activity of a technology i with vintage v in time period t , $\sum_{t \in T_i} \sum_{v \in V_i} \sum_{i \in I} \tau \gamma_{i,v,t} ACT_{i,v,t}$ represents the total emissions accountable for Pigouvian tax and β represents the energy efficiency credit level. An alternative policy which was considered as an option under EPA's Clean Power Plan (CPP) is an efficiency crediting policy. Crediting energy efficiency is equivalent to giving a subsidy on investment in energy efficiency. In other words, fixing β to 0.8 is equivalent to assuming that the price of energy efficiency is, $(1 - \beta)$, 20% lower than the original value. The subsidized price of energy efficiency encourages the buyer to invest in energy efficiency.

Conceptually, the carbon tax policy and efficiency policy can be shown in Figure 4.3. We add a new actor to Figure 4.1 which acts as a government/ central entity. In order to reduce emission, the central entity can impose tax on emission or provide subsidy for the investment in energy efficiency. By providing subsidy to energy efficiency, the central entity encourages the investment in energy efficiency. Since energy efficiency and electricity are substitute goods, the subsidy leads to decrease in demand for electricity which in turn reduces emissions.

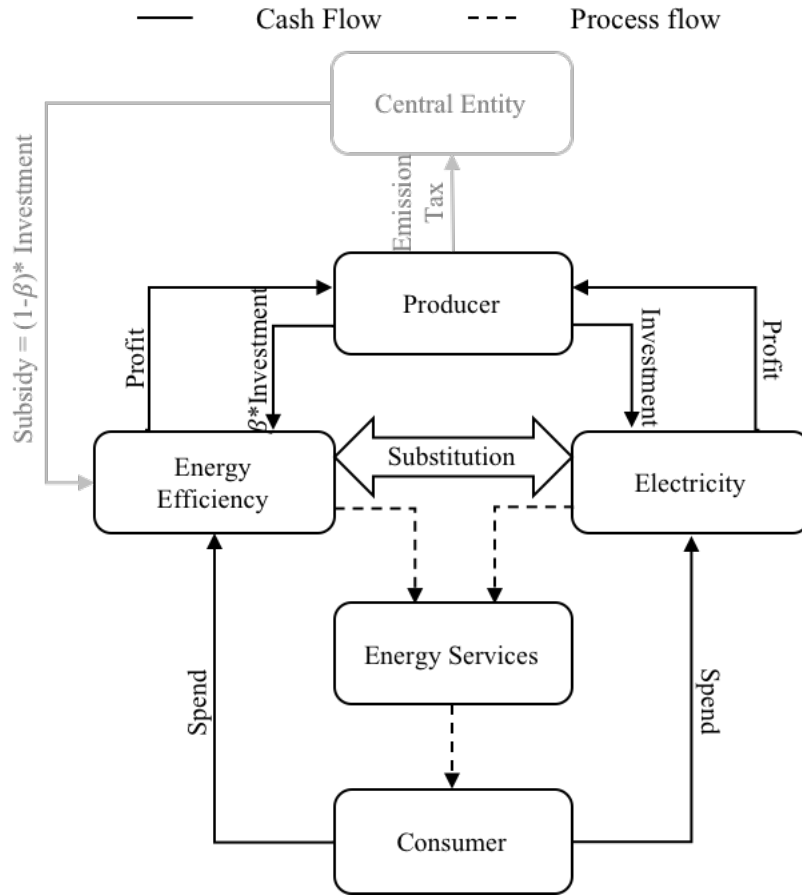


Figure 4.3: Visualization of policy scenarios along with economic and process flow in energy efficiency model.

The work presented by Fell et al. (2017) proves that the first best allocation, i.e., welfare value from carbon tax policy obtained by solving (16) subject to the constraints (14a-g), cannot be achieved with efficiency crediting policy unless the energy service demand is exogenously specified in the absence of potential capacity expansion. Since the quantity of energy service demand is price responsive, i.e. elastic, it is certain that we cannot achieve the first-best allocation with efficiency crediting. However, with an optimal choice of crediting rule, we can achieve the second-best allocation, i.e., the welfare value that is closest to the one obtained by carbon tax policy. For the following analysis, ‘no policy’ case is considered when we solve the energy efficiency model as given in (14), where $\beta = 1$. Solving the energy efficiency model with ‘efficiency credit’ policy is equivalent to solving the mathematical model given in (14) where $0 < \beta < 1$. The computation of percentage welfare gain, $\%W$, as compared to carbon tax policy, hereafter referred to as welfare recovered, is shown in Equation (17).

$$\%W = \frac{(Welfare\ from\ efficiency\ credit\ policy - Welfare\ from\ no\ policy)}{(Welfare\ from\ emission\ tax - Welfare\ from\ no\ policy)} \quad (17)$$

For comparing the change in welfare for different policies, we assume that welfare from carbon tax policy is equivalent to the optimal objective function of (16). Now, let A be the optimal objective function value of the energy efficiency model given in (14). Since the objective function for efficiency credit policy obtained by solving (14) does not include the carbon tax and the subsidy provided by the central entity for investment in energy efficiency, the welfare from the efficiency credit policy can be given as

$$\begin{aligned} & Welfare\ from\ efficiency\ credit\ policy \quad (18) \\ & = A - \sum_{t \in T} \sum_{v \in V_i} \sum_{i \in I} \tau \gamma_{i,v,t} ACT_{i,v,t} - (1 - \beta) \sum_{t \in T} P\theta_t \theta_t \end{aligned}$$

Where, $ACT_{i,v,t}$ and θ_t are the optimal values of the variables obtained by solving (14). Note that welfare from no policy can be computed from (18) by setting $\beta = 1$.

5.1 Results and Discussion

While the above sections develop a conceptual framework about efficiency crediting, simulation in this section develops additional insights about efficiency crediting with a numerical test case. We know that the quantity demanded of electricity decreases with increasing price of electricity while, the quantity demanded for energy efficiency and price of energy services increase. Crediting energy efficiency is equivalent to giving a subsidy for investment in energy efficiency. As a result, it encourages investment in energy efficiency. Since energy efficiency and electricity are substitute goods, crediting energy efficiency decreases the investment in electricity production. Hence, for a given price of electricity, quantity demanded of electricity decreases with increasing efficiency credit while quantity demanded of energy efficiency and energy service increases with increasing efficiency crediting. In (14), the decision variables, ES_t, E_t, P_t and θ_t are derived from PE_t . We plot the dependent variables as a function of independent variable to visualize the effect of increase in efficiency credit. The variation in quantity demanded of electricity (Figure 4.4(a)), quantity demanded of energy efficiency (Figure 4.4(b)), quantity demanded for energy service demand (Figure 4.4(c)), and price of energy services (Figure 4.4(d)) are plotted as a function of the electricity price for varying levels of efficiency crediting in Figure 4.4. Figure 4.4(a-d) are plotted using Equation 14(e), (f), (c) and (d), respectively.

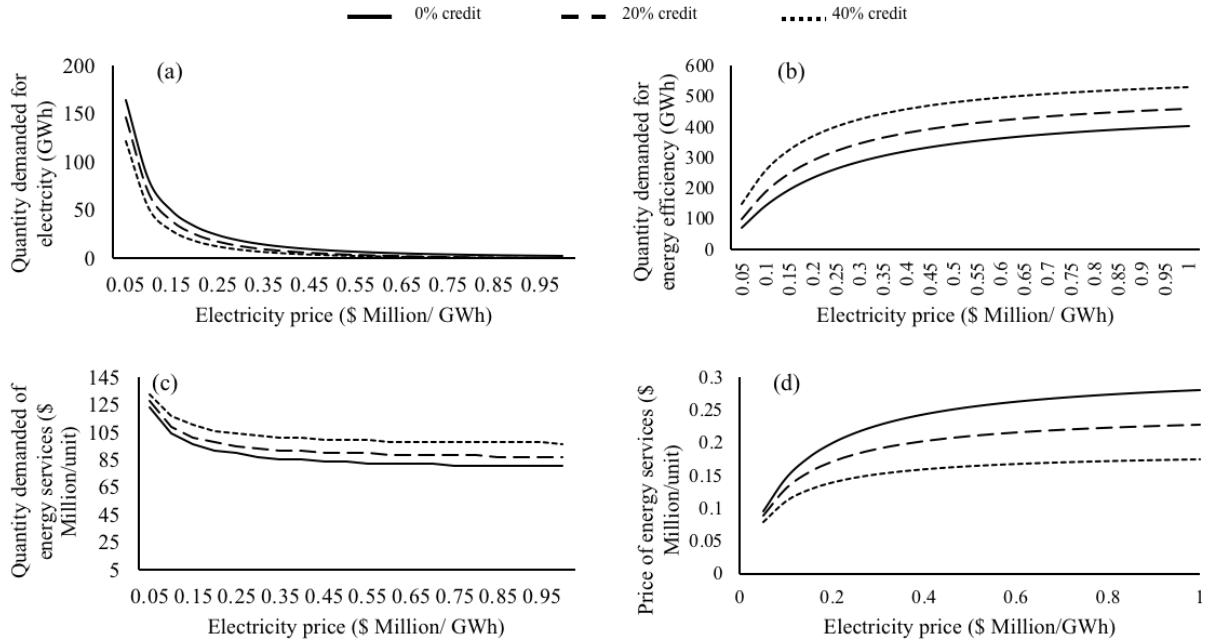


Figure 4.4: (a) For a given price of electricity, quantity demanded of electricity decreases with increasing efficiency crediting (b) Quantity demanded for energy efficiency increases with increasing efficiency crediting and (c) Quantity demanded for energy service increases with increasing efficiency crediting (d) Price of energy services decreases with increasing efficiency crediting.

We vary efficiency crediting over a large range (0% to 40%) in Figure 4.4 in order to observe that efficiency crediting also affects the rate at which quantity demanded of electricity decreases with increase in the price of electricity. By varying various parameters in the energy efficiency model, particularly the parameters in Equation 14(c-f), we can essentially incorporate various consumer behaviors as a function of the price of electricity. One particular aspect of the energy efficiency model to note here is a rebound effect where, over the long-run, consumption of energy services increases as a result of efficiency crediting-induced decline in the price of energy services. The energy efficiency model allows us to incorporate a wide range of consumer behavior, including behavior that gives rise to rebound effect. However, we do not directly isolate the exact rebound effect in this analysis. Note that the price of energy services does not have a physical significance since, in reality, we do not directly pay for energy services. The price of energy services can be thought of as a function of the price of electricity and the price of energy efficiency. Hence, if one or both of the price of electricity and the price of energy efficiency increases then it leads to increase in price of energy services, as can be observed in Figure 4.4(d).

The hypothetical test case, described in Section 4, is further used to demonstrate the welfare gain from varying levels of efficiency credit as compared to the welfare gain from a carbon tax as shown in Figure 4.5. One of the effects of efficiency crediting policy is a reduction in electricity demand which in turn reduces emissions. As a result, investing in energy efficiency reduces the total emissions tax. The results show that efficiency credit of 6% achieves maximum welfare, which is 39% of the welfare gain from carbon tax case. Beyond 12% efficiency crediting, the cost savings from the emissions reduction becomes lower than the expenditure on energy efficiency leading to the negative welfare gain from efficiency crediting.

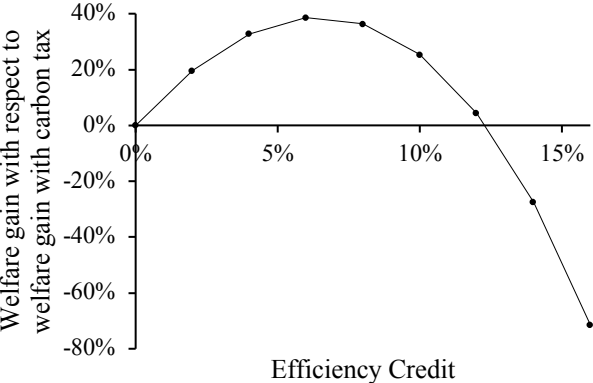


Figure 4.5: Welfare gain as a function of the efficiency credit. The gain is expressed as the fraction of welfare recovered through the energy efficiency policy compared with respect to welfare gain with a Pigouvian carbon tax set at 40 \$/ton of CO₂.

The difference between the optimal quantity of various decision variable for carbon tax case and efficiency crediting case is given in Figure 4.6. As can be observed from the Figure 4.6, emissions are 8% higher under no policy (0% efficiency credit) and gradually decrease with increase in efficiency crediting due to a decrease in quantity demanded of electricity. Noticing from Equation (14d), increasing efficiency credit, $(1 - \beta)$, decreases price of energy services, P_t . From Equation (14c), decrease in price of energy services leads to increase in demand for energy services, ES_t . In other words, efficiency crediting leads to an increase in the quantity demanded of energy efficiency and decreases in the unit price of energy services which in turn increase the quantity demanded of energy services. Crediting energy efficiency decreases the quantity demanded of electricity. As a result, the capacity expansion of a diesel power plant which required to satisfy the sudden surge in energy service demand decreases. Note that in Figure 4.6, the graph of CO₂ emissions overlaps with the graph of quantity demanded for electricity due to the simplicity of the test case.

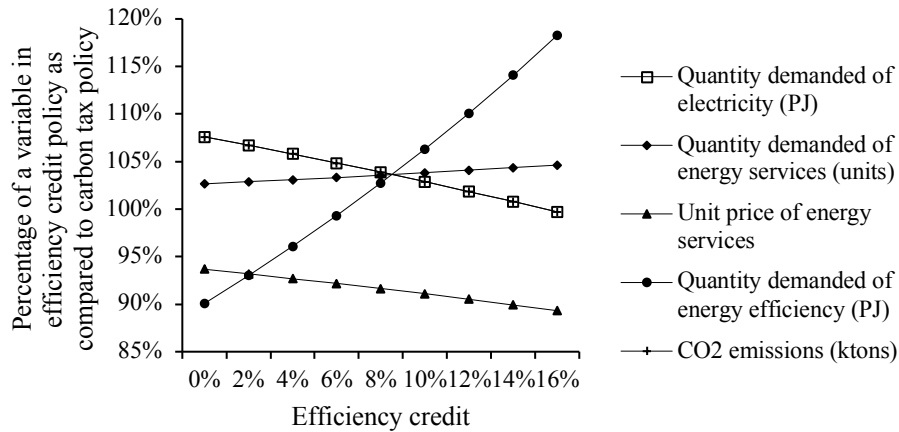


Figure 4.6: For a given efficiency credit a point of a variable represents the percentage quantity of a variable as compared to the quantity of a variable under carbon tax policy.

5.2 Sensitivity Analysis

In the energy efficiency model, the substitution parameter, σ , represents the consumer's willingness to invest in energy efficient technologies for a marginal increase in the price of electricity. The higher willingness to substitute electricity with energy efficiency leads to higher value of the substitution parameter, σ . The price elasticity parameter, ϵ , denotes the importance of energy services for the consumer. The higher elasticity values, ϵ , says that the consumer is more willing to sacrifice the energy service usage if they are marginally expensive. Moreover, the productivity parameter, α , represents the consumer's perspective of the energy services obtained from energy efficient technology. If the consumer views investing in energy efficiency as a superior option, then the productivity of energy efficiency is higher leading to a higher value of α . Such consumer behaviors are inherently uncertain, and they can vary over a broad range for different groups of consumers depending on their social and economic status. Also, a carbon tax across the world varies from 0 \$/ton to 126.84 \$/ton of carbon (World Bank and Ecofys, 2018). In this analysis, we assume a scalar value for energy efficiency cost, however, in reality, the cost of energy efficiency, $P\theta_t$, can vary over a wide range. In order to understand the overall impact of these system parameters on the welfare, we perform a sensitivity analysis as given below.

We consider the model parameters from the test case given in Table 4.1 as base case parameters. We vary all the system parameters mentioned earlier over $\pm 50\%$ from the base case value given in Table 4.1 except elasticity of substitution, σ . Decreasing the elasticity of substitution by 50% from the base value leads to model infeasibility since the CES production function used for this analysis is undefined for $\sigma = 1$. The sensitivity analysis on the productivity of energy efficiency, α , suggests that for very low ($\alpha < 0.2$) or very

high ($\alpha > 0.7$) productivity of energy efficiency, the relative welfare gain with efficiency crediting policy is not significant. The relatively high productivity of energy efficiency reduces the need to subsidize it while the relatively low productivity reduces the effect of subsidy. Figure 4.7 below shows the effect of the remaining four uncertain parameters on the relative welfare gain from the efficiency crediting policy.

Figure 4.7(a) suggests that lower cost of energy efficiency leads to higher welfare recovered. Effect of increased degree of substitution between electricity and energy efficiency on the welfare recovered is shown in Figure 4.7(b). Figure 4.7(c) suggests that lower own price elasticity of end-use energy service demand increases the welfare recovered at a given efficiency crediting. Effect of increase in carbon tax on welfare recovered, Figure 4.7(d), suggests that higher efficiency crediting is needed to recover the same level of welfare for a higher carbon tax.

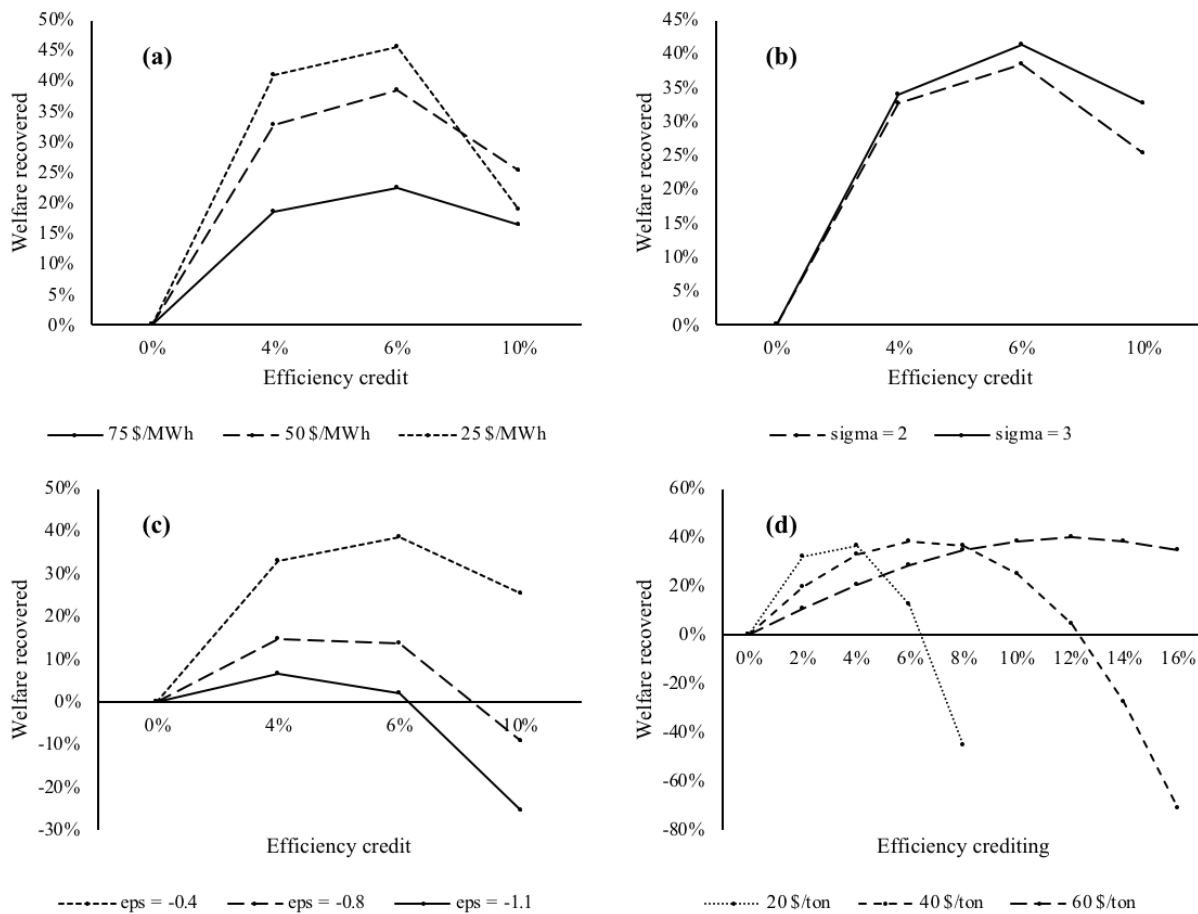


Figure 4.7: Effect of uncertain model parameters on the welfare recovered through energy efficiency credit policy as compared with the Pigouvian tax policy. Uncertain parameters are (a) Energy efficiency cost (b) Substitutability between electricity and energy efficiency (c) Own price elasticity of energy service demand (d) Carbon tax.

Now, the purpose of carbon tax policy and efficiency credit policy is to reduce emissions by discouraging electricity usage. The former achieves emission reduction by increasing price of electricity while the later does so by decreasing the price of energy efficiency. The relative welfare gain from efficiency credit policy to that of carbon tax policy relies on the efficiency crediting-induced saving on carbon tax and the increased expenditure on energy efficiency. When the saving on carbon tax is greater than the expenditure on energy efficiency, the relative welfare recovered from an efficiency credit policy is positive. As can be observed from Figure 4.5, the difference between the two peaks at 6% efficiency crediting.

To analyze Figure 4.7(a) further, note that electricity and energy efficiency are substitute goods. As a result, the effect of marginal reduction in energy efficiency cost on the quantity demanded of electricity is higher for lower energy efficiency cost. In other words, the reduction in electricity generation is higher when we give 10% credit when $P\theta_t$ is 25 \$/MWh than when $P\theta_t$ is 75 \$/MWh. This leads to a higher difference between efficiency crediting-induced saving on carbon tax and the increased expenditure on energy efficiency when $P\theta_t$ is 25 \$/MWh. Hence, relative welfare recovered from efficiency credit policy increases with a decrease in energy efficiency cost. Similar logic can be applied to Figure 4.7(b). Increase in substitutability of energy efficiency, σ , increases the reduction in electricity generation for a marginal decrease in $P\theta_t$. Consequently, 10% efficiency credit produce a larger reduction in electricity production for a higher value of σ which leads to higher relative welfare recovered. As for Figure 4.7(c), the price elasticity of demand is higher when an increase in quantity demanded of a good is higher for a marginal reduction in the price of a good. Therefore, the higher elasticity values observe a larger increase in energy service demand and consequently, energy efficiency demand as a result of 10% energy efficiency credit. Now, the rate of increase in energy efficiency demand or decrease in electricity demand depends on other model parameters such as productivity of energy efficiency, α . However, for the set of parameters given in Table 4.1, Figure 4.7(c) suggests that increase in energy efficiency expenditure is greater than efficiency credit-induced savings on emissions tax for more elastic energy service demand. As a result, the relative welfare gain from efficiency credit policy decreases as the elasticity of energy service demand increases. Figure 4.7(d) suggests that we need higher efficiency crediting for a higher carbon tax to recover the same amount of relative welfare. Higher carbon tax leads to higher emission reduction. To achieve equivalent emission reduction, we need lower electricity demand and higher energy efficiency demand. It can be achieved when cost of energy efficiency is low or equivalently, crediting for energy efficiency is high. Note that in reality, we cannot satisfy 100% of the end-use energy service demand by energy efficiency since the reduction in electricity supply is limited.

6 Conclusion and Future work

We successfully formulated the energy efficiency model for capacity expansion planning and demonstrated the model functionality using a simplified hypothetical test case. We apply the model to the test case with and without emissions tax policy to analyze the percentage of welfare recovered with efficiency crediting as compared to the welfare gain from carbon tax. We also perform parametric sensitivity analysis on the uncertain model parameters to recognize the effects of uncertain parameters on the welfare that can be recovered by crediting energy efficiency.

The primary goal of this research was to introduce consumer behavior in ESOMs and formulate them in a way that is consistent with the microeconomic theory. To do so, we build a capacity expansion model for energy systems with the representation of energy efficiency, based on (Fell et al., 2017), in an open-source energy system modeling framework. We apply the methodology to perform policy analysis for a hypothetical test case. We point out the differences between a traditional bottom-up model where we define energy efficiency through separate technologies with associated variable costs and an energy efficiency model where we can explicitly model the substitutability between electricity and energy efficiency in the form of a production function. The secondary goal is to analyze the effect of uncertain consumer behavior on system welfare. Substitutability between electricity and energy efficiency, the productivity of energy efficiency in satisfying energy service demand or price responsiveness of energy service demand are some aspects of consumer behavior. By varying these model parameters, we can potentially incorporate a wide range of consumer behavior related to energy consumption into traditional ESOMs. For example, productivity parameter, α , represents the consumers view on how good or bad the energy efficient technology is as compared to the traditionally used technology. So, if the consumer views energy efficient technology better than the traditionally used technology then energy efficiency will be very productive in generating energy services, i.e., the value of α is higher.

Although ESOMs can benefit from the introduction of a methodology that considers consumer behavior, it has some limitations. One limitation is the narrow literature on quantifying consumer behavior regarding energy efficiency given the cost-minimizing rational of the consumer. In other words, determining the appropriate value of the substitution parameter, σ , the productivity of energy efficiency, α , and the price elasticity of energy services, ϵ , is a challenging task. However, performing sensitivity analysis on these parameters provide valuable insights regarding the effect of efficiency crediting policy on overall system behavior. In recent years, multitudes of studies (Buchanan et al., 2014; Ito, 2014) have examined the empirical effects and biases in consumer behavior that might be relevant to the decisions related to investment in energy efficiency. Whether these biases lead to significant biases in decision making is still

an ongoing research debate (Gillingham et al., 2009). Another limitation of energy efficiency model arises from its highly nonlinear nature. It limits the size of the problem that can be solved within a reasonable computational time and capacity. Moreover, we have to rely on nonlinear solvers such as Ipopt for determining global optimality of the resulting solution. Despite these limitations, the energy efficiency model provides a theoretically consistent methodology to consider some of the consumer behaviors that traditional ESOMs have not considered yet.

For future work, we plan to analyze the alternative policies for emission reduction (e.g., carbon cap and renewable portfolio standard) for the electric sector of single region US database to find the second-best solution for emission reduction. Moreover, we plan to analyze and improve the computational performance of the energy efficiency model. One could also apply the same methodology for modeling a substitution effect between different fuels or different technologies for specific sectors in the ESOMs. For example, one could model a substitution effect between electric vehicles and fossil fueled vehicles in the transportation sector or substitution effect between solar PV and natural gas generators when investment in solar PV is subsidized. Ongoing work by the authors is to include the time index for the parameter β which represents the subsidy given for energy efficiency since the subsidies usually vary over time. Moreover, incorporating a supply curve for energy efficiency instead of assuming a scalar value for the cost of energy efficiency will also lead to more realistic results.

Acknowledgements

The authors acknowledge the financial support provided under the NSF grant 0812121.

Chapter 5 Conclusion and Future Work

1 Research contribution

The key contribution of this thesis is to quantify various types of uncertainty – from conflict-related damage to technology investment costs to consumer behavior– and apply rigorous uncertainty analysis to examine its effect on energy systems. Energy system models are often fraught with both parametric and structural uncertainties that arise from technical, economic, political, geographical, policy, and environmental factors. In this dissertation, several methods have been employed to address uncertainty in energy system optimization models: SA (SA), scenario analysis, stochastic linear programming (SLP), and robust optimization (RO). The resultant analysis yields insight that can inform investors, electric utilities, and policy analysts working to build cleaner, more affordable, and more resilient energy systems.

In the second chapter, the South Sudan modeling exercise demonstrates the need for conflict prone countries to explicitly consider the risk of conflict as they build out their electric power systems. We begin by describing the Method of Morris results, which inform the analysis performed with the stochastic version of the model. We construct an analytical framework that employs an energy system optimization model (ESOM) along with SA and SLP to examine how potential future conflict can affect near-term electricity planning. Next, we presented the results from the stochastic optimization under different assumed conflict scenarios. We discuss the stochastic output metrics to quantify the value of considering uncertainty while developing resilient power system infrastructure. In the results, we draw insights about future electric power development in South Sudan. We conclude that considering conflict-related uncertainty adds another dimension to future analysis, ensuring resilient energy supply in the face of conflict, fragility, and violence.

In the third chapter, while exploring the parametric uncertainty in a US-focused ESOM, we observe that previous natural gas price forecasts from AEO (2018) were often inaccurate. There is no evidence to suggest that fuel price projections have improved over the years (Moret, 2019). Thus, highly uncertain input data is a reality of utilizing ESOMs. Since the insights obtained from ESOMs are often used to inform policy, future uncertainties must be considered to build robust policies. The main goal of the third chapter is to find alternative greenhouse gas (GHG) emission mitigation pathways that are robust under fuel price and investment cost uncertainty. A key limitation of parametric SA is that it does not provide a hedging strategy against the uncertainty. To obtain the hedging strategy, we implement a RO framework that considers the correlation (CR-ESOM) in the uncertain parameters and represents the first-ever application to an ESOM. The robust solution suggests diversifying the resources used to satisfy energy demand and encourage

investment in wide range of more expensive technologies with low carbon emissions. Moreover, we show that ignoring uncertainty may have significant financial consequences.

In the fourth chapter, the primary goal was to build a capacity expansion model for energy systems with a representation of energy efficiency that is consistent with the microeconomic theory. The secondary goal was to analyze the effect of uncertain consumer response on system welfare. The substitutability between electricity and energy efficiency, the productivity of energy efficiency in satisfying energy service demand, or price responsiveness of energy service demand are examples of the consumer response. By varying these model parameters, we can incorporate a wide range of consumer responses related to energy consumption into traditional ESOMs. We successfully formulated the Energy Efficiency (EE) model for capacity expansion planning and demonstrated the model functionality using a simplified hypothetical test case. In this chapter, the goal of the uncertainty analysis was to analyze the impact of individual uncertain parameters on total system welfare. Therefore, we perform parametric SA on the uncertain model parameters to recognize their effects on the welfare recovered by crediting energy efficiency as compared to the carbon tax.

One of the high-level insights obtained from these analyses is that the hedging strategies developed with SLP and RO work best when uncertainty is highest. For example, in chapter 2, if the conflict-related damage and associated probabilities are low, the solution looks like the naïve case. On the other hand, when they are both high, the solution looks like a single run where non-distributed technologies are too expensive. The most interesting hedging strategies – and where you see the highest expected cost of perfect information (EVPI) – is when the conflict probabilities and damages are somewhere in the middle, and the best course of action is not evident. This observation is also true in the RO case. When the budget of uncertainty is very high, the results look like a single run where all the uncertain parameters take on their worst values.

Another insight obtained from the analysis in chapter 2 is that the benefits of uncertainty analysis are lower when the cost of unmet electricity demand is very low or very high. For the lower cost of unmet demand, curtailing the demand is the cheapest option while for the higher cost, meeting the demand is the cheapest option irrespective of other uncertainties present in the system. Similarly, in chapter 4, very low or very high efficiency crediting reduces the need for uncertainty analysis. For low efficiency crediting, efficiency induced emission reduction is low. In contrast, for high efficiency crediting, the expenditure on energy efficiency is higher than the value of emission reduction. In both cases, the relative welfare recovered is low. Hence, insights obtained by performing uncertainty analysis are less impactful. Even though the RO and SA are not as computationally demanding as SLP, computational tractability is still an issue for large

scale ESOMs. The analysis in these chapters assists in directing the computational resources where the uncertainty analysis can have a more significant impact.

2 Final remarks and future research goals

The work presented in this dissertation can be extended by considering additional parametric uncertainties. Given the complexity of real-world conflict in Chapter 2, we made a number of simplifying assumptions. For simplicity, we assume a constant discount rate of 5% for all technologies (García-Gusano, 2016), which is based on the expert's judgment. However, given the high risk of centralized power plants in South Sudan, the discount rate for hydro power plant can be increased (Steinbach, 2015) in the future analysis. Moreover, we assume an exogenously specified demand increase over time, with demand curtailment occurring at a specified cost. The analysis showed that the results presented are sensitive to the curtailment cost. Future efforts that characterize willingness to pay for electricity in South Sudan or elasticities for electricity demand would help narrow the assumed range of curtailment cost. Another limitation in the current work is the assumption of static load profiles in which the proportion of electricity demand with each season and time of day remains the same from one time period to another. However, electricity consumption patterns may be shifted depending on the devices used for satisfying end-use services such as cooking, heating, lighting, or cooling. For example, increased electricity consumption for residential lighting during night time can change the electricity demand distribution. Moreover, in addition to considering the damage to generators, future analysis should consider the damage to transmission and distribution lines, fuel supply infrastructure, and the resultant effect on cost and delay associated with maintenance. For considering a wide range of uncertainties in power system planning, RO might be a more appropriate option than SLP, which suffers the curse of dimensionality. We perform SA to gauge the impact of uncertain probability of damage to electricity infrastructure. As RO works with nominal and worst-case values, it eliminates the need to perform SA on the probability distribution. Therefore, RO can help in obtaining a hedging strategy under uncertain curtailment cost. Future work aimed at refining the range of input assumptions and applying RO can help in developing electric sector planning strategies under conflict.

Several open issues presented in Chapter 3 deserve further investigation. One is the issue of determining the level of temporal correlation of an uncertain parameter as data for computing correlation is limited. For example, to compute the correlation coefficient for industrial coal, we use the weighted average of the other types of coal. For future work, SA is needed for the correlation coefficients to ensure the robustness of the strategy. Another area of future work is iteratively improving the data and methodology used to determine the intervals for uncertain parameters. With more time and resources like Open EI, this part of the analysis can be improved further. Crowdsourcing the data collection and making the community effort to refine the

input data can help in defining the uncertainty set more accurately, which will increase our confidence in the insights provided by the RO analysis. Moreover, the robust formulation ignores the information about the distribution of the parameter, as it works with nominal value and deviation of the parameter. As a result, some technologies might have an unfair disadvantage for a chosen robust strategy. For example, if a budget of uncertainty is set equal to 1, the RO model selects one technology that has the highest impact on the objective function. The model provides a solution assuming worst-case value of that technology. As a result, for the US case study, light-duty electric vehicles assume worst-case value while the other uncertain parameters assume nominal value. Hence, the robust strategy gives an unfair disadvantage to light-duty electric vehicles when the budget of uncertainty is equal to 1. Furthermore, the formulation in this thesis only considers temporal autocorrelation for an uncertain parameter but does not consider the correlation between different uncertain parameters, which does exist (e.g., between fuel prices). Hence, another future direction is to extend the current formulation to include the correlation between different parameters.

As presented in the last chapter, though ESOMs can benefit from the introduction of a methodology that considers consumer response, it has some limitations. One limitation is the narrow literature on quantifying consumer adoption of energy efficiency measures. To address this issue, performing SA on the relevant parameters provide valuable insights regarding the effect of efficiency crediting policy on overall system behavior. In recent years, multitudes of studies (Buchanan et al., 2014; Ito, 2014) have examined the empirical effects and biases in consumer behavior that might be relevant to the decisions related to investment in energy efficiency. The study of the role of these biases on decision making is an ongoing research area (Gillingham et al., 2006). These studies might provide more data to better characterize consumer response in neoclassical framework. We can apply the methodologies used in Chapter 2 and 3 to find hedging strategy under uncertain consumer preferences, however, nonlinear nature of EE limits their usage. The nonlinear nature of EE limits the size of the problem that can be solved within a reasonable computational time. Moreover, we have to rely on nonlinear solvers such as Ipopt for determining global optimality of the resulting solution. Development of new methodologies to solve the nonlinear EE model more efficiently is a future research direction.

Lastly, parametric uncertainty stems from imperfect information for model input data, while structural uncertainty reflects the imperfect mathematical formulation of ESOMs. The underlying dynamics driving decision making in real world energy systems are complex and evolving over time, while ESOMs are formulated based on simplified and static assumptions (Wong-Parodi et al., 2006). Temoa considers least cost optimization from the perspective of a social planner. However, real energy systems involve many different stakeholders with competing interests and objectives. For example, due to higher capital costs the

model does not consider distributed rooftop solar photovoltaics (PV) to be cost-effective compared with centralized solar PV. However, Temoa's simple objective function does not capture the non-monetary benefits that lead consumers to install rooftop solar PV. In this way, structural uncertainties in the model can potentially miss large technology shifts in the future. One potential way to capture structural uncertainty in future analysis is to apply modeling-to-generate alternatives, an algorithm that searches the feasible, near optimal solution space for alternative solutions that are maximally different in decision space (Brill et al, 1982; DeCarolis, 2011). Other methods to systematically vary the model structure and test the effect on outputs of interest should also be explored. In the end, methods and approaches should be selected in a way that best addresses the research questions at hand, however, only a subset of results should be presented (Kann and Weyant, 2000). Uncertainty analysis, in general, should be used for increasing our confidence in the model and the results.

REFERENCES

Chapter 1

Ben-Tal, A., & Nemirovski, A. (2000). Robust solutions of linear programming problems contaminated with uncertain data. *Mathematical programming*, 88(3), 411-424.

Baranzini, A., Van den Bergh, J. C., Carattini, S., Howarth, R. B., Padilla, E., & Roca, J. (2015). Seven reasons to use carbon pricing in climate policy.

Craig, P. P., Gadgil, A., & Koomey, J. G. (2002). What can history teach us? A retrospective examination of long-term energy forecasts for the United States. *Annual Review of Energy and the Environment*, 27(1), 83-118.

DeCarolis, J., Daly, H., Dodds, P., Keppo, I., Li, F., McDowall, W., ... & Winning, M. (2017). Formalizing best practice for energy system optimization modelling. *Applied Energy*, 194, 184-198.

EAPP (2011). Final master plan report. Volume II: regional power system master plan and grid code study. East Africa Power Pool (EAPP). <http://eappool.org/the-master-plan-2011/>. Date Accessed: 05/15/2018.

Howells, M., Rogner, H., Strachan, N., Heaps, C., Huntington, H., Kypreos, S., ... & Roehrl, A. (2011). OSeMOSYS: the open source energy modeling system: an introduction to its ethos, structure and development. *Energy Policy*, 39(10), 5850-5870.

Hunter, K., Sreepathi, S., & DeCarolis, J. F. (2013). Modeling for insight using tools for energy model optimization and analysis (Temoa). *Energy Economics*, 40, 339-349.

Kanudia, A., & Loulou, R. (1998). Robust responses to climate change via stochastic MARKAL: The case of Québec. *European Journal of Operational Research*, 106(1), 15-30.

Loulou, R., & Lehtila, A. (2012). Stochastic programming and tradeoff analysis in TIMES. *TIMES*

Messner, S., Golodnikov, A., & Gritsevskii, A. (1996). A stochastic version of the dynamic linear programming model MESSAGE III. *Energy*, 21(9), 775-784.

Moret, S., Babonneau, F., Bierlaire, M., & Maréchal, F. (2019). Decision support for strategic energy planning: a robust optimization framework. *European Journal of Operational Research*.

Shapiro, A., Dentcheva, D., & Ruszczyński, A. (2009). *Lectures on stochastic programming: modeling and theory*. Society for Industrial and Applied Mathematics.

TemoProject, 2019. <https://github.com/TemoaProject/> (accessed on July 13, 2019)

Yue, X., Pye, S., DeCarolis, J., Li, F. G., Rogan, F., & Gallachóir, B. Ó. (2018). A review of approaches to uncertainty assessment in energy system optimization models. *Energy strategy reviews*, 21, 204-217.

Chapter 2

AfDB, (2013). South Sudan: An Infrastructure Action Plan, A Program for Sustained Strong Economic Growth. <https://www.afdb.org/en/countries/east-africa/south-sudan/infrastructure-action-plan-in-south-sudan-a-program-for-sustained-strong-economic-growth/>. Date accessed: 05/03/2018

Africa Progress Report, (2015). Power, People and Planet: seizing Africa's energy and climate opportunities. <http://cleancookstoves.org/resources/389.html>. Date accessed: 05/03/2018

AREI, (2017). Africa Renewable Energy Initiative: Progress Report. http://www.arei.org/wp-content/uploads/2017/01/AREI-Progress-report-Jan-2017_ENG.pdf. Date accessed: 05/15/2018

Bazilian, M., Chattopadhyay, D. (2016). Considering power system planning in fragile and conflict states. *Energy for Sustainable Development*, 32, 110-120.

Birge, J. R. (1982). The value of the stochastic solution in stochastic linear programs with fixed recourse. *Mathematical programming*, 24(1), 314-325.

Birge, J. R., Louveaux, F. (2011). *Introduction to stochastic programming*. Springer Science & Business Media.

Cacuci, D.G., Ionesco-Bujor, M. (2004). A comparative review of sensitivity and uncertainty analysis of large-scale systems-II: statistical methods. *Nuclear Science and Engineering* 147, 204-217

Campolongo, F., Cariboni, J., Saltelli, A. (2007). An effective screening design for sensitivity analysis of large models. *Environmental Modelling & Software*, 22(10), 1509-1518.

CIA World Factbook, (2018). South Sudan. <https://www.cia.gov/library/publications/the-world-factbook/geos/od.html>. Date accessed: 5/3/2018

Collier, P. (2003). *Breaking the conflict trap: Civil war and development policy*. World Bank Publications.
Dantzig, G. B. (2010). *Linear programming under uncertainty*. In *Stochastic programming* (pp. 1-11). Springer, New York, NY.

Deichmann, U., Meisner, C., Murray, S., & Wheeler, D. (2011). The economics of renewable energy expansion in rural Sub-Saharan Africa. *Energy Policy*, 39(1), 215-227.

de Queiroz, A.R., (2016) Stochastic Hydro-thermal Scheduling Optimization: An Overview, *Renewable and Sustainable Energy Reviews*, 62: 382-395

EAPP (2011). Final master plan report. Volume II: regional power system master plan and grid code study. East Africa Power Pool (EAPP). <http://eappool.org/the-master-plan-2011/>. Date Accessed: 05/15/2018.

Escudero, L. F., Garín, A., Merino, M., Pérez, G. (2007). The value of the stochastic solution in multistage problems. *TOP*, 15(1), 48-64.

EIA (2013). Updated capital cost estimates for utility scale electricity generating plants. US Energy Information Administration (EIA). https://www.eia.gov/outlooks/capitalcost/pdf/updated_capcost.pdf. Date accessed: 5/15/2018.

Fishbone, L. G., Abilock, H. (1981). Markal, a linear-programming model for energy systems analysis: Technical description of the bnl version. *International Journal of Energy Research*, 5(4), 353-375.

Fund for Peace, (2017). Fragile States Index. <http://fundforpeace.org/fsi/data/> Date accessed: 05/03/2018

Goldstone, J. A. (2008). Pathways to state failure. *Conflict Management and Peace Science*, 25(4), 285-296.

Hatch (2014). Hydropower Expansion Plan and Regional Integration Plan of South Sudan into Regional Electricity Grid, prepared as part of the Nile Basin Initiative, Report # H4569953.

Herman, J. Usher, W. (2017). SALib: An open-source Python library for sensitivity analysis. *Journal of Open Source Software*, 2(9), 97. <http://salib.github.io/SALib/>. Date accessed: 01/07/2019.

Howells, M., Rogner, H., Strachan, N., Heaps, C., Huntington, H., Kypreos, S., Hughes, A., Silveira, S., DeCarolis, J., Bazillian, M., and Roehrl, A. (2011). OSeMOSYS: the open source energy modeling system: an introduction to its ethos, structure and development. *Energy Policy*, 39(10), 5850-5870.

Hunter, K., Sreepathi, S., DeCarolis, J. F. (2013). Modeling for insight using tools for energy model optimization and analysis (Temoa). *Energy Economics*, 40, 339-349.

IEA, (2014). Partner Country Series - Boosting the Power Sector in Sub-Saharan Africa. <https://webstore.iea.org/partner-country-series-boosting-the-power-sector-in-sub-saharan-africa>. Date accessed: 05/03/2018

IRENA, (2018). South Sudan. <http://resourceirena.irena.org/gateway/countrySearch/?countryCode=SSD>
Date accessed: 05/03/2018

Kann, A. and Weyant, J.P., (2000). Approaches for performing uncertainty analysis in large-scale energy/economic policy models. *Environmental Modeling & Assessment*, 5(1), 29-46.

Lucas, P., Dagnachew, A., Hof, A. (2017). Towards universal electricity access in Sub-Saharan Africa. PBL Netherlands Environmental Assessment Agency, 22-05-2017.

Madansky, A. (1960). Inequalities for stochastic linear programming problems. *Management science*, 6(2), 197-204.

Mercier, L., Van Hentenryck, P. (2007). Performance Analysis of Online Anticipatory Algorithms for Large Multistage Stochastic Integer Programs. *International Joint Conferences on Artificial Intelligence (IJCAI)*, pp. 1979-1984.

Messner, S., & Strubegger, M. (1995). User's Guide for MESSAGE III.

Morris, M. D. (1991). Factorial sampling plans for preliminary computational experiments. *Technometrics*, 33(2), 161-174.

Mozersky, D., & Kammen, D. M. (2018). South Sudan's Renewable Energy Potential: A Building Block for Peace. United States Institute for Peace, Special Report. https://energies-media.com/wp-content/uploads/2018/01/Report_Soudan-du-Sud_Renewable-Energy_012018.pdf Date Accessed: 05/15/2018.

Oseni, M. O., Pollitt, M. G. (2013). The economic costs of unsupplied electricity: Evidence from backup generation among African firms. University of Cambridge, Faculty of Economics.

Pappenberger, F., Iorgulescu, I., Beven, K. J. (2006). Sensitivity analysis based on regional splits and regression trees (SARS-RT). *Environmental Modelling & Software*, 21(7), 976-990.

Pereira, M. V., Pinto, L. M. (1991). Multi-stage stochastic optimization applied to energy planning. *Mathematical Programming*, 52(1-3), 359-375.

Raleigh, C., Linke, A., Hegre, H., Karlsen, J. (2010). Introducing ACLED: an armed conflict location and event dataset: special data feature. *Journal of Peace Research*, 47(5), 651-660. Current database accessed from <https://www.acleddata.com/data/>.

Saltelli, A., Tarantola, S., Campolongo, F., Ratto, M. (2004). *Sensitivity analysis in practice: a guide to assessing scientific models*. John Wiley & Sons.

Shapiro, A., Dentcheva, D., Ruszczyński, A. (2009). *Lectures on stochastic programming: modeling and theory*. Society for Industrial and Applied Mathematics.

Steinbuks, J., Foster, V. (2010). When do firms generate? Evidence on in-house electricity supply in Africa. *Energy Economics*, 32(3), 505-514.

TemoaProject, (2018). <https://github.com/TemoaProject/temoa/> Date accessed: 05/03/2018

The Guardian, (2016). <https://www.theguardian.com/global-development/2015/aug/27/south-sudan-peace-deal-greeted-with-quiet-optimism-by-humanitarian-world> Date accessed: 05/03/2018

Trüby, J. (2014). *Thermal Power Plant Economics and Variable Renewable Energies: A Model-Based Case Study for Germany*. International Energy Agency Insight Series. https://www.iea.org/publications/insights/insightpublications/TRUEBY_PowerPlantEconomicsFINAL.PDF Date accessed: 05/15/2018.

Van der Weijde, A. H., Hobbs, B. F. (2012). The economics of planning electricity transmission to accommodate renewables: Using two-stage optimisation to evaluate flexibility and the cost of disregarding uncertainty. *Energy Economics*, 34(6), 2089-2101.

World Bank. (2013). *Toward a sustainable energy future for all: directions for the World Bank Group's energy sector*.

World Bank, (2015). *Fragility, Conflict and Violence Overview*,
<http://www.worldbank.org/en/topic/fragilityconflictviolence/overview>. Date accessed: 05/03/2018

World Bank, (2016). *South Sudan*. <http://pubdocs.worldbank.org/en/744081477329274990/mpo-am16-ssd.pdf>. Date accessed: 05/03/2018

World Bank, (2017). *Pump price for diesel fuel (US\$ per liter)*.
<https://data.worldbank.org/indicator/EP.PMP.DESL.CD>. Date accessed: 05/03/2018

Wu, G.C., Deshmukh, R., Ndhlukula, K., Radojicic, T., Reilly-Moman, J., Phadke, A., Kammen, D.M. and Callaway, D.S. (2017). Strategic siting and regional grid interconnections key to low-carbon futures in African countries. *Proceedings of the National Academy of Sciences (PNAS)*: 201611845.

Zerriffi, H., Dowlatabadi, H., Strachan, N. (2002). Electricity and conflict: Advantages of a distributed system. *The Electricity Journal*, 15(1), 55-65.

Chapter 3

Allen, M., & Wilkinson, B. (1999). *Parallel Programming, Techniques and Applications Using Networked Workstations and Parallel Computers*.

Alizadeh, B., Dehghan, S., Amjady, N., Jadid, S., and Kazemi, A. (2013). Robust transmission system expansion considering planning uncertainties. *IET Generation, Transmission and Distribution*, 7(11), 1318-1331.

Annual Energy Outlook 2018 with Projections to 2050; U.S. Energy Information Administration (EIA), 2018; <https://www.eia.gov/outlooks/aeo/pdf/AEO2018.pdf>

Assumptions to the Annual Energy Outlook 2018, U.S. Energy Information Administration (EIA), 2018, Available online: <https://www.eia.gov/outlooks/aeo/assumptions/>

Babonneau, F., J-P. Vial, and R. Apparigliato. "Robust optimization for environmental and energy planning." In *Uncertainty and Environmental Decision Making*, pp. 79-126. Springer, Boston, MA, 2009.

Babaei, S., A. Nagpure, and J. DeCarolis (2014), "How much do electric drive vehicles matter to future U.S. emissions," *Environmental Science and Technology*, 48: 1382-1390.

Baringo, L., and Baringo, A. (2018). A stochastic adaptive robust optimization approach for the generation and transmission expansion planning. *IEEE Transactions on Power Systems*, 33(1), 792-802.

Bayraksan, G. and Morton, D.P., 2006. Assessing solution quality in stochastic programs. *Mathematical Programming*, 108(2-3), pp.495-514.

Bayraksan, G. and Morton, D.P., 2009. Assessing solution quality in stochastic programs via sampling. In *Decision Technologies and Applications* (pp. 102-122). Inform

Ben-Tal, A., & Nemirovski, A. (2000). Robust solutions of linear programming problems contaminated with uncertain data. *Mathematical programming*, 88(3), 411-424.

Bertsimas, Dimitris, and Melvyn Sim. "The price of robustness." *Operations research* 52, no. 1 (2004): 35-53.

Bertsimas, Dimitris, and Aurélie Thiele. "Robust and data-driven optimization: modern decision making under uncertainty." In *Models, Methods, and Applications for Innovative Decision Making*, pp. 95-122. INFORMS, 2006.

Bertsimas, D., Brown, D. B., and Caramanis, C. (2011). Theory and applications of robust optimization. *SIAM review*, 53(3), 464-501.

Bertsimas, D., & Tsitsiklis, J. N. (1997). *Introduction to linear optimization* (Vol. 6, pp. 479-530). Belmont, MA: Athena Scientific.

Cacuci, D.G., Ionesco-Bujor, M. (2004). A comparative review of sensitivity and uncertainty analysis of large-scale systems-II: statistical methods. *Nuclear Science and Engineering* 147, 204e217

Campolongo, F., Cariboni, J., and Saltelli, A. (2007). An effective screening design for sensitivity analysis of large models. *Environmental modelling and software*, 22(10), 1509-1518.

Chen, X., Sim, M., and Sun, P. (2007). A robust optimization perspective on stochastic programming. *Operations Research*, 55(6), 1058-1071.

Chen, C., Li, Y. P., Huang, G. H., and Li, Y. F. (2012). A robust optimization method for planning regional-scale electric power systems and managing carbon dioxide. *International Journal of Electrical Power and Energy Systems*, 40(1), 70-84.

Chen, B., Wang, J., Wang, L., He, Y., and Wang, Z. (2014). Robust optimization for transmission expansion planning: Minimax cost vs. minimax regret. *IEEE Transactions on Power Systems*, 29(6), 3069-3077.

Climate Action Tracker. <https://climateactiontracker.org/countries/usa/> (Accessed July 9, 2019)

De Villiers, M. A. R. K., & Matibe, K. H. O. R. O. M. M. B. I. (2000). Greenhouse gas baseline and mitigation options for the residential sector. Energy & Development Research Centre, Cape Town, 11.

Dehghan, S., Amjady, N., and Kazemi, A. (2014). Two-stage robust generation expansion planning: a mixed integer linear programming model. *IEEE Trans. Power Syst*, 29(2), 584-597.

Department of Energy, <https://energy.gov/savings/renewable-electricity-production-tax-credit-ptc> (Accessed January 9, 2018) (B) U.S. Energy Information Administration (EIA). Assumptions to the

de Queiroz, A. R. (2011). A sampling-based decomposition algorithm with application to hydrothermal scheduling: cut formation and solution quality. The University of Texas at Austin.

DSIRE, <http://programs.dsireusa.org/system/program/detail/658> (Accessed January 9, 2018)

Eshraghi, H., de Queiroz, A. R., & DeCarolis, J. F. (2018). US Energy-Related Greenhouse Gas Emissions in the Absence of Federal Climate Policy. *Environmental science & technology*, 52(17), 9595-9604.

GitHub, <https://github.com/TemoaProject> (Accessed January 9, 2018)

Hajimiragha, A. H., Canizares, C. A., Fowler, M. W., Moazeni, S., and Elkamel, A. (2011). A robust optimization approach for planning the transition to plug-in hybrid electric vehicles. *IEEE Transactions on Power Systems*, 26(4), 2264-2274.

Hosseinzadeh, M., and Salmasi, F. R. (2015). Robust optimal power management system for a hybrid AC/DC micro-grid. *IEEE Transactions on Sustainable Energy*, 6(3), 675-687.

House, W. (2016). United States mid-century strategy for deep decarbonization. In United Nations Framework Convention on Climate Change, Washington, DC.

Hunter, K., Sreepathi, S., & DeCarolis, J. F. (2013). Modeling for insight using tools for energy model optimization and analysis (TEMOA). *Energy Economics*, 40, 339-349.

Hussain, A., Bui, V. H., and Kim, H. M. (2016). Robust optimization-based scheduling of multi-microgrids considering uncertainties. *Energies*, 9(4), 278.

joblib 0.11 : Python Package Index, <https://pypi.python.org/pypi/joblib> (Accessed July 9, 2019)

Kanudia, A., & Loulou, R. (1998). Robust responses to climate change via stochastic MARKAL: The case of Québec. *European Journal of Operational Research*, 106(1), 15-30.

Kusumadewi, T. V., & Limmeechokchai, B. (2015). Energy efficiency improvement and CO2 mitigation in residential sector: comparison between Indonesia and Thailand. *Energy Procedia*, 79, 994-1000.

Labriet, Maryse, Claire Nicolas, Stéphane Tchong-Ming, Amit Kanudia, and Richard Loulou. "Energy decisions in an uncertain climate and technology outlook: how stochastic and robust methodologies can assist policy-makers." In *Informing Energy and Climate Policies Using Energy Systems Models*, pp. 69-91. Springer, Cham, 2015.

Lenox, C., R. Dodder, C. Gage, D. Loughlin, O. Kaplan, AND W. Yelverton. EPA U.S. Nine-region MARKAL DATABASE, DATABASE DOCUMENTATION. US Environmental Protection Agency, Cincinnati, OH, EPA/600/B-13/203, 2013.

Loulou, R., & Lehtila, A. (2012). Stochastic programming and tradeoff analysis in TIMES. *TIMES*

Mak, W.K., Morton, D.P. and Wood, R.K., 1999. Monte Carlo bounding techniques for determining solution quality in stochastic programs. *Operations research letters*, 24(1-2), pp.47-56.

Martinez-Mares, A., and Fuerte-Esquivel, C. R. (2013). A robust optimization approach for the interdependency analysis of integrated energy systems considering wind power uncertainty. *IEEE Transactions on Power Systems*, 28(4), 3964-3976.

Messner, S., Golodnikov, A., & Gritsevskii, A. (1996). A stochastic version of the dynamic linear programming model MESSAGE III. *Energy*, 21(9), 775-784.

Moret, Stefano, Michel Bierlaire, and François Maréchal. "Robust optimization for strategic energy planning." *Informatica* 27, no. 3 (2016): 625-648.

Moret, S., Babonneau, F., Bierlaire, M., and Maréchal, F. (2019). Decision support for strategic energy planning: a robust optimization framework. *European Journal of Operational Research*.

Mulvey, John M., Robert J. Vanderbei, and Stavros A. Zenios. "Robust optimization of large-scale systems." *Operations research* 43, no. 2 (1995): 264-281.

Malcolm, S. A., and Zenios, S. A. (1994). Robust optimization for power systems capacity expansion under uncertainty. *Journal of the operational research society*, 45(9), 1040-1049.

NREL. (2019). https://openei.org/wiki/Main_Page (Accessed June 30, 2019)

Pappenberger, F., Iorgulescu, I., and Beven, K. J. (2006). Sensitivity analysis based on regional splits and regression trees (SARS-RT). *Environmental Modelling and Software*, 21(7), 976-990.

Ruiz, C., and Conejo, A. J. (2015). Robust transmission expansion planning. *European Journal of Operational Research*, 242(2), 390-401.

Saltelli, A., Tarantola, S., Campolongo, F., and Ratto, M. (2004). *Sensitivity analysis in practice: a guide to assessing scientific models*. John Wiley and Sons.

Soroudi, Alireza, and Turaj Amraee. "Decision making under uncertainty in energy systems: State of the art." *Renewable and Sustainable Energy Reviews* 28 (2013): 376-384.

Soyster, Allen L. "Convex programming with set-inclusive constraints and applications to inexact linear programming." *Operations research* 21, no. 5 (1973): 1154-1157.

Shapiro, A., Dentcheva, D., & Ruszczyński, A. (2009). *Lectures on stochastic programming: modeling and theory*. Society for Industrial and Applied Mathematics.

(a) U.S. Energy Information Administration (EIA). *Annual Energy Outlook 2017 with Projections to 2050*. Available online: [https://www.eia.gov/outlooks/aeo/pdf/0383\(2017\).pdf](https://www.eia.gov/outlooks/aeo/pdf/0383(2017).pdf) (Accessed January 9, 2018).

U.S. EPA (U.S. Environmental Protection Agency). 2016. *Inventory of U.S. greenhouse gas emissions and sinks: 1990–2014*. EPA 430-R-16-002. Available online: <https://www.epa.gov/sites/production/files/2016-04/documents/us-ghg-inventory-2016-main-text.pdf>

Wei, W., Liu, F., Mei, S., and Hou, Y. (2015). Robust energy and reserve dispatch under variable renewable generation. *IEEE Transactions on Smart Grid*, 6(1), 369-380.

Yu, N., Kang, J. S., Chang, C. C., Lee, T. Y., and Lee, D. Y. (2016). Robust economic optimization and environmental policy analysis for microgrid planning: An application to Taichung Industrial Park, Taiwan. *Energy*, 113, 671-682.

Yuan, W., Wang, J., Qiu, F., Chen, C., Kang, C., and Zeng, B. (2016). Robust optimization-based resilient distribution network planning against natural disasters. *IEEE Transactions on Smart Grid*, 7(6), 2817-2826.

Zhao, C., Wang, J., Watson, J. P., and Guan, Y. (2013). Multi-stage robust unit commitment considering wind and demand response uncertainties. *IEEE Transactions on Power Systems*, 28(3), 2708-2717.

Zhang, C., Xu, Y., Dong, Z. Y., and Wong, K. P. (2018). Robust coordination of distributed generation and price-based demand response in microgrids. *IEEE Transactions on Smart Grid*, 9(5), 4236-4247.

Chapter 4

Arrow, K. J., Chenery, H. B., Minhas, B. S., & Solow, R. M. (1961). Capital-labor substitution and economic efficiency. *The Review of Economics and Statistics*, 225-250.

Baranzini, A., Van den Bergh, J. C., Carattini, S., Howarth, R. B., Padilla, E., & Roca, J. (2015). Seven reasons to use carbon pricing in climate policy.

Böhringer, C., & Rutherford, T. F. (2008). Combining bottom-up and top-down. *Energy Economics*, 30(2), 574-596.

DeCarolus, J., Hunter, K., & Sreepathi, S. (2010, June). The TEMOA project: Tools for energy model optimization and analysis. In *International Energy Workshop* (pp. 21-23).

DeCarolus, J., Daly, H., Dodds, P., Keppo, I., Li, F., McDowall, W., ... & Winning, M. (2017). Formalizing best practice for energy system optimization modelling. *Applied Energy*, 194, 184-198.

Department of Energy, <https://energy.gov/savings/renewable-electricity-production-tax-credit-ptc>

DSIRE, <http://programs.dsireusa.org/system/program/detail/658> (

Fell, H., Kaffine, D., & Steinberg, D. (2017). Energy efficiency and emissions intensity standards. *Journal of the Association of Environmental and Resource Economists*, 4(S1), S201-S226.

Gillingham, K., Newell, R. G., & Palmer, K. (2009). Energy efficiency economics and policy. *Annu. Rev. Resour. Econ.*, 1(1), 597-620.

GitHub, <https://github.com/TemoaProject> (Accessed January 9, 2018)

Herbst, A., Toro, F., Reitze, F., & Jochem, E. (2012). Introduction to energy systems modelling. *Swiss journal of economics and statistics*, 148(2), 111-135.

Hourcade, J.-C., Jaccard, M., Bataille, C., Gershi, F., 2006. Hybrid modeling: new answers to old challenges. *Energy Journal-Special Issue* 1–12.

Howells M, Rogner H, Strachan N, Heaps C, Huntington H, Kypreos S, et al. OSeMOSYS: the open source energy modeling system: an introduction to its ethos, structure and development. *Energy Policy* 2011; 39:5850–70. <http://dx.doi.org/10.1016/j.enpol.2011.06.033>.

Hunter, K., Sreepathi, S., & DeCarolus, J. F. (2013). Modeling for insight using tools for energy model optimization and analysis (TEMOA). *Energy Economics*, 40, 339-349.

IEA (2017). <https://www.iea.org/efficiency/>

IIASA (International Institute for Applied Systems Analysis), 2011. Energy Modeling Framework: Model for Energy Supply Strategy Alternatives and their General Environmental Impact (MESSAGE) <http://www.iiasa.ac.at/Research/ENE/model/message.html>. (Accessed January 9, 2018)

Jones, R. V., Fuertes, A., & Lomas, K. J. (2015). The socio-economic, dwelling and appliance related factors affecting electricity consumption in domestic buildings. *Renewable and Sustainable Energy Reviews*, 43, 901-917.

Lenox, C., R. Dodder, C. Gage, D. Loughlin, O. Kaplan, AND W. Yelverton. EPA U.S. Nine-region MARKAL DATABASE, DATABASE DOCUMENTATION. US Environmental Protection Agency, Cincinnati, OH, EPA/600/B-13/203, 2013.

Loulou R, Goldstein G, Noble K. (2004). Documentation for the MARKAL Family of Models. Energy Technology Systems Analysis Programme. Available at: <http://www.etsap.org/documentation.asp>

Manne, A.S., Mendelsohn, R., Richels, R.G., 2006. MERGE: a model for evaluating regional and global effects of GHG reduction policies. *Energy Policy* 23, 17–34.

Morgan, M. G., Henrion, M., & Small, M. (1992). *Uncertainty: a guide to dealing with uncertainty in quantitative risk and policy analysis*. Cambridge university press.

Nardelli, P. H., Karhinen, S., & Svento, R. (2017). Implementing Flexible Demand: Real-time Price vs. Market Integration. [arXiv.org](https://arxiv.org/).

Palmer, Karen, and Anthony Paul. 2015. A primer on comprehensive policy options for states to comply with the Clean Power Plan. RFF Working Chapter DP 15-15, Resources for the Future, Washington, DC.

Temoa GitHub. www.github.com/TemoaProject/temoa/

The TEMOA Project | Tools for Energy Model Optimization and Analysis, <http://temoaproject.org/> (Accessed January 9, 2018)

U.S. EPA (U.S. Environmental Protection Agency). 2016. Inventory of U.S. greenhouse gas emissions and sinks: 1990–2014. EPA 430-R-16-002. Available online: <https://www.epa.gov/sites/production/files/2016-04/documents/us-ghg-inventory-2016-main-text.pdf>

U.S. Energy Information Administration (EIA). Annual Energy Outlook 2017 with Projections to 2050. Available online: [https://www.eia.gov/outlooks/aeo/pdf/0383\(2017\).pdf](https://www.eia.gov/outlooks/aeo/pdf/0383(2017).pdf)

Van Beeck, N. (2000). Classification of energy models. Tilburg University, Faculty of Economics and Business Administration.

Chapter 5

Annual Energy Outlook 2018 with Projections to 2050; U.S. Energy Information Administration (EIA), 2018; <https://www.eia.gov/outlooks/aeo/pdf/AEO2018.pdf>

Assumptions to the Annual Energy Outlook 2018, U.S. Energy Information Administration (EIA), 2018, Available online: <https://www.eia.gov/outlooks/aeo/assumptions/>

Brill Jr, E. D., Chang, S. Y., & Hopkins, L. D. (1982). Modeling to generate alternatives: The HSJ approach and an illustration using a problem in land use planning. *Management Science*, 28(3), 221-235.

Buchanan, K., Russo, R., & Anderson, B. (2014). Feeding back about eco-feedback: How do consumers use and respond to energy monitors?. *Energy Policy*, 73, 138-146.

Craig, P. P., Gadgil, A., & Koomey, J. G. (2002). What can history teach us? A retrospective examination of long-term energy forecasts for the United States. *Annual Review of Energy and the Environment*, 27(1), 83-118.

DeCarolis, J. F. (2011). Using modeling to generate alternatives (MGA) to expand our thinking on energy futures. *Energy Economics*, 33(2), 145-152.

García-Gusano, D., Espegren, K., Lind, A., & Kirkengen, M. (2016). The role of the discount rates in energy systems optimisation models. *Renewable and Sustainable Energy Reviews*, 59, 56-72.

Gillingham, K., Ne well, R., & Palmer, K. (2006). Energy efficiency policies: a retrospective examination. *Annu. Rev. Environ. Resour.*, 31, 161-192.

Ito, K. (2014). Do consumers respond to marginal or average price? Evidence from nonlinear electricity pricing. *American Economic Review*, 104(2), 537-63.

Kann, A., & Weyant, J. P. (2000). Approaches for performing uncertainty analysis in large-scale energy/economic policy models. *Environmental Modeling & Assessment*, 5(1), 29-46.

Moret, S., Babonneau, F., Bierlaire, M., and Maréchal, F. (2019). Decision support for strategic energy planning: a robust optimization framework. *European Journal of Operational Research*.

Smil, V. (2000). Perils of long-range energy forecasting: reflections on looking far ahead. *Technological Forecasting and Social Change*, 65(3), 251-264.

Steinbach, J., & Staniaszek, D. (2015). Discount rates in energy system analysis Discussion Chapter. *BPIE: Berlin, Germany*.

Wong-Parodi, G., Dale, L., & Lekov, A. (2006). Comparing price forecast accuracy of natural gas models and futures markets. *Energy policy*, 34(18), 4115-4122.

Smil, V. (2000). Perils of long-range energy forecasting: reflections on looking far ahead. *Technological Forecasting and Social Change*, 65(3), 251-264.

APPENDICES

Chapter 2

1 Technology representation

The base system includes the electric generating units and transmission lines shown in Appendix Table 2.1. The base case assumes no conflict in South Sudan. All thermal power plants run on diesel. For simplicity, we assume that the investment cost, fixed and variable operations and maintenance costs, capacity factor, and efficiency of a technology remain unchanged for the entire time horizon. We also assume that fixed and variable cost for transmission lines and the variable cost for solar PV are negligible compared to their investment cost and therefore can be ignored. Moreover, solar PV cannot generate electricity at night and is thus assigned a capacity factor of zero at night. Location and status (new/existing) of the power plants, proposed transmission grid, all cost coefficients for proposed hydro power plants, investment and variable cost for thermal power plants, capacity factor and efficiency of hydro power plants, thermal power plants and transmission lines, and investment cost of transmission lines are taken from HATCH (2014). Fixed operations and maintenance costs for solar PV are considered 15% higher than given in EIA (2017). The investment cost of all solar PV is assumed to be 3350 \$/GW. This value is specific to Africa and is the average of the range of total installed cost (1820 - 4880 \$/kW) (IRENA, 2015). Along with the equipment cost, it depends on the maturity of the domestic market, local labor, manufacturing cost, incentive levels, and structure. Data for location-specific capacity factors of solar PV are obtained from average annual direct solar irradiation taken from (Solargis, 2017). The most recent data available for the fuel price for thermal generators is \$1.98/liter (World Bank, 2017).

Appendix Table 2.1: Technology cost and performance assumptions

Location of the proposed power plants	Technology Name ^a	New or Existing (N/E)	Starting year	Variable cost (\$/GWh)	Fixed cost (\$/GWyr)	Investment cost (\$/GWyr)	Capacity Factor	Efficiency
Juba	SO1	N	2017	0	25	3350	0.3424	0.2
Yambio	SO2	N	2017	0	25	3350	0.3196	0.2
Maridi	SO3	N	2017	0	25	3350	0.3196	0.2
Yei	SO4	N	2017	0	25	3350	0.3196	0.2
Kapoeta	SO5	N	2017	0	25	3350	0.3424	0.2
Torit	SO6	N	2017	0	25	3350	0.3424	0.2
Benitu	SO7	N	2017	0	25	3350	0.3881	0.2
Malakal	SO8	N	2017	0	25	3350	0.3424	0.2
Bor	SO9	N	2017	0	25	3350	0.3196	0.2
Rumbek	SO10	N	2017	0	25	3350	0.3424	0.2

Appendix Table 2.1: (continued)

Wau	SO11	N	2017	0	25	3350	0.3881	0.2
Kuajok	SO12	N	2017	0	25	3350	0.3881	0.2
Aweil	SO13	N	2017	0	25	3350	0.4109	0.2
Juba	TH1	E	2016	0.0464	20	0	0.75	0.42
Yambio	TH2	E	2016	0.0464	20	0	0.75	0.36
Maridi	TH3	E	2016	0.0464	20	0	0.75	0.34
Yei	TH4	E	2016	0.0464	20	0	0.75	0.35
Kapoeta	TH5	E	2016	0.0464	20	0	0.75	0.34
Tharjath	TH6	N	2019	0.0399	20	1500	0.75	0.46
Malakal	TH7	E	2016	0.0464	20	0	0.75	0.37
Bor	TH8	E	2016	0.0464	20	0	0.75	0.36
Rumbek	TH9	E	2016	0.0464	20	0	0.75	0.35
Wau	TH10	E	2016	0.0464	20	0	0.75	0.34
Palogue	TH11	N	2019	0.0399	20	1500	0.75	0.48
Bedden	HY1	N	2031	0.0045	20	2500	0.3	0.9
Shukoli	HY2	N	2031	0.0070	20	1800	0.32	0.9
Lakki	HY3	N	2031	0.0022	20	2200	0.28	0.9
Fula Rapids	HY4	N	2019	0.0004	20	3700	0.65	0.9
Wau_HPP	HY5	N	2019	0.0004	20	13100	0.33	0.9
Bedden-Juba	trans_Be_J	N	2017	0	0	7.8	1	0.95
Shukoli-Juba	trans_S_J	N	2017	0	0	49.4	1	0.95
Lakki-Juba	trans_L_J	N	2017	0	0	30	1	0.95
Fula rapids- Juba	trans_F_J	N	2017	0	0	26.4	1	0.95
Juba-Yei	trans_J_Y	E	2016	0	0	0	1	0.95
Juba-Torit	trans_J_T	N	2017	0	0	37.9	1	0.95
Juba-Bor	trans_J_B	N	2017	0	0	59.6	1	0.95
Yei-Maridi	trans_Y_Ma	E	2016	0	0	0	1	0.95
Maridi- Yambio	trans_Ma_Ym	E	2016	0	0	0	1	0.95
Kapoeta-Torit	trans_K_T	E	2016	0	0	0	1	0.95
Bor-Malakal	trans_B_M	N	2017	0	0	91.3	1	0.95
Malakal- Benitu	trans_M_Bu	N	2017	0	0	42.2	1	0.95
Tharjath- Benitu	trans_Th_Bu	E	2016	0	0	0	1	0.95
Bor-Rumbek	trans_B_R	N	2017	0	0	86.1	1	0.95
Rumbek-Wau	trans_R_W	N	2017	0	0	82.6	1	0.95
Wau-Kuajok	trans_W_Kj	N	2017	0	0	23.1	1	0.95
Kuajok-Aweil	trans_Kj_A	N	2017	0	0	16.2	1	0.95

Appendix Table 2.1: (continued)

Palogue-Malakal	trans_P_M	N	2017	0	0	16.2	1	0.95
Wau_HPP-Wau	trans_Wa_W	N	2017	0	0	16.2	1	0.95

^a ‘SO’ indicates solar PV, ‘TH’ indicates thermal plants running on diesel, ‘HY’ indicates hydro, and ‘trans’ indicates transmission lines.

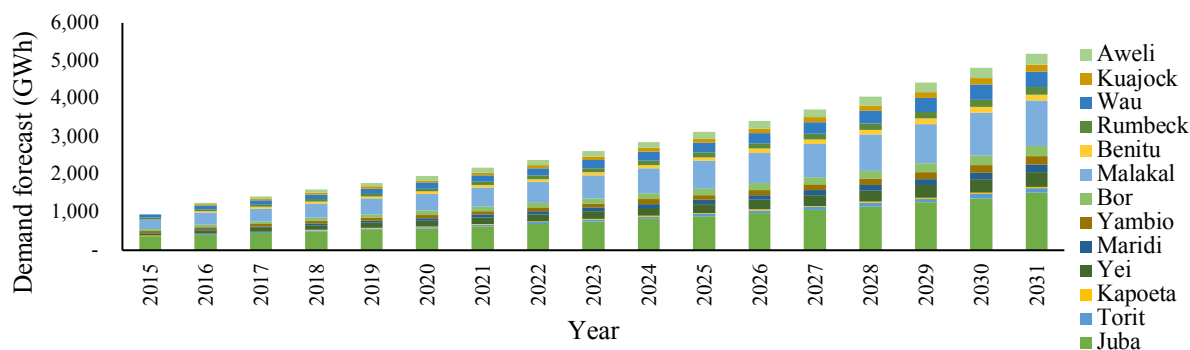
Appendix Table 2.2 represents the region where each thermal and hydro power plant is located. For each region listed in Appendix Table 2.2, there are one or more demand centers. The model allows one solar PV installation at each of the 13 demand centers. The electric power system under consideration also has 9 existing and 2 proposed thermal power plants as well as 5 proposed hydro power plants. Note that two of the biggest proposed hydro power plants (1 and 4) are located in Central Equatoria where the highest numbers of conflicts were observed in 2016.

Appendix Table 2.2: Location of all the generators by region

Region	Thermal power plant (TH)											Solar PV (SO)													Hydro power plant (HY)				
	1	2	3	4	5	6	7	8	9	10	11	1	2	3	4	5	6	7	8	9	10	11	12	13	1	2	3	4	5
Central Equatoria	■			■								■			■										■			■	
Eastern Equatoria				■											■	■												■	
Jonglei								■													■								
Lakes									■													■							
Northern Bahr-el-Ghazal																								■					
Unity						■													■										
Upper Nile							■				■									■									
Warap																							■						
Western Bahr-el-Ghazal										■													■						■
Western Equatoria		■	■									■	■																

2 Electricity demand

Given the new country’s challenging situation, there has not been a formal South Sudan Master Plan since its independence in 2011. Electricity demand is an exogenous input taken from a comprehensive infrastructure action plan produced by the African Development Bank Group in 2013 for South Sudan (AfDB, 2013). Electricity demand for each of the 13 demand locations considered for this analysis is given in Appendix Figure 2.1.



Appendix Figure 2.1: Electricity demand forecast for South Sudan, drawn from AfDB (2013).

3 Damage Value Estimation

3.1 Regional Conflict Rate

The regional conflict rate (RCR) is estimated using the ACLED database (Raleigh et al., 2010), which has monitored the conflicts occurring in South Sudan since its independence in 2011. South Sudan is constitutionally divided into 10 regions. We assume that conflict occurs in each of these regions with the frequency values reported in Appendix Table 2.3. The frequency represents the number of conflict incidences recorded in a given region during year 2016.

Appendix Table 2.3: Regional conflict rate (RCR) calculated from frequency of conflict incidences in 2016 for 10 states in South Sudan (Raleigh et al., 2010).

Regions	Abbreviation	Regional	
		Conflict	Rate
Central Equatoria	CE	0.298	268
Eastern Equatoria	EE	0.0855	77
Jonglei	J	0.0989	89
Lakes	L	0.0411	37
Northern Bahr-el-Ghazal	NB	0.0311	28
Unity	U	0.106	95
Upper Nile	UN	0.0767	69
Warap	W	0.0378	34
Western Bahr-el-Ghazal	WB	0.123	111
Western Equatoria	WE	0.102	92

3.2 Damage Rate

For hydro and thermal power plants, the damage rate (DR) represents the fractional increase in the fixed operations and maintenance cost (FOM) equivalent to the annual payment on investment cost. The increase

in FOM or decrease in CF remains in effect for 5-year time period. The investment cost (IC) is amortized over 30 years with a 3% discount rate (r). The following example illustrates the calculation of DR for a thermal power plant, DR_{TH} , with an investment cost (IC) of \$1500 million/GW and FOM of \$20 million/GW-yr

$$DR = \frac{\left(FOM + IC \left(\frac{r}{(1 - (1 + r)^{-p})} \right) \right)}{FOM}$$

$$DR_{TH} = \frac{\left(20 + 1500 \left(\frac{0.03}{(1 - (1 + 0.03)^{-30})} \right) \right)}{20}$$

$$DR_{TH} = 4.83$$

Similarly, due to the distributed nature of solar PV, we assume that DR_{SO} is the rate of increase in FOM equivalent to 10% of the annual payment on investment. For solar PV with an investment cost (IC) of \$3350 million/GW and FOM of \$25 million/GW-yr, DR_{SO} is calculated as follows:

$$DR_{SO} = \frac{\left(20 + 0.1 \times 3550 \left(\frac{0.03}{(1 - (1 + 0.03)^{-30})} \right) \right)}{25}$$

$$DR_{TH} = 1.68$$

In the event of damage to generators, Appendix Table 2.4 shows the estimated increase in FOM represented as the equivalent increase in investment cost and decrease in CF for each power plant, calculated using the three methods: Regional Damage, Intensified Regional Damage, and Maximum Damage. TH1, TH4, SO1, SO4, HY1 and HY3 are located in Central Ectoria where maximum conflict incidences are recorded in 2016. Hence, these power plants observe the highest increase in FOM and decrease in CF during conflict.

Appendix Table 2.4: *EFOM* represents percent equivalent increase in investment cost while *ECF* represents equivalent percent of capacity factor remaining for each power plant after damage. *EFOM* and *ECF* for Regional damage \leq Intensified regional damage \leq Maximum damage. ‘SO’ indicates solar PV, ‘TH’ indicates thermal plants running on diesel, ‘HY’ indicates hydro power plant.

Power plant ^a	Region	Equivalent capital cost increase			Capacity factor change		
		Regional Damage	Intensified Regional Damage	Maximum damage	Regional Damage	Intensified Regional Damage	Maximum damage
Thermal	Juba	0.31	1.00	1.00	0.78	0.10	0.10
Thermal	Yambio	0.09	0.28	1.00	0.94	0.75	0.10
Thermal	Maridi	0.09	0.28	1.00	0.94	0.75	0.10
Thermal	Yei	0.31	1.00	1.00	0.78	0.10	0.10
Thermal	Kapoetta	0.09	0.31	1.00	0.93	0.72	0.10
Thermal	Tharjath	0.08	0.26	1.00	0.94	0.77	0.10
Thermal	Malakal	0.08	0.27	1.00	0.94	0.76	0.10
Thermal	Bor	0.17	0.55	1.00	0.88	0.51	0.10
Thermal	Rumbek	0.07	0.24	1.00	0.95	0.79	0.10
Thermal	Wau	0.13	0.41	1.00	0.91	0.63	0.10
Thermal	Palouge	0.08	0.27	1.00	0.94	0.76	0.10
Hydro	Bedden	0.25	0.97	1.00	0.78	0.10	0.10
Hydro	Shukoli	0.08	0.30	1.00	0.93	0.72	0.10
Hydro	Lakki	0.26	1.00	1.00	0.78	0.10	0.10
Hydro	Fula Rapids	0.09	0.35	1.00	0.93	0.72	0.10
Hydro	Wau	0.12	0.48	1.00	0.91	0.63	0.10
Solar	Juba	0.06	0.10	0.10	0.98	0.90	0.90
Solar	Yambio	0.02	0.03	0.10	0.99	0.97	0.90
Solar	Maridi	0.02	0.03	0.10	0.99	0.97	0.90
Solar	Yei	0.06	0.10	0.10	0.98	0.90	0.90
Solar	Kapoeta	0.02	0.03	0.10	0.99	0.97	0.90
Solar	Torit	0.02	0.03	0.10	0.99	0.97	0.90
Solar	Bentiu	0.02	0.03	0.10	0.99	0.97	0.90
Solar	Malakal	0.02	0.03	0.10	0.99	0.97	0.90
Solar	Bor	0.03	0.05	0.10	0.99	0.95	0.90
Solar	Rumbek	0.01	0.02	0.10	0.99	0.98	0.90
Solar	Wau	0.02	0.04	0.10	0.99	0.96	0.90
Solar	Kuajok	0.01	0.02	0.10	1.00	0.98	0.90
Solar	Aweil	0.01	0.02	0.10	1.00	0.98	0.90

Chapter 3

This Appendix is a collective work of everyone involved in the Temoa team. This documentation describes the inputs and assumptions to the US energy system model. In this document, an overview of the database is given. In sections 1, 2, 3, and 4, sector-specific inputs and assumptions are presented. In section 5 we expand on cross-sectoral issues. The section, 6, describes the Power to X formulation and the last section, 7, describes the biomass representation.

1 An overview of the database

This database is mostly structured on the US EPA MARKAL database (USEPA) (Lenox, et al., 2013) and US NREL ReEDs database (Eurek et al., 2014). It includes residential, commercial, transportation, industrial and electric sectors. The model time horizon spans from 2017 to 2050, with 5-year time periods. To represent seasonal and diurnal variations in energy supply and demand, the model must perform energy commodity balances across a set of time slices that represent different combinations of seasons and times of day. In the input database used in this analysis, we represent three seasons (summer, winter, intermediate) and four times of times of day: AM (6AM - 12PM), peak (12PM - 3PM), PM (3PM - 9PM), and night (9PM - 6AM).

The end-use sectors (residential, commercial, transportation and industrial sectors) include demand technologies that convert secondary energy carriers (e.g., electricity, natural gas, liquid fuels) into useful energy services (e.g., space heating, space cooling, vehicle miles traveled). These energy service demands are specified exogenously and are drawn from the USEPA database. For example, the residential sector includes demands for space heating, space cooling, water heating, freezing, refrigeration, lighting, and miscellaneous electricity for appliances.

Data on existing capacities of technologies in the residential, commercial and transportation sectors as well as their techno-economic parameters are drawn from the USEPA (Lenox, et al., 2013). These parameters include overnight investment costs, conversion efficiencies and technology lifetime. Existing capacities data on electric sector technologies are drawn from 2018 EIA data. Instead of using USEPA data on industrial sector, we developed a more simplified model of industrial sector. Finally, instead of modeling regional extraction and transport of fossil fuels such as natural gas, coal and liquid fuels we simply define import technologies for these fuels and specify a price for them drawn from the table 6.2.B and 6.2.C of the EIA Electric Power Monthly (EIA, February 2017). Other electric sector data and assumptions are described in Section 2.

Fuel prices are exogenous to the model and are taken from the AEO 2018 Outlook (AEO, 2018). While we make the simplifying assumption that fuel prices are not responsive to endogenous changes within the model, retrospective analysis indicates that there is considerable uncertainty associated with the projection of future fuel prices (AEO, 2018).

1.1 Electric sector

The electric sector modeled in this analysis includes a representation of existing and new generation technologies. Thermal power plants include coal-fired steam, integrated gasification combined-cycle (IGCC) with and without carbon capture and storage (CCS), oil-based steam plants, natural gas steam plants, open cycle and combined-cycle natural gas turbines with and without CCS, and light water nuclear reactors. Renewable sources include conventional hydro, solar photovoltaics, concentrating solar thermal, wind, biomass IGCC, and geothermal. In addition to these electric generating technologies, the model represents air pollution retrofit technologies for NO_x removal, including low NO_x burners (LNB), selective catalytic reduction (SCR), and selective non-catalytic reduction (SNCR). In addition, flue gas desulfurization (FGD) can remove SO₂ associated with coal-fired generation.

In sections 2.1 through section 2.6, we expand on our assumptions and modeling approach to the electric sector. The rest of the input parameters not discussed here, are exactly similar to that of the USEPA.

1.1.1 Investment costs of electric sector technologies

Investment costs of electric sector technologies are drawn from the mid scenario of the National Renewable Energy Laboratory (NREL) Annual Technology Baseline (ATB) 2018 (Cole, et al., 2018). Representative plants for solar are single axis tracking with capacity of 100 MW or higher. All wind classes are specified with the techno-resource group 4 of ATB.

1.1.2 Renewable energies representation

1.1.2.1 Solar

For US energy system, we defined one utility-scale photovoltaic (UPV), one distributed photovoltaic (DPV) and one solar thermal (STH) technology. UPV and DPV capacity factors come from NREL's National Solar Radiation Database (NSRDB) (Habte and Sengupta, 2017), which are also used in the ReEDS model (Furek, et al., 2016). NREL's study represents UPV potential sites in the US based on multiple criteria for appropriate sites (Habte and Sengupta, 2017). This resource potential is based on large parcels of land outside of urban areas, excluding federally protected lands, roadless areas, areas of environmental concern,

and excluding areas with a slope greater than 5%. UPV modules are based on a 100MW and array densities of 39. DPV representation includes fixed tilt systems with a tilt equal to latitude from simulated solar data at 6,000 simulated PV plants (Habte and Sengupta, 2017).

The NREL’s database provides 5-minute power output data for each of these site in their respective states (Habte and Sengupta, 2017). The 5-minute power output data is used to calculate the average capacity factors for each time slice. STH capacity factors are drawn from the USEPA by averaging capacity factors of various solar thermal classes and cost categories (Lenox, et al., 2013). STH classes defined in USEPA are class 1 to class 5, and each class includes 5 different cost categories. Thus, there are 25 different STH technologies, and each technology is represented by an upper bound that indicates available capacities from the technology (Lenox, et al., 2013). By performing a weighted-average across all the 25 technologies, we are able to calculate the STH capacity factors. Appendix Table 3.1 to 3.3 show DC capacity factors of solar technologies. In the database, we multiply the investment cost and capacity factor of solar technologies by a factor of 1.3 to convert the numbers from DC to AC.

Appendix Table 3.1: UPV capacity factors

Time Slice	Fraction of Year	US
Intermediate-AM*	0.082	0.49
Intermediate-Peak*	0.003	0.68
Intermediate-PM*	0.096	0.40
Intermediate-Night*	0.153	0.00
Summer-AM*	0.098	0.50
Summer-Peak*	0.003	0.66
Summer-PM*	0.109	0.43
Summer-Night*	0.125	0.01
Winter-AM*	0.082	0.30
Winter-Peak*	0.003	0.51
Winter-PM*	0.109	0.24
Winter-Night*	0.138	0.00

Appendix Table 3.2: DPV capacity factors

Time Slice	Fraction of Year	US
Intermediate-AM*	0.082	0.26
Intermediate-Peak*	0.003	0.33
Intermediate-PM*	0.096	0.02
Intermediate-Night*	0.153	0
Summer-AM*	0.098	0.28
Summer-Peak*	0.003	0.4
Summer-PM*	0.109	0.05
Summer-Night*	0.125	0
Winter-AM*	0.082	0.16
Winter-Peak*	0.003	0.24
Winter-PM*	0.109	0
Winter-Night*	0.138	0

Appendix Table 3.3: STH capacity factors

Time Slice	Fraction of Year	US
Intermediate-AM*	0.082	0.46
Intermediate-Peak*	0.003	0.46
Intermediate-PM*	0.096	0.46
Intermediate-Night*	0.153	0.23
Summer-AM*	0.098	0.46
Summer-Peak*	0.003	0.46
Summer-PM*	0.109	0.46
Summer-Night*	0.125	0.23
Winter-AM*	0.082	0.46
Winter-Peak*	0.003	0.46
Winter-PM*	0.109	0.46
Winter-Night*	0.138	0.23

Similar to NREL’s study (Furek, et al., 2016), we specify minimum capacity constraints on DPV deployments through 2050. Minimum capacity values were obtained from NREL’s dSolar model (Gangron and Sigrin, 2016). The Solar’s output provides projections of the amount of distributed solar capacity on a state-by-state basis which is aggregated for the US energy system database. In this execution, the sum of state data in the contiguous US was used. Appendix Table 3.4 shows minimum capacity values from DPV.

Appendix Table 3.4: Solar outputs of the DPV deployments across the regions (GW)

Region	2020	2025	2030	2035	2040	2045	2050
US	29.026	32.3545	6.1082	98.4844	154.3957	178.5226	178.5226

Capacity credit of renewable technologies change with the renewable penetration the energy system. To ensure safe and reliable supply of electricity, we reduce the capacity credit of solar PV technologies with increasing share in electricity generation. We do not have an ability to specify capacity credit as a function of renewable penetration in Temoa. But we know that the renewable share increases as a function of time period. Hence, we add a time period index while representing the capacity credit of all the technologies.

For solar PV, we use the capacity credit provided by (Frew et al., 2017) as shown in Appendix Figure 3.1.

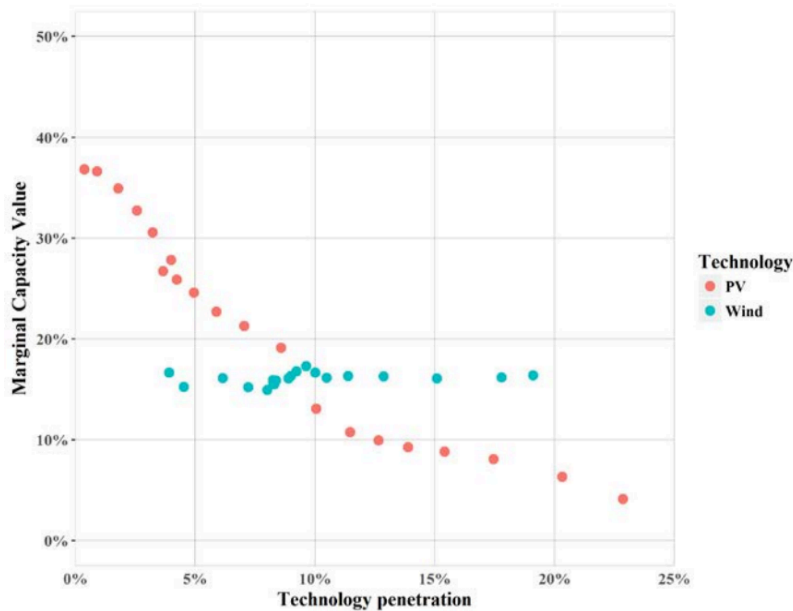


Figure 8. National median marginal CV for PV and wind as a function of their respective energy penetration level with the new ReEDS CV method

Appendix Figure 3.1: reference for capacity credit for solar PV as a function of renewable share

1.1.2.2 Wind

We use USEPA to represent wind resources in our database (Lenox, et al., 2013). Depending on availability of wind resources, various wind classes are defined along with an upper bound on each class. If a particular class represents less than 5% of total wind capacity potentials in USEPA, it is not defined in our database, Appendix Table 3.5. The capacity factors of the wind classes are taken from the USEPA

Appendix Table 3.5 : Maximum wind capacities (GW)

	Wind Class 1	Wind Class 2	Wind Class 3	Wind Class 4	Wind Class 5
US	272.27	30.96	62.03	119.67	81.89

For the capacity credit of wind resources, we refer to the Appendix Figure 3.2 given in (Voorspools and D'haeseleer, 2006). It gives the capacity credit as a function of wind share in electricity generation and capacity factor of wind.

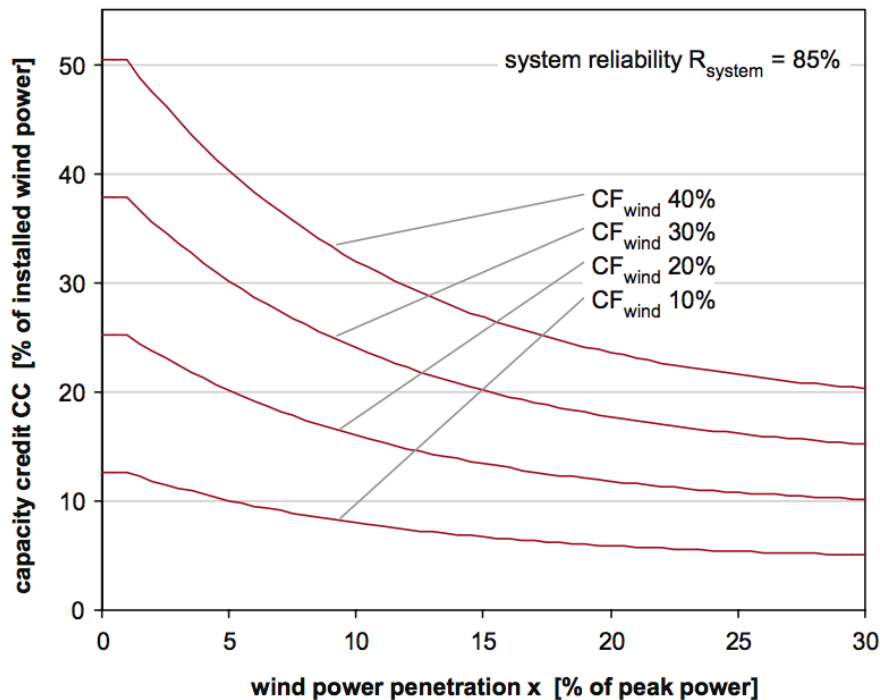


Fig. 1. Capacity credit in function of wind power penetration level for different capacity factors.

Appendix Figure 3.2: reference for capacity credit of wind as a function of wind share and capacity factor

We use the same methodology used above and interpolate the capacity credit of wind resources depending on the capacity factor of wind during summer peak time slice.

We use the following Appendix Table 3.6 to for computing the capacity credit depending on capacity factor. If the capacity factor during summer peak time slice is 29% then we use the nearest capacity factor value given in the above Appendix Figure 3.2. The capacity credit values for wind are given in Appendix Table 3.7.

Appendix Table 3.6: capacity credit values from Appendix Figure 3.2 (Voorspools and D'haeseleer, 2006).

Capacity factor	2017	2020	2025	2030	2035	2040	2045	2050
30%	0.37	0.3	0.23	0.2	0.18	0.16	0.15	0.15
20%	0.25	0.2	0.16	0.14	0.12	0.11	0.1	0.1
40%	0.51	0.41	0.33	0.26	0.23	0.22	0.2	0.2

Appendix Table 3.7: capacity credit for wind resources in the US database

Capacity factor	2017	2020	2025	2030	2035	2040	2045	2050
E_WNDCL1_N	0.29	0.36	0.29	0.22	0.19	0.17	0.15	0.15
E_WND_R	0.319	0.39	0.32	0.24	0.21	0.19	0.17	0.16
E_WNDCL2_N	0.35517628	0.45	0.36	0.29	0.23	0.20	0.20	0.18
E_WNDCL3_N	0.38335085	0.49	0.39	0.32	0.25	0.22	0.21	0.19
E_WNDCL4_N	0.40258031	0.51	0.41	0.33	0.26	0.23	0.22	0.20
E_WNDCL5_N	0.43400617	0.55	0.44	0.36	0.28	0.25	0.24	0.22

1.1.4 Capacity reserve margin

This constraint set requires Temoa to build enough capacity in each period to satisfy the capacity reserve margin. The capacity reserve margin is defined by the North American Electric Reliability Cooperation (NERC) as the amount of unused electric capacity at the time of peak load (NERC, 2009). The capacity reserve requirement ensures that peak demand plus the desired reserve can be met at all times, thereby maintaining system reliability. Equation 1 defines the constraint for the period p :

$$\sum_{t \in T} CC_t \times \mathbf{CAPAVL}_{p,t} \times C2A_t \times SEG^{s^*,d^*} \geq (1 + RES) \times \sum_{t \in T} \mathbf{ACT}_{p,s^*,d^*,t} \quad (1)$$

Where t denotes the electricity generating technologies in a set T , (s^*, d^*) indicates the peak-load time-slice, CC_t and $C2A_t$ are technology-specific capacity credit and conversion factor between capacity and activity respectively, SEG^{s^*,d^*} represents the fraction of peak-load time-slice as a fraction of year and RES is the region-specific reserve margin. $\mathbf{CAPAVL}_{p,t}$ and $\mathbf{ACT}_{p,s^*,d^*,t}$ are the two decision variables in the inequality. $\mathbf{CAPAVL}_{p,t}$ indicates total available capacity from technology t in period p , and $\mathbf{ACT}_{p,s^*,d^*,t}$ indicates activity of technology t in the peak time-slice (s^*, d^*) of period p .

While NERC minimum reserve margins vary from 12% to 18% (NERC, 2017), we assume a uniform 15% reserve rate. Having said that, due to coarse representation of time-slices, our model inherently underestimates peak demand. Our model estimation of summer peak-load for the base year (2017), is 645 GW, while the actual non-coincident peak in summer 2017 has been 20% higher, around 776 GW. To close the gap between our estimate of peak demand and actual peak demand and meet the minimum reserve margin requirement on the other hand, we assume *RES* in equation 1 is 35%.

Another important parameter in Equation 1 is the technology-specific capacity credit. Capacity credit indicates the contribution of non-dispatchable technologies to meeting electricity demand at peak-load time (IEA, 2011). Dispatchable generators, such as coal or natural gas, usually have capacity credits close to their nameplate capacity because they can be relied upon to generate during peak periods. By contrast, wind and solar receive less capacity credit because they are not dispatchable during peak demand periods. In the current database, we used a 5% capacity credit for UPV and DPV, a 20% value for all wind technologies and 100% for the rest of the technologies.

1.1.5 Renewable portfolio standards

State-level renewable portfolio standards (RPSs) are included in our regional dataset in the form of minimum production from renewables. Total state-level electricity generation from renewables are drawn from the AEO 2018 input assumptions (Assumptions to AEO, 2018) and are then aggregated into national level, Appendix Table 3.8. Since the goal of an RPS is to increase the deployment of new renewable technologies, most states restrict existing hydro plants from counting towards the RPS target. The fractions of total hydro generation that counts towards region-specific RPS constraints, are shown in Appendix Table 3.8. The shares are obtained from the USEPA (Lenox, et al., 2013).

Appendix Table 3.8: Minimum generation from renewable energies (RPS)

	Renewable hydro (as a % of regions' total hydro)	2020	2025	2030	2035	2040	2045	2050
US	37.3	207.72	230.04	252.36	272.88	293.4	313.56	333.72

1.1.6 Cross-State Air Pollution Rule

Cross-State Air Pollution Rule (CSAPR) limits SO₂ and NO_x emissions from the electric sector in 22 mostly eastern states (EPA-CSAPR). 2017 State-level budgets for SO₂ and NO_x are gathered and are then aggregated into national levels. We use 2017 emission budgets to cap SO₂ and NO_x emissions from 2017 to 2050 (EPA-CSAPR).

1.1.7 Hydrogen combustion

Hydrogen at 100 bar pressure (H2_100) can be burnt to produce electricity. We introduced a technology E_H2CC_N which has the same techno-economic parameters as E_NGAACC_N. The only difference between the two is that E_H2CC_N doesn't have any emissions.

Appendix Table 3.9: Techno economic parameters for hydrogen combustion to produce electricity

	period/vintage	E_H2CC_N
efficiency	all periods	53.0
CAPEX Mil. \$/GW	2020	1048.44
	2025	1024.69
	2030	1001.07
	2035	983.36
	2040	966.43
	2045	950.07
	2050	927.08
FOM Mil. \$/GW-yr	all periods/vintages	9.73
Cost, variable Mil. \$/PJ		0.54
Lifetime (year)		40
Discount rate		6%

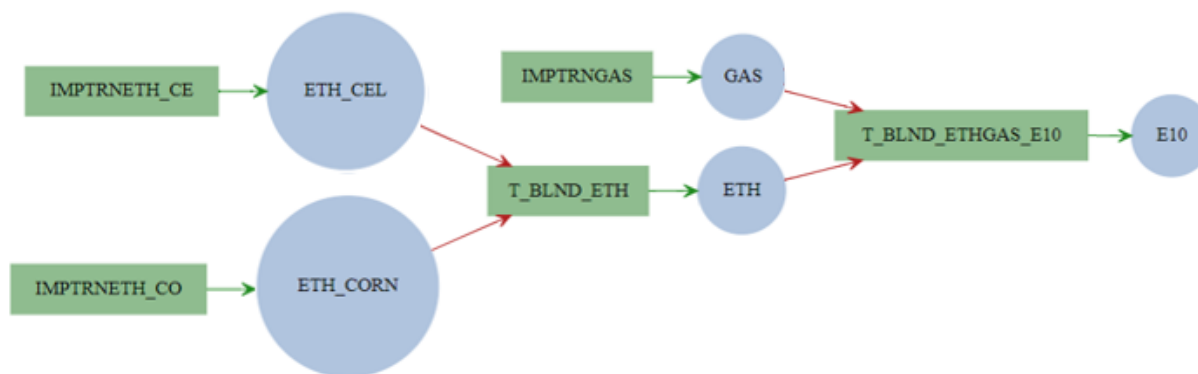
1.2 Transportation sector

In the current database, similar to the USEPA (Lenox, et al., 2013), E10 and E85 are each represented as fuels, as well as a range of transportation technologies that can utilize them. E10 is defined as an up to 10% ethanol blend and is most commonly found to be 10% ethanol. However, E85 is defined as a blend of 55 to 83% ethanol, varying seasonally based on weather.

1.2.1 Modeling of ethanol E10 and E85

Our modeling of E85 differs from the USEPA in that E85 blends in the database are represented as 55% minimum ethanol and 17% minimum gasoline. The blend ratio will then be determined based on the cost of the respective fuels and/or emissions data. In addition, we explicitly represent two main sources of ethanol, corn-based ethanol and cellulosic ethanol. The motivation for such a representation is due to Energy Independence and Security Act of 2007 (EISA) specification of where biomass must be sourced (U.S. Congress, 2007). The EISA addresses fuel economy and energy efficiency standards, but also incorporates biofuel requirements. It requires the use of “renewable biomass” to produce renewable fuels. Feedstocks sourced from new farmland cultivated after December 2007, tree crops and tree residues, federal lands, or rangeland are all excluded from the “renewable biomass” designation (U.S. Congress, 2007). This

constrains the land available for the production of biofuels. The EISA updates the renewable fuels standards (RFS) with annual biofuel requirements, culminating in requiring at least 36 billion gallons of biofuels to be used in the US by 2022 (U.S. Congress, 2007). Additionally, by 2022, at least 16 billion gallons of this must be supplied by cellulosic biofuels and a cap of 15 billion gallons is placed on corn-based biofuel (U.S. Congress, 2007). Appendix Figure 3.3 shows processes and commodities involved in producing E10 and Appendix Table 3.10 defines the notations used in Appendix Figure 3.3. E85 has a similar chain, except T_BLND_ETHGAS_E10 is replaced by T_BLND_ETHGAS_E85.



Appendix Figure 3.3: Processes and commodities defined for E10 production. E85 has a similar chain, except T_BLND_ETHGAS_E10 is replaced by T_BLND_ETHGAS_E85.

Appendix Table 3.10: Description of notations used in Appendix Figure 3.3

Name	Description	Designation
IMPTRNETH_CO	Import of corn-based ethanol to system	Technology
IMPTRNETH_CE	Import of cellulosic ethanol to system	Technology
ETH_CORN	Corn-based ethanol	Commodity
ETH_CEL	Cellulosic ethanol	Commodity
T_BLND_ETH	“Dummy” technology that blends different ethanol sources	Technology
ETH	Pure ethanol representing total mix of ethanol in system	Commodity
GAS	Pure gasoline	Commodity
T_BLND_ETHGAS_E10	Blending of ethanol and gasoline to produce E10	Technology
T_BLND_ETHGAS_E85	Blending of ethanol and gasoline to produce E85	Technology

We added constraints with regard to corn ethanol, cellulosic ethanol, and total ethanol values. For the purposes of the model, the EISA corn-biofuel cap was applied exclusively to ethanol, though biodiesel is also considered a renewable fuel. The bio-based diesel requirement includes a minimum of 1 billion gallons by 2012, representing 2.8% of the total standard (U.S. Congress, 2007). Values for the 2015, 2020, and

2025 time periods are included in Appendix Table 3.11. Except for the maximum total ethanol use constraint that reflects land availability, the rest of the constraints come from the EISA (U.S. Congress, 2007). Numerous scenarios of land availability were considered when designing the maximum total ethanol use constraint, ranging from converting all existing cropland in 2007 to biofuel feedstocks to the use of only residual lands for feedstock production. Residual lands are abandoned or degraded cropland, typically not suitable for typical food crops (Cai et al., 2010). The implemented land constraint is based on current ethanol production, plus the addition of minimum estimated residual lands on which biofuel feedstocks could be grown at a minimum yield value (Cai et al., 2010; Hay, 2015; National Agricultural Statistics Service, 2016). This produced a total biofuel potential of 42 million gallons per year – the current 14 billion gallons plus an additional 32 billion from residual lands.

Appendix Table 3.11: Constraints imposed on ethanol use. Numbers are in PJ.

Year	Minimum cellulosic ethanol use	Maximum based ethanol use	corn-ethanol use	Minimum ethanol use	total	Maximum ethanol use (land constraint)	total
2015	240.6	1203.0		1644.1		3689.0	
2020	842.1	1203.0		2406.0		3689.0	
2025	1283.2	1203.0		2887.2		3689.0	

Note: The 2025 time period reflects the federal government requirements to be implemented by 2022. The 2025 values are maintained for all of the subsequent time periods. The energy content of each ethanol type was assumed the same and equal to 80.2 MJ/gallon (Lenox, et al., 2013).

Similar to other fuels in our database, ethanol and gasoline prices are taken from the AEO 2018 (AEO, 2018). Ethanol cost data reflects the wholesale ethanol prices. However, in the AEO, gasoline is described as “motor gasoline”. Based on EIA definitions, this is not strictly pure gasoline but includes “conventional gasoline, all types of oxygenated gasoline, including gasohol; and reformulated gasoline” (AEO, 2018). Thus, this cost data does not represent a pure, wholesale price for gasoline.

1.2.2 Modeling of jet fuel and biodiesel

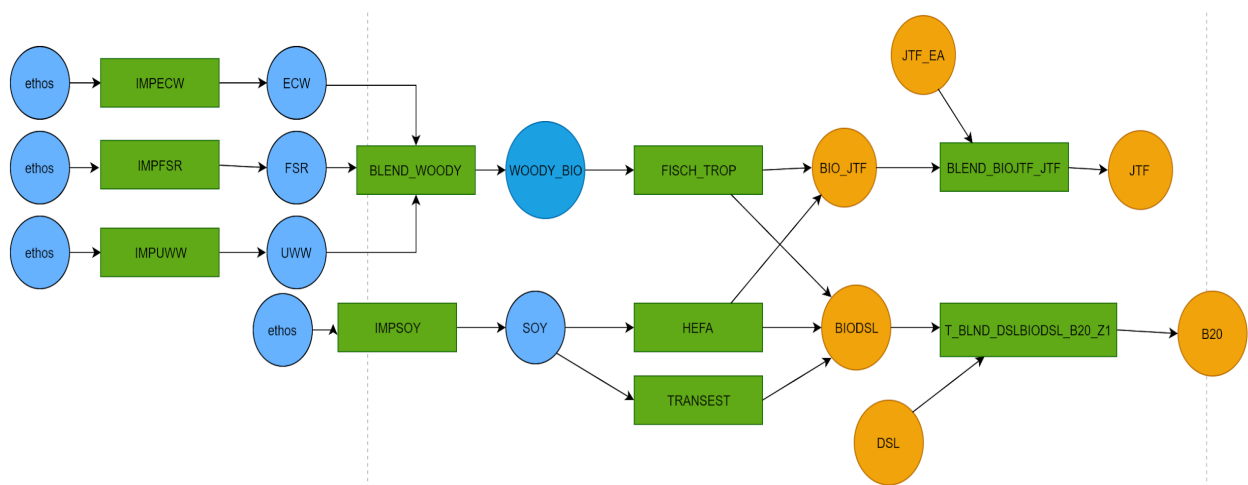
Our modeling of jet fuel and biodiesel production is given below. We have 7 different types of biomass that are fed into various process to produce bio jet fuel and biodiesel. The abbreviations used for the biomass commodities is given in Appendix Table 3.12.

Appendix Table 3.12: Biomass related commodities

Commodity name in Temoa	description
STV	Corn Stover
ECW	Energy Crops (Woody)
FSR	Forest Resources
UWW	Urban wood waste
AGR	Agricultural Residues
ECG	Energy Crops (Grass)
ECA	Energy Crop (Annual) - Sorghum
SOY	Soybeans
FISCH_TROP	Fischer-Tropsch process
HEFA	Hydro processed esters and Fatty acids

1.2.2.1 Description:

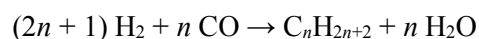
Considering the current feedstocks and processes in the EPA (and Temoa) database, two methods of bio jet fuel production can be incorporated into the model. In addition, biodiesel and cellulosic ethanol production has also been incorporated. The structure of the process as incorporated in the US database is shown in Appendix Figure 3.4.



Appendix Figure 3.4: Structure of bio jet fuel and biodiesel production in Temoa

1.2.2.1.1 Fischer-Tropsch (FISCH_TROP) process

Woody biomass is passed through a gasifier. The resultant syngas is then transformed into hydrocarbons by means of the Fischer-Tropsch process as follows:



The hydrocarbons are then processed to produce jet fuel and biodiesel, of roughly the same quality as conventional jet fuel and diesel.

In the database, ECW, UWW and FSR are blended using the tech BLEND_WOODY to produce a commodity, WOODY_BIO, which is then fed to the FISCH_TROP process to produce BIOJTF and BIODSL, since the techno-economic data of FISCH_TROP is for a lignocellulosic biomass feedstock.

1.2.2.1.2 Hydro-processed esters and fatty acids (HEFA) and Transesterification (TRANSEST)

Soybeans (SOY) are hydrotreated (treated with hydrogen), then isomerized through a cracking process, and subsequently refined to produce gasoline, jet fuel, diesel and various other light hydrocarbons (naphtha etc.).

This process has been commercially implemented, with lots of companies producing HEFA jet fuel for aviation use. It is ASTM certified, and allows for a maximum of 50% of bio-jet fuel to be blended with conventional jet fuel. Hence there is a TechInputSplit of 0.5 associated with the blending technology BLEND_BIOJTF_JTF which blends bio-jet fuel and imported jet fuel.

In the database, SOY is imported from ethos, then fed to HEFA. It produces both BIOJTF and BIODSL. The other products are ignored, since it is assumed that the process conditions are tailored to favor biodiesel and bio-jet fuel production.

Conventionally, biodiesel has been produced from vegetable oils using the transesterification process. Since the same feedstocks are used for both transesterification and HEFA, both processes are linked using a common feedstock (SOY). In this database, BIODSL is also produced using TRANSEST. Techno-economic parameters for the above mentioned processes are given in Appendix Table 3.13 and 3.14.

Appendix Table 3.13: Techno-economic data for FISCH_TROP AND HEFA

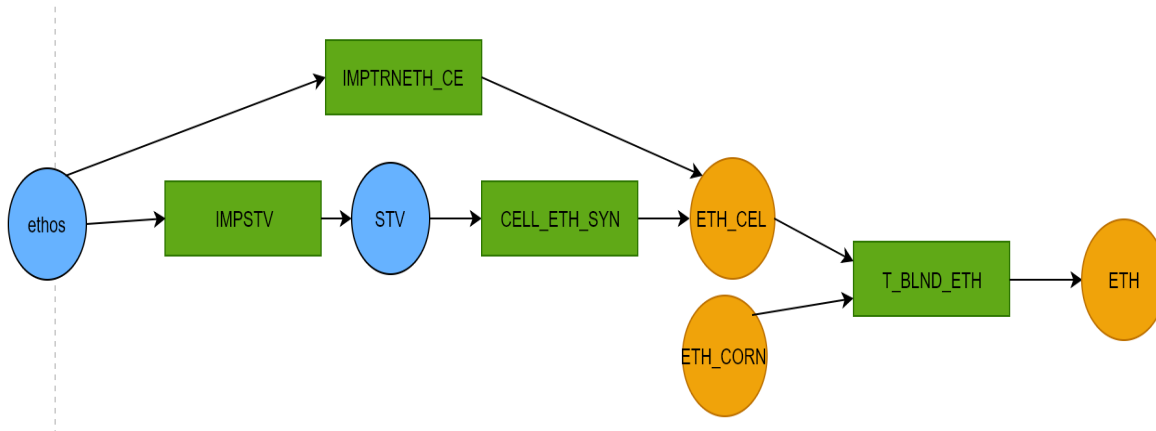
Parameter	FISCH_TROP	HEFA	Unit	Source	
Efficiency	50%	84%		(GREET, 2018; de Jong, 2018)	
Emissions					
	CO ₂	3.67	19.47	g/MJ	(GREET, 2018)
	NO _x	0.02329	0.0142	g/MJ	(GREET, 2018)
	SO _x	0.00571	0.0038	g/MJ	(GREET, 2018)
Investment cost	137.46	76.63	M\$/PJ	(Pavlenko et al., 2019; Bann et al., 2017; de Jong, 2018; Wormslev, 2016)	
Fixed cost	16.37	10.16	M\$/PJ	(Pavlenko et al., 2019; Bann et al., 2017; de Jong, 2018; Wormslev, 2016)	
Variable cost	5.52	5.52	M\$/PJ	(Pavlenko et al., 2019; Bann et al., 2017; de Jong, 2018; Wormslev, 2016)	
LCOE			¢/kWh jet fuel		

Appendix Table 3.14: Techno-economic data for TRANSEST

Parameter	FISCH_TROP	HEFA	Unit	Source	
Efficiency	90%	84%		(Huang et al., 2016)	
Emissions					
	CO ₂	7.22	19.47	g/MJ	(GREET, 2018)
	NO _x	0.0369	0.0142	g/MJ	(GREET, 2018)
	SO _x	0.00242	0.0038	g/MJ	(GREET, 2018)
Investment cost	29.1	76.63	M\$/PJ	(Huang et al., 2016)	
Fixed cost	2.59	10.16	M\$/PJ	(Huang et al., 2016)	
Variable cost	4.39	5.52	M\$/PJ	(Huang et al., 2016)	
LCOE			¢/kWh jet fuel		

1.2.2.1.3 Production of cellulosic ethanol from corn stover (CELL_ETH_SYN)

Appendix Figure 3.5 below shows the process for ethanol production.



Appendix Figure 3.5: Structure of ethanol production in Temoa

The corn stover biomass (STV) is fed to the CELL_ETH_SYN technology, which includes a gasifier. The resultant syngas is then cleaned and passed through a catalyst bed at high temperatures to produce cellulosic ethanol (ETH_CEL). ETH_CEL is then mixed with imported cellulosic ethanol and with imported corn ethanol (ETH_CORN) to produce Ethanol (ETH), which is then used to produce E10 or E85 blends. Techno-economic parameters for the ethanol production are given in Appendix Table 3.15.

Appendix Table 3.15: Techno-economic data for ethanol

Parameter	FISCH_TROP	HEFA	Unit	Source	
Efficiency	52%	84%		(Luo et al., 2009)	
Emissions	CO₂	15.16	19.47	g/MJ	(GREET, 2018)
	NO_x	0.03549	0.0142	g/MJ	(GREET, 2018)
	SO_x	0.126	0.0038	g/MJ	(GREET, 2018)
Investment cost	99.68	76.63	M\$/PJ	(Zhao et al., 2015)	
Fixed cost	24.57	10.16	M\$/PJ	(Zhao et al., 2015)	
Variable cost	9.67	5.52	M\$/PJ	(Zhao et al., 2015)	
LCOE			¢/kWh jet fuel		

1.2.2.2 Calculations

1.2.2.2.1 HEFA

Density of jet fuel = 0.804 kg/l

Energy content of jet fuel = 44 MJ/kg (GREET, 2018)

Discount rate = 6%

From (de Jong, 2018), Investment cost = 560 million \$/500 ton of jet fuel production per day (average of 265 and 855 M\$)

$$\text{Total energy generated in a year} = (0.5 \times 106 \text{ kg}) \times 365 \frac{\text{days}}{\text{year}} \times 44 \frac{\text{MJ}}{\text{kg}} = 8030 \text{ TJ}$$

$$\Rightarrow \frac{560 \times 10^6 \$}{8030 \text{ TJ} \times 10^3 \frac{\text{PJ}}{\text{TJ}}} = 69.738 \frac{\text{M\$}}{\text{PJ}}$$

Converting to 2018 dollars,

$$\text{Investment cost} = \frac{69.738 \frac{\text{M\$}}{\text{PJ}}}{0.91} = 76.64 \frac{\text{M\$}}{\text{PJ}}$$

Fixed cost = 10.2 % of Investment cost + Labor + Waste disposal

$$= 0.102 * 69.738 + (0.65+1.26) \frac{\text{€}}{\text{GJ}} * 1.12$$

(1.12 = conversion factor from euros to dollars)

$$= 9.25 \frac{\text{M\$}}{\text{PJ}}$$

Converting to 2018 dollars,

$$\text{Fixed cost} = \frac{9.25 \frac{\text{M\$}}{\text{PJ}}}{0.91} = 10.16 \frac{\text{M\$}}{\text{PJ}}$$

Variable cost = Electricity + Catalyst + Hydrogen + Natural gas

$$= (0.59+0.51+0.46+2.92) \frac{\text{€}}{\text{GJ}} * 1.12$$

$$= 5.02 \frac{\text{M\$}}{\text{PJ}}$$

Converting to 2018 dollars,

$$\text{Variable cost} = \frac{5.02 \frac{\text{M\$}}{\text{PJ}}}{0.91} = 5.52 \frac{\text{M\$}}{\text{PJ}}$$

1.2.2.2 Fischer-Tropsch

From (de Jong, 2018), Investment cost = 1004.5 M\$/500 ton jet fuel (average of 434 and 1575 M\$)

$$\text{Total energy generated in a year} = (0.5 \times 106 \text{ kg}) \times 365 \frac{\text{days}}{\text{year}} \times 44 \frac{\text{MJ}}{\text{kg}} = 8030 \text{ TJ}$$

$$\Rightarrow \frac{1004.5 \times 10^6 \$}{8030 \text{ TJ} \times 10^3 \frac{\text{PJ}}{\text{TJ}}} = 125.09 \frac{\text{M\$}}{\text{PJ}}$$

Converting to 2018 dollars,

$$\text{Investment cost} = \frac{125.09 \frac{\text{M\$}}{\text{PJ}}}{0.91} = 137.46 \frac{\text{M\$}}{\text{PJ}}$$

Fixed cost = 10.2 % of Investment cost + Labor + Waste disposal

$$= 0.102 * 125.09 + (0.65+1.26) \frac{\text{€}}{\text{GJ}} * 1.12$$

(1.12 = conversion factor from euros to dollars)

$$= 14.899 \frac{\text{M\$}}{\text{PJ}}$$

Converting to 2018 dollars,

$$\text{Fixed cost} = \frac{14.899 \frac{\text{M\$}}{\text{PJ}}}{0.91} = 16.37 \frac{\text{M\$}}{\text{PJ}}$$

Variable cost for FT is the same as that of HEFA.

1.2.2.2.3 Cellulosic ethanol

Density = 0.79 kg/l (Biofuels FactSheet)

Energy content = 26.8 MJ/kg (Biofuels FactSheet)

From (Zhao et al., 2015), Total Capital Investment = 7.26 \$/gallon

$$\Rightarrow 7.26 \frac{\$}{\text{gal yr}^{-1}} \times \frac{1 \text{ gallon}}{3.78 \text{ lit}} \times \frac{1 \text{ lit}}{0.79 \text{ kg}} \times \frac{1 \text{ kg}}{26.8 \text{ MJ}}$$

$$= 0.09071 \frac{\$}{\text{MJ}}$$

$$= 90.71 \frac{\text{M\$}}{\text{PJ}}$$

Converting to 2018 dollars,

$$\text{Investment cost} = \frac{90.71 \frac{\text{M\$}}{\text{PJ}}}{0.91} = 99.68 \frac{\text{M\$}}{\text{PJ}}$$

Fixed cost = 1.79 \$/gallon

$$\Rightarrow 1.79 \frac{\$}{\text{gal yr}^{-1}} \times \frac{1 \text{ gallon}}{3.78 \text{ lit}} \times \frac{1 \text{ lit}}{0.79 \text{ kg}} \times \frac{1 \text{ kg}}{26.8 \text{ MJ}}$$

$$= 0.02236 \frac{\$}{\text{MJ}}$$

$$= 22.36 \frac{\text{M\$}}{\text{PJ}}$$

Converting to 2018 dollars,

$$\text{Fixed cost} = \frac{22.36 \frac{\text{M\$}}{\text{PJ}}}{0.91} = 24.57 \frac{\text{M\$}}{\text{PJ}}$$

Variable cost = 0.71 \$/gallon

$$\begin{aligned} &\Rightarrow 0.71 \frac{\$}{\text{gal yr}^{-1}} \times \frac{1 \text{ gallon}}{3.78 \text{ lit}} \times \frac{1 \text{ lit}}{0.79 \text{ kg}} \times \frac{1 \text{ kg}}{26.8 \text{ MJ}} \\ &= 0.0088 \frac{\$}{\text{MJ}} \\ &= 8.8 \frac{\text{M}\$}{\text{PJ}} \end{aligned}$$

Converting to 2018 dollars,

$$\text{Variable cost} = \frac{8.8 \frac{\text{M}\$}{\text{PJ}}}{0.91} = 9.67 \frac{\text{M}\$}{\text{PJ}}$$

1.2.2.2.4 Transesterification

Density of biodiesel = 0.874 kg/l (Biodiesel)

Energy content = 37.8 MJ/kg (Energy content)

Lifetime = 20 years

From (Huang et al., 2016), Investment cost = 84 M\$ / 96 million liters of biodiesel production per year

$$\text{Total energy generated in a year} = 96 * 106 \frac{\text{litres}}{\text{yr}} \times 0.874 \frac{\text{kg}}{\text{lit}} \times 37.8 \frac{\text{MJ}}{\text{kg}} = 3.171 \frac{\text{PJ}}{\text{yr}}$$

$$\Rightarrow \frac{84 \text{ M}\$}{3.171 \frac{\text{PJ}}{\text{yr}}} = 26.49 \frac{\text{M}\$}{\text{PJ}}$$

Converting to 2018 dollars,

$$\text{Investment cost} = \frac{26.49 \frac{\text{M}\$}{\text{PJ}}}{0.91} = 29.1 \frac{\text{M}\$}{\text{PJ}}$$

Fixed cost = Labor + capital depreciation

$$\begin{aligned} &= (3.5 + 4) \frac{\text{M}\$}{3.171 \frac{\text{PJ}}{\text{yr}}} \\ &= 2.36 \frac{\text{M}\$}{\text{PJ}} \end{aligned}$$

Converting to 2018 dollars,

$$\text{Fixed cost} = \frac{2.36 \frac{\text{M}\$}{\text{PJ}}}{0.91} = 2.59 \frac{\text{M}\$}{\text{PJ}}$$

Variable cost = Other chemical costs + Utilities + Supplies + General Works

$$= (6.5 + 4 + 1.3 + 0.9) \frac{\text{M}\$}{3.171 \frac{\text{PJ}}{\text{yr}}}$$

$$= 4 \frac{M\$}{PJ}$$

Converting to 2018 dollars,

$$\text{Variable cost} = \frac{4 \frac{M\$}{PJ}}{0.91} = 4.39 \frac{M\$}{PJ}$$

1.3 Residential and commercial sectors

We made some minor changes on the USEPA representation of end-use technologies by removing the alternative technologies from the same family of technologies. For four demand services space heating, space cooling, water heating and refrigeration, various “versions” of a single technology type are defined. For instance, there are four different versions of heat pump in the USEPA that vary in their coefficient of performance and overnight capital costs (Lenox, et al., 2013). While there is value in having insight over the relative cost-effectiveness of heat pumps with respect to other space heating technologies (e.g. electric radiant heating or natural gas furnaces), we think that keeping multiple versions of heat pump, needlessly oversize the database. Therefore, for simplicity we keep the “version one” of each of the technologies with multiple versions. In all cases, “version one” has the closest costs and performances to the products found in the market today.

1.4 Industrial sector

1.4.1 Background

The industrial sector accounts for the second-largest share (32%) of primary energy consumption in the United States (33,000 PJ in 2015). Its electrification share falls between process heat and transportation, with 10,500 PJ (24%) of its primary energy from electric sector. Besides electricity, industrial energy uses rely on a mix of fossil fuels and biomass (EIA, 2017). The industrial sector in Temoa identifies energy consumption by non-manufacturing and manufacturing industry. The majority of the energy consumption in the non-manufacturing industry comes from agriculture, mining, and construction while major energy consumers of manufacturing industry are food, paper, bulk chemical, cement, iron, steel and aluminum industry.

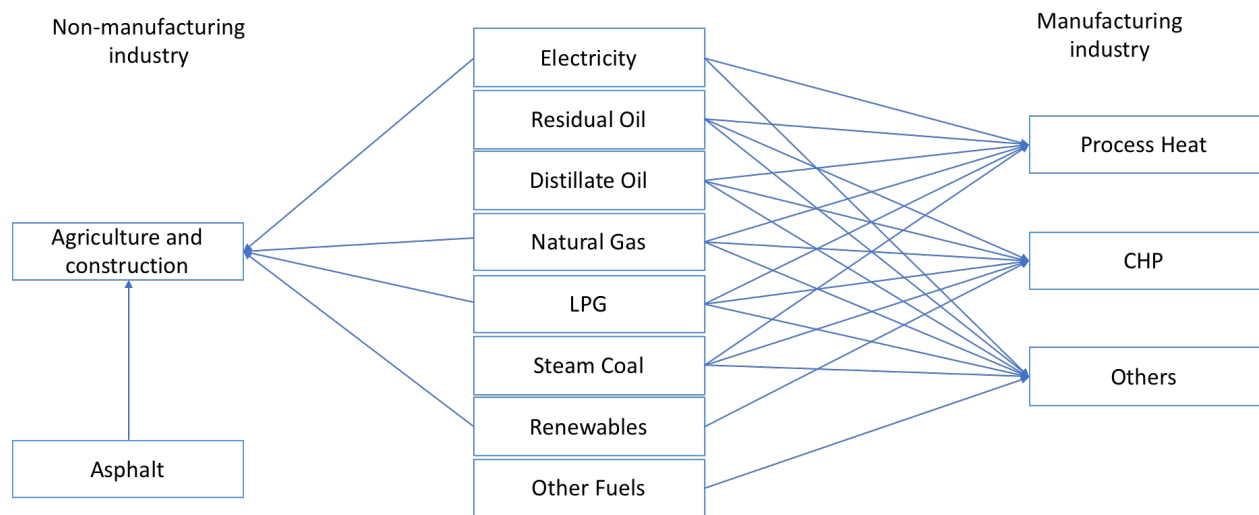
1.4.2 Structure

One of the side effects of deep decarbonization scenarios is electrification of end use sectors. The previous representation of industrial sector considered fixed fuel share which did not allow substitution of fossil fuels with electricity or renewable sources. In order to enable substitution between fuels under high renewable

penetration scenarios or other deep decarbonization scenarios, while at the same time keeping the complexity at a minimal level we choose the following approximation of the industrial sector.

The industrial sector in Temoa estimates energy consumption by energy source for manufacturing and non-manufacturing industries. The manufacturing industries are subdivided further by the end use accounting procedures. The non-manufacturing industries are modeled with less detail because processes are simpler and limited data is available. We do not have a direct representation of refining industry in Temoa. Instead we include the cost of refining in the fuel cost for electric sector. The refining industry is not included in the industrial sector.

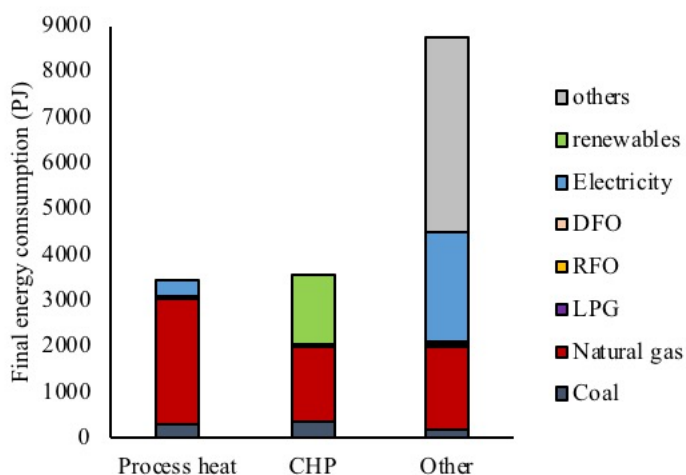
In order to simplify the manufacturing industry representation in Temoa, the energy consumption is classified by sources and three end uses: process heat, CHP and other. We also combine petroleum coke, lease, plant fuel, metallurgical coal, coke, and road oil into a single fuel commodity called ‘other fuels’ because of their significantly smaller share in energy consumption (EIA, 2017). We combined all end uses for non-manufacturing industry into one combined non-manufacturing demand commodity. Note that type of fuel consumed is dependent on the end-use process. For example, asphalt is only consumed in non-manufacturing industry. Conceptual framework of the industrial sector representation in Temoa is shown in Appendix Figure 3.6.



Appendix Figure 3.6: Conceptual framework of industrial sector.

The end uses in the manufacturing sector are classified into 13 categories in the (VT_EPAUS9rT_IND_v16.1.0.xlsx, EPA 2017) database namely: conventional boiler use, combined heat

and power (CHP), process heating, process cooling, machine drive, electro-chemical process, other process uses, facility HVAC, facility lighting, onsite transportation, conventional electricity generation, other non-process uses, and end use not reported. We consider end use categories other than process heat and CHP as ‘other’ end uses. As shown in Appendix Figure 3.7. 10, process heating and CHP account for 45% of final energy use in manufacturing.



Appendix Figure 3.7: Energy use in U.S. manufacturing (MECS, 2014).

Approximately 6,200 PJ of natural gas, 1,550 PJ of biomass and 820 PJ of coal were used directly by manufacturing industries in 2014, with most occurring in process heating and CHP. There is a potential interchangeability in fuels used for process heat and CHP. For example, natural gas can be replaced by electricity and biomass in process heat and CHP, respectively. Appendix Figure 3.8 shows the industrial subsectors and end uses that has potential for electrification.

Industrial Subsector	End Use	Representative Electrotechnology
All manufacturing industries and agriculture	Building HVAC	Industrial heat pump
	Machine drive	Electric machine drive
Food, chemicals, transportation equipment, plastics, and other manufacturing	Process heat	Electric boiler
Food	Process heat	Industrial heat pump
Chemicals	Process heat	Resistance heating
		Industrial heat pump
Glass and glass products	Process heat	Direct resistance melting (electric glass melt furnace)
Primary metals	Process heat	Induction furnace
Transportation equipment	Process heat	Induction furnace
Plastic and rubber products	Process heat	Resistance heating
	Process heat	Infrared processing
Other manufacturing	Process heat	Resistance heating
Other wood products and printing and related support	Process heat: curing	Ultraviolet curing

Appendix Figure 3.8: Industrial subsector and End Uses relevant to electrification scenarios. (Jadun et al., 2017)

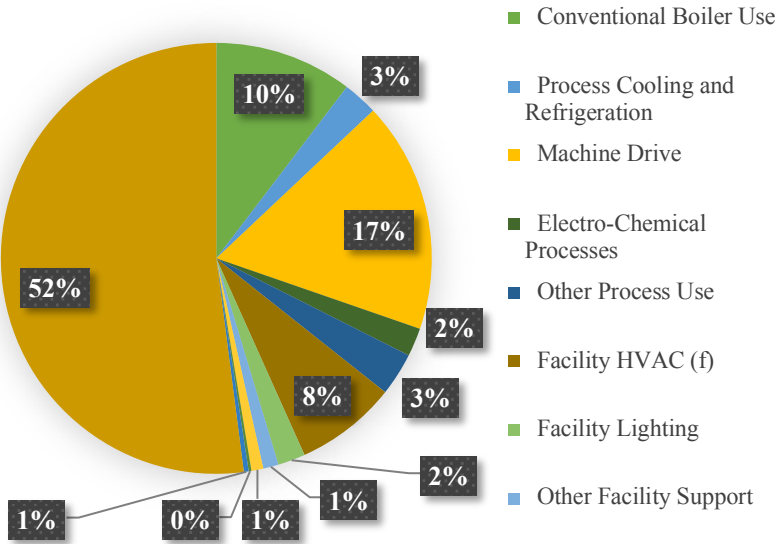
The major energy source for non-manufacturing industry is asphalt which contributes to 60% of energy consumption. Natural gas, electricity and LPG contributes 20%, 12% and 4% to final energy consumption. There might be a potential for fuel substitution for non-manufacturing industry, however, due to lack of data, we assume a fixed fuel share.

1.4.3 Key Assumptions about manufacturing sector

The time horizon assumed for US database in Temoa is 2017 to 2050. Total energy consumption data for manufacturing industry is available for our assumed time horizon. However, we do not have energy consumption data by fuel and end use. To obtain the required data, we use data from MECS (2014) and EIA (2010). The MECS (2014) provides the fuel consumption by source and end use for 2014. EIA (2010) provides energy consumption by fuel, and end use for 2010.

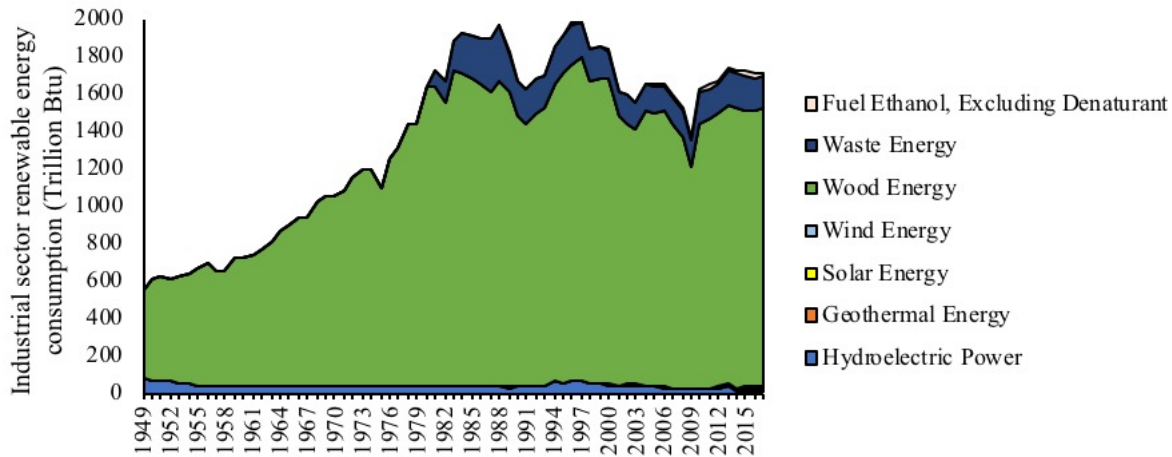
Following Appendix Figure 3.9 gives share of various end-uses which are combined to form a single category called ‘other’ end uses. 52% of the energy consumption for ‘other’ end uses is reported by fuel type. The exact end use process is not reported in (EIA, 2017). Moreover, 92% of the fuel consumption is from ‘other fuels which are petroleum coke, lease, plant fuel, etc. So, there is lack of information and relevant data for potential fuel substitution for 52% of energy consumption. Furthermore, process cooling, machine drive, lector-chemical processes, and facility lighting demand accounts for 25% of energy

consumption for 'other' end uses. More than 90% of which is satisfied by electricity. There might be a fuel substitution potential for the remaining 23% energy consumption in 'other' end uses, however, for simplicity, we assume that potential for electrification in 'other' end uses is negligible. Note that 23% of 'other' end uses is equivalent to 10.6% of the total industrial sector energy consumption (=1969/19748). Hence, we fix the fuel share of other end uses for the entire time horizon. We also fix the fuel share of the entire manufacturing industry for the base year in order to calibrate the database to a historical year. Natural gas accounts for 90% and 55% of the process heat and CHP energy consumption, respectively.



Appendix Figure 3.9: Share of energy consumption by end-uses which are included in 'other' end uses

We assume that biomass in industrial sector is a byproduct of paper industry which is used for combined heat and power (CHP). Since it is a byproduct, we assume that the cost of biomass for CHP is zero. The biomass use in industrial sector has remained approximately constant since 1979 as shown in Appendix Figure 3.10. Hence, to avoid unlimited utilization of biomass for CHP, we set a maximum activity constraint on biomass. We let the cost of technology and fuel decide the optimal fuel mix for the process heat and CHP end use.



Appendix Figure 3.10: Historical renewable energy consumption for industrial sector

We define technologies only for process heat and CHP since these end uses have the highest potential for fuel substitution (Jadun et al., 2017). The technologies are distinguished by fuel and end use. We assume that the demand for the base year is satisfied by existing technology. The existing technology has the same fixed operations and maintenance cost as the new technology. EIA (2010) provides the technology cost by manufacturing industry subsectors. Process heat and CHP are common to many industrial subsectors. Using EPA as a starting point, we calculate the average investment cost, fixed cost, and variable cost of the technologies over all the manufacturing industry subsectors. Efficiency and capacity factor of all technologies is assumed to be 1 since we assume end-use demand in PJ and input fuel is also in PJ. Life time of all technologies is assumed to be 50 years. Appendix Table 3.16 shows the techno economic parameters for the technologies.

Appendix Table 3.16: Techno-economic parameters for the technologies (EIA, 2010)

		Investment Cost (\$M/PJ)	Fixed Cost (\$M/PJ)	Variable Cost (\$M/PJ)	Efficiency	Capacity Factor	Life time (years)
Process Heat	Electricity	45.060	2.960	N/A	1	1	50
	Residual Fuel Oil	51.620	3.240	N/A	1	1	50
	Distillate Fuel Oil	55.760	3.470	N/A	1	1	50
	Natural Gas	42.390	2.770	N/A	1	1	50
	LPG	42.310	3.140	N/A	1	1	50
	Coal	44.470	3.120	N/A	1	1	50
	Renewables	N/A	N/A	N/A	N/A	N/A	N/A
	Others	N/A	N/A	N/A	N/A	N/A	N/A
CHP	Electricity	N/A	N/A	N/A	N/A	N/A	N/A
	Residual Fuel Oil	N/A	0.946	0.011	1	1	50
	Distillate Fuel Oil	17.448	1.120	0.013	1	1	50
	Natural Gas	18.255	0.867	0.025	1	1	50
	LPG	31.802	1.039	0.016	1	1	50
	Coal	N/A	4.355	0.050	1	1	50
	Renewables	7.571	0.470	0.013	1	1	50
	Others	N/A	N/A	N/A	N/A	N/A	N/A

The EPA data has no technology representation for coal and RFO used for CHP, biomass is used only for CHP and other fuels, which include petroleum coke, lease, etc., are used only for ‘other’ end uses. EPA database has no variable cost for technologies used for process heating.

1.4.4 Key assumptions about non-manufacturing sector

Table ‘TechData_OTR’ in the EPA worksheet provides residual capacity for the year 2005 and 2010 by energy source. The mining and refining industry consumption is approximately 2 quads. Total energy consumption for the non-manufacturing sector is taken from the EPA database for the model time horizon. We do not explicitly model mining in for the US database. Instead, we include the cost of mining in the imported fuel cost. Hence, for simplicity, mining and refining energy consumption are removed from the total energy consumption. The EPA worksheet provides the energy consumption for the year 2010. We use this database to estimate the demand for the non-manufacturing industry for the model time horizon. Note that the non-manufacturing demand is represented as a fuel share. Hence, we introduce a dummy technology to represent the energy transfer from fuels to end-use.

1.4.5 Fuel Cost

Fuel cost projections taken from AEO database are given in Appendix Table 3.17. Please note that fuel prices for industrial sector is different than fuel price for other sectors.

Appendix Table 3.17: Fuel cost projections from AEO (\$Million/PJ)

(\$M/PJ)	Distillate		Residual	Natural	Coal	Gasoline
	LPG	Fuel Oil	Fuel Oil	Gas		
2017	10.069	11.852	4.309	2.993	3.279	15.303
2020	10.726	16.904	9.077	3.956	3.309	15.961
2025	11.625	18.853	11.526	4.244	3.438	17.289
2030	12.083	19.937	12.448	4.367	3.467	17.770
2035	13.031	21.012	13.258	4.377	3.501	18.665
2040	13.855	22.002	14.035	4.582	3.552	19.453
2045	14.601	22.277	14.347	4.783	3.627	20.162
2050	15.331	22.324	14.630	5.069	3.734	20.852

1.4.6 Hydrogen in industrial sector

There are four ways to use hydrogen in the industrial sector. The first option is to blend at most 3.4% hydrogen with natural gas. Second option is to use the synthetic natural gas to replace natural gas. The third option is to blend at most 75% methanol with industrial gasoline. The description of all the above options is given in the power -to-X section. In this section we discuss the fourth option where we replace “other” fuels in the industrial sector with hydrogen.

Now, we don’t have much information about what the other fuels are and their properties or share. From the EPA database we know that the “other” fuels include but are not limited to lease, lubricants, coke, petroleum, etc. We assume that all of these fuels can be produced as a by-product of Fischer tropesch process. We use the technology named H2_OTH to convert H2_100 to O_OTH_H2. The techno economic parameters of H2_OTH are same as FISCH_TROP technology. In the future, we need to remove the gasification cost from the investment cost of H2_OTH. We haven’t done it yet due to lack of data.

A noteworthy point here is that the efficiency of H2_OTH is increased from 0.5 to 1.0 and the investment cost is increased from 137.46 to 274.92. We did this for plotting purposes.

1.5 Cross-sectoral issues

1.5.1 Hurdle rate

Hurdle rates represent the technology-specific discount rates used to amortize capital costs and can be used to represent non-economic costs such as time preference, risk, and uncertainty (Decarolis et al., 2017).

Without hurdle rates on new technologies in the residential and commercial sectors, the majority of existing end-use technologies are retired in the first time period and replaced with new capacity. For simplicity, Temoa does not consider the remaining capital payments on existing technology, which often makes it cost-effective to simply replace older, less efficient vintages with new ones. To remedy this issue, we assigned a uniform hurdle rate of 30% to all the new technologies in the residential and commercial sector. This rate is high enough to keep existing technologies active until they reach the end of their useful lifetimes. Since the hurdle rate is uniform for all new technologies, it doesn't incentivize one technology over another. Adhering to the same logic in the electric sector, all electric generating technologies use a uniform 6% rate, which is the rate for renewable and natural gas-fired technologies in AEO 2018 (AEO, 2018).

We used a uniform 10% hurdle rate for all the alternative vehicles in the light duty vehicle sector and 5% for conventional internal combustion engines. All the other technologies in the transportation sector have 5% hurdle rates. The assumed 10% hurdle rate is relatively low; surveys have estimated hurdle rates associated with alternative vehicle purchases in the range of 20-50% (Peterson and Michalek, 2013; Mau et al., 2008; Home et al., 2005).

1.6 Power to X

1.6.1 Introduction

The increasing share of renewable energies like solar and wind power for generation of electricity yields higher fluctuations in power production. Evidently, this is attributed to the fact that electricity generation from solar and wind is not controllable, unless it is curtailed, which evidently is the less desired option. For that reason, it will become a challenge to balance demand and production of electricity in future energy systems providing a high share of renewables.

Obviously, electrical storages are a good measure to overcome this challenge, and various technologies are available like batteries, compressed air or pumped hydro types. Since more than 10 years Power-to-Gas is discussed as a potential technology in this respect. Basically, Power-to-Gas incorporates the generation of gaseous Hydrogen by electrolysis driven by excess electricity from solar and wind plants. This Hydrogen can either be used directly for electricity generation i.e. by the use of fuel cells, or it can be converted by a

chemical process in conjunction with CO₂ to synthetic natural gas (SNG), which can be fed to gas turbines in order to yield electricity again. In any case either Hydrogen or SNG serve as the energy storage, and the timely separation of production and utilization of the gases enables for a better balancing of renewable electricity production and electrical load.

The beauty of adding the chemical process for generating SNG is twofold: Firstly, SNG can be fed into the existing grid for natural gas with no restrictions, and existing technologies like gas turbine can be used for re-generation of electricity. Secondly, the chemical process for conversion of Hydrogen to SNG serves as a sink for CO₂. This creates an interesting option for CO₂-utilization everywhere, where CO₂ occurs in higher concentrations i.e. at biogas or CCS plants or at industrial processes like production of cement or steel. However, the higher cost and the loss in efficiency introduced by the additional chemical process need to be evaluated carefully compared to the direct utilization of Hydrogen.

Besides from looking at Power-to-Gas as a technology purely applied for storage of electric energy, it offers further advantages in terms of coupling the sector of electricity generation to the heat sector and especially to the transport sector. This is, because either Hydrogen or SNG can serve as fuel for furnaces in order to produce heat for residential, commercial or industrial purposes. Similarly, Hydrogen and SNG can be used for powering fuel cell or gas driven vehicles and by this means creating an alternative pathway for integrating renewable electricity into the transport sector in addition to electric vehicles. It is even more an option to convert Hydrogen and CO₂ in further chemical processes into liquid fuel like Methanol or even synthetic gasoline, which evidently opens the door for serving the entire transport sector including i.e. large trucks and airplanes. In order to point out this option, the labelling of the technology has changed during the last years from Power-to-Gas to Power-to-X, where “X” represents the variety of fuels, which may result from the technology.

1.6.1.1 Scope of this report

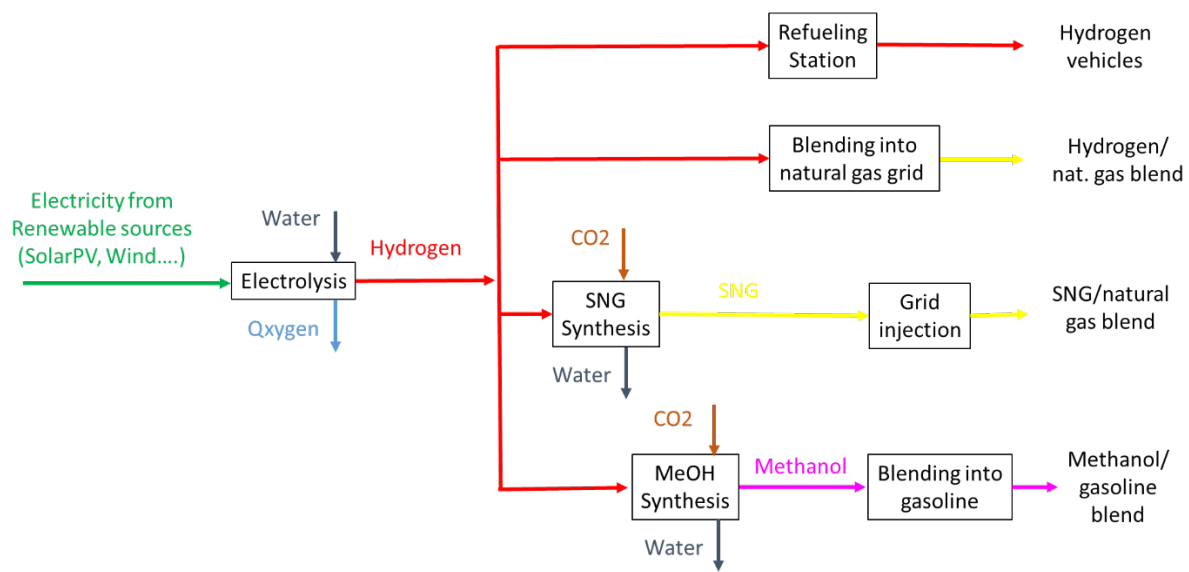
In order to evaluate the value of Power-to-X for future energy systems and its deployment under different assumptions, the technology was integrated in the Tool for Energy Model Optimization and Assessment (Temoa) developed at NC State University (Temoa Project). Since Temoa is an energy economy optimization model, it requires an adequate description of the different processes incorporated in Power-to-X in terms of energy efficiency, cost and emissions, which will be outlined in the following.

After describing the technology in this way, the second part of this report deals with the results derived from applying Temoa including the new features according to Power-to-X to the data set of the US energy

system, which already exists. As a base scenario a deep decarbonization down to 80% below the 2005 level until the year 2050 is pursued. Variation of different parameter provide insight about the dependencies related to the deployment of Power-to-X, which is used to close the report with final conclusions.

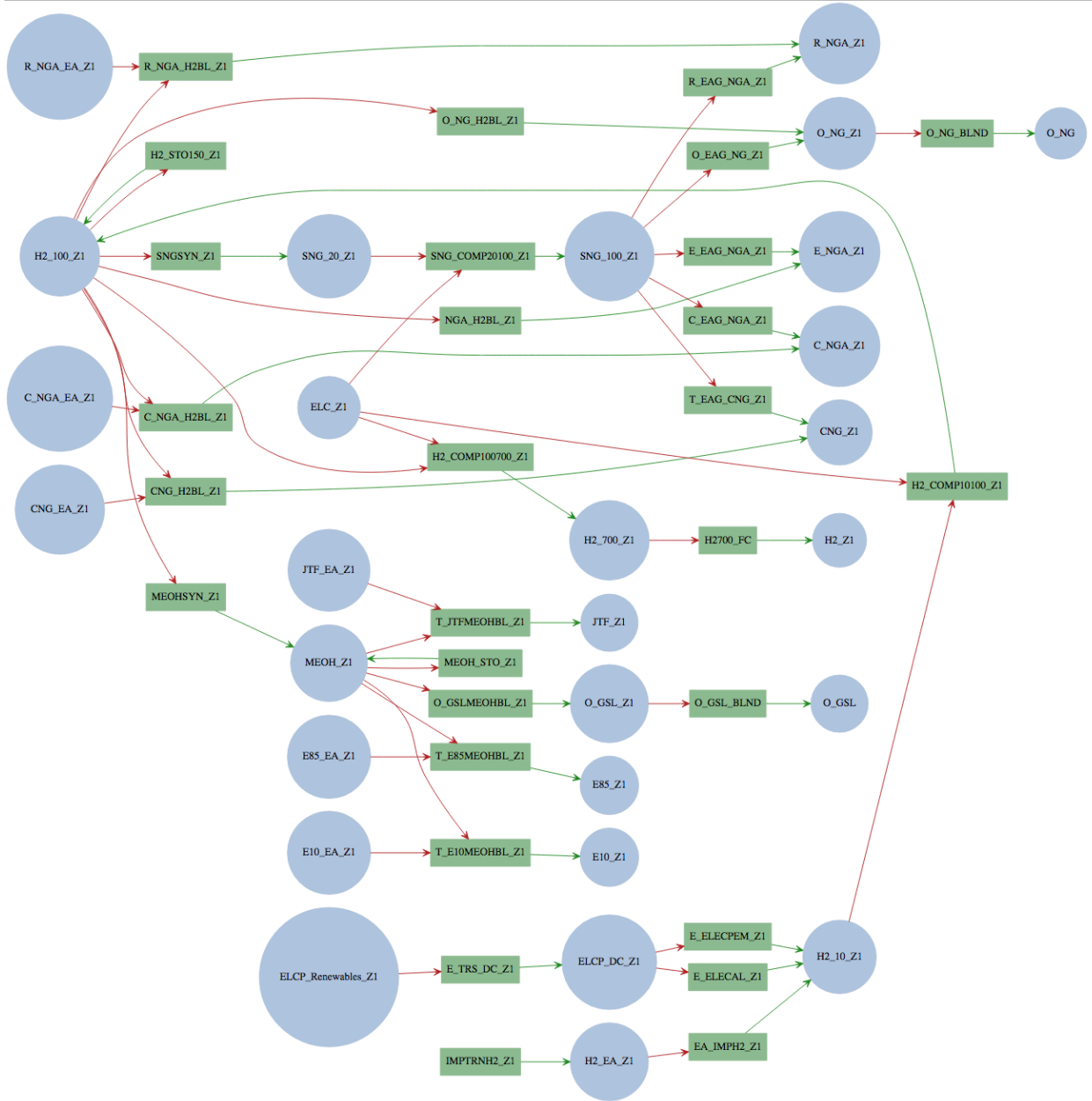
1.6.2 The Power-to-X technology

As already outlined in the introduction, Power-to-X incorporates different pathways for the conversion of renewable electricity to gaseous and liquid fuels. Evidently, each of these pathways should be adequately represented in Temoa. Appendix Figure 3.11 basically illustrates the conversion technologies pursued in this report.



Appendix Figure 3.11: Basic pathways for conversion of renewable electricity to gaseous and liquid fuels by Power-to-X pursued in this report

The following Appendix Figure 3.12 gives the schematic of the power to gas structure in Temoa.



Appendix Figure 3.12: Power to Gas representation in US database

It can be seen that in a first step electricity from renewable sources like PV or wind-plants is utilized to separate water into Hydrogen and Oxygen by electrolysis. For the economic analysis in Temoa it is assumed that the water needed is available at no cost and that no revenues are generated from the Oxygen generated by the process. While the first assumption is more than reasonable, the second may prevent the deploying of the technology due to higher cost. However, revenues from utilizing the Oxygen resulting from the electrolysis are neglected, in order to omit taking further processes for Oxygen purification into account,

on the one hand. On the other hand, considering any benefit from the produced Oxygen may help to improve the economic feasibility of Power-to-X later on.

Appendix Figure 3.12 reveals that Hydrogen from the electrolysis is used in four different ways. It is used either directly as fuel for Hydrogen powered vehicles like i.e. fuel cell cars. Another way of direct utilization is blending Hydrogen into natural gas, even though this is restricted by an upper limit. For practical applications momentarily, an upper limit of 10 Vol% is feasible (Dörr, 2016), but further efforts in R&D are intended to yield an increase of this limit (Müller-Syring et al. 2013). With respect to the current state of the art, in this report the upper value for blending Hydrogen into the natural gas grid is fixed at 10 Vol%.

A separate distribution grid for Hydrogen was not analyzed. Up to today no major Hydrogen grids exist, because the cost of implementing such grids are quite high and hard to predict accurately. Hence, this cost will dominate the results on the one hand with only minor chances for practical verification on the other hand. This will burden the results with a large proportion of uncertainty and by this means drastically reduces the significance of any conclusions.

The two additional pathways for utilization of Hydrogen from electrolysis involve a further chemical process where Hydrogen reacts with CO₂ either to SNG or to Methanol. The water leaving both processes is not considered for economic evaluation. CO₂, however, might be a side product of a biogas or a CCS-plant nearby and by this means available for free, as i.e. suggested in (US Census Bureau, 2010). However, if the CO₂ needed for the reaction with Hydrogen must be extracted from any kind of gas stream, the cost for separation and purification have to be considered. In this case prices for CO₂ from CCS-plants are reported in the literature between 20 and 60 €/to (Schiebahn et al., 2015) and 7 – 75 €/to (Ahern et al., 2015), even though it is not quite clear to what extent the investment cost of the CCS-plant are included, which seems to be questionable from the author's point of view. In (Atsonios et al., 2016) a price for CO₂ of 43.8 €/to is reported as an equivalent for average CO₂ avoidance cost for coal-fired power plants according to IEA. For biogas plants the cost for CO₂ add up to 68 – 154 €/to according to (Ahern et al., 2015); again, this cost seems high especially compared to others, like (US Census Bureau, 2010), who account CO₂ from biogas plants for free.

Other sources for CO₂ can be found in gas streams released from industrial plants like i.e. the cement or steel industry. The cost for CO₂ in these cases is, however, highly depending on concentration and availability. If it is intended to extract CO₂ from ambient air, a price up to 1000 \$/to must be considered (Götz et al, 2016), (Ahern et al., 2015).

The SNG generated from the chemical process is almost pure methane, and for this reason there is no restriction at all for directly feeding SNG into the natural gas grid. Methanol, as the product from the other chemical process is a liquid, and it can be blended into gasoline. Various simulations as well as experimental studies verify the feasibility of a high percentage of methanol in gasoline for Otto engines (Farkade and Pathre, 2012; Iliev, 2015). In the 80's and 90's a reasonable fleet of vehicles ran on 85% methanol (M85) in the state of California (Wuebben, 2015) with no major technical problems. The reasons for not continuing the program at that time were both, economical, because the price of gasoline dropped under the limit where any blending of methanol was feasible, and political, since the use of ethanol was supported with respect to the American farmers (Falco, webpage). Based on this experience the upper limit for blending methanol into gasoline for any transportation purpose is fixed at 85 Vol%.

1.6.3 Implementing Power-to-X into Temoa

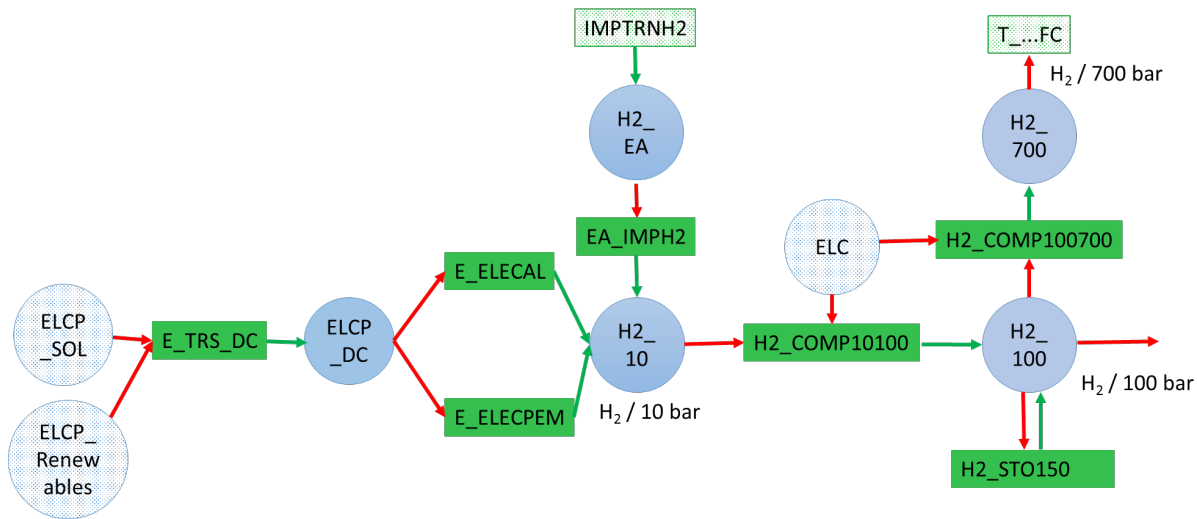
In the following the implementation of the schematic from Appendix Figure 3.12 in Temoa will be outlined. This includes an introduction of all new technologies and commodities as well as a brief description of all related parameter like cost, efficiencies, emission activity, life time etc. A report by ENEA consulting “The potential of Power-to-gas” from 2016 (ENEA, 2016) served as a good summary in in this respect, but further literature has been studied, in order to verify the data from the report as well as to gather more recent data. Starting from the input of electricity to Power-to-X, it can be seen from Appendix Figure 3.13 that the technologies are connected to the existing commodities for renewable electricity (ELCP_SOL, ELCP_Renewables) in Temoa.

1.6.3.1 Transformation of electricity from AC to DC (E_TRS_DC)

Since the electrolysis is driven by DC electricity, the AC current from the grid has to converted to DC beforehand. This might not be always necessary having small units directly coupled to solar-PV in mind, but in general the renewable electricity needs be transferred to the Power-to-X plant by using standard AC transmission lines.

In the ENEA report (Götz et al., 2016) an efficiency of 97.5% is given for the transformation from AC to DC, and this value has been adapted to Temoa as well as the lifetime of 40 years. Regarding investment cost a value of 0.2 Mio €/MW (= 0.24 Mio \$/MW) was taken from a report for planning the reinforcement of the German transmission grid from 2016 (Felix et al., 2016). However, this value for CAPEX is in good agreement to the data from the ENEA report (ENEA, 2016). OPEX and variable cost are neglected.

The resulting output commodity is DC electricity ELCP_DC, which is fed to the electrolysis technologies.



Appendix Figure 3.13: Implementation of the processes for Hydrogen generation in Temoa (textured commodities/ technologies already existing in Temoa, fully colored commodities/technologies new to Temoa)

1.6.3.2 Technologies for electrolysis (E_ELECAL and E_ELECPEM)

For Hydrogen generation from electrolysis three different technologies are currently discussed: Alkaline, PEM and High temperature (SOEC). While Alkaline electrolysis is the only mature technology, PEM electrolysis is in the status of field testing and SOEC is still in the lab. However, PEM and SOEC technologies offer higher efficiencies and lower cost compared to Alkaline, and for that reason major efforts in R&D are spent on both technologies, momentarily. For PEM electrolysis estimates for CAPEX and OPEX already exist, for SOEC rough approximation are available in this respect, only. Hence, it was decided to implement Alkaline and PEM electrolysis into Temoa at this point. Whenever more advanced data will be available for SOEC, this technology can be added quite easily.

Regarding cost, lifetime and efficiencies there are meanwhile several studies and reports available from the literature. Besides the report by ENEA, sources (Götz et al., 2016; Schiebahn et al., 2015; Ahern et al., 2015; Smolinka et al., 2016; Bertuccioli et al., 2014; Smolinka et al., 2010) have been used to derive the data needed. Evidently, the data from the different publications does not coincide entirely, even though they are in the same range. Often, it is reported, that the data has been taken and averaged from various other sources, which span a certain range as well.

Regarding efficiencies, the data for Temoa is taken from (Bertuccioli et al., 2014) applying one correction for alkaline electrolysis as follows: Since Hydrogen should be supplied at a pressure level of 10 bar after

electrolysis, the additional efforts for compression need to be incorporated in the numbers for efficiencies. While PEM electrolysis works at elevated pressure anyhow, no correction is necessary for this type. In contrast, the efficiency for alkaline electrolysis drops from 74 to 66%, if pressure is increased from ambient to 10 bar according to (ENEA, 2016). For that reason, all efficiencies for alkaline electrolysis taken from (Bertuccioli et al., 2014) were corrected by a factor of 66/74.

Investment cost (CAPEX) are taken from (Bertuccioli et al., 2014), as well. At this point it should be noted that cost for electrolysis are in most cases referred to electric input. Since cost in Temoa are based on output, the cost from (Bertuccioli et al., 2014) need to be divided by efficiency for each period. In addition, factors of 1.1 and 1.2 are applied; the former for taking installation cost into account, the latter for currency conversion from € to US\$. Operating and maintenance cost (OPEX) are calculated at 3% from CAPEX, taken as mean value from (ENEA, 2016), and variable cost are neglected. Lifetime is assumed to reach 25 years for both types of electrolysis. This accounts for low numbers of operational hours, if the technologies are applied in the near future, and for technical improvement, if applied later on.

Appendix Table 3.18 summarized all relevant data for the two technologies for electrolysis E_ELECAL and E_ELECPM:

Appendix Table 3.18: Data for electrolysis technologies E_ELECAL and E_ELECPEM entered to Temoa

	period/vintage	E_ELECAL	E_ELECPEM
efficiency / %	2015	66.3	75.8
	2020	67.6	82.1
	2025	68.9	82.1
	2030	70.3	83.8
	2035	71.0	83.8
	2040	71.7	85.6
	CAPEX / Mio. \$/GWout	2015	1852
2020		1231	1609
2025		1169	1399
2030		1090	1197
2035		1060	1055
2040		1031	925
OPEX / Mio. \$/GWout		2015	55.6
	2020	36.9	48.3
	2025	35.1	42.0
	2030	32.7	35.9
	2035	31.8	31.7
	2040	30.9	27.7
	Cost, variable		0
Lifetime / a		25	25

1.6.3.3 Technology for import of Hydrogen (IMPTRNH2)

As displayed in Appendix Figure 3.13, at the pressure level of 10 bar after electrolysis additional amounts of Hydrogen can enter the system as an import. This stream of Hydrogen is most likely generated from fossil fuels by steam generation from methane. As the technology IMPTRNH2 is already existing in Temoa, all data, especially the cost of the Hydrogen, are already available. The only data missing is the emissions accounting for CO₂, and for that reason technology EA_IMP2 has been added serving just for this purpose. In a NREL report from 2001 specific emissions of 10.62 kg CO₂/kg H₂ are reported for the steam reforming process (Spath and Mann, 2001), which converts to 0.483 mole CO₂/mol H₂ or 74.9 kt CO₂/PJ H₂. A more recent source from the internet reports 0.45 mol CO₂/mol H₂ or 69.8 kt CO₂/PJ H₂ (energyportal, accessed 2017) taking further improvements in the efficiency of the process into account. For that reason, the smaller value of 69.8 kt CO₂/PJ is entered to technology **(EA_IMP2) in Temoa.**

1.6.3.4 Technology for compression of Hydrogen to 100 bar (H2_COMP10100)

From the 10 bar pressure level after electrolysis Hydrogen is compressed to 100 bar serving as a sufficient pressure for any further utilization including feed in to high pressure transmission lines. However, this assumption prevents any cost savings from delivering Hydrogen right at the pressure level needed for each individual purpose, which might be applied later on for optimization purposes. At this stage the drawback from the higher cost is small and by this means not significant for the general conclusions derived from the analysis.

In order to derive the efficiency for technology H2_COMP10100, the equation for the electric power necessary to drive an adiabatic compressor is introduced:

$$P_{el} = \dot{m}_{H_2} \cdot \frac{c_p \cdot T_1}{\eta_{mot} \cdot \eta_{mech} \cdot \eta_{SC}} \cdot \left(\pi^{R_i/c_p} - 1 \right) \quad (2)$$

Dividing this number by output activity yields the related loss. Hence, efficiency calculates as follows:

$$\eta_{compr} = 1 - \frac{P_{el}}{\dot{m}_{H_2} \cdot HHV_{H_2}} \quad (3)$$

Using the property data of Hydrogen for c_p , R_i and HHV_{H_2} , setting input temperature $T_1 = 30^\circ\text{C}$ and pressure ratio $\pi = 100 \text{ bar} / 10 \text{ bar} = 10$ and selecting efficiencies for the driving electric motor including controls $\eta_{mot} = 0.8$, for mechanical drive $\eta_{mech} = 0.9$ and for isentropic compression $\eta_{SC} = 0.7$, an efficiency $\eta_{compr} = 0.94$ for compressor technology H2_COMP101000 can be derived. It is assumed that compressor efficiency stays constant for all periods.

Generally, there are two different options to consider for the consumption of electricity according to compressor efficiency. At first, and probably as the straight forward approach, it might be reasonable to account for the electricity as variable cost, only. However, since electricity is a commodity in the system by itself, it seems to be more appropriate to account for its activity instead of its cost. Actually, by this means the cost for generating the amount of electricity consumed is incorporated as well. This implies to connect commodity ELC to technology H2_COMP10100, as shown in Appendix Figure 3.12, which, evidently, needs to be recognized when accounting for the input and output activities, because the activity of ELC adds to the input activity of Hydrogen. On the other hand, the flow of activity through the compressor should stay constant, as long as Hydrogen is treated as an ideal gas where pressure does not account for enthalpy. In order to satisfy both constraints, ELC and Hydrogen input activity H2_10 must be

rated with compressor efficiency η_{compr} when connecting to H2_COMP10100. In addition, technology_input_split needs to be set at η_{compr} for Hydrogen input activity H2_10 and at $(1-\eta_{compr})$ for ELC, in order to maintain a fixed ratio of both commodities when entering technology H2_COMP10100.

In terms of setting CAPEX and OPEX, Niaz reports a price range of 1000 – 1500 €/kW_{el} for large scale (> 100 kW_{el}) Hydrogen compressors (Niaz et al., 2015). Scaling this cost to output activity of Hydrogen, factor $(1 - \eta_{compr})$ is applied, yielding 60 - 90 €/kW_{H2}. Taking average mean and multiplying by a factor of 1.15 for installation (acc. to (ENEA, 2016) and a second factor of 1.2 for currency conversion to US \$ finally results in CAPEX of 103.5 Mio. \$/GW for technology H2_COMP10100. Since Hydrogen compression can be termed as mature technology and no information about the potential for cost reduction in the future is available, CAPEX is kept constant for all periods. Similarly, OPEX is treated constant with 4% of CAPEX, which is an average between an OPEX of 6%, reported in (ENEA, 2016), and 2%, taken from (Ferreroa et al., 2016).

Since electricity for driving the compressor is accounted by the efficiency of the technology, further variable cost is small and therefore neglected. The lifetime of the technology is set at 15 years as suggested by ENEA (ENEA, 2016). In Appendix Table 3.19 all relevant data for compressor technology H2_COMP10100 is listed:

Appendix Table 3.19: Data for Compressor technology H2_COMP10100 entered to Temoa

	period/vintage	H2_COMP10100
efficiency ELC / %	all periods	94.0
efficiency H2_10 / %	all periods	94.0
Tech_input_split ELC / %	all periods	6.0
Tech_input_split H2_10 / %	all periods	94.0
CAPEX / Mio. \$/GWout	all vintages	103.5
OPEX / Mio. \$/GWout	all periods/vintages	4.14
Cost, variable		0
Lifetime / a		15

As stated in the beginning of this section, the pressure level of 100 bar after compression technology H2_COMP 10100 serves as common basis for all pathways for further processing or utilization of Hydrogen in terms of Power-to-X according to Appendix Figure 3.12. In addition, a Hydrogen storage is connected to this pressure level, which will be explained next.

1.6.3.5 Technology for Hydrogen storage at 150 bar (H2_STO150)

At this stage a storage for Hydrogen is necessary, in order to decouple the generation of Hydrogen by electrolysis from the chemical processes for SNG and methanol production. While the electrolysis strongly depends on the supply of renewable electricity from PV and wind-plants and by this means needs to operate flexible, the chemical processes perform best when operated in steady state. For that reason, an intermediate storage is essential for being able to run all processes in an optimal mode.

Since Hydrogen should be maintained at a pressure level of 100 bar, the pressure level for the storage must be higher, and 150 bar was selected in a first approach. Hence, compression is needed again, but for the sake of simplicity and due to the fact that the amount of electricity is small compared to the compression of the entire flow of Hydrogen, electricity is accounted in terms of cost.

Applying equation 2 and 3 with all numbers given in the last section despite a pressure ratio of $\pi = 150 \text{ bar} / 100 \text{ bar} = 1.5$, an efficiency of $\eta_{compr} = 0.99$ arises. Hence, a tariff for electricity of 0.1 \$/kWh or 27.78 Mio. \$/PJ converts by the factor $(1-\eta_{compr})$ in variable cost based on the activity flow of Hydrogen of 0.2778 Mio. \$/PJ. Since the electricity is accounted for by cost, only, the efficiency of technology H2_STO150 is 1.

Referring to Niaz (Niaz et al., 2015) with respect to investment cost, CAPEX of 12-16 \$/kWh are reported for compressed Hydrogen storages at a pressure level of 800 bar for transportation purposes. At 150 bar, the cost should be smaller. Götz reveals cost for a 1700 m³, 30-200 bar compressed Hydrogen storage of 8.3 Mio. € at a power-to-gas site. Applying ideal gas law at ambient temperature yields specific cost of 9.09 €/kWh or 10.9 \$/kWh after conversion from € to US\$ of 1.2. Götz analysis a second storage of half the size with cost of Mio. 4.8 € resulting in specific cost of 12.6 \$/kWh under the same assumptions. In conclusion, the lower bound of 12 \$/kWh reported by Niaz seem to be a good estimate for CAPEX of compressed Hydrogen storage.

However, this specific cost needs to be converted to \$/kW before it can be entered to Temoa, because a storage is sized in Temoa by its capacity in the same way as any other technology. Hence, it is important to know, which maximum capacity in terms charging or discharging power the storage should represent. Taking in mind that the Hydrogen storage is predominantly determined by the fluctuating supply of renewable electricity from PV and wind-plants, and assuming solar PV to be more flexible in time due to day and night pattern, a mean charging time with high production of solar PV of 8 hours seems appropriate

comparing to a 16-hour period of discharging. Since, charging power is higher, it determines the capacity of the storage, resulting in specific investment cost of 96 \$/kW or 96 Mio. \$/GW.

Besides the compressor, the main component of a Hydrogen storage is a pressure vessel, which doesn't need a high amount of maintenance. For that reason, OPEX and lifetime are set at 1.5 % of CAPEX and 40 years, respectively. Moreover, all data presented for Hydrogen storage are not subject to changes in periods and vintages. Appendix Table 3.20 summarizes the relevant data for Hydrogen storage technology H2_STO150:

Appendix Table 3.20: Data for Hydrogen storage technology H2_STO150 entered to Temoa

	period/vintage	H2_STO150
efficiency / %	all periods	100.0
CAPEX / Mio. \$/GWout	all vintages	96
OPEX / Mio. \$/GWout	all periods/vintages	1.44
Cost, variable / Mio. \$/PJ	all periods/vintages	0.2778
Lifetime / a		40

1.6.3.6 Technology for compression of Hydrogen to 100 bar (H2_COMP100700)

As the first pathway according to Appendix Figure 3.12 the Hydrogen generated by electrolysis from renewable electricity is utilized for in Hydrogen vehicles. In principle this can be Otto engine powered vehicles, where the engine is capable of running on Hydrogen, or vehicles driven by a fuel cell, but momentarily in Temoa are fuel cell cars implemented, only. From Appendix Figure 3.13 it can be seen that the Power-to-X technology is connected to the transport technologies already existing in Temoa. Introducing further technologies i.e. for Otto engine vehicles running on Hydrogen is optional but not intended within this study.

For utilization of Hydrogen in vehicles storage is crucial. In order to reach a reasonable mileage, tanks for compressed Hydrogen at 700 bar are currently state of the art. For that reason, another compression is needed, in order to connect these technologies to the 100 bar pressure level provided by the Power-to-X technologies introduced so far. It should be noted, that within this study any additional efforts in terms of establishing Hydrogen refueling technology and infrastructure are not included.

Hydrogen compression from 100 to 700 bar is implemented in Temoa in the same way as for technology H2_COMP10100 as described in section 3.4. The pressure ratio of $\pi = 700 \text{ bar} / 100 \text{ bar} = 7$ yields an efficiency of $\eta_{compr} = 0.95$. Similarly, to technology H2_COMP10100, the activity of the electricity needed

to drive the compressor is taking into account instead of electricity cost, only. Hence, efficiency is attributed to both input commodities, ELC and H2_100, as well as a tech_input_split of 5:95 is implemented to maintain the proper ratio between both commodities.

Regarding CAPEX an additional factor of 1.2 is applied, in order to account for the high pressure, the compressor has to endure. Thus, CAPEX is 124.2 Mio. \$/GW and OPEX is 5.0 Mio. \$/GW. Variable cost is neglected, and all data does not change with period or vintage; lifetime is again fixed at 15 years.

Appendix Table 3.21 lists all relevant data for compressor technology H2_COMP100700:

Appendix Table 3.21: Data for Compressor technology H2_COMP100700 entered to Temoa

	period/vintage	H2_COMP100700
efficiency ELC / %	all periods	95.0
efficiency H2_10 / %	all periods	95.0
Tech_input_split ELC / %	all periods	5.0
Tech_input_split H2_10 / %	all periods	95.0
CAPEX / Mio. \$/GWout	all vintages	124.2
OPEX / Mio. \$/GWout	all periods/vintages	5.0
Cost, variable		0
Lifetime / a		15

Above data is for above the ground hydrogen storage. Hydrogen can also be stored in the depleted gas reservoirs at a significantly lower cost. Regarding the roundtrip efficiency of H2 storage in underground reservoirs (Colbertaldo et al., 2019) notes the following on p. 9564:

"These leakage losses are neglected here, as both the studies on Lined Rock Caverns (LRC) [49] and the available measures from existing underground facilities have shown very low leakage rates (further investigation is expected with operation of the first installations, e.g., in the Houston, Texas area) [50]."

So, H2 storage efficiency is 100%. We have tested 2 hurdle rate for hydrogen storage (6 and 10%). Higher hurdle rate did not make a significant difference in the results. So, the hurdle rate for the underground hydrogen storage technology is 6%. We assume that underground hydrogen is stored at 150 bar pressure which is same as the above ground storage assumptions. This assumption can be updated in the future.

Dr. Bernd's estimate assumes above ground storage (engineered tank) at a cost of \$12/kWh. It is possible to storage H2 in underground caverns (e.g., depleted gas reservoirs) at costs that are two orders of magnitude lower at ~\$0.1-0.4/kWh. For example, (Amos, 1999) indicates a range of cost between \$2-30 /

kg. Conservatively taking the upper end of \$30/kg, the cost is approximately \$0.35/kWh (corrected for inflation). Now, we need to fix the duration at some value.

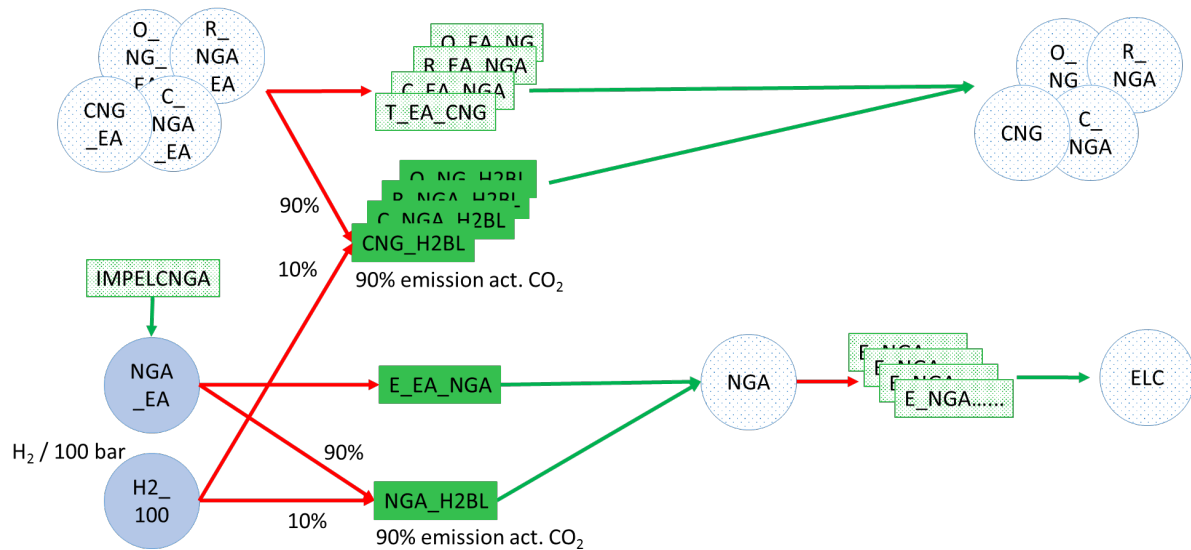
To see how the storage duration affects the results, we added a few different versions of the technology with different durations. Note that in each case, the storage cost (\$/kWh stored) is multiplied by the hours of duration to get the \$/kW investment cost specified in the model. We tested the model with the following durations: 10 hours, 300 hours, 1000 hours. (At 300 hours of duration, the cost per kW is $\$0.35/\text{kWh} \times 300 = 100$ \$/kW, which is close to Bernd's original estimate. The longest time slice is intermediate night, $\text{SegFrac}=0.1532$, which is 1342 hours.). Different storage durations did not make a significant difference in the results since we can build a fraction of the hydrogen storage with any duration. The current US data has only one hydrogen storage technology with 2000 hour duration. We do not have any above the ground storage since the model would not choose it over the cheaper underground storage option. Life time of underground hydrogen storage is 40 years. Fixed and variable cost are same as above the ground storage. These can be updated in the later revisions.

1.6.3.7 Technologies for blending Hydrogen into natural gas (..._H2BL)

According to Appendix Figure 3.12 another option considered for utilization of Hydrogen is blending it into the natural gas grid. As outlined in paragraph 2, a concentration of 10 Vol% is introduced as an upper limit for the concentration of Hydrogen in the grid.

For implementation in Temoa, the technologies for feeding natural gas into the five sectors of interest – residential, industrial, commercial, transport and electrical – have been doubled by a blending technology (R_NGA_H2BL, O_NG_H2BL, C_NGA_H2BL, CNG_H2BL and NGA_H2BL), as shown in Appendix Figure 3.14. By applying the `tech_input_split` parameter to each technology the proper mixture of 10% Hydrogen and 90% NGA is maintained. However, it should be noted that the parallel pathway of direct utilization of NGA in total allows any mixture below 10% Hydrogen in the gas.

Keeping in mind that the input data for `tech_input_split` in Temoa is based on activities and not on volume, the ratio converts to 3.43% Hydrogen and 96.57% NGA after conversion with respect to the higher heating value of the two gases involved.



Appendix Figure 3.14: Implementation of the processes for blending Hydrogen in natural gas in Temoa (textured commodities/ technologies already existing in Temoa, fully colored commodities/technologies new to Temoa)

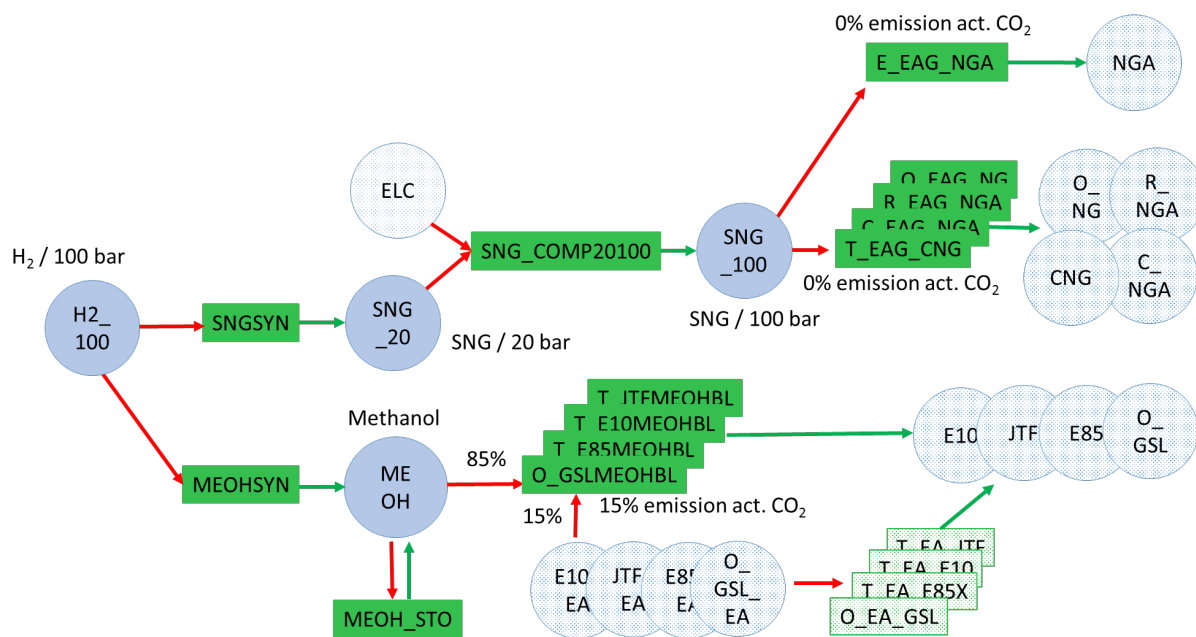
The blending technologies are in Temoa applied simply to link the commodities in a proper way; the equipment needed for the blending process is not considered, because it does not affect the results significantly. Thus, no cost is attributed to the blending technologies and their efficiency is set to 1. However, the accounting for CO₂-emissions is incorporated as another feature besides tech_input_split in the blending technologies. While in Temoa the utilization of natural gas is in general related to CO₂-emissions of 50 kt/PJ, the blended gas shows CO₂-emissions of 45 kt/PJ, only, due to the content of 10 Vol% Hydrogen, which is not burdened with CO₂-emissions, since it is generated from electrolysis driven by renewable electricity. By this means, blending natural gas with Hydrogen from Power-to-X technologies helps to reduce CO₂-emissions.

Even though the method to account for CO₂-emissions described so far has been applied to all sectors, the implementation for the electric sector differed from the other sectors. The reason for the alternate approach is that emission accounting for the electric sector is not performed in a separate technology exclusively attributed to this subject like in the other sectors. Instead, emission accounting is incorporated in the various technologies for electricity generation. But in order to account for the lower emissions of the Hydrogen blended gas, the electric sector needs to be treated similar to the other sectors with a separate technology to account for CO₂-emissions. For that reason, technology E_EA_NGA is introduced to Temoa, which attributes CO₂-emissions of 50 kt to each PJ NGA activity. In consequence, CO₂-emission activities in all technologies for electricity generation from NGA are reduced by 50 kt/PJ. For CCS-technologies, this

yields negative emission activities for the technology itself, but in combination with technology E_EA_NGA it becomes positive again. Evidently, for the blended gas burdened with smaller CO₂-emissions of 45 kt/PJ the method implemented is mathematically not completely correct, but the remaining error is small and by this means not significant with respect of the overall results.

1.6.3.8 Technology for generating SNG from Hydrogen and CO₂ (SNGSYN)

As one of the two chemical processes involved in Power-to-X the generation of methane, which is labelled as synthetic natural gas or SNG, from Hydrogen and CO₂ will be introduced next. Appendix Figure 3.15 displays the different technologies involved and the way they are linked and incorporated in Temoa.



Appendix Figure 3.15: Implementation of the processes for generating SNG and methanol in Temoa (textured commodities/ technologies already existing in Temoa, fully colored commodities/technologies new to Temoa)

The process of forming SNG from Hydrogen and CO₂ is based on the following chemical reaction also known as Sabatier or methanation process:



It is a catalytic, 2-stage chemical reaction, running at 250-550°C and 1-100 bar (Götz et al., 2016). In the first, endothermic reaction Hydrogen and CO₂ are converted to CO and water. The second reaction is meant

to convert CO with further Hydrogen to methane and another molecule of water, and it is exothermic. Since the energy release from the second reaction is higher than needed for the first, the overall process is exothermic.

Currently, a biological option to form methane from Hydrogen and CO₂ by microorganisms is under investigation, as well. Biological methanation does not require high temperatures and pressures, it runs between 20 and 70°C and at a pressure below 10 bar, and it is more tolerant in terms of impurities, which in the Sabatier process are subject to deactivate the catalyst. However, the reaction rate of biological methanation is still small and requires large reactors compared to the Sabatier process, which momentarily prevents deployment of this technology in a larger scale. For that reason, the Sabatier process working at a pressure level of 20 bar is considered throughout this study, only.

Regarding efficiency of the methanation according to the Sabatier process Götz reports of 78% (Götz et al., 2016), which is in good correspondence to the ENEA report (79.4%) (ENEA, 2016) and to Ahern et al. (80%) (Ahern et al., 2015). According to Schiebahn the maximum efficiency of the Sabatier process can reach 83% (Schiebahn et al., 2015); for that reason, the efficiency is allowed to rise slightly up to 81% in 2040 within the scope of this study.

Information about current investment cost for the methanation vary a lot; a good overview is given by Götz (Götz et al., 2016). He reports about a range from 130 to 175 €/kW for bigger plants at the lower end up to 1500 €/kW given by (ENEA, 2016). Since Götz refers to other sources at 300-500 €/kW and 600 €/kW, an intermediate value for CAPEX of 450 €/kW (SNG) is implemented in Temoa, which is equivalent to 540 \$/kW (SNG) applying the conversion rate of 1.2 between € and US\$. For future periods a significant drop of CAPEX seems plausible, ENEA assumes only 1/3 of current investment prices in 2050 (ENEA, 2016). According to this information CAPEX is allowed to decrease by ½ (down to 270 \$/kW (SNG)) until 2040 within this study. As an indicator for OPEX a fraction of 7.5% of CAPEX is taken from the ENEA report (ENEA, 2016) resulting in 40.5 \$/kW (SNG) in 2015 and 20.25 \$/kW (SNG) in 2040.

Variable cost is mainly attributed to the source of CO₂ available, and the potential cost for CO₂ have been already discussed in chapter 2. Within this study the impact of CO₂ cost will be studied by parameter variation. At this point it should be noted that for the Sabatier process, where the cost is based on output activity SNG, specific cost of 10 \$/to (CO₂) convert to 0.5 Mio. \$/PJ (SNG). Additional variable cost beside CO₂ cost are not considered.

Finally, expected lifetime of the methanation technology is 20 years as indicated in (ENEA, 2016).

Appendix Table 3.22 displays all relevant data for technology SNGSYN to represent the generation of SNG from Hydrogen and CO₂ in Temoa.

Appendix Table 3.22: Data for SNG generation technology SNGSYN entered to Temoa

	period/vintage	SNGSYN
efficiency / %	2015	79.0
	2020	80.0
	2025	80.5
	2030	81.0
	2035	81.0
	2040	81.0
	CAPEX / Mio. \$/GW (out)	2015
2020		486
2025		432
2030		378
2035		324
2040		270
OPEX / Mio. \$/GW (out)		2015
	2020	36.45
	2025	32.4
	2030	28.35
	2035	24.3
	2040	20.25
	Cost, variable	
Lifetime / a		20

1.3.6.8 Technology for compression of SNG from 20 to 100 bar (SNG_COMP20100)

In order to feed SNG into the gas grid its pressure must be elevated to the pressure level of the transmission lines, which may vary between 16 and 100 bar depending on the location of the grid and the distance the gas needs to be transferred to the consumers (American Gas Association, 2017). In order to be able to meet the highest pressure, a compression from 20 bar after methanation up to 100 bar is considered for technology SNG_COMP20100. This is in addition in accordance to the pressure level selected for Hydrogen blended into the gas grid.

Due to differing property data of SNG compared to Hydrogen, compressor efficiency is higher in terms of SNG. Applying equations 2 and 3 to compression of SNG together with the relevant pressure ratio $\pi = 100 \text{ bar} / 20 \text{ bar} = 5$ and apart from that similar data as for Hydrogen compression (input temperature $T_1 = 30^\circ\text{C}$,

efficiencies for the driving electric motor including controls $\eta_{mot} = 0.8$, for mechanical drive $\eta_{mech} = 0.9$ and for isentropic compression $\eta_{sc} = 0.7$), an efficiency $\eta_{compr} = 0.98$ arises for technology SNG_COMP20100.

Incorporating the compressor technology for SNG into Temoa follows the same schematic as already introduced and discussed for Hydrogen compression. In addition, and for the sake of simplicity, the data for cost and lifetime derived for technology H2_COMP10100 is adopted for technology SNG_COMP20100, which might not cause major errors since output pressure is the same for both technologies. Similarly, all data is assumed constant for all periods and vintages. This yields the data for compressor technology SNG_COMP20100 as listed in Appendix Table 3.23.

Appendix Table 3.23: Data for Compressor technology SNG_COMP20100 entered to Temoa

	period/vintage	SNG_COMP20100
efficiency ELC / %	all periods	98.0
efficiency H2_10 / %	all periods	98.0
Tech_input_split ELC / %	all periods	2.0
Tech_input_split H2_10 / %	all periods	98.0
CAPEX / Mio. \$/GWout	all vintages	103.5
OPEX / Mio. \$/GWout	all periods/vintages	4.14
Cost, variable		0
Lifetime / a		15

1.3.6.10 Technologies for emission accounting of SNG_100 (..._EAG_NGA)

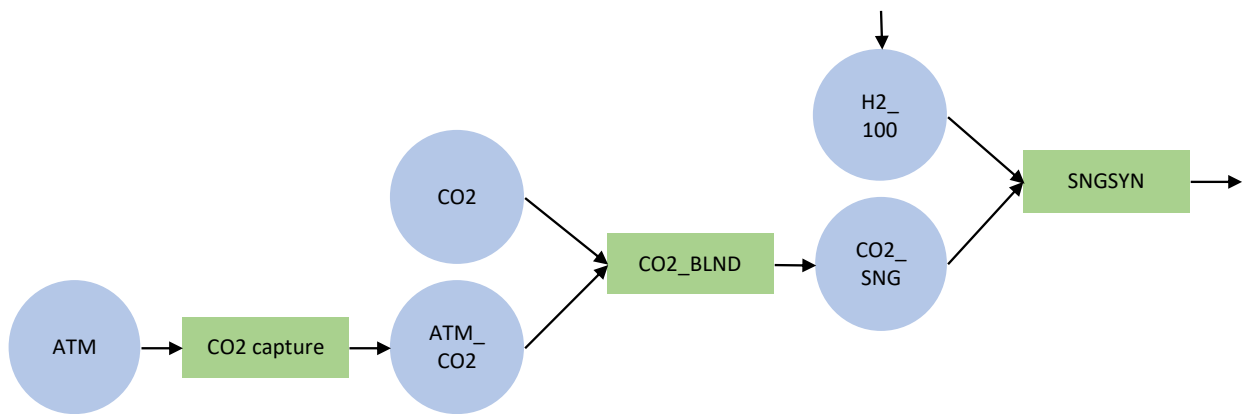
Appendix Figure 3.15 shows that SNG at the pressure level of 100 bar (SNG_100) is directly fed into the gas grid and by this means transferred to the relevant sectors electric, residential, commercial, industrial and transport. Since SNG consists of pure methane, it can be fed into the gas grid without any restrictions; all downstream conversion technologies are able to handle SNG in the same way as natural gas, hence, there is no need for blending SNG with natural gas to a certain extend only as in case of Hydrogen. Technically spoken, it is not necessary to apply parameter tech_input_split as in case of the blending technologies for Hydrogen. For that reason, the only duty of technologies E_EAG_NGA, R_EAG_NGA, C_EAG_NGA, O_EAG_NG and T_EAG_CNG is accounting for emissions associated with the use of SNG, which compares to technologies E_EA_NGA, R_EA_NGA, C_EA_NGA, O_EA_NG and T_EA_CNG from Appendix Figure 3.14.

The above was Dr. Bernd's structure where SNG would have same emissions as natural gas when burnt. In the updated structure, we assume that SNG is carbon neutral since it takes in CO₂ which is later released during SNG combustion. The emission parameters of the natural gas is not associated with the end use

technology for the residential and commercial sector. However, for transportation and industrial sector, the emission parameter is associated with the end-use technology. So, we created a different SNG commodity for the transportation (T_SNG) and the industrial (O_SNG) sector which is directly fed to the end use technologies that consume natural gas. Emission activity is defined by the input commodity, technology, and output commodity. Since the input commodity for all the industrial sector and transportation sector technologies is now changed, SNG is carbon neutral.

Now, even though SNG is carbon neutral, we need to make sure that the CO₂ that is needed to produce SNF is coming from somewhere. Specially in the deep decarbonization or high renewable penetration scenario where the emissions are going almost to zero in 2050, we need a way to capture CO₂ from the atmosphere.

We need 1 mole of CO₂ and 4 moles of hydrogen to produce 1 mole of SNG. When we convert CO₂ to kt and hydrogen to PJ, it turns out that we need 38.46 kt of CO₂ per PJ of hydrogen to produce 1 PJ of SNG. We input this number via the TechInput Split constraint. Now, there are two ways to get CO₂. The first way is from emissions from the carbon sources in the energy system and the second way is to capture the CO₂ from the atmosphere. The following Appendix Figure 3.16 shows the flow of the process.



Appendix Figure 3.16: CO₂ input for SNG production

We modified the structure of the efficiency table to allow the emission commodity (co2) to act as an input commodity. The changes are made in temoa_initialize.py and temoa_model.py. In the deep decarbonization case, if the energy system has lower CO₂ emission than what is required to produce SNG, then CO₂_Capture technology capture the CO₂ from the atmosphere. The investment cost of this technology is 109890.11 \$ million/kt of CO₂ with 6% discount rate and 40 year (default) life time. We added the ATM, CO₂_SNG and ATM_CO₂ commodities and CO₂_BLND technology.

Note that to keep the model from using excessive amount of CO₂ for SNG production, we need to make the efficiency of CO₂_SNG → SNGSYN → SNG insignificant. Currently it is 0.01.

1.3.6.11 Technology for generating Methanol from Hydrogen and CO₂ (MEOHSYN)

The second chemical process involved is for generating Methanol from Hydrogen and CO₂, which can be used as liquid fuel, and it is by this means mainly attributed to the transportation sector in order to provide a CO₂-free fuel. A good overview about the process including technical and economic assessment data is given by Atsonios (Atsonios et al., 2016) and Pérez-Fortes (Pérez-Fortes et al., 2016). The report by ENEA (ENEA, 2016) reveals some information about the process, as well.

Equation 5 presents the basic chemical reaction of the process, which splits in two separate reactions: First, CO is created from Hydrogen and CO₂ in an endothermic reaction under dismissal of water. In a second exothermic step CO reacts with two molecules of Hydrogen to Methanol.



The Methanol reactor is typically operated at 250°C and a pressure of 65 bar according to (Atsonios et al., 2016). Obviously, a high pressure shifts the reaction displayed by eq. 4 to the right hand side.

For the state of the art efficiency of the process a value of 75.5% is taken from the report by ENEA (ENEA, 2016). The more advanced CCU process yields an efficiency of 80.4% according to (Pérez-Fortes et al., 2016), which is considered for 2020. For the following periods until 2040 only a minor increase in efficiency up to 82% is considered.

Atsonios (Atsonios et al., 2016) provides a specific price of 133.4 €/to (MeOH) for CAPEX and OPEX as a yearly rate. With 5% OPEX and 2% insurance, a capital recovery factor of 0.11 and the higher heating value of Methanol this converts to 1575 €/kW (MeOH) for CAPEX. This value is in good agreement to the ENEA report (ENEA, 2016), where 1,500,000 €/MW(MeOH) are stated for the year 2015, even though they assume an additional cost of 50%, which is already included in the analysis presented by Atsonios. Since Atsonios gives more details about his cost analysis, the value for CAPEX according to his work is considered in this study, resulting in 1890 \$/kW (MeOH) for CAPEX of technology MEOHSYN after conversion of currency from € to US\$ by a factor of 1.2.

Regarding potential reduction in cost for the future, only the ENEA report provides an estimate. According to (ENEA, 2016) CAPEX for technology MEOHSYN should reduce by 1/3 until 2030 and by 53.3% until 2050. This decline has been adopted to the data entered to Temoa. OPEX is as well taken from the ENEA report (ENEA, 2016) with 7.5% of CAPEX. The value suggested by Atsonios is close by, if their data for OPEX (5%) and insurance (2%) is added.

Similarly, as in case of technology SNGSYN, variable cost is mainly attributed to utilization of CO₂. For that reason, no values are fixed in this section. Instead, the impact of CO₂ cost will be studied by parameter variation in the next paragraph. In contrast to the process of generating SNG, for Methanol production specific cost of 10 \$/to (CO₂) convert to 0.6 Mio. \$/PJ(MeOH) due to the different stoichiometric of the chemical reactions (compare eqs. 3 and 4). Any other variable cost besides the cost for CO₂ are neglected. Finally, lifetime of technology MEOHSYN is fixed at 20 years as indicated in (ENEA, 2016). Appendix Table 3.24 summarizes all relevant data for technology MEOHSYN for the generation of Methanol from Hydrogen and CO₂ in Temoa.

Appendix Table 3.24: Data for Methanol generation technology MEOHSYN entered to Temoa

	period/vintage	MEOHSYN
efficiency / %	2015	75.5
	2020	80.4
	2025	81.0
	2030	81.5
	2035	82.0
	2040	82.0
	CAPEX / Mio. \$/GW (out)	2015
2020		1650
2025		1440
2030		1260
2035		1120
2040		1000
OPEX / Mio. \$/GW (out)		2015
	2020	123.75
	2025	108.0
	2030	94.5
	2035	84.0
	2040	75.0
	Cost, variable	
Lifetime / a		20

1.3.6.12 Technology for storing Methanol (MEOH_STO)

While for SNG the gas grid and the storages associated to it are accessible, in case of Methanol a separate storage should be available at the production site. For that reason, technology MEOH_STO is implemented in Temoa in order to serve in this way. However, the technology itself is quite simple, because Methanol is stored as a liquid at ambient or slightly elevated pressure. Therefore, any cost for the storage of Methanol are neglected at this early stage of the analysis, since they are small compared to the cost of all other technologies involved. In addition, energy losses mainly caused by pumping are small in this terms and by this means negligible as well, resulting in an efficiency of 1 for technology MEOH_STO in Temoa. Expected lifetime of the technology is fixed to 20 years.

1.3.6.13 Technologies for blending Methanol into gasoline for utilization in the transport sector (..._MEOHBL)

As outlined in paragraph 2, Methanol can be blended to a high extent into gasoline. Based on the discussion at the end of paragraph 2, a content of 85 Vol% Methanol in gasoline is feasible. It has been outlined as well that this pathway of Power-to-X opens the field for liquid fuels in addition to SNG and by this means allows renewable electricity entering the transport sector in a second way in addition to the direct use in form of e-mobility.

For blending Methanol into gasoline commodities E10, E85, JTF and O_GSL are involved in Temoa, as shown in Appendix Figure 3.15. Consequently, technologies T_E10MEOHBL, T_E85MEOHBL, T_JTFMEOHBL and O_GSLMEOHBL are implemented. By applying parameter tech_input_split the proper content of Methanol is maintained for each type of gasoline. As in case of blending Hydrogen into natural gas, it must be kept in mind that the input parameter for tech_input_split is based on activity rather than on volume. Therefore, the percentages need to be converted based on the high heating values of the liquids involved. In case of E10, JTF and O_GSL the same higher heating value is assumed resulting in parameter for tech_input_split of 75.69% Methanol and 24.31% gasoline. In case of E85 the lower higher heating value due to the high percentage of Ethanol is considered resulting in 80.32% Methanol and 19.68% E85 as input parameter for tech_input_split in terms of technology T_E85MEOHBL.

It should be noted here as well that any blending with a smaller percentage of Methanol is feasible, because the pathway of direct utilization of the gasoline fuels is still active in parallel as displayed in Appendix Figure 3.15.

Again, similar to implementing the blending technologies for Hydrogen in Temoa, they are used for emission accounting as well. Since Methanol from Power-to-X is produced from renewable electricity, it is not burdened with emissions of CO₂. Therefore, any fuel blended with 85% Methanol from Power-to-X shows 85% less CO₂-emissions, which is incorporated in technologies T_E10MEOHBL, T_E85MEOHBL, T_JTFMEOHBL and O_GSLMEOHBL.

1.7 Biomass

We have following 8 types of biomasses going to power plant and transportation sector. All the types have a maximum activity constraint. The variable cost of the biomass is taken from (DoE BTS, 2016) using the following query:

Filter the data by year and feedstock. For 2017 use the data for the base case all energy crop. For all subsequent year use the data from 4% yield increase scenario. Download the dataset as .csv file. Sum over the data by time period and unit price. If the unit of production is in bushels, then convert it to dry tons by multiplying by 0.0254. The BTS (DoE BTS, 2016) reports out the feedstock values as cumulative amount for each step. So, subtract out the values from the previous step to get the incremental amount that the model can use at each price step to avoid double counting. For example, Appendix Table 3.25 shows the calculation for corn stover (IMPSTV).

Appendix Table 3.25: sample calculation for IMPSTV

IMPSTV	USD (Mil. \$)	2017	2020	2025	2030	2035	2040
(before) R4	30	0	0	6.26	16.29	27.3	31.64
	40	22.92	25.55	29.98	33.21	37.39	40.99
	50	50.36	55.86	65.67	75.29	83.12	91
	60	57.24	62.96	72.77	80.12	88.02	95.96
	70	60.06	65.6	76.19	84.72	92.8	99.92
	80	63.17	69.43	79.49	87.34	96.47	103.82
	90	65.05	70.77	81.7	90.15	98.14	104.31
	100	66.63	71.75	82.58	90.49	98.13	104.22
(After) R4	30	0	0	6.26	16.29	27.3	31.64
	40	22.92	25.55	23.71	16.92	10.09	9.35
	50	27.44	30.31	35.69	42.08	45.73	50.01
	60	6.88	7.1	7.1	4.83	4.9	4.96
	70	2.81	2.64	3.42	4.6	4.78	3.96
	80	3.12	3.83	3.3	2.63	3.67	3.9
	90	1.88	1.34	2.21	2.8	1.66	0.49
	100	1.58	0.98	0.88	0.34	0	-0.09
	Prod. (MMt)	66.63	71.75	82.57	90.49	98.13	104.22
	Mil. \$/MMT	52.155	51.196	50.103	48.378	46.680	45.534
Mil. \$/PJ	3.863	3.792	3.711	3.584	3.458	3.373	

Following Appendix Table 3.26 shows the energy content of all the biomasses which is used for the above calculations.

Appendix Table 3.26: Energy content of the biomass

Energy content (PJ/Mt)	Reference
STV 13.5	Demirbas, (2004).
AGR 13.5	Demirbas, (2004).
ECG 13.083	Tillman, (2000)
ECW 15	Demirbas, (2004).
ECA 15	Tillman, (2000)
UWW 15	Tillman, (2000)
FSR 15	Demirbas, (2005).

For IMPSOY, cost was an order of magnitude off with the above calculations. The above cost might not consider the transportations cost. This part needs more research and is currently left for future students. The IMPSOTY cost comes from (Market Insider).

Chapter 4

1 Proving global optimality of the IPOPT solution:

Simplified form of the energy efficiency model can be given as follows:

$$\max f(E_t, \theta_t, CAP_{i,v}, ACT_{i,v,t}) \quad (1)$$

$$= \sum_{t \in T} \int_{ES_t^{min}}^{ES_t} (q/\varphi)^{1/\epsilon} dq - \beta \sum_{t \in T} P\theta_t \theta_t - \sum_{v \in V_i} \sum_{i \in I} IC_{i,v} CAP_{i,v} \\ - \sum_{t \in T} \sum_{v \in V_i} \sum_{i \in I} FC_{i,v,t} CAP_{i,v} - \sum_{t \in T} \sum_{v \in V_i} \sum_{i \in I} VC_{i,v,t} ACT_{i,v,t}$$

$$\text{s. t. } \sum_{v \in V_i} \sum_{i \in I} ACT_{i,v,t} \geq E_t \quad \forall t \in T \quad (1a)$$

$$\zeta_{i,v,t} CAP_{i,v} \geq ACT_{i,v,t} \quad \forall t \in T, v \in V_i, i \in I \quad (1b)$$

$$BX \geq b \quad (1c)$$

Where, ES_t is defined as a production function of θ_t and E_t , given in Equation 5. Hence, ES_t is equivalent to $\left(\alpha\theta_t^{(\sigma-1)/\sigma} + (1-\alpha)E_t^{(\sigma-1)/\sigma}\right)^{\sigma/\sigma-1}$. Assume that the above problem has n decision variables and m constraints. The proofs of the propositions 1 to 5 are given in Convex analysis and monotone operator theory in Hilbert spaces, chapter 8 (Bauschke & Combettes, 2017).

Definition 1: For the $n \times n$ matrix A , the k^{th} order principal submatrix is obtained by deleting the last $n - k$ rows and columns of A . The determinant of this matrix is called leading principal minor of A .

We denote the k^{th} order leading principal submatrix of A by A_k and the k^{th} order leading principal minor by $|A_k|$.

Proposition 1: The matrix A is negative semidefinite if and only if every principal minor of odd order is ≤ 0 and every principal minor of even order is ≥ 0 .

Proposition 2: Let f be a twice differentiable function on Z such that $Z \in R^n$ and x^* is an interior point of Z . Then, f is concave if and only if Hessian matrix of f , $H_f(x^*)$, is negative semidefinite at all $x^* \in Z$.

Proposition 3: Let f_1 and f_2 are concave functions then $f_1 + f_2$ is also a concave function

Proposition 4: Feasible region S where, $S = \{X \in R^n, X|AX \geq b\}$ is convex where, $X, X \in R^n$, is a vector of decision variable, A is the constraint coefficient matrix and b is the right-hand side of the constraint.

Proposition 5: Let f be a concave function on a convex feasible domain $S \in R^n$ and x^* be an interior point of S . If x^* is a local maximum of a f then x^* is also a global maximum.

For our analysis Appendix Table 4.1 represents the ranges of the parameters used for sensitivity analysis. Note that close interval denotes that the boundary values are included while open interval denotes that they are not.

Appendix Table 4.1: Valid range of the model parameters

Parameter	Range
α	(0,1)
β	(0,1)
ϵ	$(-\infty, 0)$
σ	$(1, \infty)$
P_{θ_t}	$(0, \infty)$

For the simplification purpose, we drop the summation over time period since from Proposition 3, we know that summation of concave functions is concave. For a given \tilde{t} , where $\tilde{t} \in T$, after simplifying the integral and ignoring the summation over time period, $f(E_{\tilde{t}}, \theta_{\tilde{t}}, CAP_{i,v}, ACT_{i,v,\tilde{t}})$ can be given as

$$\begin{aligned}
 & f(E_{\tilde{t}}, \theta_{\tilde{t}}, CAP_{i,v}, ACT_{i,v,\tilde{t}}) \tag{2} \\
 & = \frac{1}{1 + \epsilon} \left(\epsilon \varphi_{\tilde{t}} \left(\frac{\left(\alpha \theta_{\tilde{t}}^{(\sigma-1)/\sigma} + (1 - \alpha) E_{\tilde{t}}^{(\sigma-1)/\sigma} \right)^{\sigma/(\sigma-1)}}{\varphi_{\tilde{t}}} \right)^{1+1/\epsilon} \right. \\
 & \quad \left. - \epsilon \varphi_{\tilde{t}} \left(\frac{ES_{\tilde{t}}^{min}}{\varphi_{\tilde{t}}} \right)^{1+1/\epsilon} \right) - \beta P \theta_{\tilde{t}} \theta_{\tilde{t}} - \sum_{v \in V_i} \sum_{i \in I} IC_{i,v} CAP_{i,v}
 \end{aligned}$$

Proposition 6: The function $f(E_{\tilde{t}}, \theta_{\tilde{t}}, CAP_{i,v}, ACT_{i,v,\tilde{t}})$ given in (2) is concave

We are ignoring the constant term in the objective function. The Hessian matrix, $H_f(E_{\tilde{t}}, \theta_{\tilde{t}}, CAP_{i,v}, ACT_{i,v,\tilde{t}})$ is computed as follows

$$H_f(E_{\bar{t}}, \theta_{\bar{t}}, CAP_{i,v}, ACT_{i,v,\bar{t}}) = \begin{bmatrix} \frac{\partial^2 f}{\partial E_{\bar{t}}^2} & \frac{\partial^2 f}{\partial E_{\bar{t}} \partial \theta_{\bar{t}}} & \frac{\partial^2 f}{\partial E_{\bar{t}} \partial CAP_{i,v}} & \frac{\partial^2 f}{\partial E_{\bar{t}} \partial ACT_{i,v,\bar{t}}} \\ \frac{\partial^2 f}{\partial \theta_{\bar{t}} \partial E_{\bar{t}}} & \frac{\partial^2 f}{\partial \theta_{\bar{t}}^2} & \frac{\partial^2 f}{\partial \theta_{\bar{t}} \partial CAP_{i,v}} & \frac{\partial^2 f}{\partial \theta_{\bar{t}} \partial ACT_{i,v,\bar{t}}} \\ \frac{\partial^2 f}{\partial CAP_{i,v} \partial E_{\bar{t}}} & \frac{\partial^2 f}{\partial CAP_{i,v} \partial \theta_{\bar{t}}} & \frac{\partial^2 f}{\partial CAP_{i,v}^2} & \frac{\partial^2 f}{\partial CAP_{i,v} \partial ACT_{i,v,\bar{t}}} \\ \frac{\partial^2 f}{\partial ACT_{i,v,\bar{t}} \partial E_{\bar{t}}} & \frac{\partial^2 f}{\partial ACT_{i,v,\bar{t}} \partial \theta_{\bar{t}}} & \frac{\partial^2 f}{\partial ACT_{i,v,\bar{t}} \partial CAP_{i,v}} & \frac{\partial^2 f}{\partial ACT_{i,v,\bar{t}}^2} \end{bmatrix}$$

Where, the partial derivative with respect to $CAP_{i,v}$ is equivalent to taking a partial derivative with respect to $CAP_{i,\tilde{v}}, \forall i \in I, \tilde{v} \in V_i$. Hence, the dimension of the $H_f(E_{\bar{t}}, \theta_{\bar{t}}, CAP_{i,v}, ACT_{i,v,\bar{t}})$ is $[(2 + IV_i + IV_i) \times (2 + IV_i + IV_i)]$. The leading principal minor $|A_1|$ which is equivalent to $\left| \frac{\partial^2 f}{\partial E_{\bar{t}}^2} \right|$ is given by (3):

$$\frac{(-1 + \alpha)\theta_{\bar{t}}^{\frac{1}{\sigma}}\varphi_{\bar{t}} \left(\alpha E_{\bar{t}}^{\frac{1}{\sigma}} \epsilon \theta_{\bar{t}} + (-1 + \alpha)E_{\bar{t}} \sigma \theta_{\bar{t}}^{\frac{1}{\sigma}} \right) \left(\frac{\left((1 - \alpha)E_{\bar{t}}^{\frac{-1+\sigma}{\sigma}} + \alpha \theta_{\bar{t}}^{\frac{-1+\sigma}{\sigma}} \right)^{\frac{\sigma}{-1+\sigma}}}{\varphi_{\bar{t}}} \right)^{1+\frac{1}{\epsilon}}}{\epsilon \sigma E_{\bar{t}} \left(\alpha E_{\bar{t}}^{\frac{1}{\sigma}} \theta_{\bar{t}} + (1 - \alpha)E_{\bar{t}} \theta_{\bar{t}}^{\frac{1}{\sigma}} \right)^2} \quad (3)$$

Assume that

$$a = (-1 + \alpha)\theta_{\bar{t}}^{\frac{1}{\sigma}}\varphi_{\bar{t}}$$

$$b = \left(\alpha E_{\bar{t}}^{\frac{1}{\sigma}} \epsilon \theta_{\bar{t}} + (-1 + \alpha)E_{\bar{t}} \sigma \theta_{\bar{t}}^{\frac{1}{\sigma}} \right)$$

$$c = \left(\frac{\left((1 - \alpha)E_{\bar{t}}^{\frac{-1+\sigma}{\sigma}} + \alpha \theta_{\bar{t}}^{\frac{-1+\sigma}{\sigma}} \right)^{\frac{\sigma}{-1+\sigma}}}{\varphi_{\bar{t}}} \right)^{1+\frac{1}{\epsilon}}$$

$$d = \epsilon \sigma E_{\bar{t}} \left(\alpha E_{\bar{t}}^{\frac{1}{\sigma}} \theta_{\bar{t}} + (1 - \alpha)E_{\bar{t}} \theta_{\bar{t}}^{\frac{1}{\sigma}} \right)^2$$

Hence, the Expression (3) can be written as $(abc)/d$. We compute $\varphi_{\bar{t}}$ in equation (13). Since the demand of electricity $E_{\bar{t}}^0$ and price of electricity $PE_{\bar{t}}^0$ are always positive, $\varphi_{\bar{t}}$ is always positive. The decision variables $\theta_{\bar{t}}$ and $E_{\bar{t}}$ are nonnegative. Hence for the assumed parameter values given in Appendix Table 4.1, a, b and d are always negative while c is always positive. Hence, $(abc)/d$ is always negative, i.e., is the first principal minor is always negative.

The leading principal minor $|A_2|$ where,

$$A_2 = \begin{bmatrix} \frac{\partial^2 f}{\partial E_{\bar{t}}^2} & \frac{\partial^2 f}{\partial E_{\bar{t}} \partial \theta_{\bar{t}}} \\ \frac{\partial^2 f}{\partial \theta_{\bar{t}} \partial E_{\bar{t}}} & \frac{\partial^2 f}{\partial \theta_{\bar{t}}^2} \end{bmatrix}$$

is given as (4):

$$\frac{(-1 + \alpha)\alpha E_{\bar{t}}^{-1+\frac{1}{\sigma}} \theta_{\bar{t}}^{-1+\frac{1}{\sigma}} \left((1 - \alpha) E_{\bar{t}}^{\frac{-1+\sigma}{\sigma}} + \alpha \theta_{\bar{t}}^{\frac{-1+\sigma}{\sigma}} \right)^{\frac{2\sigma}{-1+\sigma}} \left(\frac{\left((1 - \alpha) E_{\bar{t}}^{\frac{-1+\sigma}{\sigma}} + \alpha \theta_{\bar{t}}^{\frac{-1+\sigma}{\sigma}} \right)^{\frac{\sigma}{-1+\sigma}}}{\varphi_{\bar{t}}} \right)^{2/\epsilon}}{\epsilon \sigma \left(\alpha E_{\bar{t}}^{\frac{1}{\sigma}} \theta_{\bar{t}} - (-1 + \alpha) E_{\bar{t}} \theta_{\bar{t}}^{\frac{1}{\sigma}} \right)^2} \quad (4)$$

Assume that

$$a = (-1 + \alpha)\alpha E_{\bar{t}}^{-1+\frac{1}{\sigma}} \theta_{\bar{t}}^{-1+\frac{1}{\sigma}}$$

$$b = \left((1 - \alpha) E_{\bar{t}}^{\frac{-1+\sigma}{\sigma}} + \alpha \theta_{\bar{t}}^{\frac{-1+\sigma}{\sigma}} \right)^{\frac{2\sigma}{-1+\sigma}}$$

$$c = \left(\frac{\left((1 - \alpha) E_{\bar{t}}^{\frac{-1+\sigma}{\sigma}} + \alpha \theta_{\bar{t}}^{\frac{-1+\sigma}{\sigma}} \right)^{\frac{\sigma}{-1+\sigma}}}{\varphi_{\bar{t}}} \right)^{2/\epsilon}$$

$$d = \epsilon \sigma \left(\alpha E_{\bar{t}}^{\frac{1}{\sigma}} \theta_{\bar{t}} - (-1 + \alpha) E_{\bar{t}} \theta_{\bar{t}}^{\frac{1}{\sigma}} \right)^2$$

Hence, (4) can be given as $(abc)/d$. Upon closer inspection, we can see that for the assumed parameter values given in Appendix Table 4.1, a and d are always negative while b and c are always positive. Hence, $(abc)/d$ is always positive, i.e., the second principal minor is always positive.

From above, $|A_1| \leq 0$, $|A_2| \geq 0$ and $|A_k| = 0, \forall k > 2$. Hence, from proposition 1, the Hessian matrix $H_f(E_{\bar{t}}^*, \theta_{\bar{t}}^*, CAP_{i,v}^*, ACT_{i,v,\bar{t}}^*)$ is negative semidefinite for all $E_{\bar{t}}^*, \theta_{\bar{t}}^*, CAP_{i,v}^*, ACT_{i,v,\bar{t}}^* \in S_2$ where, S_2 is a feasible domain defined by constraints (1a-c). Therefore, from proposition 2, the function is concave.

If we add more electricity generation technologies, time periods and vintages then the resulting function will still be concave since from proposition 3, the sum of concave function will be concave.

Proposition 7: Feasible region defined by constraints (1a-c) is convex

Constraints (1a-c) are of the form $AX \geq b$. Since, all the constraints are linear, from proposition 4, the feasible domain is convex.

Theorem 1: The solution obtained by a nonlinear optimization solver is a global optimal solution.

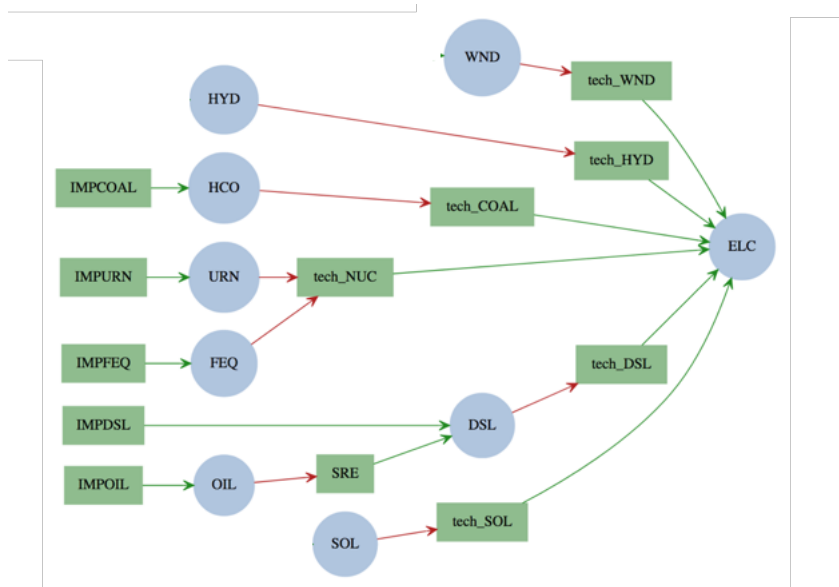
The objective function $f(E_t, \theta_t, CAP_{i,v}, ACT_{i,v,t})$ is concave from proposition 6 and the feasible region is convex from proposition 7. Hence from proposition 5, the local maxima obtained from a nonlinear optimization solver (e.g. IPOPT from the Coin-OR initiative (Biegler, L. T., and Zavala, V. M., 2009)) is a global maximum.

2 Data

We modify an example energy system called ‘utopia’ to include solar and wind technology for electricity generation. This test case was, introduced in MARKAL, described in (Hewells et al., 2011) and extended in (Lavingne, 2017). Since the energy efficiency model is described for electric sector, we run the base case utopia model described by (Hewells et al., 2011) to determine the quantity demanded for electricity to meet the heating, lighting and transportation demand given in (Hewells et al., 2011).

In the modified utopia example, a single region is represented which has electricity demand. The electricity demand fluctuates depending on the season and time of the day: in general, more electricity is required during the day time and in winter. To generate electricity, six different power stations are available: coal (tech_COAL), nuclear(tech_NUC), hydro (tech_HY), diesel (tech_DSL), solar (tech_SOL)

and wind (tech_WND). Diesel is imported (IMPDSL) and/or produced by a refinery (SRE) that converts imported crude oil (IMPOIL). Uranium and coal are also imported (via technologies IMPURN and IMPCOAL, respectively). The nuclear technology (tech_NUC) also take in fossil equivalent (FEQ) imported as (IMPFEQ) along with (URN) for electricity generation. The network diagram for the ‘utopia’ energy system is given in Appendix Figure 4.1.



Appendix Figure 4.1: Graphical representation of a modified version of a test case called 'utopia' (developed for MARKAL). Energy technology is represented by green arrows, flow out by red arrows. Energy sources are shown on the left edge of the diagram (i.e., the import technologies), and on the right edge are the end-use electricity demand. This image was dynamically generated with an open source graphing utility called Graphviz

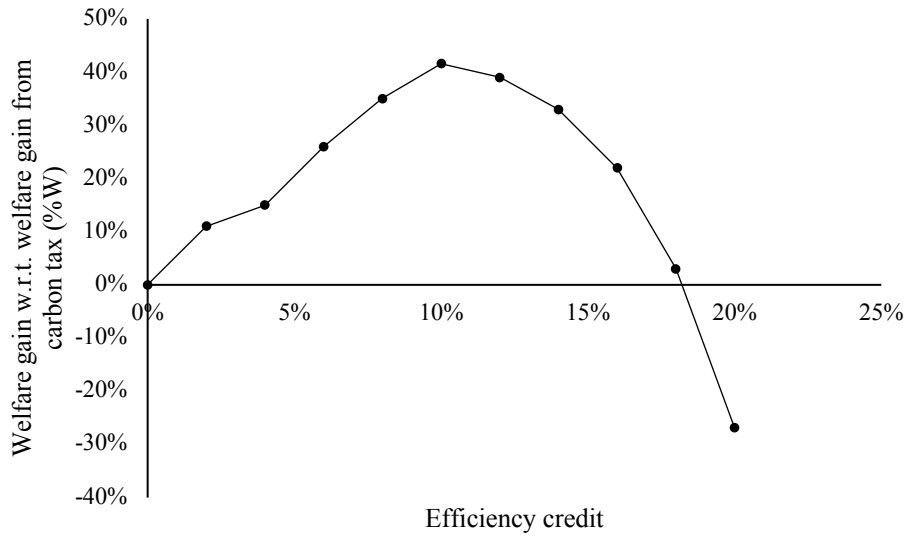
The basic data used to calibrate the utopia application are summarized in Appendix Table 4.2. The future time horizon is from 1990 to 2010 while vintages of existing capacity is from 1960 to 1980. We assume that capacity factor of solar is zero during night time. Cost and performance data for wind and solar is taken from (EIA, 2018).

Appendix Table 4.2: Technology specifications for utopia database

Parameter	Input	Efficiency	Output	Capital	Variable	Fixed	Capacity to	Capacity	Life	Existing capacity		
				Cost	cost	cost	activity	factor		1960	1970	1980
Unit				\$M/GW	\$M/PJ	\$M/GW			years	GW	GW	GW
Technology												
Tech_COAL	Coal	0.32	Electricity	2000	0.3	40	31.54	0.8	40	0.175	0.175	0.15
Tech_NUC	Uranium	0.4	Electricity	4000	1.5	500	31.54	0.8	40	0	0	0
Tech_NUC	FEQ	0.32	Electricity	4000	0	0	31.54	1	1000	0	0	0
Tech_HYD	Hydro	0.32	Electricity	3000	0	75	31.54	0.275	100	0	0	0.1
Tech_DSL	Diesel	0.294	Electricity	1000	0.4	30	31.54	0.8	40	0.005	0.005	0.2
Tech_WND	Wind	0.34	Electricity	1600	12	41	31.54	0.4	40	0	0	0
Tech_SOL	Solar	0.34	Electricity	2000	11	25	31.54	0.4	40	0	0	0
Unit				\$M/PJ/a	\$M/PJ/a	\$M/PJ/a			years	PJ/a	PJ/a	PJ/a
IMPDSL		1	Diesel	0	5	0	1	1	1000	N/A	N/A	N/A
IMP_COAL		1	Coal	0	2	0	1	1	1000	N/A	N/A	N/A
IMP_OIL		1	Oil	0	8	0	1	1	1000	N/A	N/A	N/A
IMPURN		1	Uranium	0	2	0	1	1	1000	N/A	N/A	N/A
SRE	Oil	1	Diesel	100	10	0	1	1	50	N/A	N/A	N/A
Year	1990	2000	2010	For season:		Inter	Summer		Winter			
Demand	PJ/a	PJ/a	PJ/a	For time slice:		Day	Night	Day	Night	Day	Night	
Electricity	6.42	29.85	35.17	Year split:		0.1256	.0594	0.0755	0.0344	0.4801	0.2248	
						0.1667	0.0833	0.1667	0.0833	0.3333	0.1667	

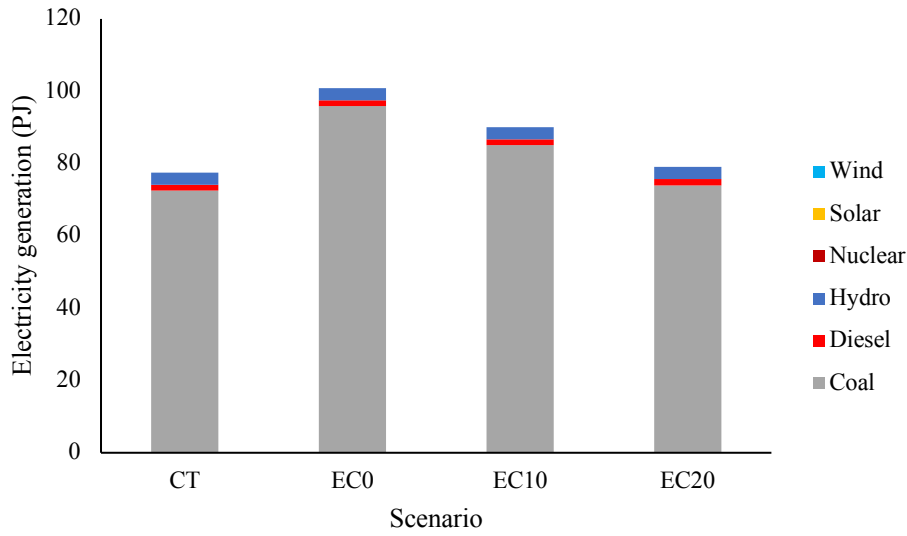
3 Policy Analysis

Welfare gain from efficiency credit scenarios as compared to welfare gain from 40 \$/ton carbon tax scenario is shown in Appendix Figure 4.2. The results show that 42% of the welfare can be recovered with 10% efficiency credit as compared to the welfare gain from carbon tax of 40 \$/ton.

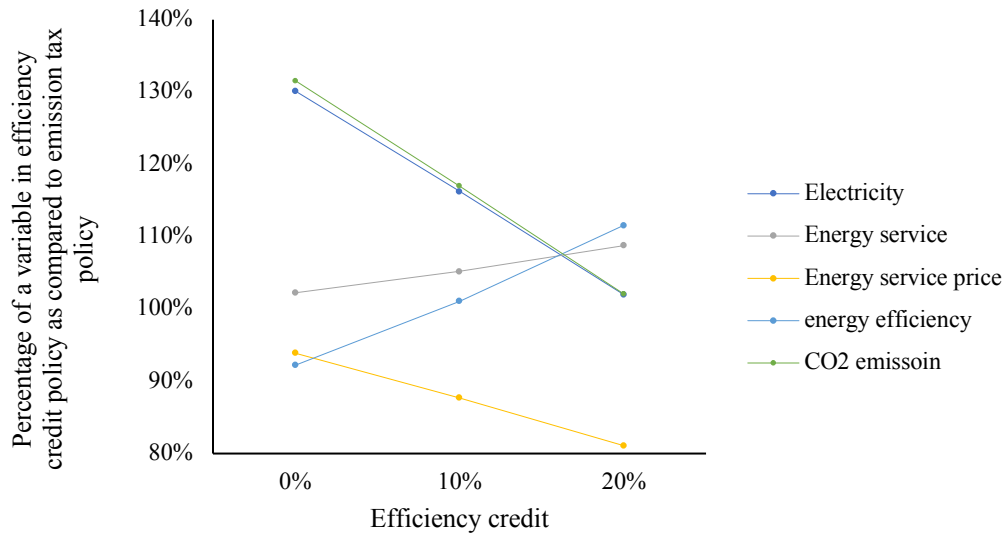


Appendix Figure 4.2: Welfare gain with respect to welfare gain with carbon tax = 40 \$/tonCO₂

Capacity expansion for different policy scenarios is shown in Appendix Figure 4.3. Majority of the capacity expansion is in coal power plant since it is the cheapest available technology. Capacity expansion of Hydro and crude oil processor (SRE) is due to the lower limit set on the capacity expansion in the utopia database. As can be observed, capacity expansion is lowest in carbon tax scenario. Also, increase in efficiency credit leads to lower electricity demand. As a result, overall capacity expansion decreases with increase in efficiency credit.



Appendix Figure 4.3: Capacity expansion in GW for 40 \$/ton Carbon tax (CT), no efficiency credit (EC0), 10% efficiency credit (EC10) and 20% efficiency credit (EC20)



Appendix Figure 4.4: For a given efficiency credit a point of a variable represents the percentage quantity of a variable as compared to the quantity of a variable under emission tax policy

Appendix of Chapter 2

AfDB, (2013). South Sudan: An Infrastructure Action Plan, A Program for Sustained Strong Economic Growth. <https://www.afdb.org/en/countries/east-africa/south-sudan/infrastructure-action-plan-in-south-sudan-a-program-for-sustained-strong-economic-growth/> Date accessed: 05/03/2018

EIA (2017). Annual Energy Outlook 2017. US Energy Information Administration, Washington, DC.

Hatch (2014). Hydropower Expansion Plan and Regional Integration Plan of South Sudan into Regional Electricity Grid, prepared as part of the Nile Basin Initiative, Report # H4569953.

IRENA (2015), Africa 2030: Roadmap for a Renewable Energy Future. IRENA, Abu Dhabi. www.irena.org/remap Date accessed: 05/03/2018

Raleigh, C., Linke, A., Hegre, H., Karlsen, J. (2010). Introducing ACLED: an armed conflict location and event dataset: special data feature. *Journal of Peace Research*, 47(5), 651-660. Current database accessed from <https://www.acleddata.com/data/>.

Solargis (2017). <https://solargis.info/> Date accessed: 05/03/2018

World Bank, (2017). <https://data.worldbank.org/indicator/EP.PMP.DESL.CD> Date accessed: 05/03/2018

Appendix of Chapter 3

Ahern, E. P., Deane, P., Persson, T., Ó Gallachóir, B., Murphy, J. D.: “A perspective on the potential role of renewable gas in a smart energy island system”, *Renewable Energy* 78 (2015) p. 648-656

American Gas Association: „How Does the Natural Gas Delivery System Work?”, published online <https://www.aga.org/natural-gas/delivery/how-does-the-natural-gas-delivery-system-work/>, accessed Dec. 2017

Amos, W. A. (1999). Costs of storing and transporting hydrogen (No. NREL/TP-570-25106; ON: DE00006574). National Renewable Energy Lab., Golden, CO (US).

Annual Energy Outlook 2018 with Projections to 2050; U.S. Energy Information Administration (EIA), 2018; <https://www.eia.gov/outlooks/aeo/pdf/AEO2018.pdf>

Assumptions to the Annual Energy Outlook 2018, U.S. Energy Information Administration (EIA), 2018, Available online: <https://www.eia.gov/outlooks/aeo/assumptions/>

Atsonios, K., Panopoulos, K.D., Kakaras, E.: „Investigation of technical and economic aspects for methanol production through CO₂ hydrogenation“, *international journal of hydrogen energy* 41 (2016), p. 2202-2214

Bann, S., Malina, R., Staples, M. D., Suresh, P., Pearlson, M., Tyner, W. E., Hileman, J. I., & Barrett, S. (2017). The costs of production of alternative jet fuel: A harmonized stochastic assessment. *Bioresource Technology*, 227, 179–187;

Bertuccioli, L., Chan, A., Hart, D., Lehner, F., Madden, B., Standen, E.: „Study on development of water electrolysis in the EU“, Final Report, program: Fuel cells and Hydrogen - Joint undertaking, 2014

Biofuels FactSheet, E., B. F. Sheet, and M. Formula, Ethanol. <http://www.etipbioenergy.eu/images/ethanol-fact-sheet.pdf>

Biodiesel - <https://www.aqua-calc.com/page/density-table/substance/biodiesel>

Cai, X., Zhang, X., & Wang, D. (2010). Land availability for biofuel production. *Environmental science & technology*, 45(1), 334-339.

Colbertaldo, P., Agustin, S. B., Campanari, S., & Brouwer, J. (2019). Impact of hydrogen energy storage on California electric power system: towards 100% renewable electricity. *International Journal of Hydrogen Energy*.

Cole, W. J., Hand, M. M., Eberle, A., Beiter, P. C., Kurup, P., Turchi, C. S., ... & O'Connor, P. (2018). 2018 Annual Technology Baseline (No. NREL/PR-6A20-70015). National Renewable Energy Lab. (NREL), Golden, CO (United States)

Congress, U.S. (2007). Energy Independence and Security Act of 2007. Public Law, 111(140). Retrieved from GPO's Federal Digital System: <https://www.gpo.gov/fdsys/pkg/BILLS-110hr6enr/pdf/BILLS-110hr6enr.pdf>

DeCarolis, F. J. et al. Formalizing best practices for energy system optimization modelling. *Applied Energy*, 2017, vol. 194, pp. 184-198. DOI: j.apenergy.2017.03.001

de Jong, S. A. (2018). Green Horizons: On the production costs, climate impact and future supply of renewable jet fuels (Doctoral dissertation, Utrecht University).

Demirbas, A. (2004). Combustion characteristics of different biomass fuels. *Progress in energy and combustion science*, 30(2), 219-230.

Demirbas, A. (2005). Potential applications of renewable energy sources, biomass combustion problems in boiler power systems and combustion related environmental issues. *Progress in energy and combustion science*, 31(2), 171-192.

DoE BTS (2016). <https://bioenergykdf.net/bt16-download-tool/state> accessed 06/10/2019

Dörr, H., Kröger, K., Graf, F., Köppel, W., Burmeister, F., Senner, J., Nitschke-Kowsky, P., Weßing, W.: "Untersuchungen zur Einspeisung von Wasserstoff in ein Erdgasnetz", *energie wasser-praxis* 11 (2016), p. 50-59

EIA, U.S. Electric Power Monthly (February 2017), Tables 6.2.B and 6.2.C

ENEA consulting: The potential of power-to-gas”, Paris, Jan. 2016

Energy content - https://en.wikipedia.org/wiki/Energy_content_of_biofuel

Energyportal, (2017) <http://www.energieportal24.de/cms1/wissensportale/brennkraftstoffe/wasserstoff/h2-herstellung/>, accessed on 12/7/2017

EPA-CSAPR <https://www.epa.gov/csapr/overview-cross-state-air-pollution-rule-csapr>

Eurek, K., Wesley, C., Bielen, D., 2016. Regional Energy Deployment System (ReEDS) Model Documentation: Version 2016.

Falco, R.: “California's Methanol Fuel Experience”,

http://www.energyresourcefulness.org/Fuels/methanol_fuels/California_methanol_experiment_1.html

Farkade, H. S., Pathre, A. P.,: “Experimental investigation of methanol, ethanol and butanol blends with gasoline on SI engine”, International Journal of Emerging Technology and Advanced Engineering, ISSN 2250-2459, Volume 2, Issue 4 (2012), p. 205-215

Felix, O., Wiede, T., Meinecke, M., König, R.: “Netzentwicklungsplan 2025, 2. Entwurf”, 2016

Ferreroa, D., Gamba, M., Lanzinia, A., Santarellia, M.: “Power-to-Gas Hydrogen: techno-economic assessment of processes towards a multi-purpose energy carrier”, Energy Procedia 101 (2016) p. 50–57

Frew, B. A., Cole, W. J., Sun, Y., Mai, T. T., & Richards, J. (2017). 8760-based method for representing variable generation capacity value in capacity expansion models (No. NREL/CP-6A20-68869). National Renewable Energy Lab.(NREL), Golden, CO (United States).

Eurek, K., Wesley, C., Bielen, D., 2016. Regional Energy Deployment System (ReEDS) Model Documentation: Version 2016.

Gagnon, P., & Sigrin, B. (2016). Distributed PV Adoption-Sensitivity to Market Factors (No. NREL/PR-6A20-65984); U.S. Department of Energy. Golden, CO.

Götz, M., Lefebvre, J., Mörs, F., McDaniel Koch, A., Graf, F., Bajohr, S., Reimert, R., Kolb, T.: „Renewable Power-to-Gas: A technological and economic review“, *Renewable Energy* 85 (2016), p. 1371-1390

GREET, 2018. GREET.Net framework by Argonne National Laboratory. <https://greet.es.anl.gov/net>

Habte, A., Sengupta, M., 2017. Evaluation of the National Solar Radiation Database (NSRDB): 1998–2015. National Renewable Energy Laboratory.

Hay, J.F. (2015). Corn for Biofuel Production. eXtension Foundation. Kansas City, MO. <http://articles.extension.org/pages/27536/corn-for-biofuel-production>

Horne, M; Jaccard, M.; Tiedemann, K. Improving behavioral realism in hybrid energy economy models using discrete choice studies of personal transportation decisions. *Energy Economics*, 2005, 27, 59-77. DOI: j.eneco.2004.11.003

Huang, H., Long, S., & Singh, V. (2016). Techno-economic analysis of biodiesel and ethanol co-production from lipid-producing sugarcane. *Biofuels, Bioproducts and Biorefining*, 10(3), 299-315.

International Energy Agency. Modelling the capacity credit of renewable energy sources; International Energy Agency, Paris, France, 2011.

Iliev, S., “A Comparison of Ethanol and Methanol Blending with Gasoline Using a 1-D Engine Model”, *Procedia Engineering* 100 (2015), p. 1013–1022

Jadun, Paige, Colin McMillan, Daniel Steinberg, Matteo Muratori, Laura Vimmerstedt, and Trieu Mai. 2017. Electrification Futures Study: End-Use Electric Technology Cost and Performance Projections through 2050. Golden, CO: National Renewable Energy Laboratory. NREL/TP-6A20-7048

Lenox, C., Dodder, R., Gage, C., Kaplan, O., Loughlin, D., & Yelverton, W. (2013). EPA US Nine-region MARKAL Database: database documentation. US Environmental.

Luo, L., Van der Voet, E., & Huppes, G. (2009). An energy analysis of ethanol from cellulosic feedstock–Corn stover. *Renewable and Sustainable Energy Reviews*, 13(8), 2003-2011.

MacDonald, A. E., Clack, C. T., Alexander, A., Dunbar, A., Wilczak, J., & Xie, Y. (2016). Future cost-competitive electricity systems and their impact on US CO₂ emissions. *Nature Climate Change*, 6(5), 526.
Markey Insider - <https://markets.businessinsider.com/commodities/soybeans-price> accessed on 06/10.2019

Mau, P.; Eyzaguirre, J.; Jaccard, M.; Collins-Dodd, C.; Tiedemann, K. The neighbor effect: Simulating dynamics in consumer preferences for new vehicle technologies. *Ecological Economics*, 2008, 68, 504-516. DOI: [j.ecolecon.2008.05.007](https://doi.org/10.1016/j.ecolecon.2008.05.007)

MECS 2017 “2014 MECS Survey Data.” Manufacturing Energy Consumption Survey (MECS) - Data - U.S. Energy Information Administration (EIA). 2017.
<https://www.eia.gov/consumption/manufacturing/data/2014/>.

Müller-Syring, M., Henel, M., Köppel, W., Mlaker, H., Sterner, M., Höcher, T.: „Entwicklung von modularen Konzepten zur Erzeugung, Speicherung und Einspeisung von Wasserstoff und Methan ins Erdgasnetz“, final report, DVGW-project G1-07-10, DVGW, 2013

National Agricultural Statistics Service. (2016). Crop Production 2015 Summary. United States Department of Agriculture. Washington, D.C. <https://www.usda.gov/nass/PUBS/TODAYRPT/cropan16.pdf>

Niaz, S., Manzoor, T., Pandith, A.H.: “Hydrogen storage: Materials, methods and perspectives”, *Renewable and Sustainable Energy Reviews* 50 (2015), p. 457–469

Nikita Pavlenko, Stephanie Searle, and Adam Christensen, The cost of supporting alternative jet fuels in the European Union, ICCT (Working paper)
https://www.theicct.org/sites/default/files/publications/Alternative_jet_fuels_cost_EU_20190320.pdf

North American Electric Reliability Corporation. NERC Reliability Metrics Specifications Sheet; North American Electric Reliability Corporation, Washington, DC, 2009.

North American Electric Reliability Corporation, 2017 Summer Reliability Assessment, Available on: <https://www.nerc.com/pa/RAPA/ra/Reliability%20Assessments%20DL/2017%20Summer%20Assessment.pdf>

Peterson, S.B.; Michalek, J.J. Cost-effectiveness of plug-in hybrid electric vehicle battery capacity and charging infrastructure investment for reducing US gasoline consumption. *Energy Policy*. 2013, 52, 429-438. DOI: j.enpol.2012.09.059

Pérez-Fortes, M., Schöneberger, J.C., Boulamanti, A, Tzimas, E.: „Methanol synthesis using captured CO₂ as raw material: Techno-economic and environmental assessment“, *Applied Energy* 161 (2016) p. 718–732

Schiebahn, S., Grube, T., Robinius, M., Tietze, V., Kumar, B., Stolten, D.: „Power to gas: Technological overview, systems analysis and economic assessment for a case study in Germany“, *Int. journal of Hydrogen energy* 40 (2015), p. 4285-4294

Smolinka, T., Thomassen, M., Oyarce, A., Marchal, F.: “Cost benefit analysis and cost and performance target for large scale PEM electrolyser stack”, public summary from the project MEASTACK, 2016

Smolinka, T., Günther, M., Garche, J.: „Stand und Entwicklungspotenzial der Wasserelektrolyse zur Herstellung von Wasserstoff aus regenerativen Energien“, NOW Studie, Kurzfassung des Abschlussberichtes, 2010

Spath, P.L., Mann, M.K.: (2001) “Life cycle assessment of Hydrogen production via natural gas steam reforming”, NREL-report NREL/TP-570-27637, 2001

The TEMOA Project, www.temoaproject.org

Tillman, D. A. (2000). Biomass cofiring: the technology, the experience, the combustion consequences. *Biomass and bioenergy*, 19(6), 365-384.

US Census Bureau. (2010). Census regions and divisions of the United States. US Census Bureau website.

U.S. Energy Information Administration, Office of Energy Consumption and Efficiency Statistics, Form EIA-846, '2014 Manufacturing Energy Consumption Survey.'

Voorspools, K. R., & D'haeseleer, W. D. (2006). An analytical formula for the capacity credit of wind power. *Renewable Energy*, 31(1), 45-54.

Wormslev, E. C. (2016). Sustainable jet fuel for aviation: Nordic perspectives on the use of advanced sustainable jet fuel for aviation. Nordic Council of Ministers.

Wuebben, P.: “Back to the Future - Lessons Learned from California’s 1990s Methanol Program and Renewed Interest in Petroleum Reduction”, 2015 European Methanol Forum, Brussels, Oct. 13th – 14th 2015

Zhao, L., Zhang, X., Xu, J., Ou, X., Chang, S., & Wu, M. (2015). Techno-economic analysis of bioethanol production from lignocellulosic biomass in China: Dilute-acid pretreatment and enzymatic hydrolysis of corn stover. *Energies*, 8(5), 4096-4117.

Appendix of Chapter 4

Biegler, L. T., & Zavala, V. M. (2009). Large-scale nonlinear programming using IPOPT: An integrating framework for enterprise-wide dynamic optimization. *Computers & Chemical Engineering*, 33(3), 575-582.

Bauschke, H. H., & Combettes, P. L. (2017). *Convex analysis and monotone operator theory in Hilbert spaces* (Vol. 2011). New York: Springer.

EIA. (2018). https://www.eia.gov/forecasts/aeo/assumptions/pdf/table_8.2.pdf

Howells, M., Rogner, H., Strachan, N., Heaps, C., Huntington, H., Kypreos, S., ... & Roehrl, A. (2011). OSeMOSYS: the open source energy modeling system: an introduction to its ethos, structure and development. *Energy Policy*, 39(10), 5850-5870.

Lavigne, D. (2017). OSeMOSYS Energy Modeling Using an Extended UTOPIA Model. *Universal Journal of Educational Research*, 5(1), 162-169.